DESIGN AND SYNTHESIS OF MOLECULAR ACTUATORS AND SENSORS

by

CHANGSIK SONG

B.S., Chemistry
Korea Advanced Institute of Science and Technology, 2001

Submitted to the Department of Chemistry
in Partial Fulfillment of the Requirements for the Degree of

DOCTOR OF PHILOSOPHY IN CHEMISTRY

at the

MASSACHUSETTS INSTITUTE OF TECHNOLOGY

September 2007

© 2007 Massachusetts Institute of Technology. All Rights Reserved

Signature of Author: ____
Department of Chemistry
June 27, 2007

Certified by: ____
Timothy M. Swager
John D. MacArthur Professor of Chemistry
Thesis Supervisor

Accepted by: ____
Robert W. Field
Haslam and Dewey Professor of Chemistry
Chairman, Departmental Committee on Graduate Students

This doctoral thesis has been examined by a Committee of the Department of Chemistry as follows:

Professor Gregory C. Fu: ____
Chairman

Professor Timothy M. Swager: ____
Thesis Advisor

Professor Sarah E. O'Connor: ____

To God,

my family, and Yunmi

Design and Synthesis of Molecular Actuators and Sensors

by

Changsik Song

Submitted to the Department of Chemistry
on June 27, 2007 in Partial Fulfillment of the
Requirements for the Degree of
Doctor of Philosophy in Chemistry

ABSTRACT

To date, the most successful conducting polymer actuators are based on polypyrrole, which operates through incorporating and expelling counterions and solvent molecules to balance the charges generated by electrochemical stimuli (swelling mechanism). Although significant progress has been made, there still exists a need for developing new materials that would overcome the intrinsic limitations in the swelling mechanism, such as slow diffusion rate, limited expansion volume, etc. Our group has contributed this area with a different approach – molecular mechanisms, which utilize a dimensional change of a single polymer chain. We propose two types of molecular mechanisms: contracting and expanding. We proposed earlier a calix[4]arene-based molecular actuator for the contracting mechanism, in which π-dimer formation was proposed as a driving force. In this dissertation, we first confirm by model studies that π-dimer formation can indeed be a driving force for the calix[4]arene-based system. We propose another molecular hinge, binaphthol moiety, for the contracting model. The syntheses of polymers with binaphthols and their characterization, including signatures of oligothiophene interactions, are described. Due to its chirality, we examined the possibilities of the binaphthol polymer as a chiral amine sensor. To create actuators that make use of the expanding model, we propose new conjugated seven-membered ring systems with heteroatoms (*thiepin* with sulfur and *azepine* with nitrogen) and their syntheses and characterization will be described. Inspired by the fact that sulfoxide has very low extrusion barrier in the related system, we applied the thiepin molecules to create a peroxide sensor. In addition, during the investigation of phenol functional groups in conducting polymers, we found interesting properties that strategic positioning of phenol groups can render a conjugation-broken *meta*-linked system just as conductive as a fully conjugated *para*-linked isomeric system.

Thesis Supervisor: Timothy M. Swager
Title: John. D. MacArthur Professor of Chemistry

Table of Contents

Dedication 3
Abstract 4
Table of Contents 5

Chapter 1. Introduction: Molecular Mechanism for Actuators 8
  Molecular Machines: From Biological to Synthetic 9
  Molecular Machines at Work: Artificial Muscles 12
  Conducting Polymer Actuators: The Conventional Mechanisms 15
  Molecular Actuators: Mechanisms and Designs 17
  References and Notes 21

Chapter 2. π-Dimer Formation as the Driving Force for Calix[4]arene-based Molecular Actuators 23
  Calix[4]arene-based Molecular Actuator 24
  π-Dimers 25
  Synthesis of Model Compounds 27
  π-Dimers between Oxidized Oligothiophene Derivatives: UV-vis 28
  EPR and DPV 32
  Conclusion 34
  Experimental Section 35
  References and Notes 44
  Appendix 46

Chapter 3. Binaphthyl-Hinged Molecular Actuators 55
  Binaphthyl – A Molecular Hinge 56
  Synthesis of Binaphthyl Polymers: The First Generation 58
  Preparation of Free-Standing Films and Actuation Testing 63
  Design of New Scaffold: The Second Generation 65
  O-Alkylated Binaphthol Polymers 71
  Alignment of Polymers: Ring Opening Metathesis Polymerization 80
  Conclusion 84
  Experimental Section 85
  References and Notes 97
  Appendix 100

Chapter 4. Electroactive Polymer Chiral Sensors 113
  Introduction and Design Principles 114

Synthesis of Monomers 116
Electropolymerization........ 117
Attempts for Chiral Sensing........ 120
Discussion 124
Conclusion 127
Experimental Section........ 128
References and Notes 133
Appendix........ 134

Chapter 5. Annulated Thiepins as Building Blocks for Actuating and Sensory Materials 139
Introduction........ 140
Thermal Stability of Thiepins and Design of the Molecular Scaffold 141
Synthesis of Thiophene-Annulated Thiepins........ 143
Cyclic Voltammograms of Annulated Thiepins........ 145
Electropolymerization of Extended Thiepins........ 148
Properties of Thiepin 1-Oxide (Sulfoxide) 154
Conclusion 161
Experimental Section........ 162
References and Notes 175
Appendix........ 177

Chapter 6. Polymers Incorporating Azepines: Redox Stable Materials For Actuation.... 193
Introduction........ 194
Synthesis of Annulated Azepines via Buchwald-Hartwig Aminations........ 196
Functionalization of Annulated Azepines........ 199
Cyclic Voltammetry 201
Electrochemistry of Azepine-Incorporated Polymers 204
Conclusion 209
Experimental Section........ 210
References and Notes 221
Appendix........ 222

Chapter 7. Highly Conductive Poly(phenylene theienylene)s: *m*-Phenylene Linkages Are Not Always Bad........ 232
Introduction........ 233
Monomer Synthesis 235
Electropolymerization........ 236
Deprotection to Give Free –OH Groups 238
Polymer Electrochemistry Comparison of *meta* vesus *para*........ 240

Meta vesus *para*: *In situ* Conductivity Measurement ... 242
Meta vesus *para*: Spectroelectrochemistry ... 244
Substituent Effects in PMPTs ... 245
Conclusion ... 248
Experimental Section ... 249
References and Notes ... 258
Appendix ... 260

Curriculum Vitae ... 271
Acknowledgements ... 273

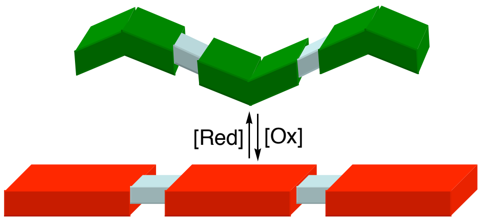

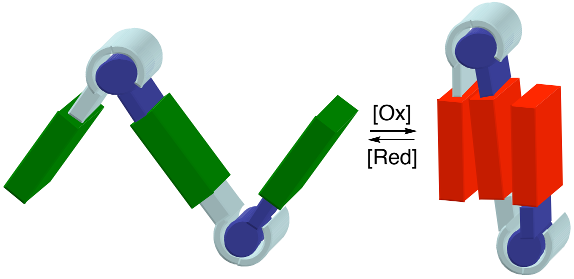

Chapter 1

Introduction: Molecular Mechanism for Actuators

Molecular Machines: From Biological to Synthetic

Significant progress in molecular biology has made it possible to understand biological phenomena at the molecular level. The molecular structures of proteins or protein assemblies have been determined to the point where the operations of some classes of proteins can be precisely described.[1] Of particular interest are the biological motor proteins, which are responsible for various tasks, including moving cargos inside cells and contracting muscles.[2] Similar to machines in everyday use, those nanometer-sized molecular machines (motors) convert fuels (chemical energy inputs, for example, ATP) to useful linear or rotary motions. Examples of these molecular machines are myosins, kinesins, dyneines, ATPase, and bacterial flagella. Much has been revealed about how these molecular machines operate in response to biological stimuli at the molecular level.[2] For instance, myosins move along the actin filaments via the cycle of myosin's binding to actin, followed by myosin's stroke and dissociation. As a fuel, ATP plays a key role in the operation cycle. Association of ATP enhances the binding of myosin to actin. The stroke of myosin occurs by hydrolyzing ATP and concomitant release of a pyrophosphate. Finally, the dissociation upon release of ADP allows the next cycle.

Revelations from these biological molecular machines have inspired chemists to build synthetic systems that mimic the functions of the molecular machines.[2b,3] For example, Kelly and coworkers reported a molecular ratchet that conducts unidirectional 120° rotation around a single bond with phosgene as a fuel (Figure 1a).[4] Feringa *et al.* reported the synthetic rotary motor which is reminiscent of ATPase's unidirectional motion (Figure 1b).[5] By using light as a fuel, they realized the continuous unidirectional motion (360°). Photochemical *cis-trans* isomerization results in a rotation that places bulky groups in high-energy positions. The molecular rotor then undergoes thermal relaxation that accomplishes 180° rotation. Repeating the above steps allows the unidirectional rotation in a continuous way. It is noteworthy that light is a highly desirable fuel because it does not produce any waste. For the same reason, electrochemical stimulation is also a suitable mechanism.

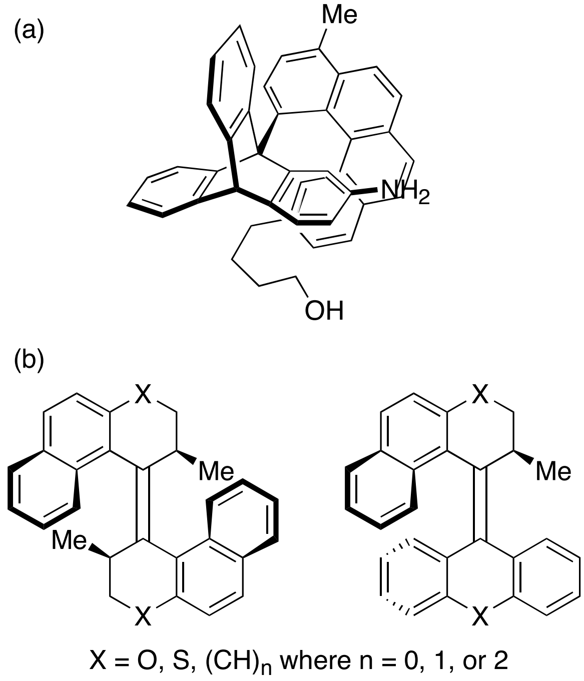

Figure 1. (a) Chemically powered molecular rachet.[4] (b) Light-driven unidirectional molecular rotors.[5]

Molecular systems of the directed linear motion have been based mainly on the rotaxanes and related structures.[3] Rotaxanes are supramolecular complexes that consist of a macrocylic ring component surrounded by a dumbbell-shaped molecule. The key to linear motion is the presence of two recognition sites on the dumbbell-shaped molecule, which makes the rotaxane a bistable molecular switch. For example, tetrathiafulvalene (TTF) and naphthalene units can be competing recognition sites for the tetracationic cyclophane ring (Figure 2a).[6] In the neutral state of TTF, the tetracationic ring stays in the TTF moiety due to the greater affinity. However, once TTF is oxidized, coulombic repulsion pushes the tetracationic ring immediately to the naphthalene moiety. Upon reduction, the tetracationic ring is thermally relaxed to the TTF moiety again.

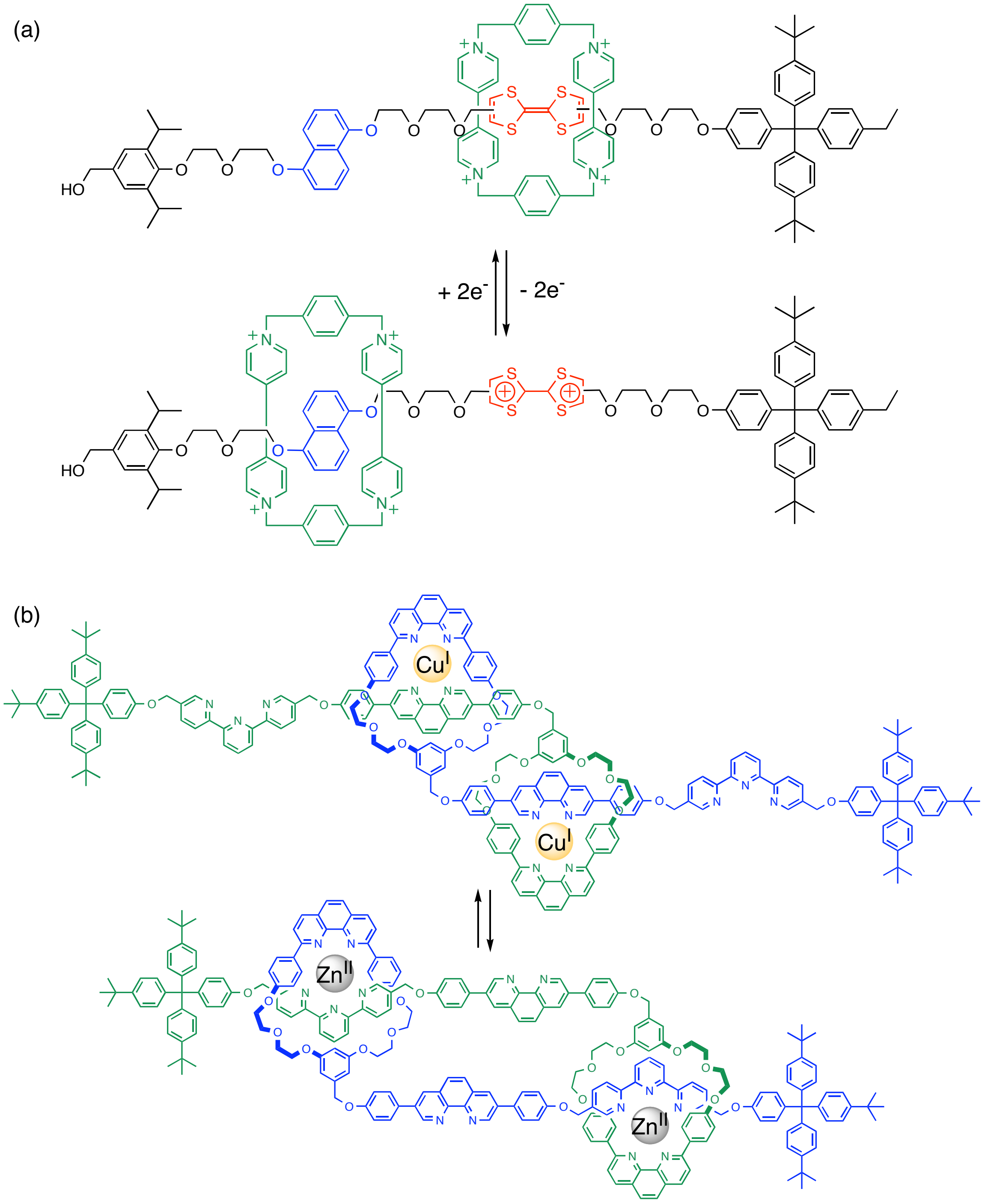

Figure 2. (a) Bistable [2]rotaxane with TTF and naphthalene moieties.[6] (b) Artificial molecular muscle driven by metal ion bindings.[3a]

Sauvage *et al*. reported a very elegant system that has two interlocked rotaxanes and is driven by different metal ion bindings.[3a] The system mimics the sliding movement of actin and myosin filaments in natural muscles.[2] In addition to donor-acceptor and metal-ligand binding interactions, other non-covalent interactions, such as hydrogen bonding, π-π stacking, coulombic, and hydrophobic-hydrophilic interactions, are exploited in a number of rotaxane and related systems.

Molecular Machines at Work: Artificial Muscles

For practical reasons, much effort is being made to take advantage of such molecular machines and create useful functions. In many cases, the synthetic molecular machines act as a switch, moving from one state to another state, which can produce useful output signals. However, it is not always easy to extract useful mechanical work from molecular machines because in the nanoscale world you should "accommodate to the brownian storms."[7] To overcome the brownian terbulance, either the size of molecular machines needs to be very large, or they should be mounted on surfaces. However, even though the system works in the solution state, immobilization often leads to malfunctions due to loss of degrees of freedom in structured environments.[3e] Moreover, bringing nanoscale events to macroscopic (useful) movements is always challenging. In this regard, the demonstration that molecular machines can perform work is very important, and some have already been achieved.

The indirect movement of a much larger object by collective change in host matrix was reported by Feringa and coworkers.[8] They embedded a chiral molecular rotor (Figure 3a) in a liquid crystal film. As the rotation of the molecular rotor was performed by photochemical isomerization and subsequent thermal relaxation, the liquid-crystal film was reorganized because of the induced helicity by the guest molecule. The reorganization of the matrix was harnessed to move a micron-sized object (a glass rod) in a rotary fashion (Figure 3b).

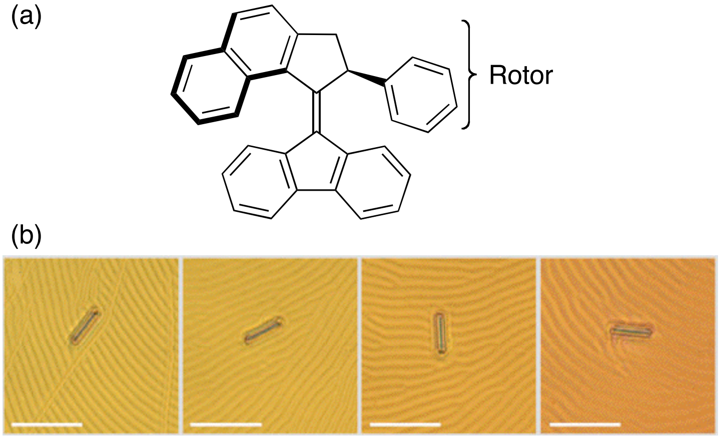

Figure 3. Rotation of a microscale glass rod (b) in a liquid-crystal film doped with a light-driven molecular rotor (a). Scale bars in b are 50 μm. Reproduced with permission from ref 8.

The macroscopic transport of liquid drops was demonstrated by the surface-energy switching that originated from a light-responsive molecular shuttle (rotaxane)[9] (Figure 4). The rotaxane, which is physisorbed on the surface, has fumaramide and tetrafluorosuccinamide groups, and in the unperturbed state the macrocycle resides with the former by hydrogen bonding. However, UV irradiation induces the *E*→*Z* isomerization of fumaramide to maleamide, which has a low affinity to the macrocycle. By masking the fluoroalkyl moiety, the surface energy can be changed from "polarophobic" to "polarophilic", which results in the movement of a liquid drop (CH_2I_2).

Another approach was the direct bending of microcantilever beams by electrochemically switchable [3]rotaxanes directly assembled on the surface. The design elegantly resembles the natural muscle's actin and myosin structure. The rotaxane has four stations and two macrocyclic rings, and the rings have disulfide tethers that are attached to the surface of the cantilever beams in the self-assembly. The electrochemical switching of two stations from neutral to positively charged states results in the contraction of the distance between the rings, which is translated into the bending of cantilever beams.

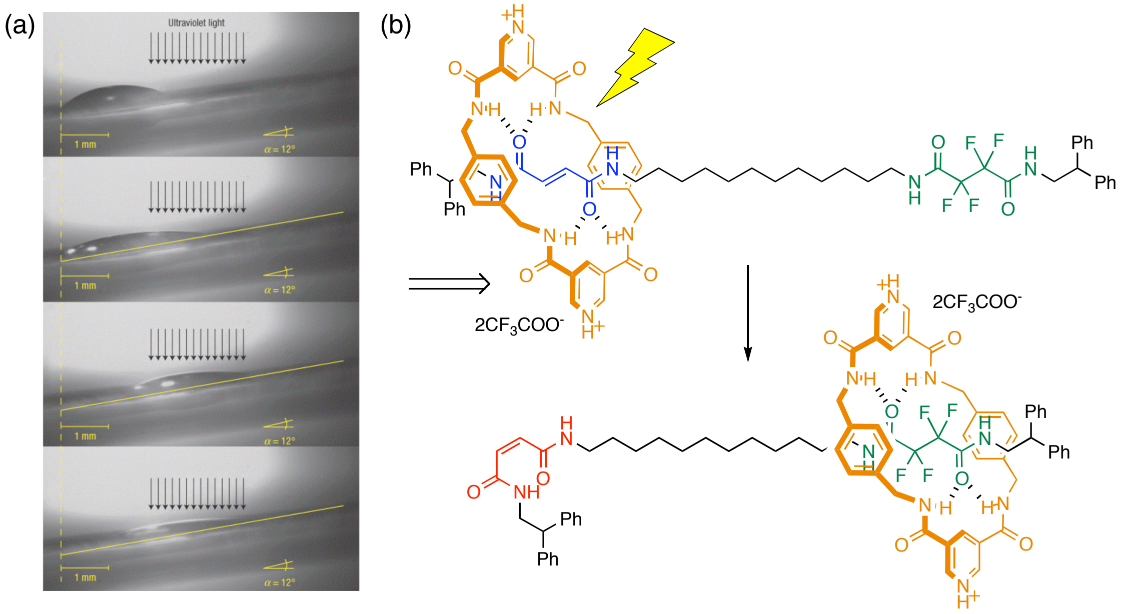

Figure 4. Light-driven transport (a) of a liquid drop (CH_2I_2) on a self-assembled monolayer (SAM) of 11-mercaptodecanoic acid on gold deposited on mica. The light-switchable rotaxane (b) was physisorbed onto the SAM. Reproduced with permission from ref 9.

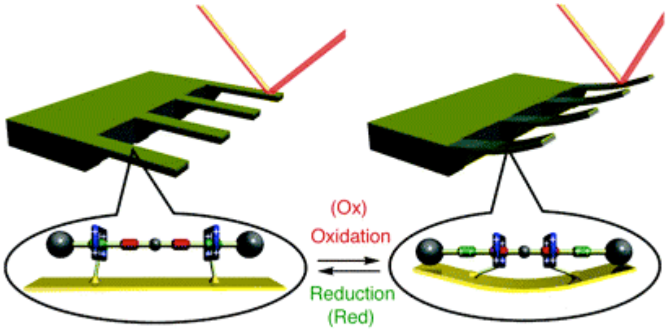

Figure 5. Design of a molecular muscle based on rotaxanes and its operation (bending of cantilever beams) under redox control. Reproduced with permission from ref 10. Copyright (2005) American Chemical Society.

We are interested in those types of molecular machines that generate useful mechanical outputs (artificial muscles). We believe that the incorporation of molecular machines into a polymeric form, if aligned properly, can enable us to effectively translate the nanoscopic events into macroscopic work. In this dissertation, we propose new molecular systems, which change their conformations under external stimuli (molecular machines), and their syntheses and installment into polymers will be described. We seek to exploit dimensional changes of the molecular machines to create systems that can be considered as molecular muscles, or artificial muscles. To accomplish our goals, we make use of electroactive polymers (EAPs), which are a class of polymeric materials that has been spotlighted as artificial muscles.[11] However, our approach is in sharp contrast to conventional EAP actuators in that we would like to take advantage of molecular events, not just bulk phase behavior.

Conducting Polymer Actuators: The Conventional Mechanisms

EAP actuators exhibit dimensional changes in response to electrical stimulation. EAPs can be classified into two basic groups depending on the activation mechanism: electronic and ionic.[11] The electronic EAPs change their dimensions by the attraction force due to the applied electric field. Although the electronic EAPs exhibit relatively large force and rapid response time, they generally require very high voltages (~100 MV/m) that are close to dielectric breakdowns. On the contrary, ionic EAPs only need very low driving voltages (1~5 V); they are driven by diffusion of ions. However, they require an electrolyte, which may cause problems in open-air conditions, or with long-term use.

Conducting polymers can be classified as the ionic EAP because the ions' egress and ingress are responsible for the polymers' deformation.[12] As shown in Figure 6, a conducting polymer gains positive charge due to oxidation caused by the applied voltage. Then, counter-ions and accompanying solvent molecules are incorporated to balance the charge, which causes the expansion of volume. This process is reversible, so upon reduction the polymer returns to its original volume by expelling the counter-ions. This mechanism is often referred to as a "swelling" mechanism.

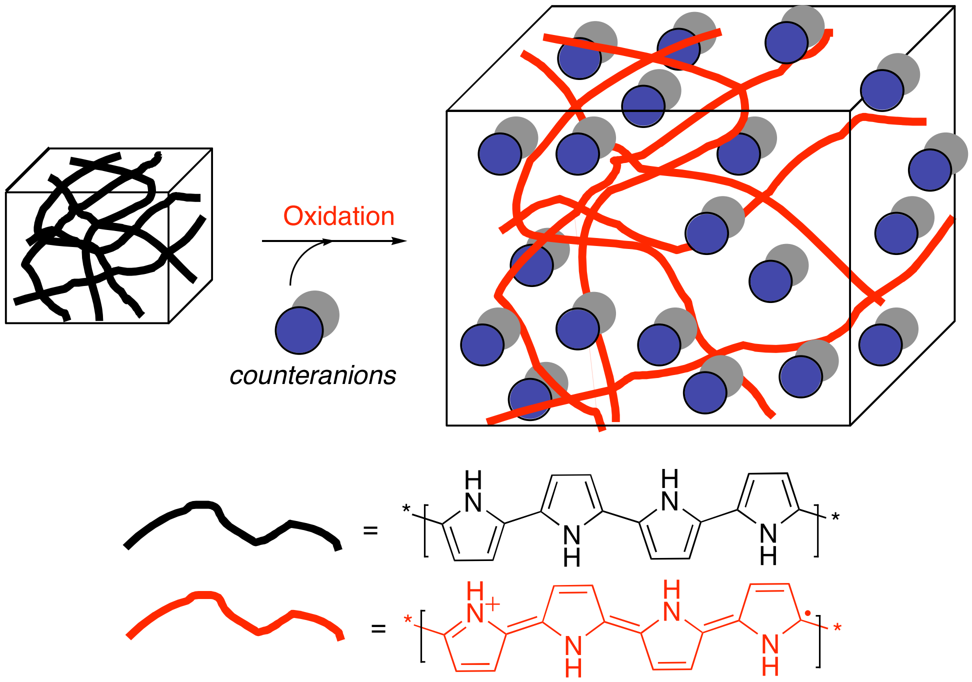

Figure 6. Swelling mechanism represented by polypyrrole. The polymer increases in dimension when oxidized due to the ingress of counterions (typically PF_6^- in organic solvents).

Polypyrrole and related systems are the most developed conducting polymers for actuators.[12,13] Polypyrroles are often fabricated into the tri-layer system, in which two polypyrrole films sandwich a polymeric electrolyte layer.[14] This tri-layer actuator can bend in either direction according to the voltage polarities. Polypyrrole can also be easily deposited onto conductive substrates via an electrochemical oxidative polymerization method using pyrrole monomers. This makes them useful for microfabrication.

Optimization for the polypyrrole's performance has been continued to create materials that display one or two performance metrics that are equal or exceed that of natural muscle.[15] However, the performance that allows proper comparison with natural muscle has not been realized in a single device. Therefore, continuing efforts are still needed and our group has contributed to this area with a different approach – molecular mechanisms.

Molecular Actuators: Mechanisms and Designs

In a conventional swelling mechanism, speed is intrinsically limited by the ion's mobility. In addition, strain cannot exceed values imposed by the space that is occupied by the ions and associated solvent molecules. It should be noted that the individual polymer chains remain chemically unchanged and the reversible oxidation and reduction process in the polymer causes the ion flow. The macroscopic polymer object retains its shape and the incorporation of counterions causes the swelling-based volume change.

Throughout this thesis, we will refer to materials having geometrical changes at the molecular level to create volume changes as *molecular actuators*. It should be noted that unlike bulk actuators (e.g., polypyrrole), molecular actuators harness the dimensional variation of the single strands of the polymer. We envision that if we utilize the conformational changes of single polymer chains, we may obtain fast responses and large strains, which are not limited to the ion's mobility. These single molecule actuators have potential applications to the bottom-up development of nano-devices and machines. The conformational change of the single strand would come from the monomer unit's response to the external stimulation, namely electrochemical. We propose two types of molecular mechanisms: expanding and contracting (Figure 7).

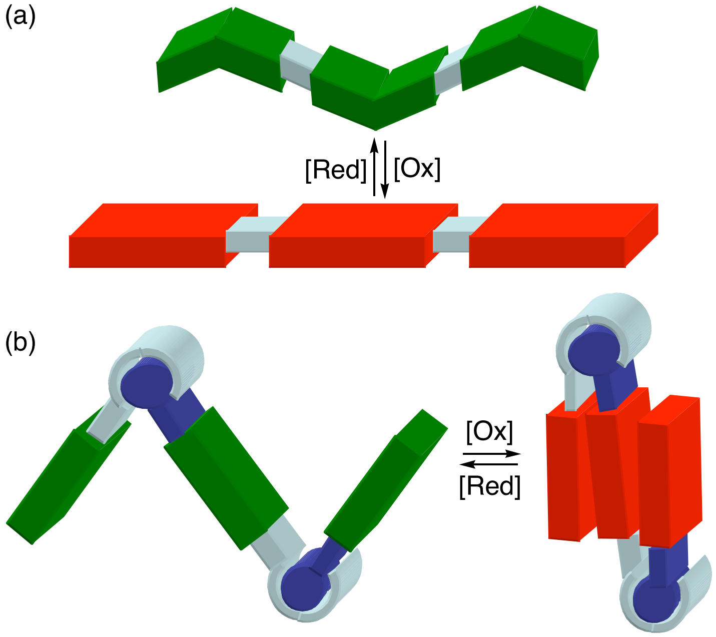

Figure 7. Expanding (a) and contracting (b) molecular mechanisms for actuation under redox control. Expanding model exploits the conformational changes of monomer units, while in the contracting model new chemical bond induces the contraction through a molecular hinge.

In the expanding model, the monomer moiety has a bent geometry in its neutral state. However, it becomes planar when it is oxidized, resulting in expansion. We can exploit the aromatization of non-aromatic system as the driving force. For example, we proposed thianthrene as the candidate, which is bent in its neutral state, and calculations showed about 7% increase upon oxidation (Figure 8a).[16] Marsella *et al*. reported a polymer which was based on the bent-to-planar transformation of cyclooctatetraene moiety under redox control (Figure 8b).[17] Although not experimentally confirmed, theoretical calculations predicted ~6% increase when oxidized.

In the contracting model, the key in the design is a hinged molecule that connects electroactive segments. Upon electrochemical oxidation, new chemical bonds between the oxidized species (π-dimer or π-stacks, for example) induce a large conformational change through the molecular hinge. We proposed a calix[4]arene moiety as the molecular hinge and oligothiophenes as the electroactive segments (Figure 9).[18] The driving force for contraction is the π-dimer formation between the radical cations of oligothiophenes.

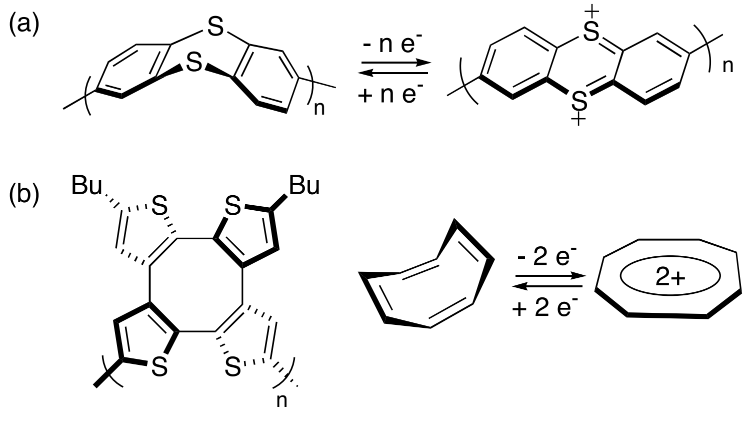
(a)
S
S
- n e⁻
+ n e⁻
n
S
S
+
+
n
(b)
Bu
Bu
S
S
S
S
n
- 2 e⁻
+ 2 e⁻
2+

Figure 8. Expanding molecular actuators: a thianthrene-based polymer (a) and a cyclooctatetraene-based polymer (b). They utilize a bent-to-planar transformation caused by the aromatization from 8 to 6-π electrons.

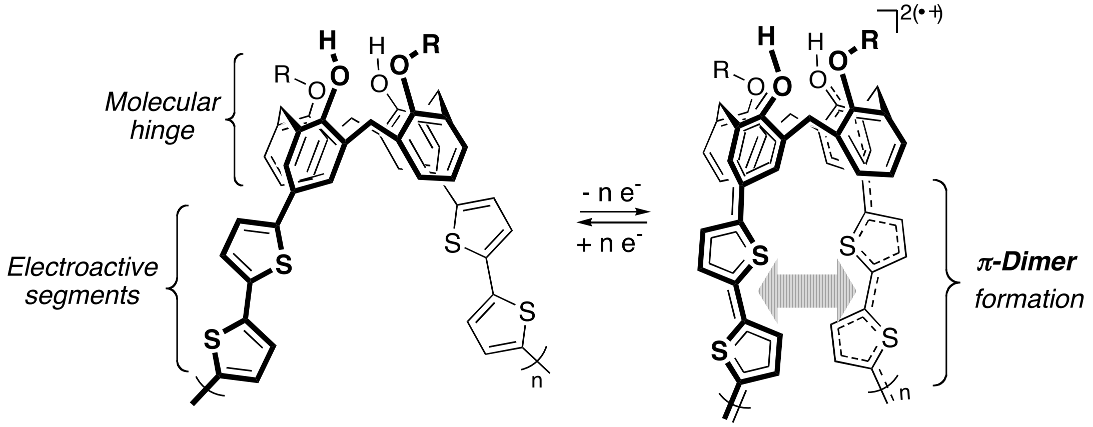
Molecular hinge
Electroactive segments
H
H
R
R
O
O
O
O
S
S
S
S
n
- n e⁻
+ n e⁻
2(•+)
H
H
R
R
O
O
O
O
S
S
S
S
n
π-Dimer formation

Figure 9. Contracting molecular actuator with a calix[4]arene as a molecular hinge. The new chemical bond (π-dimer) would be the driving force for the transformation.

In this dissertation, we first confirm by the model compound study that π-dimer formation can indeed be a driving force for the calix[4]arene-based molecular actuator (Chapter 2). We propose another molecular hinge, binaphthol moiety, for the contracting model. The syntheses of polymers with binaphthols and their characterization, including signatures of oligothiophene interactions, are the subject of Chapter 3. Due to its chirality, we examined the possibilities of the binaphthol polymer as a chiral amine sensor in Chapter 4. To create actuators that make use of the expanding model, we propose new conjugated seven-membered ring systems with heteroatoms (*thiepin* with sulfur, Chapter 5, and *azepine* with nitrogen, Chapter 6) and their syntheses and characterizations will be described. Inspired by the fact that sulfoxide has very low extrusion barrier in the related system, we applied the thiepin molecules to create a peroxide sensor (Chapter 5). In addition, during the investigation of phenol functional groups in conducting polymers, we found that strategic positioning of phenol groups can render a conjugation-broken *meta*-linked system just as conductive as a fully conjugated *para*-linked isomeric system, which will be described in Chapter 7.

References and Notes

(1) Borman, S. *Chemical & Engineering News* **2007,** *85,* 13–16.

(2) (a) Mavroidis, C.; Dubey, A.; Yarmush, M. L. *Annu. Rev. Biomed. Eng.* **2004,** *6,* 363–395. (b) Kinbara, K.; Aida, T. *Chem. Rev.* **2005,** *105,* 1377–1400.

(3) For reviews: (a) Jimenez-Molero, M. C.; Dietrich-Buchecker, C.; Sauvage, J. –P. *Chem. Comm.* **2003,** 1613–1616. (b) Kottas, G. S.; Clarke, L. I.; Horinek, D.; Michl, J. *Chem. Rev.* **2005,** *105,* 1281–1376. (c) Balzani, V.; Credi, A.; Ferrer, B.; Silvi, S.; Venturi, M. *Top. Curr. Chem.* **2005,** *262,* 1–27. (d) Braunschweig, A. B.; Northrop, B. H.; Stoddart, J. F. *J. Mater. Chem.* **2006,** *16,* 32–44. (e) Browne, W.; Feringa, B. L. *Nature Nanotech.* **2006,** *1,* 25–35. (f) Kay, E. R.; Leigh, D. A.; Zerbetto, F. *Angew. Chem. Int. Ed.* **2007,** *46,* 72–191.

(4) Kelly, T. R.; De Silva, H.; Silva, R. A. *Nature* **1999,** *401,* 150–152.

(5) (a) Koumura, N.; Zijlstra, R. W.; van Delden, R. A.; Harada, N.; Feringa, B. L. *Nature* **1999,** *401,* 152–155. (b) Feringa, B. L.; van Delden, R. A.; ter Wiel, M. K. J. *Pure Appl. Chem.* **2003,** *75,* 563–575.

(6) Tseng, H. –R.; Wu, D. M.; Fang, N. X. L.; Zhang, X.; Stoddart, J. F. *ChemPhysChem* **2004,** *5,* 111–116.

(7) Whitesides, G. M. *Sci. Am.* **2001,** *285,* 78–84.

(8) Vicario, J.; Katsonis, N.; Ramon, B. S.; Bastiaansen, C. W. M.; Broer, D. J.; Feringa, B. L. *Nature* **2006,** *440,* 163.

(9) Berná, J.; Leigh, D.; Lubomsak, M.; Mendoza, S. M.; Pérez, E. M.; Rudolf, P.; Teobaldi, G.; Zerbetto, F. *Nature Mater.* **2005,** *4,* 704–710.

(10) Liu, Y.; Flood, A. H. Bonvallet, P. A.; Vignon, S. A.; Northrop, B. H.; Tseng, H. –R.; Jeppesen, J. O.; Huang, T. J.; Brough, B.; Baller, M.; Magonov, S.; Solares, S. D.; Goddard, W. A.; Ho, C. –M.; Stoddart, J. F. *J. Am. Chem. Soc.* **2005,** *127,* 9745–9759.

(11) *Electroactive Polymer (EAP) Actuators as Artificial Muscles – Reality, Potential, and Challenges*; Bar-Cohen, Y., Ed.; SPIE Press: Bellingham, 2001.

(12) Baughman, R. H. *Synth. Met.* **1996,** *78,* 339–353.

(13) Smela, E. *Adv. Mater.* **2003,** *15,* 481–494, and references therein.

(14) Madden, P. G. A. Ph.D. Thesis, Massachusetts Institute of Technology, 2003.

(15) (a) Hunter, I.; Lafontaine, S. In *Tech. Dig. IEEE. Solid State Sensors Actuators Workshop* **1992**, 178–185. (b) Madden, J. D. W. Ph.D. Thesis, Massachusetts Institute of Technology, 2000.

(16) Yu, H. –h. Ph.D. Thesis, Massachusetts Institute of Technology, 2003.

(17) (a) Marsella, M. J. *Acc. Chem. Res.* **2002**, *35*, 944–951. (b) Marsella, M. J.; Reid, R. J.; Estassi, S.; Wang, L. -S. *J. Am. Chem. Soc.* **2002**, *124*, 12507–12510.

(18) (a) Anquetil, P. A.; Yu, H. -h.; Madden, J. D.; Madden, P. G.; Swager, T. M.; Hunter, I. W. *Smart Structures and Materials 2002: EAPAD, Proc. Of SPIE* **2002,** *4695,* 424–434. (b) Yu, H. -h.; Xu, B.; Swager, T. M. *J. Am. Chem. Soc.* **2003,** *125,* 1142–1143. (c) Yu, H. -h.; Swager, T. M. *IEEE J. Oceanic Eng.* **2004,** *29,* 692–695.

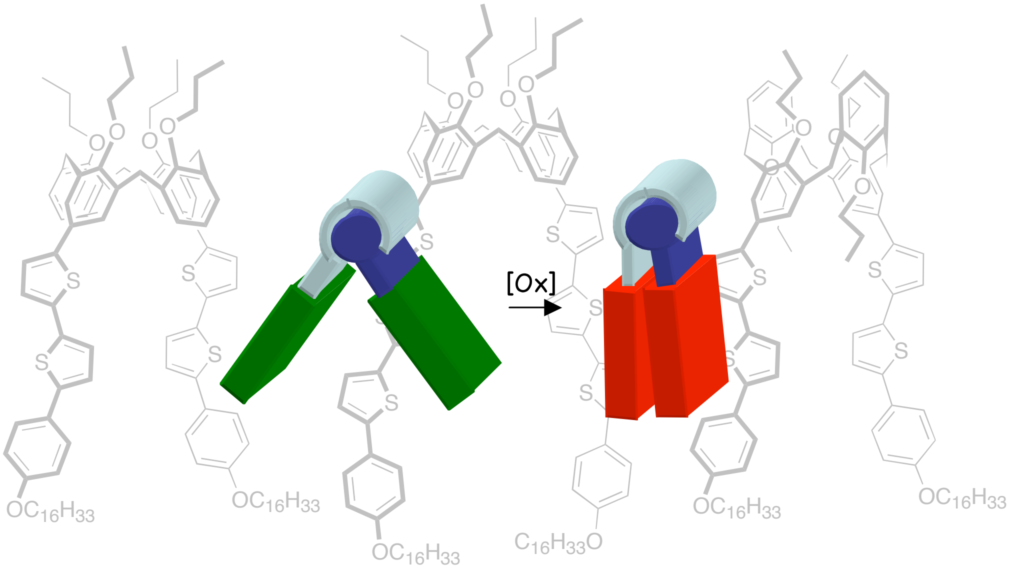
[Ox]
OC16H33
OC16H33
OC16H33
C16H33O
OC16H33
OC16H33
S
O

Chapter 2.

π-Dimer Formation as the Driving Force for Calix[4]arene-based Molecular Actuators

Calix[4]arene-based Molecular Actuator

Our group designed a calix[4]arene-based molecular actuator (Scheme 1), in which electroactive oligothiophenes are connected by the calix[4]arene scaffold.[1] We proposed that each calix[4]arene moiety acts as a molecular hinge and that new noncovalent interactions between oxidized oligothiophenes (i.e., π-dimer or π-stack) can drive the dimensional changes. The π-dimer (or π-stack) is a nonconventional interaction that has drawn particular attention as a charge transporting entity in conducting polymers.[2] π-Dimer formation has been demonstrated in solution and in the solid state for oligothiophene derviatives.[3,4]

Scheme 1. Model of the Calix[4]arene-based Molecular Actuator.

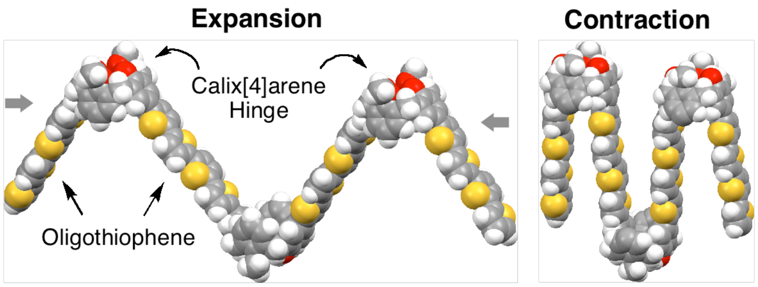

In order to take advantage of such interactions as a driving force for molecular actuators, we considered that a segmented polymer would be more suitable than a fully conjugated one because it is able to attain the maximum interaction due to the spatial confinement of the radical cation's wavefunctions. It should be noted, however, that higher degrees of spatial confinement would be expected to result in coulombic repulsion of like charges and hence counterion and solvent effects are expected.

The *ab initio* calculations by Scherlis and Marzari modeling the behavior of one actuating unit supported the concept that π-dimer formation (or π-stacking) between oxidized oligothiophenes induces conformational changes.[5,6] Based on their investigations about the energetics of calix[4]arene hinges and the stacking interactions between oligothiophenes, they demonstrated with molecular dynamic simulations that the model molecules can change their shape in response to electrochemical oxidation.[5b] The π-dimers of oxidized oligothiophenes are found unstable in gas phase but a polarizable solvent (e.g., acetonitrile) can dramatically stabilize the charged dimers with a moderate binding energy (5.2 kcal/mol for therthiophene).[5a] Herein, we present a series of model studies designed to test the hypothesis that π-dimer formation can indeed be a driving force for the calix[4]arene-based molecular actuator.

π-Dimers

Conduction in doped conjugated polymers is understood in terms of the polaron/bipolaron model[7] which has been widely investigated experimentally and computationally. In simplified terms, a polaron is a radical cation delocalized to a few repeating units in a conjugated polymer, and a bipolaron is as a dication with no unpaired electrons. Due to the spinless nature of the highly doped polythiophenes as revealed by electron paramagnetic resonance (EPR), bipolarons (not polarons) were believed to be the charge carriers. However, since Hill and coworkers first reported the dimerization of oligothiophene cation radicals, the π-dimer (also a spinless entity) has emerged as an alternative model for the bonding in doped polythiophenes.[2,3,8,9] This is not to say that it is incompatible with the polaron/bipolaron model. Indeed, a diamagnetic π-dimer is best considered an inter-chain bipolaron. Nevertheless, the study of this new type of chemical bonding (π-dimer or π-stack) is very important for understanding charge transport through polymer chains.

π-Dimer formation has been observed upon oxidation of various substituted oligothiophenes.[3] In most cases, dimer formation has been observed in the solution state, particularly at low temperatures or at high concentration. π-Dimers have also been observed in the solid state; in particular, our group reported π-dimer formation in polythiophene hybrids of transition-metal bis(salicylidenimine)s.[4]

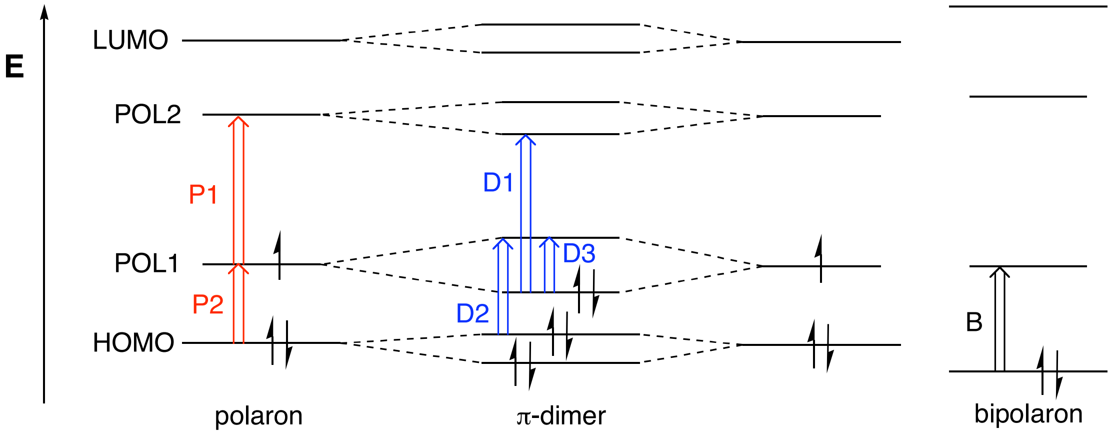

Figure 1. Schematic representation of electronic structures of three oxidized states. (Adapted from ref 3d)

When two oligothiphenes are linked with an alkyl chain[3c,d] or constrained to a cofacial arrangement,[3e] π-dimer formation is greatly enhanced and observed even at room temperature. π-Dimers can be easily detected by spectroscopic methods; diminished EPR intensities and shifted UV-vis-NIR absorptions are considered to be diagnostic indicators of π-dimer formation. Electronic structures of these π-electron species have been proposed by several groups (Figure 1).[3a,b,d] When one electron is removed from the π-electron system, two new energy levels emerge due to the relaxation of the nuclear coordinates (polaron-like structure), allowing two sub-bandgap transitions (P1 and P2). In the π-dimer state, two singly occupied molecular orbitals (SOMOs) mix together and form a new bond, resulting in the disappearance of EPR signals. In optical spectroscopy, three allowed transitions (D1–D3) are observed. In addition to the charge transfer transition (D3), D1 and D2 are comparable to polaronic transitions P1 and P2, respectively, but blue-shifted due to the perturbation of molecular orbitals.

Synthesis of Model Compounds

To conduct model studies of the actuating unit, we synthesized **1–4**, which contain a calix[4]arene hinge and two oligothiophene derivatives as electroactive segments (Scheme 2). Firstly, we sought to examine which, if any, of these compounds would give rise to stable radical cations when oxidized, and whether π-dimer formation would take place. Secondly, the effect of the calix[4]arene's conformation (cone vs. 1,3-alternate) was the subject of investigation.

Oligothiophene derivatives were connected to the upper rim of the calix[4]arene moiety. Compound **1** has free hydroxy groups on the benzene ring (lower rim) whereas compounds **2–4** contain alkoxy groups. Calix[4]arenes **1–3** existed predominantly in the cone conformation as determined by ^{1}H-NMR spectroscopy, whereas **4** adopted the 1,3-alternate conformation. We postulate that the calix[4]arene moiety of **1** is conformationally more rigid than that of **2**, **3**, or **4** due to lower rim hydrogen bonding.[10] A long alkyl chain (n-$C_{16}H_{33}$) was installed to oligothiophene moieties in order to increase their solubility.

Calix[4]arene precursors **6**, **7** and **9** were prepared according to literature procedures (see Experimental Section). Compound **8** was synthesized from **7** via Stille coupling with 2-tributylstannylthiophene, followed by electrophilic iodination. The Stille cross-coupling reactions between calix[4]arenes **6–9** and tributylstannylated bithiophene derivative **12** furnished the desired compounds **1–4** in moderate yields. For the comparison, compound **5** was also prepared as a monomeric version of compound **2**.

Scheme 2.^{a}

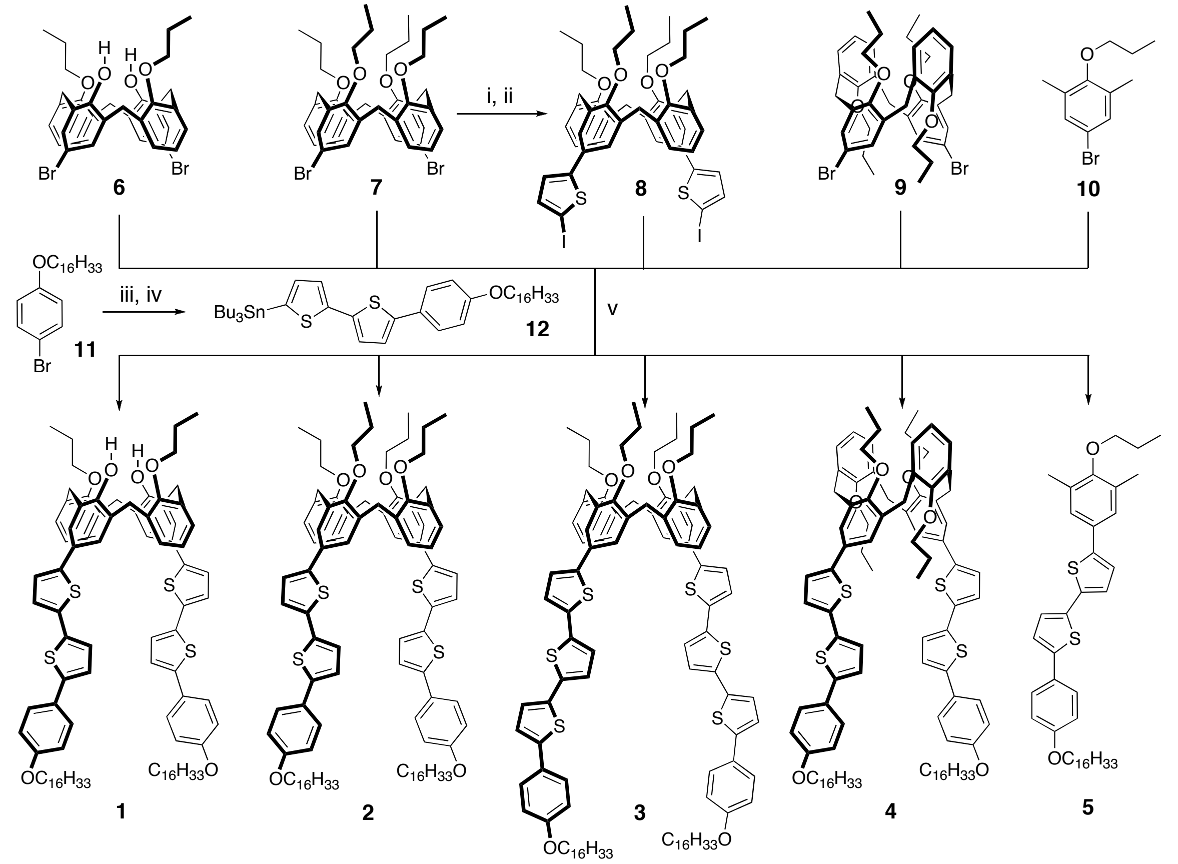

^{a}Reagents: (i) 2-Tributylstannylthiophene, $Pd_2(dba)_3$, (t-$Bu_3PH)BF_4$, KF, DMF, 80 °C, 6 h, 93%. (ii) n-BuLi, -40 °C, then I_2, 36%. (iii) 5-Tributylstannyl-2,2'-bithiophene, $Pd_2(dba)_3$, (t-$Bu_3PH)BF_4$, KF, DMF, 80 °C, 6 h, 72%. (iv) n-BuLi, Bu_3SnCl, -40 °C to room temperature, 86%. (v) $Pd_2(dba)_3$, (t-$Bu_3PH)BF_4$, KF, THF/DMF, 70 °C, 6 h, 41% (**1**), 61% (**2**), 49% (**3**), 59% (**4**), 83% (**5**)

π-Dimers between Oxidized Oligothiophene Derivatives: UV-vis

We examined several oxidizing agents to produce radical cations of **1–5** and finally chose Et_3OSbCl_6, a Meerwein's salt, as a 1-electron oxidant[11] (not as an alkylating agent) because it is relatively easy to handle and more importantly, it does not exhibit a strong absorbance above 300 nm in the UV-vis spectrum. Therefore, we were able to monitor the diminution of the neutral absorption and the concurrent evolution of new absorptions without any interference (Figure 2). Upon addition of the oxidant, all oligothiophenes were converted to deep-blue or violet radical cations, which were stable to moisture. However, the color was slowly lost (returned to their neutral state) when air was bubbled into the solution.

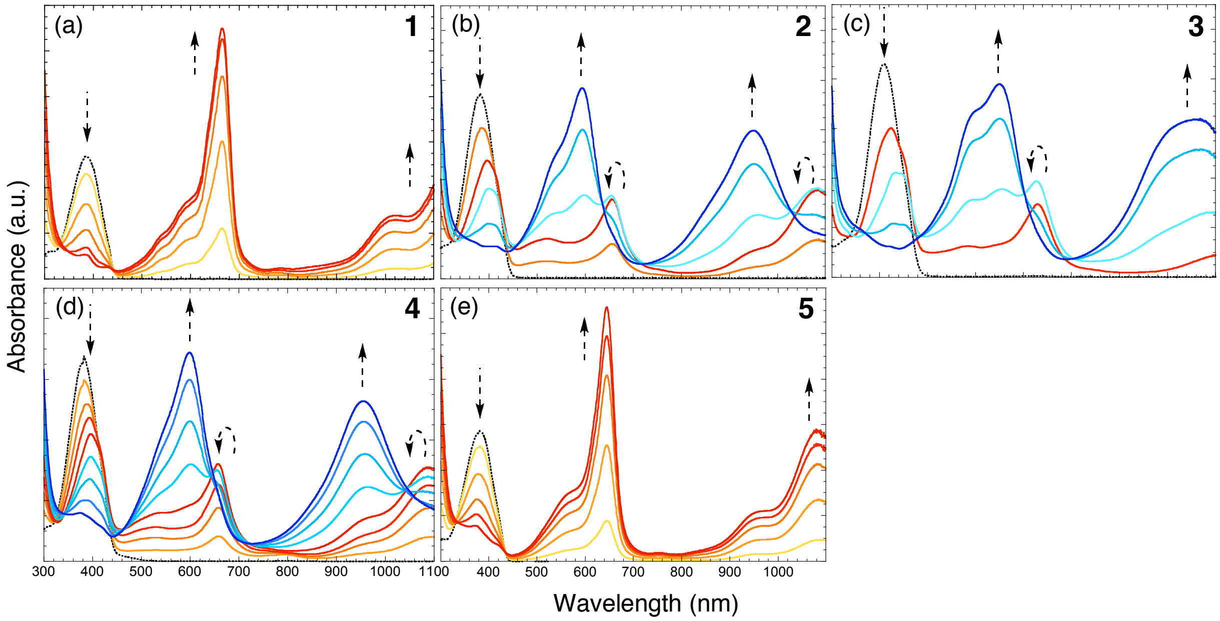

Figure 2. UV-vis spectral changes of **1**–**5** in CH_2Cl_2 at room temperature upon the increasing addition of the oxidant Et_3OSbCl_6. Spectra of neutral absorptions of **1**–**5** are displayed by dashed lines.

For the oxidation of monomeric **5** in CH_2Cl_2 under ambient conditions (Figure 2e), the initial π-π* absorption (382 nm) decreased and new peaks (645, 1079 nm) developed, which can be attributed to the polaronic absorptions (radical cations, Figure 1). These sub-bandgap transitions with vibronic structures are in good accord with literature precedent.[3] We were not able to observe the formation of dications even after adding excess amounts of Et_3OSbCl_6 under the above conditions.

Remarkably distinct behavior was observed upon oxidation of **2** (Figure 2b). Polaronic peaks, similar in shape to those of $\mathbf{5}^{\bullet+}$, were dominant at the low levels of oxidation (Figure 2e). However, as more oxidant was added, blue-shifted absorptions were evident. Such blue-shifts are characteristic of π-dimer formation, as discussed above. The same phenomenon was observed upon oxidation of **3**, the terthiophene-substituted version (Figure 2c). It is known that longer oligothiophene forms stronger dimers, probably due to the reduced coulombic repulsion.[7c] The results of the present study are noteworthy in that a stable π-dimer is generated at room temperature in a solvent of low dielectric constant (CH_2Cl_2) from a framework as short as two thiophenes.

Table 1. Absorption Maxima[a] and Half-Wave Potentials[b] of **1~5**

Compounds	Absorption Maxima / nm			Half-Wave Potentials / V	
	Neutral	Polaronic	π-Dimeric	$E_{1/2}^1$	$E_{1/2}^2$
1	384	665, >1100	-	0.33	0.57
2	382	655, 1084	593, 948	0.33	0.83
3	409	730, >1100	663, 1062	0.23	0.71
4	382	658, 1094	598, 955	0.33	0.82
5	382	645, 1079	-	0.42	0.76

[a]Absorption were measured in CH_2Cl_2 upon addition of oxidant Et_3OSbCl_6 at room temperature. [b]Half-wave potentials (all vs. Fc/Fc^+) were measured in CH_2Cl_2 with 0.1 M $TBAPF_6$ as a supporting electrolyte under ambient conditions.

Interestingly, when we added the oxidant Et_3OSbCl_6 to **1**, only polaronic absorptions were observed in the UV-vis spectra (Figure 2a). The only difference is that **1** has free hydroxyl groups at the lower rim of the calix[4]arene moiety. We attribute this reluctance to form π-dimer formation to the calix[4]arene's conformational rigidity resulting from lower-rim hydrogen bonding. However, it should be noted here that the π-dimer formation is coupled to the "motional" flexibility of the calix[4]arene hinge (hydrogen-bonded vs. tetraalkylated).

There is a possibility that the hydroxyl groups of **1** were alkylated by the Meerwein's salt. To address this, we reduced the oxidized solution of **1** by NH_4OH and took the ^{1}H-NMR from the recovered compound. Indeed, we found the phenolic protons were no longer evident and calix[4]arene's conformational behavior became complicated. However, it is not clear at which point the alkylation took place. That is, was it during the oxidation, or during the reduction step with NH_4OH? If the alkylation occurred during oxidation, the absorption of **1** should have resembled that of **2**. However, the different electronic absorption spectra of oxidized **1** and **2** suggest that the oxidation of **1** with the Meerwein's salt was not accompanied by alkylation. Moreover, oxidation of **1** with $FeCl_3$ resulted in a similar absorption spectrum to that obtained using Et_3OSbF_6 (Figure 3).

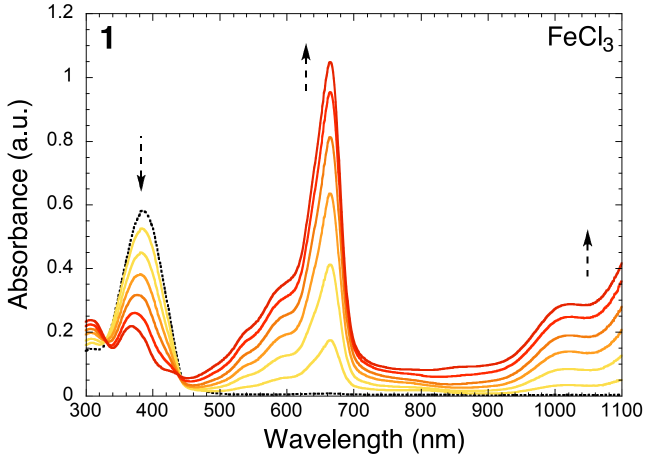

Figure 3. UV-vis spectral changes of **1** in CH_2Cl_2 at room temperature upon the increasing addition of the oxidant $FeCl_3$. The dashed line represents the neutral absorption of **1**.

The effect of the calix[4]arene's conformation on the dimer formation appeared minimal. Oxidation profiles of 1,3-alternate **4** are very similar to those of cone **2** (Figure 2d vs. 2b). Literature precedent suggests that these conformations should be fixed; when the hydroxyl groups on the lower rim of the calix[4]arene are alkylated with propyl groups or larger substituents, rotation through the annulus of the macrocycle is not observed at room temperature.[10] Therefore, there is no possibility of interconversion of **4** to **2**, and vice versa. We can conclude that the cone and 1,3-alternate conformations of **2** and **4** are sufficiently flexible to allow π-dimer formation when oxidized.

EPR and DPV

π-Dimer formation was further confirmed by EPR spectroscopy. EPR spectra were acquired for each of the CH_2Cl_2 solutions (0.2 mM for **1–2**, 0.4 mM for **5**) at room temperature. As expected, bis(radical cation) $\mathbf{1}^{2(\bullet+)}$ (Figure 1, blue) was EPR active, showing a rather broad and featureless signal, which is very similar to radical cation $\mathbf{5}^{\bullet+}$ (black). Note that $\mathbf{1}^{2(\bullet+)}$ consists of two independent radical cations. In contrast, $\mathbf{2}^{2(\bullet+)}$ (red) was almost EPR silent, which indicates that the two radical cations are bound to form a π-dimer.

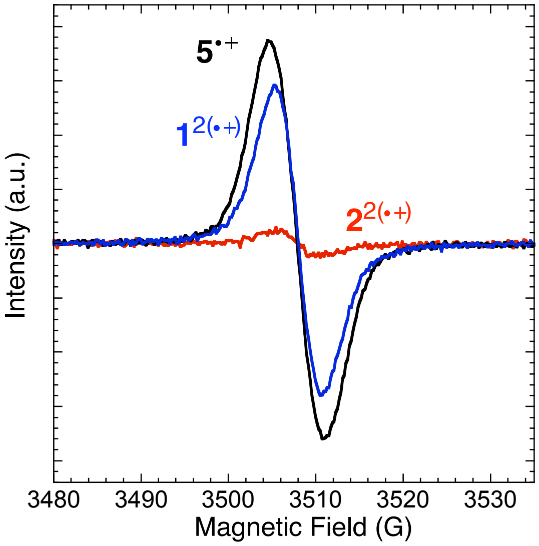

Figure 4. 9-GHz EPR spectra of radical cations $\mathbf{1}^{2(\bullet+)}$ (blue), $\mathbf{2}^{2(\bullet+)}$ (red), and $\mathbf{5}^{\bullet+}$ (black) in CH_2Cl_2 at room temperature.

The evolution of the EPR signals of oxidized **2** and **5** was monitored as the oxidant (Et_3OSbCl_6 in CH_2Cl_2) was added incrementally (Figure 5). In the case of **5**, the signal increased gradually to maximum. However, the initially developed signal for **2** decreased as more oxidant was added. This is in accord with what was observed by the UV-vis spectroscopy (Figure 2b); in **2**, radical cations appeared at the initial stages of oxidation, but the π-dimer dominated at higher oxidation levels.

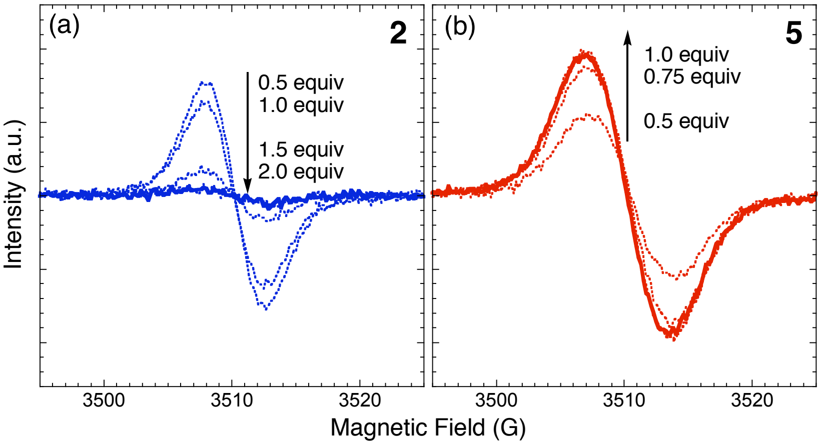

Figure 5. 9-GHz EPR spectra of **2** (a) and **5** (b) measured in CH_2Cl_2 at room temperature with increasing addition of oxidant Et_3OSbCl_6.

Oxidation potentials of dimeric **2** and monomeric **5** were measured in CH_2Cl_2 solutions with 0.1 M $TBAPF_6$ as a supporting electrolyte under ambient conditions (Figure 6). In cyclic voltammetry, both **2** and **5** showed two 1-electron oxidation peaks, which correspond to radical cation(s) and dication(s), respectively. However, the first oxidation of **2** took place at lower potential than that of **5** (0.33 and 0.42 V, respectively, vs. Fc/Fc^+), and the peak was broader. In contrast, the second oxidation of **2** was shifted to the higher potential. Differential pulse voltammetry (DPV, Figure 6b) reveals the differences more clearly. The first oxidation of the dimeric **2** occurred at a lower potential and the peak was broader, while the second oxidation was at higher potential when compared to the monomeric **5**. These data also are consistent with the π-dimer formation because an over-potential would be required to oxidize the π-dimer, which is a stabilized species.

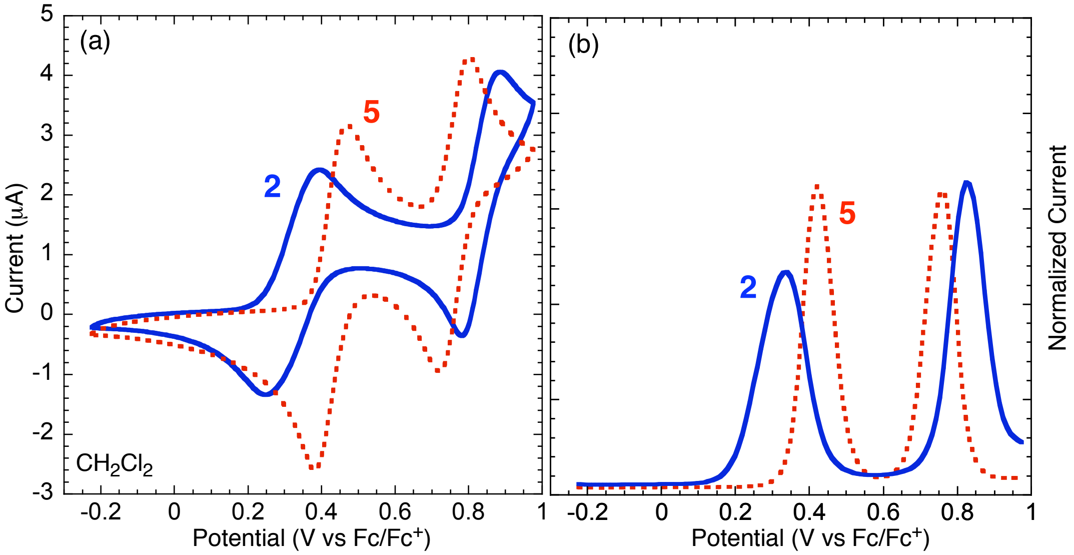

Figure 6. Cyclic voltammograms (a) and differential pulse voltammograms (b) of **2** (blue) and **5** (red) in CH_2Cl_2 solution (~ 0.5 mM) on Pt button electrodes with 0.1 M $TBAPF_6$ as a supporting electrolyte.

Conclusion

We have demonstrated that a stable π-dimer is formed upon oxidation of compounds **2**, **3**, and **4**, the model units of the proposed *molecular actuator*, in the solvent of low dielectric constant (CH_2Cl_2) at room temperature. Evidence from UV-vis, EPR, and DPV are all in agreement with the π-dimer formation. In addition, we found that π-dimer formation is dependent upon the conformational flexibility of the calix[4]arene hinge. We are currently investigating polymeric materials of these compounds.

Experimental Section

General. NMR spectra were recorded on a Varian Mercury-300, Bruker Advance-400, or Varian Inova-500 spectrometer. Chemical shifts were reported in ppm and referenced to residual solvent peaks ($CDCl_3$: δ 7.27 ppm for ^1H, δ 77.23 ppm for ^{13}C). High-resolution mass spectra (HR-MS) were obtained on a Bruker Daltonics APEX II 3 Tesla FT-ICR-MS. UV-vis spectra were obtained using a HP 8453 diode array spectrometer. Electrochemical measurements were carried out using an Autolab PGSTAT 10 or PGSTAT 20 potentiostat (Eco Chemie) in a three-electrode cell configuration consisting of a quasi-internal Ag wire reference electrode (BioAnalytical Systems) submerged in 0.01 $AgNO_3$ / 0.1 M tetrabutylammonium hexafluorophosphate ($TBAPF_6$) in anhydrous CH_3CN, a Pt button (1.6 mm in diameter) electrode as the working electrode, and a Pt coil as the counter electrode. The ferrocene/ferrocenium (Fc/Fc^+) redox couple was used as an external reference. Half-wave potentials of Fc/Fc^+ were observed between 210-245 mV vs Ag/Ag^+ in CH_2Cl_2. EPR spectra were obtained using a Bruker Model EMX Electron Paramagnetic Resonance Spectrometer operating as the X-band with 100 kHz modulation at room temperature. All air and water sensitive synthetic manipulations were performed under an argon or nitrogen atmosphere using standard Schlenk techniques.

Materials. Spectroscopic grade CH_2Cl_2 was purchased from Aldrich for electrochemistry. $TBAPF_6$ was recrystallized in ethanol prior to use. Anhydrous DMF was purchased from Aldrich as Sure-Seal Bottles and used as received. THF was purified by passage through two alumina columns of an Innovative Technologies purification system. All other chemicals were of reagent grade and used as received. Compounds **6**, **7** and **9** were prepared by literature procedures.[12] Compounds **10**[13] and **11** were synthesized from commercially available bromophenols by a standard Williamson ether synthesis with alkyl bromides. 5-Tributylstannyl-2,2'-bithiophene was synthesized by a known procedure.[14]

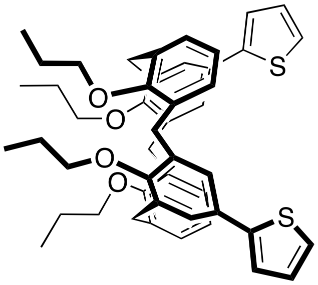

11,23-Bis(thiophen-2-yl)-25,26,27,28-tetrapropoxycalix[4]arene (A). In a Schlenk tube equipped with a stir bar were combined **6** (0.766 g, 1 mmol), $Pd_2(dba)_3 \cdot CHCl_3$ (31 mg, 3 mol %), and t-$Bu_3PH \cdot BF_4$ (19 mg, 6.6 mol %). To the mixture, after purging three times with Ar, were added 2-tributylstannylthiophene (0.827 mL, 2.5 mmol), KF (0.349 g, 6 mmol), and anhydrous DMF (3 mL). The mixture was allowed to stir at 80 °C for 6 h, at which time it was cooled to room temperature and methanol was added to precipitate product. The crude product was isolated by filtration and thoroughly washed with methanol. It was then passed through a short silica gel pad (dichloromethane as eluent). The concentrated product was further purified by recrystallization (dichloromethane/methanol), yielding 0.705 g (93%) of white solid. ^{1}H-NMR (400 MHz, $CDCl_3$) δ: 7.22 (s, 4H), 7.17 (dd, 2H, J = 5.1, 1.0 Hz), 7.13 (dd, 2H, J = 3.6, 1.0 Hz), 7.00 (dd, 2H, J = 5.1, 3.6 Hz), 6.39 (s, 6H), 4.48 (d, 4H, J = 13 Hz), 4.00 (t, 4H, J = 8.0 Hz), 3.77 (t, 4H, J = 7.0 Hz), 3.21 (d, 4H, J = 13 Hz), 1.96 (m, 8H), 1.09 (t, 6H, J = 7.5 Hz), 0.96 (t, 6H, J = 7.4 Hz). ^{13}C-NMR (125 MHz, $CDCl_3$) δ: 157.57, 155.81, 145.02, 136.94, 133.70, 128.26, 128.01, 127.99, 126.36, 123.82, 122.43, 122.16, 77.12, 76.89, 31.22, 23.65, 23.33, 10.89, 10.25. HR-MS (ESI): calcd for $C_{48}H_{52}O_4S_2$ $[M+Na]^+$, 779.3199; found, 779.3204.

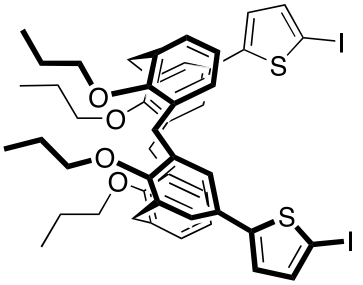

11,23-Bis(5-iodothiophen-2-yl)-25,26,27,28-tetrapropoxycalix[4]arene (8). To **A** (0.250 g, 0.33 mmol) dissolved in THF (10 mL) was added *n*-BuLi (0.413 mL, 0.66 mmol) at –40 °C. It was then removed from the cooling bath and allowed to stir for 1 h at room temperature. The mixture was cooled to –40 °C again and then quenched with iodine (0.168 mg, 0.66 mmol). After being diluted with ethyl acetate at room temperaure, the organic layer was washed with a saturated aqueous solution of $Na_2S_2O_3$ and brine, dried over $MgSO_4$, and evaporated under reduced pressure. The crude product was purified by column chromatography (chloroform:hexane 1:3), yielding 0.120 g (36 %) of a white solid. ^{1}H-NMR (400 MHz, $CDCl_3$) δ: 6.98 (d, 2H, *J* = 3.8 Hz), 6.78 (d, 4H, *J* = 6.5 Hz), 6.72 (*pseudo*-t, 2H, *J* = 6.5 Hz), 6.70 (s, 4H), 6.42 (d, 2H, *J* = 3.8 Hz), 4.48 (d, 4H, *J* = 13 Hz), 3.93 (t, 4H, *J* = 7.7 Hz), 3.85 (t, 4H, *J* = 7.4 Hz), 3.19 (d, 4H, *J* = 13 Hz), 1.96 (m, 8H), 1.05 (t, 6H, *J* = 7.4 Hz), 1.02 (t, 6H, *J* = 7.5 Hz). ^{13}C-NMR (125 MHz, $CDCl_3$) δ: 156.85, 156.72, 150.79, 137.71, 135.54, 135.21, 128.60, 127.58, 125.54, 123.14, 122.47, 77.11, 76.92, 31.15, 23.52, 23.39, 10.63, 10.45. HR-MS (ESI): calcd for $C_{48}H_{50}I_2O_4S_2$ $[M+Na]^+$, 1031.1132; found, 1031.1133.

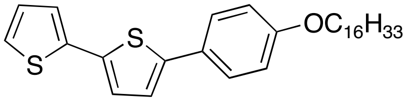

5-(4-Hexadecyloxyphenyl)-2,2'-bithiophene (B). In a Schlenk tube equipped with a stir bar were combined **11** (4.06 g, 10 mmol), $Pd_2(dba)_3$·$CHCl_3$ (104 mg, 1 mol %), *t*-Bu_3PH·BF_4 (58 mg, 2 mol %), and 5-tributylstannyl-2,2'-bithiophene (4.89 mL, 13 mmol). After purging three times with Ar, KF (1.74 g, 30 mmol) and anhydrous DMF (20 mL) were added. The mixture was then allowed to stir at 80 °C for 6 h, at which time it was cooled to room temperature and methanol was added. The suspension was filtered and the resulting solid washed thoroughly with methanol. It was then passed through a short pad of silica gel, eluting with chloroform. The concentrated product was further purified by recrystallization (chloroform/methanol), yielding 3.46 g (72%) of white solid. ^{1}H-NMR (300 MHz, $CDCl_3$) δ: 7.52 (*pseudo*-d, 2H, *J* = 8.7 Hz), 7.21 (dd, 1H, *J* = 5.1, 1.2 Hz), 7.19 (dd, 1H, *J* = 3.6, 1.2 Hz), 7.13 (d, 1H, *J* = 3.7 Hz), 7.11 (d, 1H, *J* = 3.7 Hz), 7.03 (dd, 1H, *J* = 5.1, 3.6 Hz), 6.92 (*pseudo*-d, 2H, *J* = 8.7 Hz) 3.99 (t, 2H, *J* = 6.6 Hz), 1.81 (m, 2H), 1.54–1.20 (m, 26H), 0.89 (t, 3H, *J* = 6.9 Hz). HR-MS (ESI): calcd for $C_{30}H_{42}OS_2$ $[M+H]^+$, 483.2750; found, 483.2754.

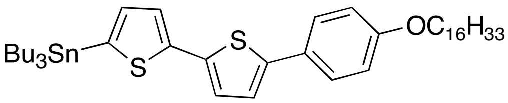

5-Tributylstannyl-5'-(4-Hexadecyloxyphenyl)-2,2'-bithiophene (12). To **B** (0.950 g, 1.9 mmol) dissolved in THF (50 mL) was added *n*-BuLi (1.31 mL, 2.1 mmol) at –40 °C. It was then removed from the cooling bath and allowed to stir for 1 h at room temperature. The mixture was cooled to –40 °C again and then quenched with tributylstannyl chloride (0.814 mL, 2.2 mmol). After being diluted with ethyl acetate at room temperaure, the organic layer was washed with water and brine, dried over $MgSO_4$, and evaporated under reduced pressure. The crude product was used without further purification. Yield: 1.41 g (86 %, assuming 90% purity) of pale yellow solid. ^{1}H-NMR (400 MHz, $CDCl_3$) δ: 7.52 (*pseudo*-d, 2H, *J* = 8.9 Hz), 7.30 (d, 1H, *J* = 3.4 Hz), 7.13 (d, 1H, *J* = 3.7 Hz), 7.11 (d, 1H, *J* = 3.7 Hz), 7.08 (d, 1H, *J* = 3.4 Hz), 6.91 (*pseudo*-d, 2H, *J* = 8.9 Hz), 3.99 (t, 2H, *J* = 6.6 Hz), 1.80 (m, 2H), 1.59 (m, 6H), 1.53–1.21 (m, 38H), 0.92 (t, 9H,

J = 7.3 Hz), 0.89 (t, 3H, J = 7.0 Hz). ^{13}C-NMR (125 MHz, $CDCl_3$) δ: 158.97, 143.15, 142.99, 136.60, 136.33, 136.11, 127.04, 127.00, 124.75, 124.48, 122.74, 115.06, 68.33, 32.16, 29.91~29.94 (5C), 29.89, 29.83, 29.80, 29.62, 29.60, 29.47, 29.17, 27.49, 26.26, 22.93, 14.37, 13.91, 11.08. HR-MS (ESI): calcd for $C_{42}H_{68}OS_2Sn$ $[M]^+$, 772.3704; found, 772.3742.

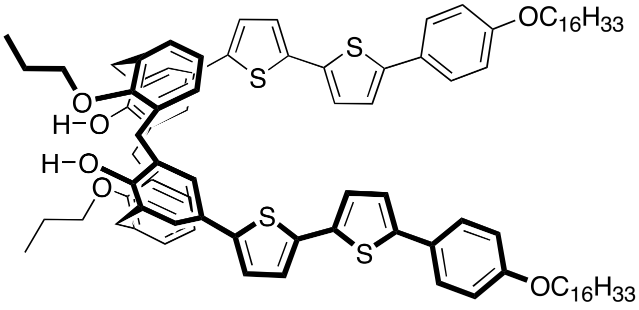

11,23-Bis[5'-(4-hexadecyloxyphenyl)-2,2'-bithiophen-5-yl]-25,27-dihydroxy-26,28-dipropoxycalix[4]arene (1). In a Schlenk tube equipped with a stir bar were combined **6** (0.081 g, 0.12 mmol), $Pd_2(dba)_3 \cdot CHCl_3$ (6.2 mg, 5 mol %), *t*-$Bu_3PH \cdot BF_4$ (3.8 mg, 11 mol %), **12** (0.198 g, 0.25 mmol), THF (0.8 mL), and DMF (0.4 mL). To the mixture, which was degassed by free-pump-thaw (three times), was added KF (0.049 g, 0.72 mmol) under Ar. The mixture was allowed to stir at 70 °C for 6 h, at which time it was cooled to room temperature and methanol was added. The crude product was isolated by filtration and thoroughly washed with methanol. It was then passed through a short pad of silica gel, eluding with dichloromethane. The concentrated product was further purified by recrystallization (dichloromethane/methanol, two times). Yield: 0.072 g (41%) of yellow solid. ^{1}H-NMR (300 MHz, $CDCl_3$) δ: 8.52 (s, 2H), 7.52 (*pseudo*-d, 4H, J = 9.0 Hz), 7.32 (s, 4H), 7.27 (d, 2H, J = 2.1 Hz), 7.14–7.10 (m, 4H), 7.08 (d, 2H, J = 3.9 Hz), 7.01 (d, 4H, J = 7.5 Hz), 6.92 (*pseudo*-d, 4H, J = 9.0 Hz), 6.82 (t, 2H, J = 7.5 Hz), 4.35 (d, 4H, J = 13 Hz), 4.02 (t, 4H, J = 6.0 Hz), 3.99 (t, 4H, J = 6.6 Hz), 3.45 (d, 4H, J = 13 Hz), 2.09 (m, 4H), 1.80 (m, 4H), 1.53–1.20 (m, 58H), 0.89 (t, 6H, J = 6.9 Hz). ^{13}C-NMR (125

MHz, $CDCl_3$) δ: 159.02, 153.73, 152.11, 143.89, 142.92, 136.23, 135.46, 133.27, 129.38, 128.77, 127.02, 126.98, 126.24, 125.67, 125.47, 124.29, 124.14, 122.79, 122.36, 115.09, 77.23, 76.97, 68.35, 32.15, 31.68, 29.92–29.89, 29.83, 29.80, 29.62, 29.59, 29.46, 26.25, 23.72, 22.92, 14.36, 11.15. HR-MS (ESI): calcd for $C_{94}H_{116}O_6S_4$ $[M+Na]^+$, 1491.7547; found, 1491.7527.

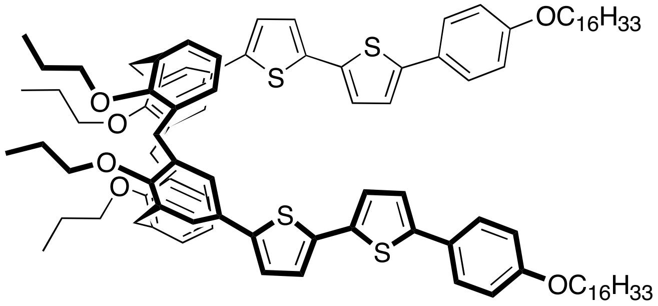

11,23-Bis[5’-(4-hexadecyloxyphenyl)-2,2’-bithiophen-5-yl]-25,26,27,28-tetrapropoxycalix[4]arene (2). Using the similar procedure for the synthesis of **1**, compound **7** (0.171 g, 0.22 mmol) was treated with $Pd_2(dba)_3 \cdot CHCl_3$ (11 mg, 5 mol %), *t*-$Bu_3PH \cdot BF_4$ (7 mg, 11 mol %), **12** (0.386 g, 0.51 mmol), THF (1.4 mL), DMF (0.7 mL), and KF (0.077 g, 1.3 mmol). Yield: 0.207 g (61%) of yellow solid. ^{1}H-NMR (400 MHz, $CDCl_3$) δ: 7.43 (*pseudo*-d, 4H, *J* = 8.8 Hz), 7.00 (d, 2H, *J* = 3.8 Hz), 6.96 (d, 2H, *J* = 3.8 Hz), 6.83 (*pseudo*-d, 4H, *J* = 8.8 Hz), 6.82–6.78 (m, 10H), 6.72 (*pseudo*-t, 2H, *J* = 7.5 Hz), 6.65 (d, 2H, *J* = 3.7 Hz), 4.49 (d, 4H, *J* = 13 Hz), 3.96 (t, 4H, *J* = 6.6 Hz), 3.93 (t, 4H, *J* = 7.6 Hz), 3.86 (t, 4H, *J* = 7.4 Hz), 3.20 (d, 4H, *J* = 13 Hz), 1.96 (m, 8H), 1.78 (m, 4H), 1.57–1.28 (m, 52H), 1.04 (t, 6H, *J* = 7.4 Hz), 1.02 (t, 6H, *J* = 7.4 Hz), 0.90 (t, 6H, *J* = 7.0 Hz). ^{13}C-NMR (125 MHz, $CDCl_3$) δ: 158.83, 156.85, 156.55, 143.33, 142.54, 136.42, 135.53, 135.53. 135.47, 135.23, 128.62, 128.12, 127.04, 126.87, 125.48, 124.21, 123.92, 122.56, 122.46, 114.97, 77.11, 76.97, 68.30, 32.16, 31.22, 29.93–29.94, 29.91, 29.89, 29.86, 29.84, 29.68, 29.60, 29.54, 26.30, 23.53, 23.43, 22.92, 14.36, 10.64, 10.49. HR-MS (ESI): calcd for $C_{100}H_{128}O_6S_4$ $[M+Na]^+$, 1575.8486; found, 1575.8439.

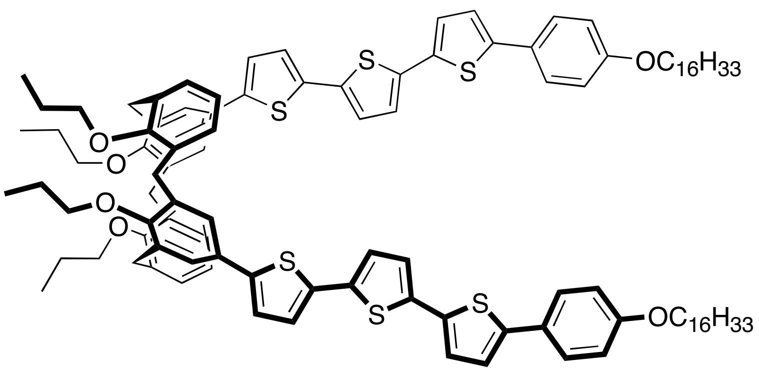

11,23-Bis[5’-(4-hexadecyloxyphenyl)-2,2’-bithiophen-5-yl]-25,26,27,28-tetrapropoxycalix[4]arene (3). Using the similar procedure for the synthesis of **1**, compound **8** (0.075 g, 0.073 mmol) was treated with $Pd_2(dba)_3 \cdot CHCl_3$ (3.8 mg, 5 mol %), *t*-$Bu_3PH \cdot BF_4$ (2.3 mg, 11 mol %), **12** (0.128 g, 0.17 mmol), THF (1 mL), DMF (0.5 mL), and KF (0.025 g, 1.3 mmol). Yield: 0.062 g (61%) of orange solid. ^{1}H-NMR (400 MHz, $CDCl_3$) δ: 7.41 (*pseudo*-d, 4H, *J* = 8.7 Hz), 6.96 (s, 4H), 6.95 (d, 4H, *J* = 8.7 Hz), 6.92 (d, 2H, *J* = 3.7 Hz), 6.85 (m, 4H), 6.38 (*pseudo*-d, 4H, *J* = 8.7 Hz), 6.71 (d, 2H, *J* = 3.7 Hz), 6.63 (s, 4H), 6.51 (d, 2H, *J* = 3.7 Hz), 4.49 (d, 4H, *J* = 13 Hz), 3.98 (t, 4H, *J* = 7.9 Hz), 3.96 (t, 4H, *J* = 6.6 Hz), 3.79 (t, 4H, *J* = 7.0 Hz), 3.20 (d, 4H, *J* = 13 Hz), 1.96 (m, 8H), 1.77 (m, 4H), 1.42–1.27 (m, 52H), 1.07 (t, 6H, *J* = 7.4 Hz), 0.98 (t, 6H, *J* = 7.4 Hz), 0.89 (t, 6H, *J* = 7.0 Hz). ^{13}C-NMR (125 MHz, $CDCl_3$) δ: 158.94, 157.30, 156.17, 143.67, 142.93, 136.69, 135.87, 135.81, 135.73, 135.04, 134.96, 128.87, 128.11, 127.08, 126.92, 125.31, 124.32, 123.81, 123.54, 122.73, 122.48, 122.34, 115.12, 115.00, 77.21, 76.93, 68.32, 32.17, 31.22, 29.95–29.93, 29.91, 29.88, 29.85, 29.70, 29.61, 29.54, 26.31, 23.62, 23.35, 22.94, 14.38, 10.81, 10.33. HR-MS (ESI): calcd for $C_{108}H_{132}O_6S_6$ $[M+Na]^+$, 1739.8240; found, 1739.8210.

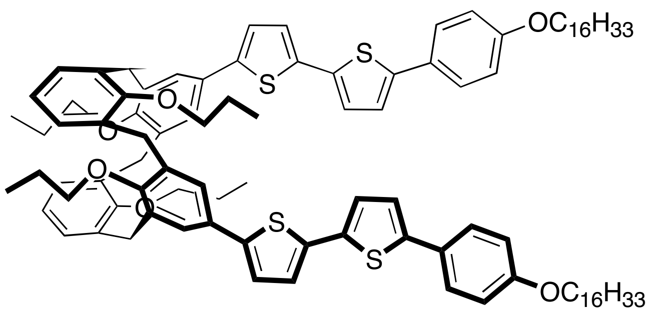

11,23-Bis[5'-(4-hexadecyloxyphenyl)-2,2'-bithiophen-5-yl]-25,26,27,28-tetrapropoxycalix[4]arene (4). Using the similar procedure for the synthesis of **1**, compound **9** (0.072 g, 0.094 mmol) was treated with $Pd_2(dba)_3 \cdot CHCl_3$ (4.9 mg, 5 mol %), *t*-$Bu_3PH \cdot BF_4$ (3.0 mg, 11 mol %), **12** (0.155 g, 0.20 mmol), THF (0.8 mL), DMF (0.4 mL), and KF (0.033 g, 0.56 mmol). Yield: 0.087 g (59%) of yellow solid. ^{1}H-NMR (300 MHz, $CDCl_3$) δ: 7.42 (*pseudo*-d, 4H, *J* = 8.7 Hz), 7.25 (s, 4H), 7.04 (d, 4H, *J* = 7.5 Hz), 7.00 (d, 2H, *J* = 3.9 Hz), 6.94 (d, 2H, *J* = 3.9 Hz), 6.84 (s, 4H), 6.82 (*pseudo*-d, 4H, *J* = 8.7 Hz), 6.69 (t, 2H, *J* = 7.5 Hz), 4.00 (t, 4H, *J* = 6.6 Hz), 3.73 (t, 4H, *J* = 6.9 Hz), 3.67 (t, 4H, *J* = 7.2 Hz), 3.59 (s, 8H), 1.97 (m, 4H), 1.83 (m, 8H), 1.50–1.28 (m, 52H), 1.15 (t, 6H, *J* = 7.5 Hz), 1.05 (t, 6H, *J* = 7.5 Hz), 0.90 (t, 6H, *J* = 6.9 Hz). ^{13}C-NMR (125 MHz, $CDCl_3$) δ: 158.76, 156.51, 156.43, 143.75, 142.32, 136.76, 135.23, 133.94, 133.30, 130.22, 127.50, 127.34, 127.14, 126.84, 124.30, 123.68, 122.53, 122.25, 121.69, 114.95, 74.87, 74.81, 68.30, 35.81, 32.16, 29.95–29.93, 29.90, 29.89, 29.86, 29.72, 29.61, 29.58, 26.32, 24.30, 24.15, 22.93, 14.37, 11.34, 10.97, 10.90. HR-MS (ESI): calcd for $C_{100}H_{128}O_6S_4$ $[M+Na]^+$, 1575.8486; found, 1575.8463.

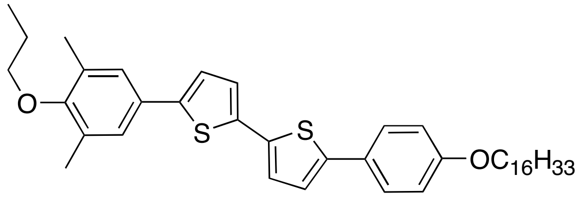

11,23-Bis[5’-(4-hexadecyloxyphenyl)-2,2’-bithiophen-5-yl]-25,26,27,28-tetrapropoxycalix[4]arene (5). Using the similar procedure for the synthesis of **1**, compound **10** (0.016 g, 0.065 mmol) was treated with $Pd_2(dba)_3 \cdot CHCl_3$ (2.0 mg, 3 mol %), *t*-$Bu_3PH \cdot BF_4$ (1.2 mg, 6.6 mol %), **12** (0.083 g, 0.098 mmol), DMF (0.7 mL), and KF (0.023 g, 0.39 mmol). Yield: 0.035 g (83%) of yellow solid. ^{1}H-NMR (400 MHz, $CDCl_3$) δ: 7.52 (*pseudo*-d, 2H, *J* = 8.8 Hz), 7.27 (s, 2H), 7.14 (d, 1H, *J* = 3.7 Hz), 7.12 (*pseudo*-s, 2H), 7.11 (d, 1H, *J* = 3.7 Hz), 6.92 (*pseudo*-d, 2H, *J* = 8.8 Hz), 3.99 (t, 2H, *J* = 6.6 Hz), 3.76 (t, 2H, *J* = 6.6 Hz), 2.33 (s, 6H), 1.85 (m, 4H), 1.56–1.27 (m, 26H), 1.10 (t, 3H, *J* = 7.4 Hz), 0.89 (t, 3H, *J* = 7.0 Hz). ^{13}C-NMR (125 MHz, $CDCl_3$) δ: 159.08, 156.09, 143.22, 143.08, 136.40, 136.01, 131.76, 129.65, 127.05, 126.91, 126.26, 124.40, 124.32, 123.31, 122.81, 115.10, 74.21, 68.35, 32.15, 29.91~29.93 (5C), 29.89, 29.83, 29.80, 29.62, 29.60, 29.46, 26.25, 23.86, 22.92, 16.61, 14.36, 10.88. HR-MS (ESI): calcd for $C_{41}H_{56}O_2S_2$ $[M]^+$, 644.3716; found, 644.3725.

References and Notes

(1) (a) Anquetil, P. A.; Yu, H. -h.; Madden, J. D.; Madden, P. G.; Swager, T. M.; Hunter, I. W. *Smart Structures and Materials 2002: EAPAD, Proc. Of SPIE* **2002,** *4695,* 424–434. (b) Yu, H. -h.; Xu, B.; Swager, T. M. *J. Am. Chem. Soc.* **2003,** *125,* 1142–1143. (c) Yu, H. -h.; Swager, T. M. *IEEE J. Oceanic Eng.* **2004,** *29,* 692–695.

(2) Miller, L. L.; Mann, K. R. *Acc. Chem. Res.* **1996,** *29,* 417–423.

(3) For example, see (a) Bäuerle, P.; Segelbacher, U.; Maier, A.; Mehring, M. *J. Am. Chem. Soc.* **1993,** *115,* 10217–10223. (b) Graf, D. D.; Duan, R. G.; Campbell, J. P.; Miller, L. L.; Mann, K. R. *J. Am. Chem. Soc.* **1997,** *119,* 5888–5899. (c) Satou, T.; Sakai, T.; Kaikawa, T.; Takimiya, K.; Otsubo, T.; Aso, Y. *Org. Lett.* **2004,** *6,* 997–1000. (d) Sakai, T.; Satou, T.; Kaikawa, T.; Takimiya, K.; Otsubo, T.; Aso, Y. *J. Am. Chem. Soc.* **2005,** *127,* 8082–8089. (e) Knoblock, K. M.; Silvestri, C. J.; Collard, D. M. *J. Am. Chem. Soc.* **2006,** *128,* 13680–13681. (f) Yamazaki, D.; Nishinaga, T.; Tanino, N.; Komatsu, K. *J. Am. Chem. Soc.* **2006,** *128,* 14470–14471.

(4) Kingsborough, R. P.; Swager, T. M. *J. Am. Chem. Soc.* **1999,** *121,* 8825–8834.

(5) (a) Scherlis, D.; Marzari, N. *J. Phys. Chem. B* **2004,** *108,* 17791–17795. (b) Scherlis, D.; Marzari, N. *J. Am. Chem. Soc.* **2005,** *127,* 3207–3212.

(6) A different mechanism involving a repulsive electrostatic interaction, rather than by an attractive π-π stacking, was suggested: see Casanovas, J.; Zanuy, D.; Alemán, C. *Angew. Chem. Int. Ed.* **2006,** *45,* 1103–1105.

(7) Bredas, L. L.; Street, G. B. *Acc. Chem. Res.* **1985,** *18,* 309–315.

(8) (a) Hill, M. G.; Mann, K. R.; Miller, L. L.; Penneau, J. -F. *J. Am. Chem. Soc.* **1992,** *114,* 2728–2730. (b) Hill, M. G.; Penneau, J. –F., Zinger, B.; Mann, K. R.; Miller, L. L. *Chem.*

Mater. **1992,** *4,* 1106–1113. (c) Bäuerle, P.; Segelbacher, U.; Gaudl, K. –U.; Huttenlocher, D.; Mehring, M. *Angew. Chem. Int. Ed.* **1993,** *32,* 76–78.

(9) As a spinless entity, chain dimer (two polarons on a single chain) and σ-dimer were also proposed. For the chain dimer, see: van Haare, J. A. E. H.; Havinga, E. E.; van Dongen, J. L. J.; Janssen, R. A. J.; Cornil, J., Brédas, J. -L. *Chem. Eur. J.* **1998,** *4,* 1509–1522. For the σ-dimer, see: Smie, A.; Heinze, J. *Angew. Chem. Int. Ed.* **1997,** *36,* 363–367.

(10) Shinkai, S. *Tetrahedron* **1993,** *49,* 8933–8968.

(11) Rathore, R.; Kumar, A. S.; Lindeman, S. V.; Kochi, J. K. *J. Org. Chem.* **1998,** *63,* 5847–5856.

(12) (a) Stastny, V.; Lhoták, P,; Stibor, I.; König, B. *Tetrahedron* **2006,** *62,* 5748–5755. (b) Casnati, A.; Fochi, M.; Minari, P.; Pochini, A.; Reggiani, M. *Gazz. Chim. Ital.* **1996,** *126,* 99–106. (c) Linnane, P.; James, T. D.; Shinkai, S. *J. Chem. Soc., Chem. Commun.* **1995,** 1997–1998.

(13) Larsen, M.; Krebs, F. C.; Harrit, N.; Jorgensen, M. *J. Chem. Soc., Perkin Trans. 2,* **1999,** 1749–1757.

(14) Zhu, S. S.; Swager, T. M. *J. Am. Chem. Soc.* **1997,** *119,* 12568–12577.

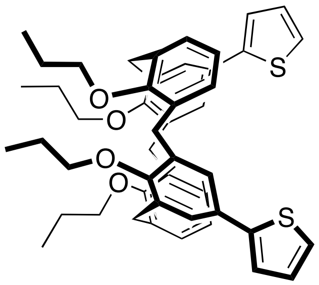

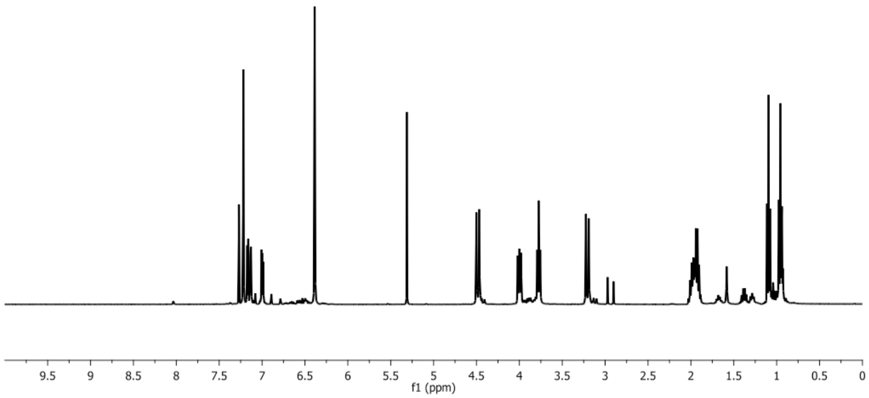

Spectrum 1. ^{1}H-NMR spectrum of **A** (400 MHz, $CDCl_3$).

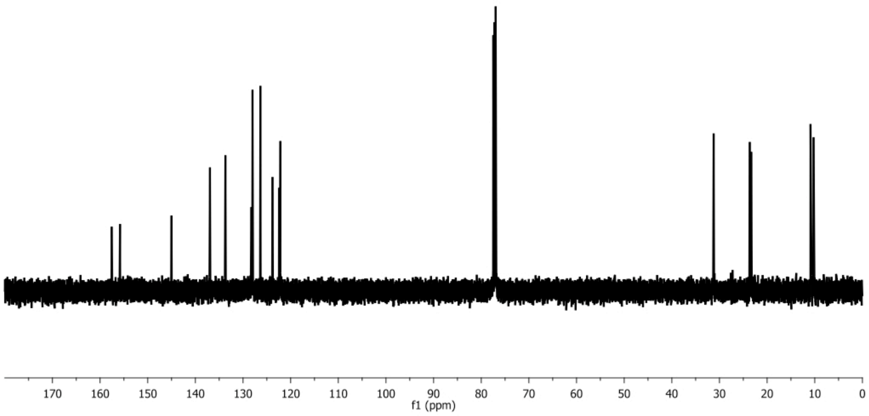

Spectrum 2. ^{13}C-NMR spectrum of **A** (125 MHz, $CDCl_3$).

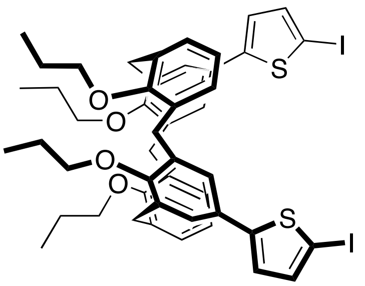

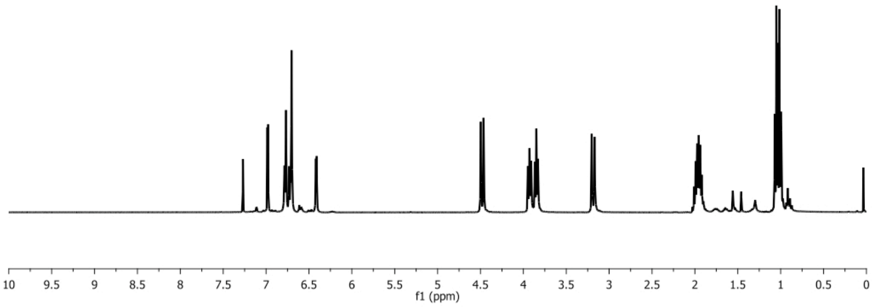

Spectrum 3. ^{1}H-NMR spectrum of **8** (400 MHz, $CDCl_3$).

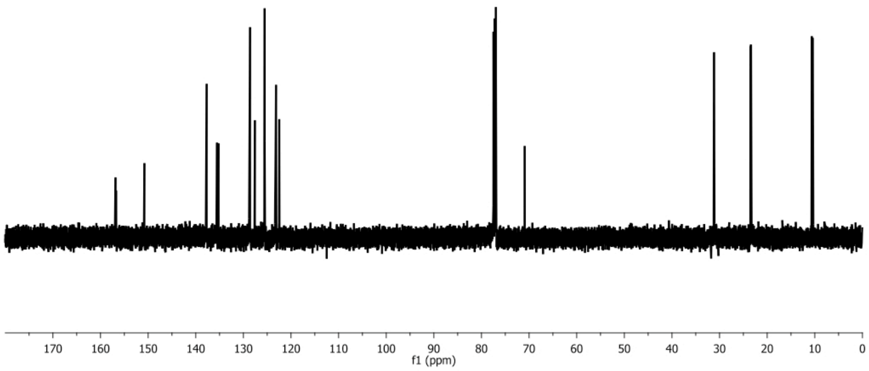

Spectrum 4. ^{13}C-NMR spectrum of **8** (125 MHz, $CDCl_3$).

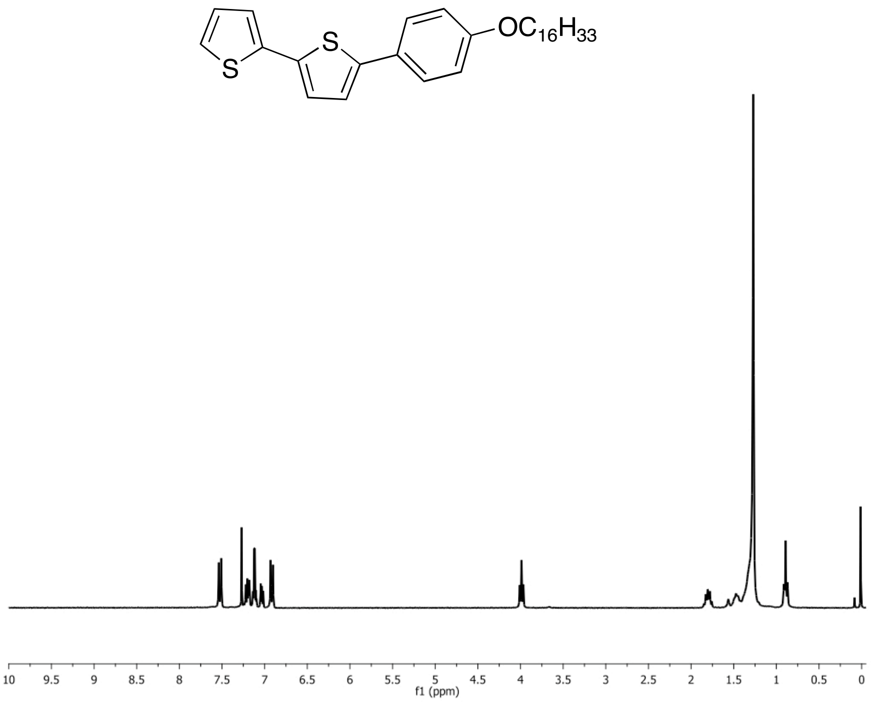

Spectrum 5. ^{1}H-NMR spectrum of **B** (300 MHz, $CDCl_3$).

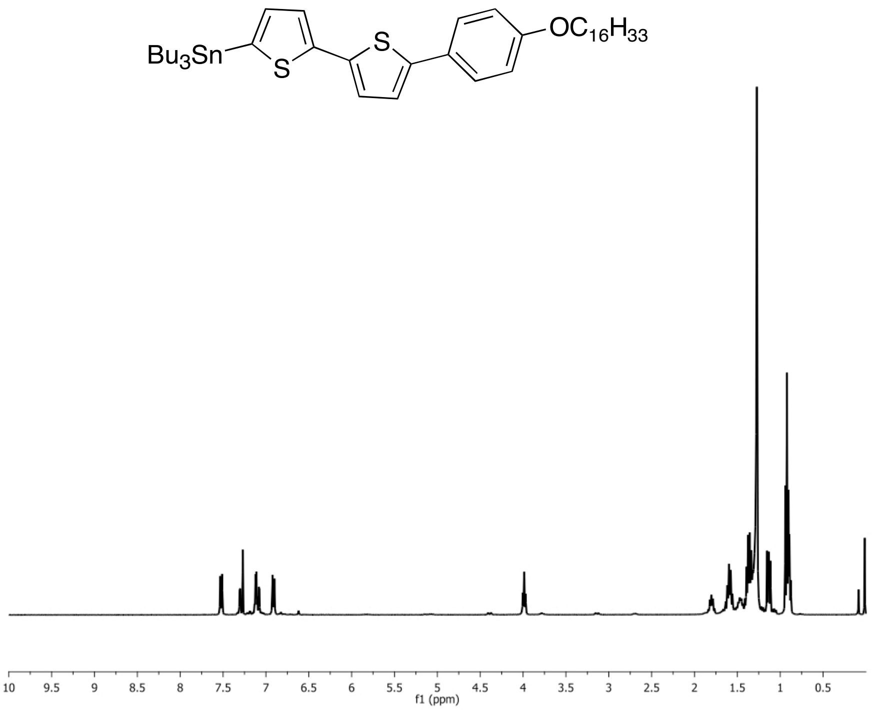

Spectrum 6. ^{1}H-NMR spectrum of **12** (400 MHz, CDCl$_3$).

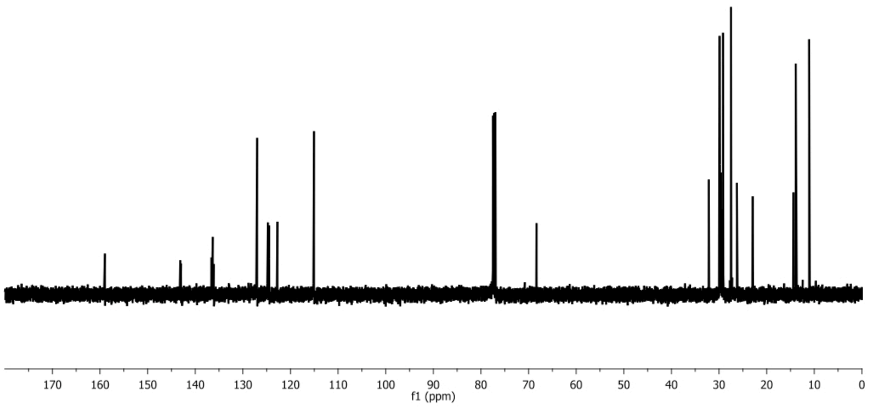

Spectrum 7. ^{13}C-NMR spectrum of **12** (125 MHz, CDCl$_3$).

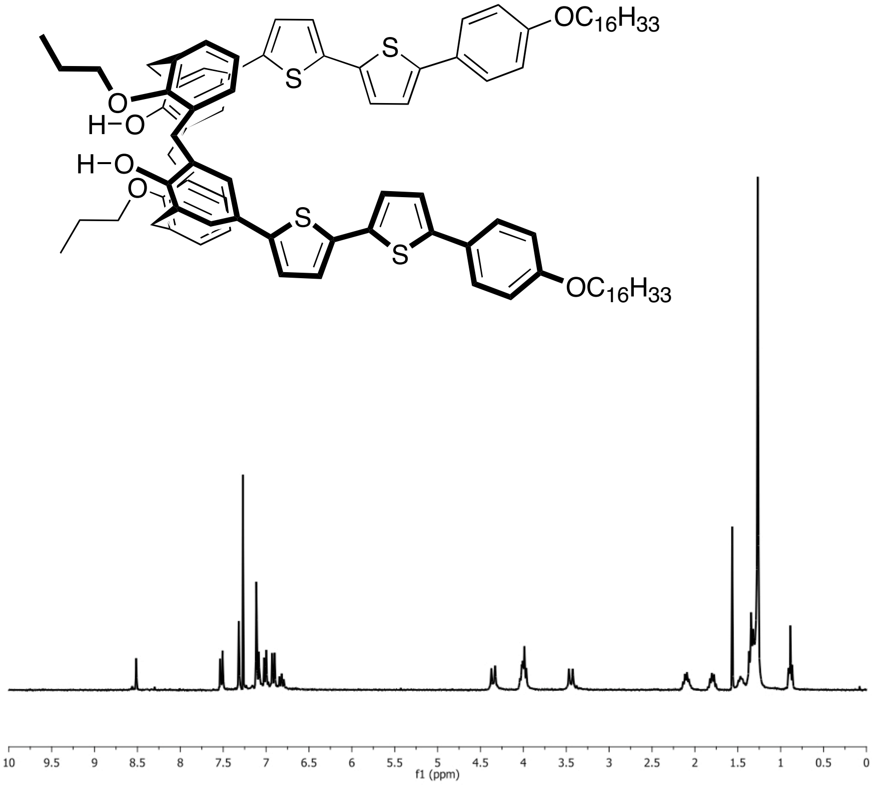

Spectrum 8. ^{1}H-NMR spectrum of **1** (300 MHz, $CDCl_3$).

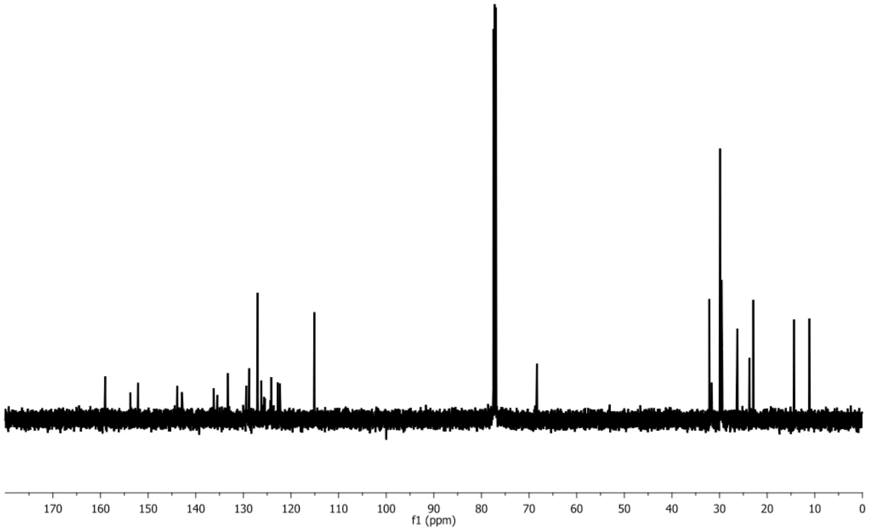

Spectrum 9. ^{13}C-NMR spectrum of **1** (125 MHz, $CDCl_3$).

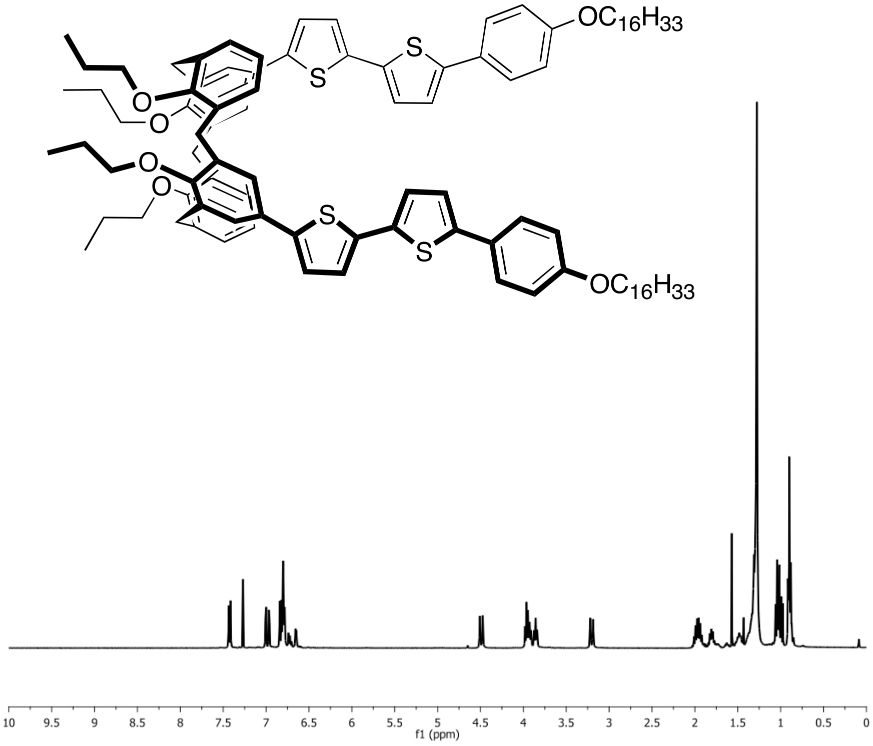

***Spectrum 10**.* ^{1}H-NMR spectrum of **2** (400 MHz, $CDCl_3$).

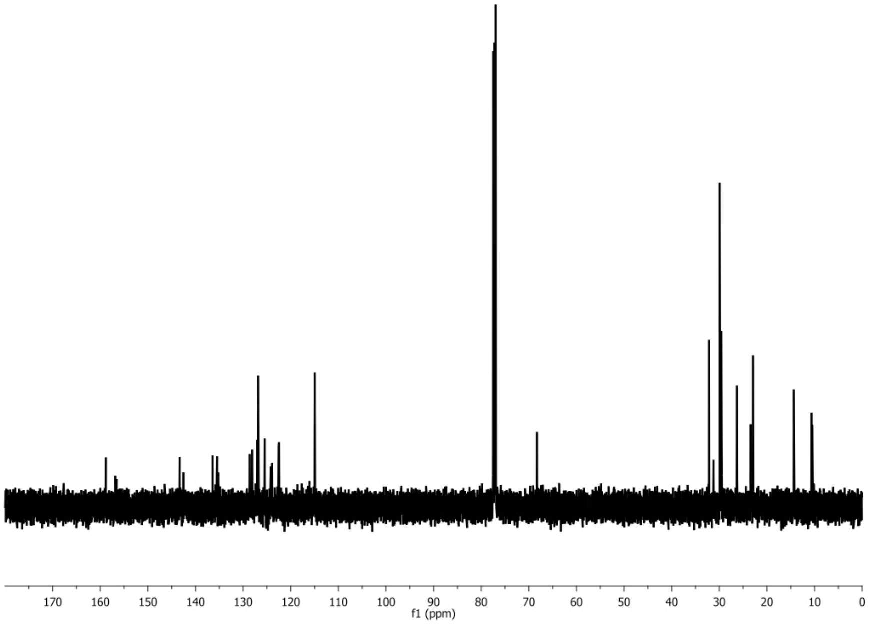

***Spectrum 11**.* ^{13}C-NMR spectrum of **2** (125 MHz, $CDCl_3$).

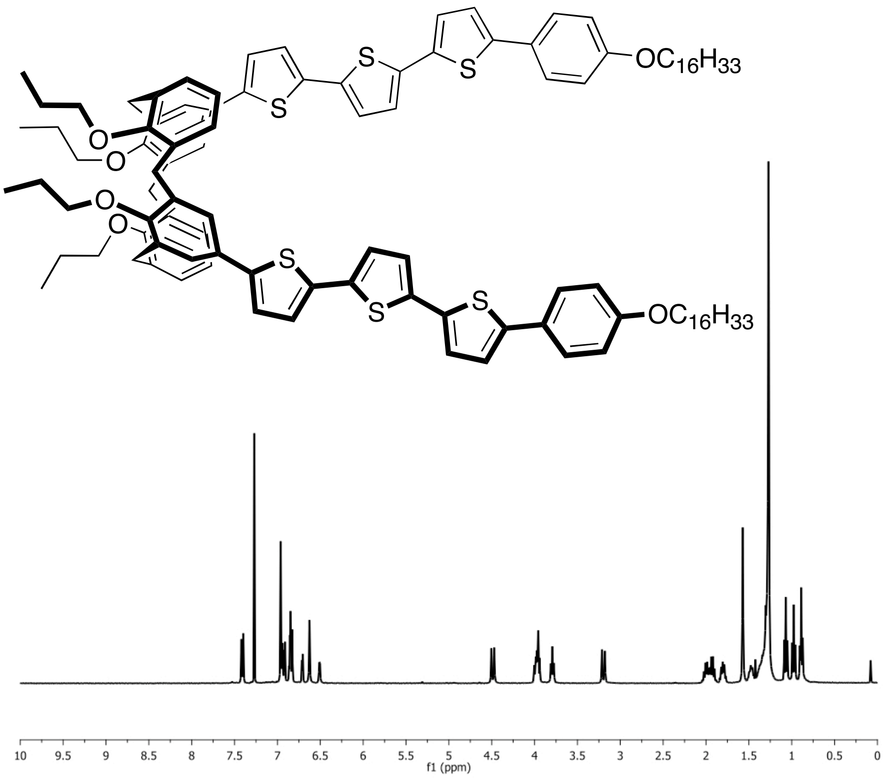

Spectrum 12. ^{1}H-NMR spectrum of **3** (400 MHz, $CDCl_3$).

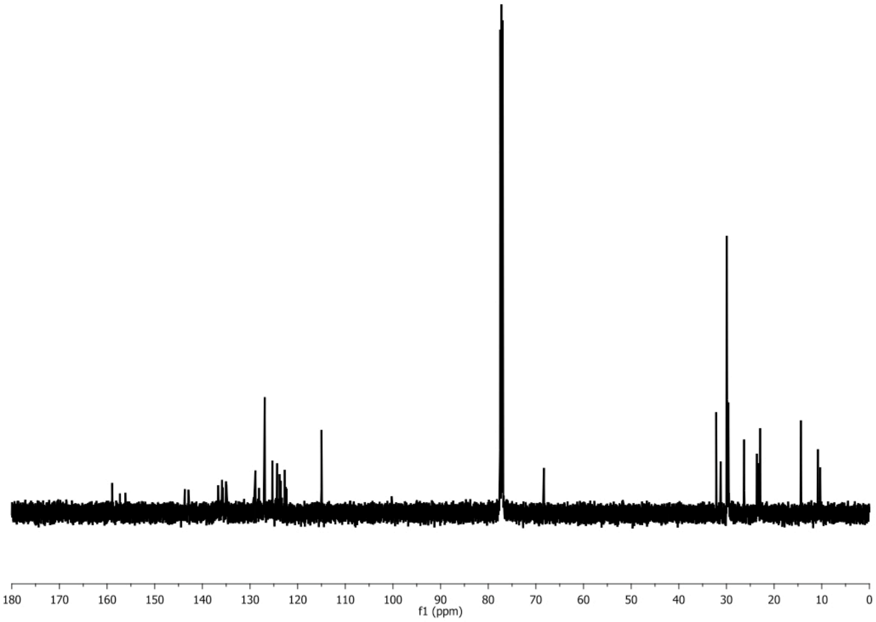

Spectrum 13. ^{13}C-NMR spectrum of **3** (125 MHz, $CDCl_3$).

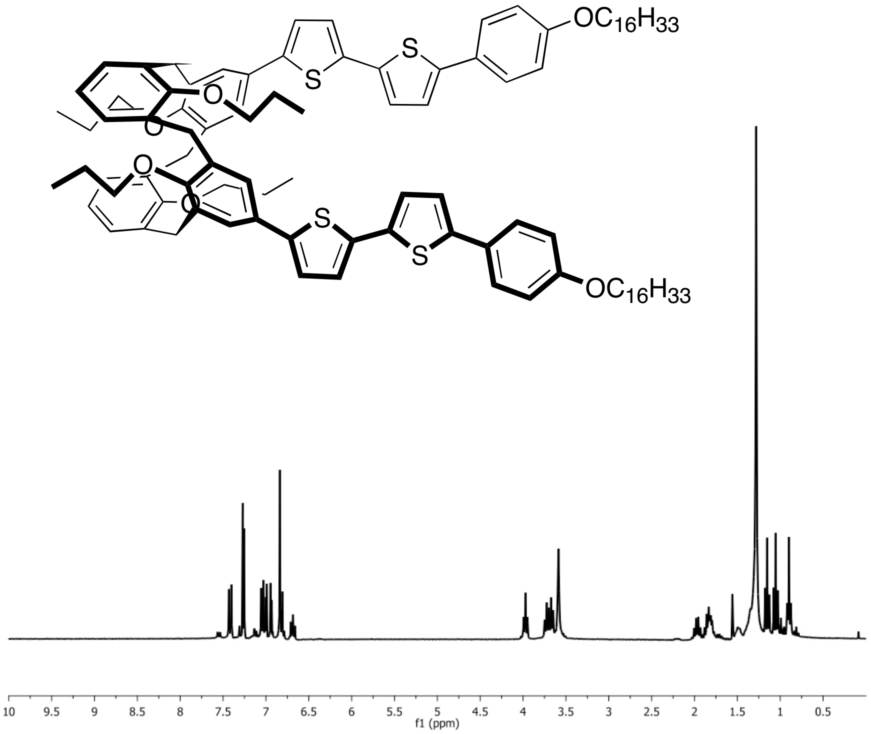

Spectrum 14. ^{1}H-NMR spectrum of **4** (400 MHz, $CDCl_3$).

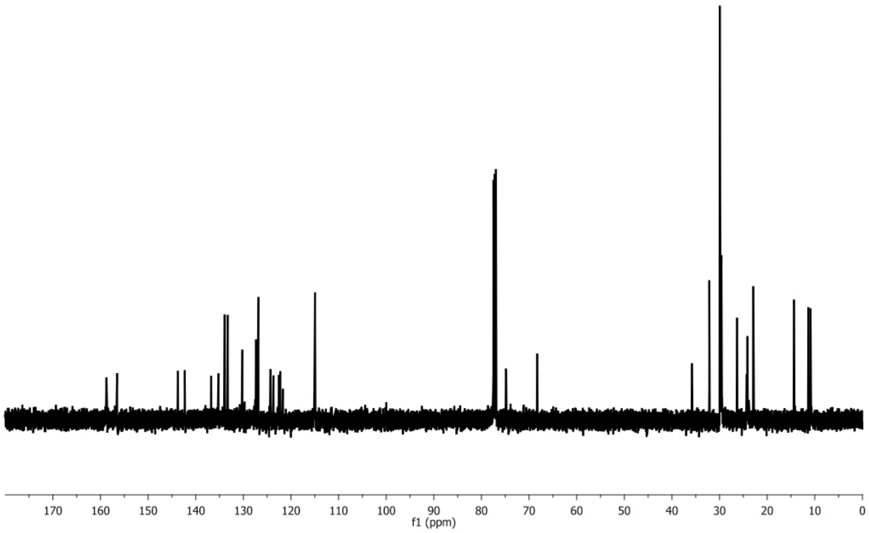

Spectrum 15. ^{13}C-NMR spectrum of **4** (125 MHz, $CDCl_3$).

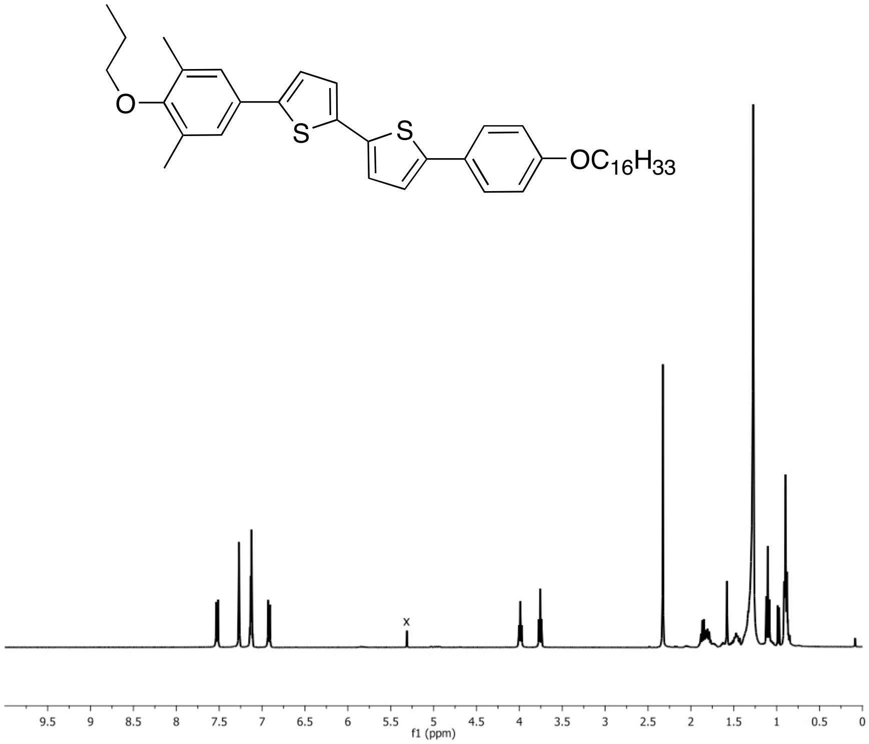

Spectrum 16. ^{1}H-NMR spectrum of **5** (400 MHz, $CDCl_3$).

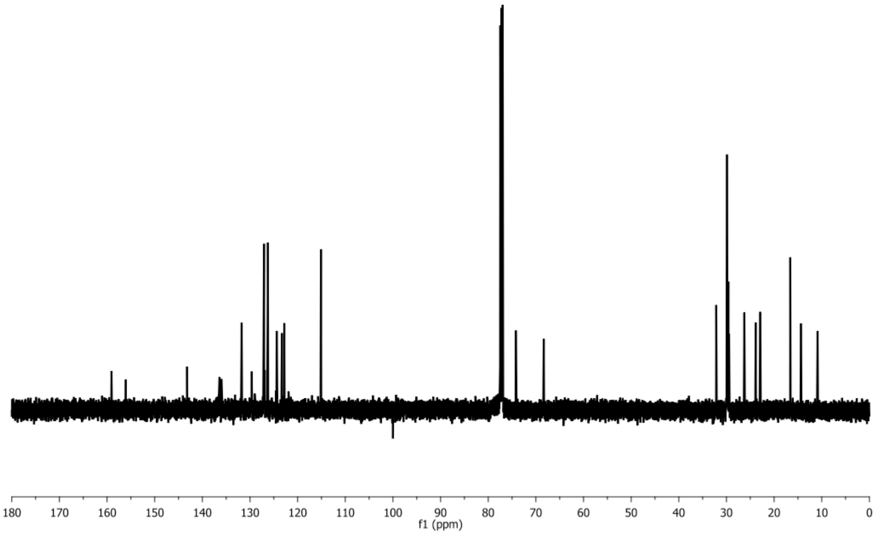

Spectrum 17. ^{13}C-NMR spectrum of **5** (125 MHz, $CDCl_3$).

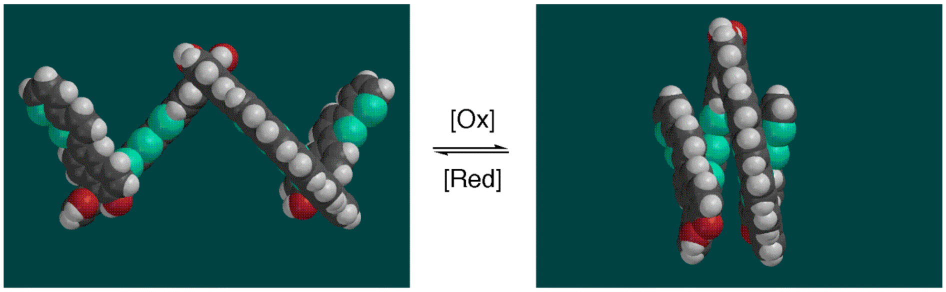

Chapter 3.

Binaphthyl-Hinged Molecular Actuators

Binaphthyl – A Molecular Hinge

We have proposed "molecular actuators" that change their dimensions via a novel molecular mechanism in Chapter 1.[1] In contrast to conventional conducting polymer actuators, which operate through absorption and release of counter-ions and solvents under electrochemical oxidation and reduction, our molecular actuator designs utilize the conformational changes of the individual polymer chain at the molecular level. Following this concept, we proposed two mechanisms for molecular actuators; the expansion and the contraction. In the expanding mechanism, the initially bent moieties are forced to be flat under redox control. The driving force is the aromatization, gained by oxidizing a non-aromatic system. Cyclooctatetraene[2] and thianthrene[3] have been suggested as possible candidates to produce this behavior.

To display a contracting mechanism, we have developed a calix[4]arene-based conducting polymer.[1b] In this system, the calix[4]arene scaffold functions as a molecular hinge, through which electroactive segments are brought together and apart to form a reversible (intermolecular) bond. We utilize π-dimer formation as the driving force for the actuation, which we unequivocally proved in model compound studies (see Chapter 2).

In parallel with the calix[4]arene-based system, a new building block containing binaphthyl units was developed as another potential hinge candidate. The binaphthyl has a hinge comprised of a 1,1' C-C bond between two naphthyl units. As described in Figure 1a, our design involves the electroactive segments (oligothiophenes, for example) that are connected through a binaphthyl hinge. As we oxidize the electroactive segments, radical cations are generated and the new chemical bond called π-dimer can potentially drive the dimensional changes. Figure 1b illustrates the computer-generated model of how the binaphthyl polymer changes its dimensions employing the hinge.

We have long pursued development of segmented electroactive polymers that lack extended conjugation. We believe that if we confine the wavefunctions into a finite region, we can expect a better interaction due to the large coefficients. However, the stability of charged species is generally improved when the species have more delocalized structures. It is also important to consider that the generated charges will display coulombic repulsion, which can offset any effects gained by the wavefunction confinement.

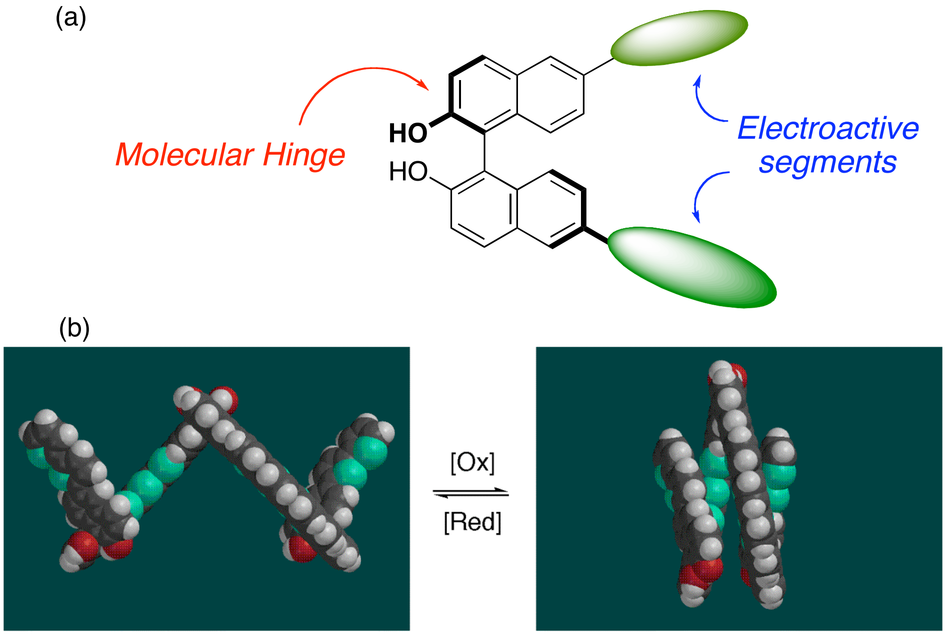

Figure 1. (a) Design of binaphthyl containing molecular actuators. (b) The computer-generated model of the binaphthyl polymer’s conformational change under redox control.

In this chapter, we describe the synthesis of this new class of materials and their electrochemical properties. We also developed a new binaphthyl monomer with oligothiophenes of different connectivity to promote a better interaction.

Synthesis of Binaphthyl Polymers: The First Generation

As a result of the richness in chemistry of binaphthyls,[4] dibromobinaphthol **1** is commercially available both in racemic and enantiomeric forms (*R* and *S*). Thus, we were able to synthesize the electropolymerizable monomers **2** and **3** in a single step with a Stille coupling reaction in moderate yields (Scheme 1). Compound **2** is stable for storage in the solid state, but we observed slow decomposition under air in case of compound **3**, perhaps due to oxidation.

Scheme 1.[a]

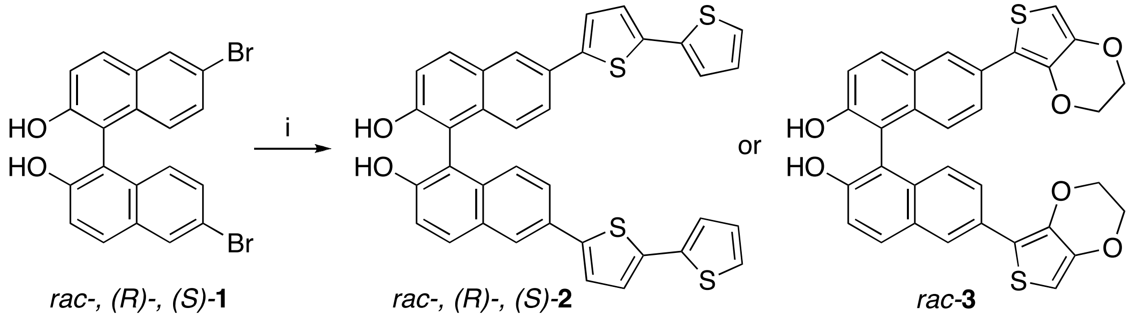

[a]Reagents: (i) $Pd_2(dba)_3 \cdot CHCl_3$, *t*-Bu_3P, 5-tributylstannyl-2,2'-bithiophene, KF, NMP, 70 °C, 24 h, 61~66%.

Figure 2 shows the electropolymerization of monomer **2** (racemic) to create electrode-surface confined polymer films and the scan-rate dependence of the electroactive polymers in CH_2Cl_2. The electrodeposition was performed under swept potential conditions with 0.1 M $TBAPF_6$ as a supporting electrolyte in air. The shift of the onset potential of the second scan (Figure 2a), when compared to the first scan, is indicative of generating a more extended conjugated system (i.e., thiophene-thiophene coupling).[5] As more films were deposited, the peak potentials slightly shifted and the increase in current with each scan slightly diminished. These effects are common with sluggish diffusion of ions into and out of the film, and the overall resistive loss through the thickness of the film results in a reduced potential (IR drop) at the film surface. We observed two oxidation and reduction couples, which is consistent with the generation of polaron (radical cation) and bipolaron (dication) types of species.[6]

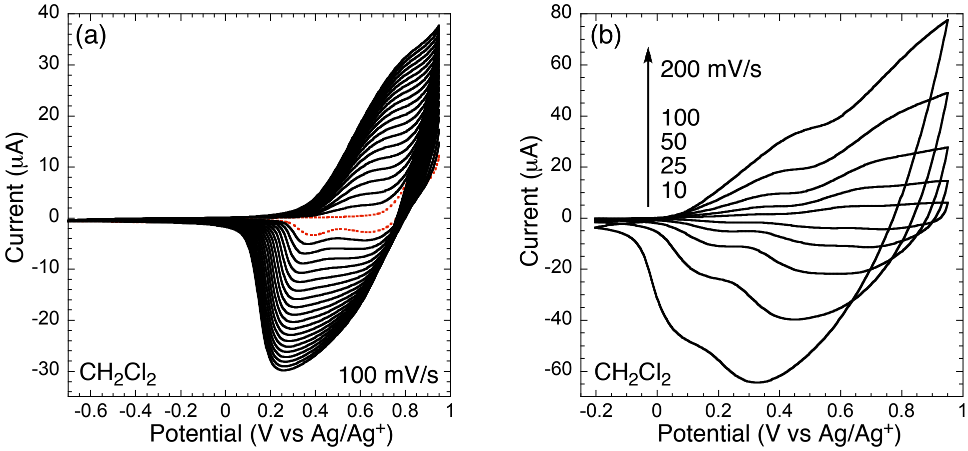

Figure 2. (a) Electropolymerization of *rac*-**2** (~1.5 mM) on a Pt button electrode. The dotted line represents the first scan. (b) CVs of a poly(*rac*-**2**) film at different scan rates in a monomer free solution. All measurements were carried out in CH_2Cl_2 with 0.1 M $TBAPF_6$ as a supporting electrolyte.

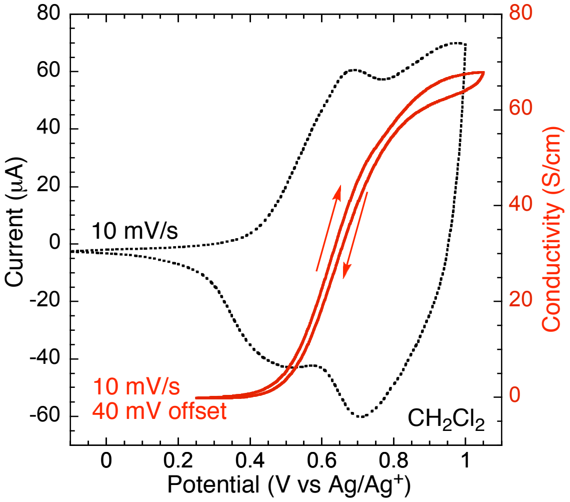

Figure 3. The CV (dotted line) and *in situ* conductivity measurement (solid line) of a film of poy(*rac*-**2**) on 5-μm interdigitated Pt microelectrode in CH_2Cl_2 with 0.1 M $TBAPF_6$ as a supporting electrolyte.

The *in situ* conductivity measurement of the poly(*rac*-**2**) was shown in Figure 3. The initially insulating film became conductive as the oxidation occurred (electrochemical doping), giving the maximum conductivity of ~60 S/cm. The conductivity profile of poly(*rac*-**2**) was distinguished from that of the related calix[4]arene-based polymer,[1b] in that it did not have a bell-shape. Rather, it represented a plateau before the degradation occurred. In the self-exchange mechanism[7] where charges are hopping between localized oxidized states, it is known that the conductivity reaches maximum when there are equal amounts of the conducting states. As was shown in the calix[4]arene-based polymer,[1b] the maximum conductivity was achieved when radical cations and dications existed in roughly equal amounts. Poly(*rac*-**2**) are segmented too and are expected to conduct charges through the self-exchange mechanism. However, it is possible that some other mechanisms exist at high oxidation levels.

Electropolymerization of *rac*-**3** was very different from that of *rac*-**2** (Figure 4). Firstly, the polymer was not stable in the ambient conditions, so the polymerization was performed under inert atmosphere (glove box). Secondly, the first and the second oxidation were well separated. Thirdly, it showed very interesting electron-injected states (n-doping). It is not usual that the n-doped states are observed in such an electron-rich system.[8]

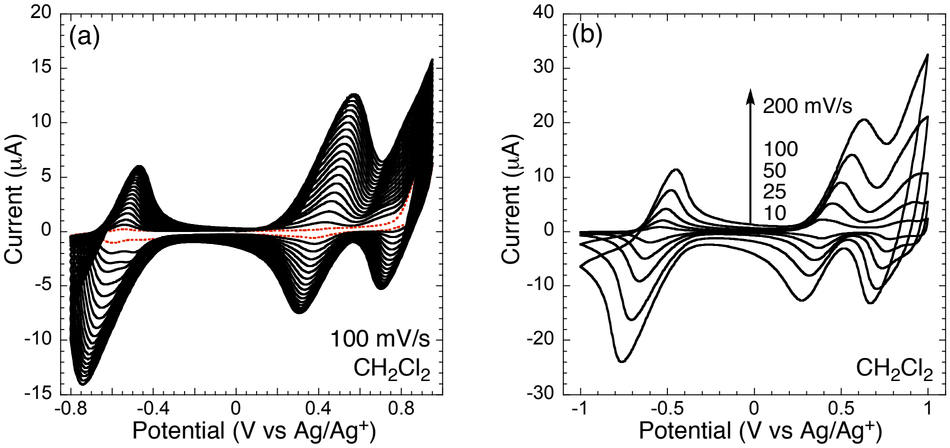

Figure 4. (a) Electropolymerization of *rac*-**3** (~1 mM) on a Pt button electrode. The dotted line represents the first scan. (b) CVs of a poly(*rac*-**3**) film at different scan rates. All measurements were carried out in CH_2Cl_2 with 0.1 M $TBAPF_6$ as a supporting electrolyte under inert atmosphere.

We noticed that the redox couples in the cyclic voltammograms (CVs) were asymmetric in oxidation and reduction current intensities, especially for the n-doping couple. The current for electron injection (reduction, the scanning from 0 V to –1 V) was bigger than that for the electron recovery (oxidation, from –1 V to 0 V). The same was true for the hole injection scans; the current from 0 V to +1 V was bigger than the backward current. We can postulate that, as we scanned the positive potential first, not all of the oxidized states were reduced in the first (positive) potential cycle, but they recovered at the negative potential scans together with n-doping process.

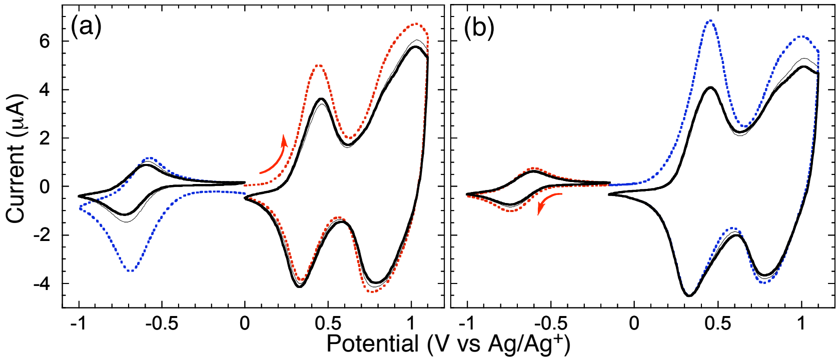

Figure 5. (a) CVs of a poly(**3**) film cycled first at the p-doping (positive potential) region (red dots), and then the n-doping (negative potential) region (blue dots). (b) CVs of a poly(**3**) film cycled at the n-doping region (red dots) first, then at the p-doping region (blue dots).

This "charge trapping" hypothesis was tested by scanning different directions (Figure 5). We first cycled the positive potential regions with the poly(*rac*-**3**) under inert atmosphere (Figure 5a). The current of the second scan (Figure 5a, gray solid above the red dots) was smaller than that of the first (Figure 5a, red dots), while the third (Figure 5a, black solid) was very similar to the second. This strongly suggested some of the charges were trapped at the first scan. Successively, we cycled the potentials to the negative regions (0 V to –1 V). As clearly shown in Figure 5a, the trapped charges appeared to be released at the first scan (blue dots). When we tried to inject the electrons first to the pristine poly(*rac*-**3**) (Figure 5b, red dots), we did not observe the same feature. Again, when cycled in the positive potentials, a portion of the charges from the first scan (Figure 5b, blue dots) were trapped.

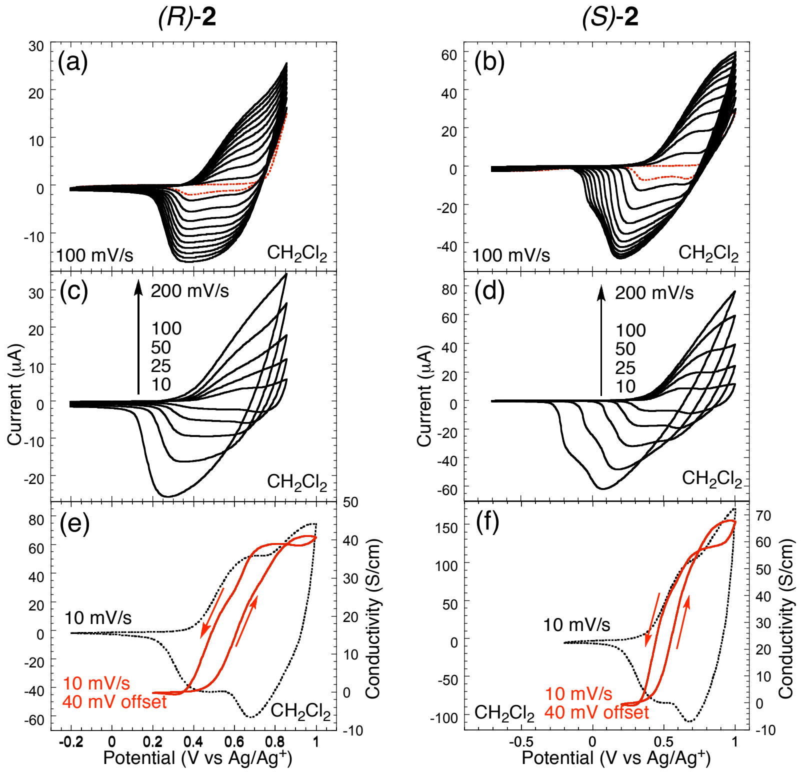

Figure 6. (top) Electropolymerizations of *R*-**2** (a, ~1.5 mM) and *S*-**2** (b, ~1.5 mM) on Pt button electrodes. The red dotted lines represent the first scan. (middle) CVs of films of poly(*R*-**2**) (c) and poly(*S*-**2**) (d) at different scan rates. (bottom) The CV (dotted line) and *in situ* conductivity measurement (solid line) of films of poly(*R*-**2**) film (e) and poly(*S*-**2**) (f) on 5-μm interdigitated Pt microelectrodes. All measurements were carried out in CH_2Cl_2 with 0.1 M $TBAPF_6$ as a supporting electrolyte.

Electropolymerization of the enantiometrically pure (*R*)- or (*S*)-**2** was conducted following the same conditions, and we found no significant differences from the results of the racemic counterpart. This is not surprising considering that the electronic structures should be the same regardless of the chirality. The polymers may have different morphologies according to the stereo-regularity. However, the stereo-regularity, if any, seems to affect the electrochemical properties very little.

Preparation of Free-Standing Films and Actuation Testing

We were able to obtain conductive free-standing films from the electropolymerization of monomer **2** employing a waveform that couples a brief mode of constant current to a swept current condition.[9] This galvanodynamic waveform, developed in our group, promotes more mass to be deposited while retaining the swept current conditions. Note that we controlled the current here, rather than potential, in order to ensure a sufficient polymerization rate even in the thick films. With thick films in a potential-controlling method, the potential at the film surface may be reduced due to a resistive drop and hence the polymerization rate is reduced. We performed the electropolymerization in CH_2Cl_2 with 0.1 M $TBAPF_6$ as a supporting electrolyte at –20 °C for 12 hours. The thickness of the peeled-off polymer film was measured as 30 μm, and the conductivity was 0.05 S/cm by the four-point probe method. The conductivity was very low compared to the value we obtained via the *in situ* method (Figure 3). However, it should be noted that the *in situ* method measures the relative value from the microscopic regions and utilizes only two probes.[10]

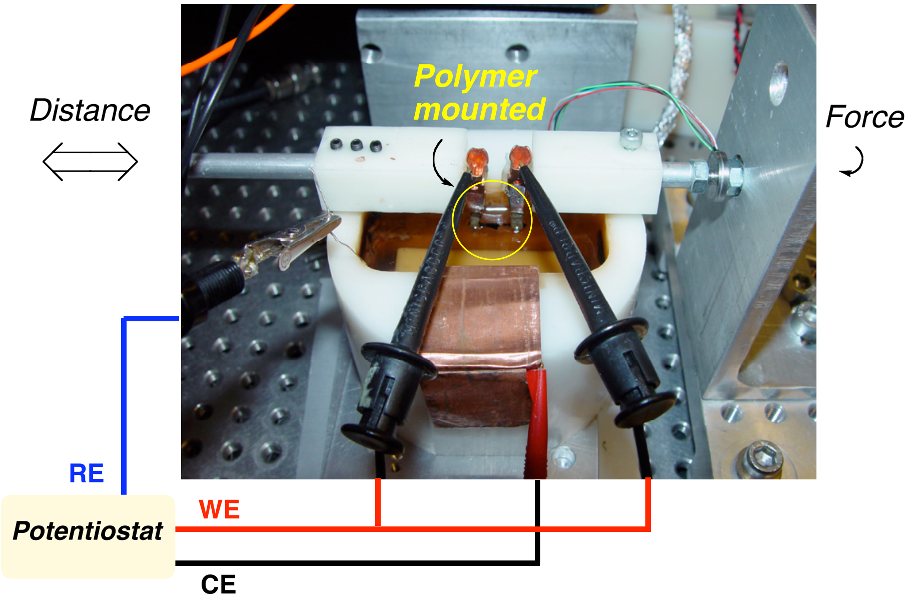

Figure 7. Dynamic mechanical analyzer for a polymer's actuation test (developed in Biointrumentation Lab, MIT).

Figure 7 illustrates the actuation test instrument (dynamic mechanical analyzer) developed in the Bioinstrumentation Lab of Professor Ian Hunter at MIT. The polymer film is mounted to two conductive clips (the working electrodes). One clip is connected to a force sensor, and the other clip is attached to a distance controller. It is then placed into an electrochemical cell including the reference and counter electrodes. Despite multiple attempts, however, we were not able to detect a correlation between injected charges and a strain (dimensional change) or stress (force change) (Figure 8). What we observed was the relaxation of the film in response to the stress applied. We suspect that the pristine polymer has highly entangled structures arising from the twisted nature of the binaphthyl monomer.

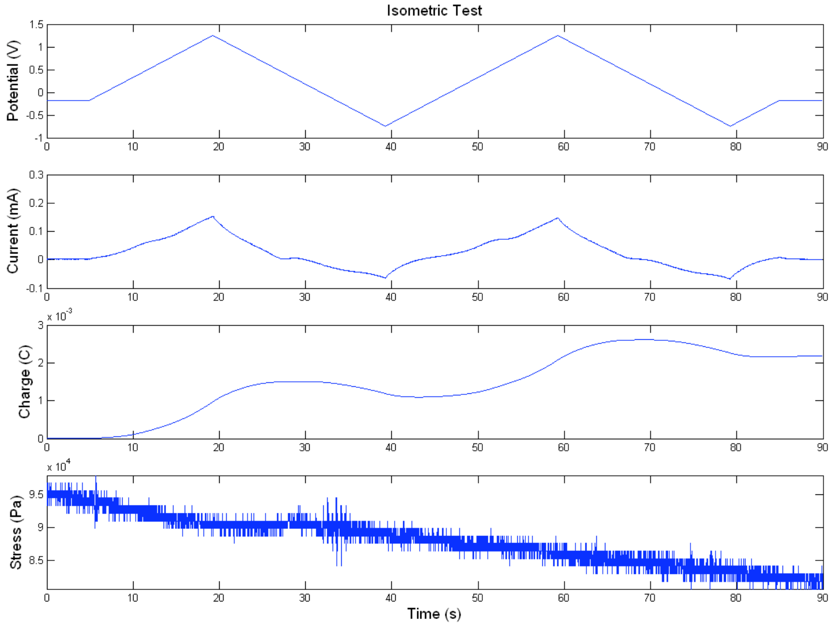

Figure 8. Actuation test results of a poly(*rac*-**2**) film. Stress (force/length, bottom) was measured in response to the applied cyclic potentials (top). No correlation was found between the stress and the injected charges.

What we have learned from actuation tests is that the alignment of the polymer strands will be key to the success of molecular actuators. Rather than the entangled structures, structures with a long-range order are needed. We will discuss efforts toward the alignments of the binaphthyl-incorpoated polymers at the end of this chapter.

Design of New Scaffold: The Second Generation

After our limited success with initial binaphthyl monomers, we turned our attention to the design of other monomer isomers containing a binaphthyl group. By simply changing the connectivity of oligothiophenes from 6-position to 7-position to the naphthol unit, we can expect a better interaction between the electroactive groups as shown.

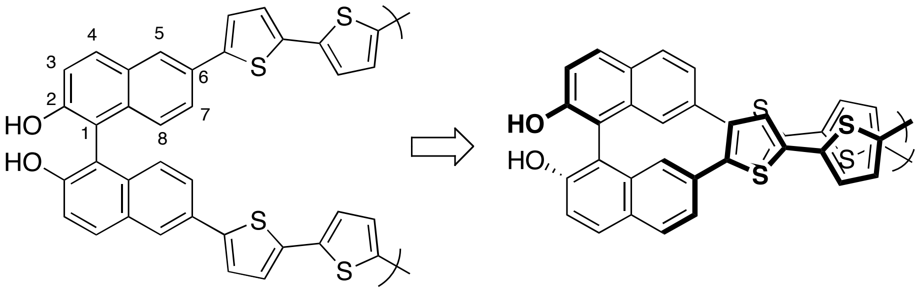

In contrast to the conventional 6,6’-disubstituted binaphthols, 7,7’-disubstitued binaphthols are rare and only recently are they utilized in catalyst development.[11] Nevertheless, the synthesis of 7,7’-dibromobinaphthol **4** was described in the literature[11b] via oxidative coupling with a copper-amine catalyst. The desired new monomer **5** was synthesized by a Stille coupling reaction in a good yield (Scheme 2).

Scheme 2.[a]

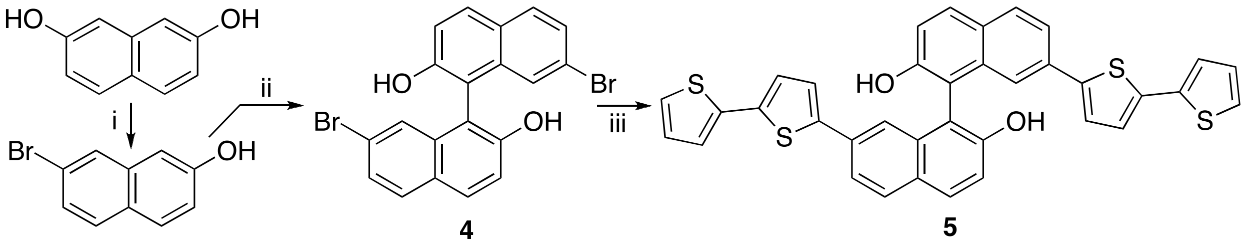

4

5

[a]Reagents: (i) $PPh_3•Br_2$, 300 °C , 67%. (ii) CuCl(OH)(TMEDA), CH_2Cl_2, 15 h, 92%. (iii) $PdCl_2(PPh_3)_2$, 5-tributylstannyl-2,2’-bithiophene, toluene, 80 °C, 18 h, 81%.

The electropolymerization of **5** (Figure 9) was performed with swept potential conditions (in CH_2Cl_2 with 0.1 M $TBAPF_6$ as a supporting electrolyte under air), similar to what was used to synthesize poly(**2**). Compared to the 6,6’-substituted monomers (e.g., **2**), 7,7’-susbstituted monomer **5** has hydroxyl groups at the non-conjugated position to the oligothiophenes. Thus, the monomer oxidation occurred at a slightly higher potential, and the peak potentials of the polymer’s oxidation were also higher. Poly(**5**) showed two one-electron oxidation and reduction couples, which were only resolved at slow scan rates.

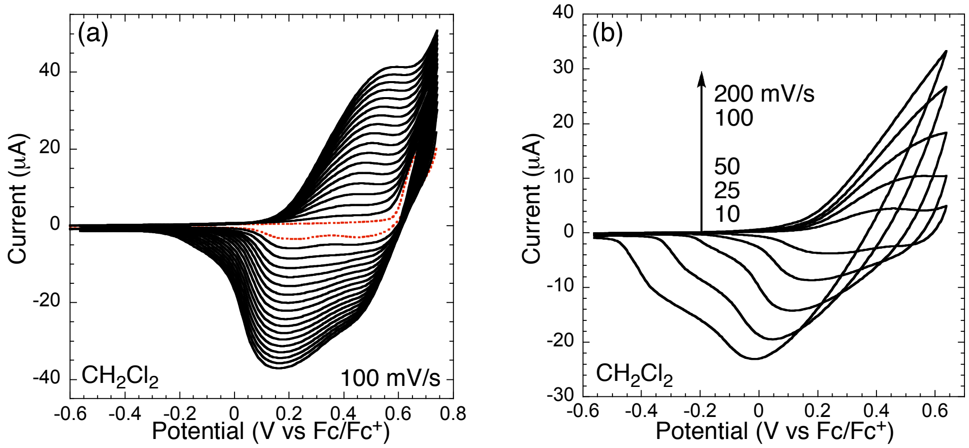

Figure 9. (a) Electropolymerization of **5** (~1.5 mM) on a Pt button electrode. The dotted line represents the first scan. (b) CVs of a poly(**5**) film at different scan rates. All measurements were carried out in CH_2Cl_2 with 0.1 M $TBAPF_6$ as a supporting electrolyte.

In situ conductivity measurements of a film of poly(**5**) revealed very interesting properties that are different from the isomeric poly(**2**)'s. We found that scanning to potentials higher than the second redox wave (~0.9 V vs Fc/Fc^+) resulted in increased conductivity (Figure 10) without degradation. When we limited the potential cyclings around the first oxidation (up to ~0.65 V vs Fc/Fc^+), the CVs were reproducible (Figure 10a, dotted line) and we see a clear correlation between the conductivity and the redox activity characteristic of self-exchange redox processes that would be expected of a hopping condition (Figure 10b, dotted line).

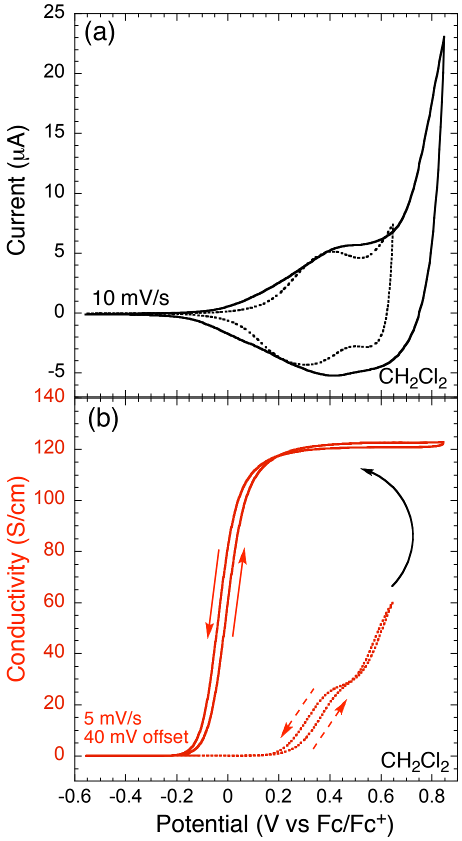

Figure 10. The CVs (a) and in-situ conductivity measurements (b) of a poly(**5**) film. Dotted lines represent the scans of potentials up to 0.65 V (vs. Fc/Fc$^+$). At higher potentials (>0.7 V), additional irreversible oxidation occurred (a, solid line) and conductivity was increased (b, solid line). Measurements were performed on a 5-µm interdigitated Pt microelectrode in CH_2Cl_2 with 0.1 M $TBAPF_6$ as a supporting electrolyte.

It appears that scanning to the higher potentials resulted in irreversible chemical reactions that produced a more conductive and delocalized polymer structure. The irreversible spike of the oxidative current in Figure 10a (solid) suggests that the oxidation results in new bonds being formed with loss of protons. The onset potential shifted to the lower potential and the electroactivity (integration of the current) did not diminish even after oxidation at the higher potential, both of which suggest a more delocalized structure is being produced. The conductivity profile (Figure 10b, solid) was very different after the high potential oxidation. The conductivity onset was shifted to lower potential as in the CV and the maximum conductivity was almost doubled. The conductivity also displayed a plateau, which is usually found in fully-conjugated polymers.[12] Segmented polymers show more structured conductivity profiles due to their hopping conduction.

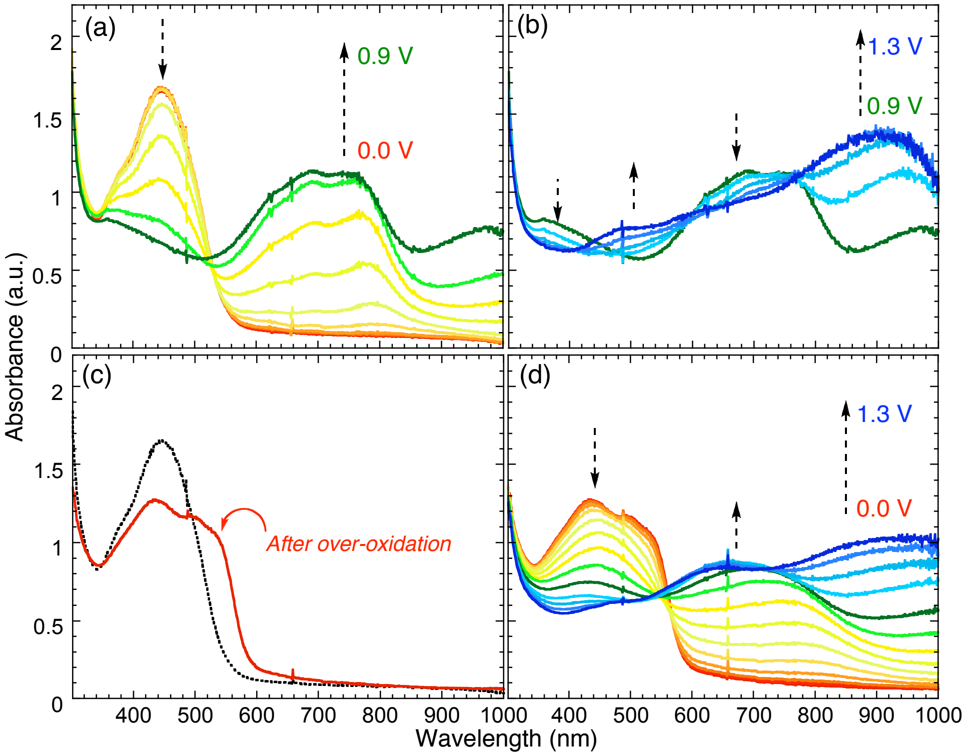

Figure 11. (a, b) Electronic absorption spectra of freshly-deposited poly(**5**) on a ITO-coated glass electrode as a function of oxidation potential from 0 V to 0.9 V (a) and 0.9 V to 1.3 V (b, high potential oxidation) vs. Ag/Ag$^+$ (0.01 M). (c) Comparison of neutral absorptions of poly(**5**) before (dotted line) and after (solid line) high potential oxidation. (d) Absorption spectra of the poly(**5**) film after high potential oxidatioin as a function of oxidation potential from 0 V to 1.3 V vs. Ag/Ag$^+$ (0.01 M). All measurements were carried out in CH_2Cl_2 with 0.1 M $TBAPF_6$ as a supporting electrolyte.

The spectroelectrochemical measurements provide evidence that the conjugation is increased after high potential oxidation. When we measured at the low potential region (Figure 11a), the development of the new optical transitions was very similar to that of polaron-like absorptions (radical cations, Chapter 2). The vibrational fine structures in the absorptions implied that the radical cations were localized to the finite segments.[13] With further oxidation as shown in Figure 11b (over-oxidation), dication species seem to dominate as a peak at around 900 nm.

After the high potential oxidation, we found that the bandgap, determined by the onset of the optical absorption, decreased significantly (Figure 11c, red line). When the polymer was oxidized again, the sub-gap transitions lost the vibrational fine structures and became featureless (Figure 11d), which is similar to fully-conjugated polythiophenes.[5,12,14] Based on the results, it seems highly likely that a chemical transformation at the high potentials leads to the increase in conjugation. Considering the structure, we postulate that 8- and 8'-positions are prone to nucleophilic attacks (Scheme 3). The phenolic oxygens, which do not actively participate in the stabilization of the generated charges, may attack those positions, resulting in the extended aromatic structures. Although we obtained much more conductive material, it seems likely that the hinges we intended to incorporate were removed through the process. Thus, we have continued to protect the phenolic oxygens with alkyl groups.

Scheme 3. Proposed Chemical Transformation of poly(**5**) at High Oxidation States

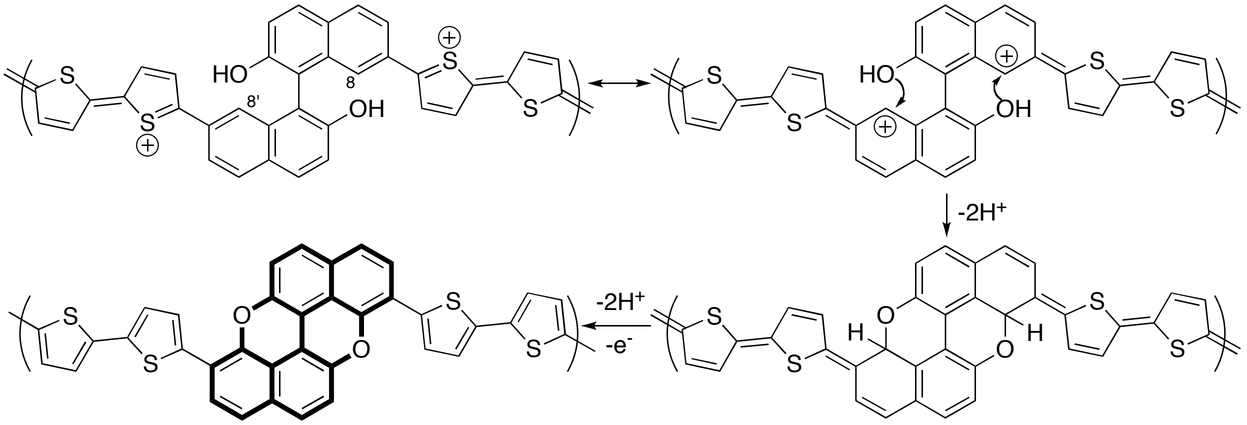

O-Alkylated Binaphthol Polymers

We installed the alkyl groups to the binaphthol monomers (Scheme 4) in the hope that *O*-alkylation will prevent any further transformation at high oxidation states. In addition, with long alkyl chains we may obtain soluble polymers, which is highly desirable for processing. Compound **7** was easily prepared from dibromobinaphthol **4** by Williamson etherification and Stille coupling. Macrocyclic monomer **9** was synthesized for ring opening metathesis polymerization (ROMP), which will be discussed later. 6,6'-Substituted counterparts **10** and **11** were also synthesized using similar methods.

Scheme 4.[a]

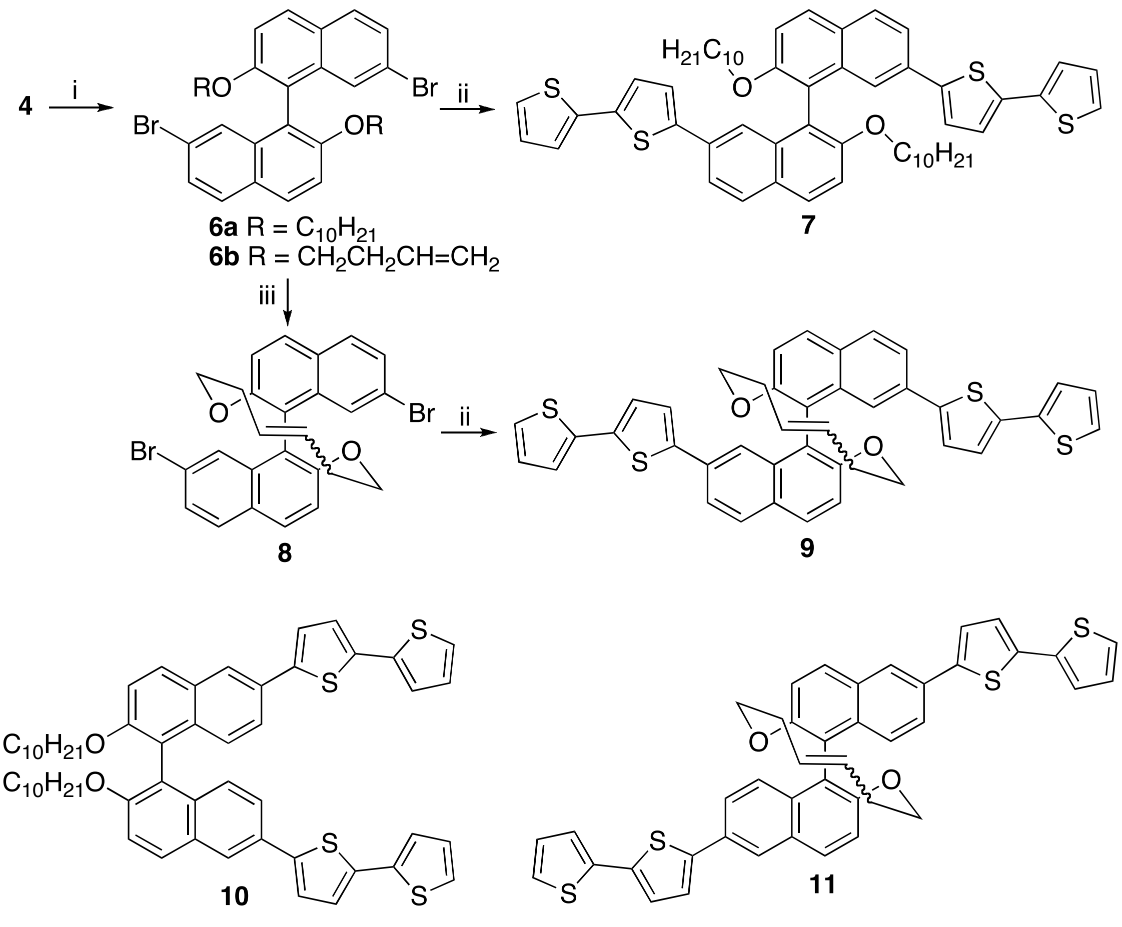
4
i
RO
Br
Br
OR
ii
6a R = C10H21
6b R = CH2CH2CH=CH2
H21C10
O
S
S
S
S
O
C10H21
7
iii
O
Br
Br
O
ii
8
9
C10H21O
C10H21O
10
11

[a]Reagents: (i) R-Br, K_2CO_3, acetone, reflux, 15 h, 78~86%. (ii) $PdCl_2(PPh_3)_2$, 5-tributylstannyl-2,2'-bithiophene, toluene, 80 °C, 18 h, 81%. (iii) $(Cy_3P)_2Cl_2Ru{=}C(H)Ph$, CH_2Cl_2, 2 h, 73%.

The electropolymerization of **7** or **10** was performed in a 1:1 mixture of CH_2Cl_2:CH_3CN, which facilitated the polymer's deposition on a electrode surface better than using CH_2Cl_2 alone. This result likely reflects the solubility of initially coupled oligomeric products. Interestingly, we were able to conduct the electropolymerization of **9** or **11** in CH_2Cl_2 solution only and hence the additional rigidity of these monomers likely decreases the solubility. All other conditions were similar to the case of other binaphtyl monomers (**2** and **5**).

Figure 12 shows the polymerizations (a–d) and the resulting polymers' scan-rate dependences in CH_2Cl_2 (e–h), and in CH_3CN (i–l). All polymers showed two 1-electron redox waves, although their peak potentials were different depending on the structures and the solvent used. In the case of poly(**7**) and poly(**10**) in CH_3CN, we needed to apply higher potentials to achieve the first oxidation, which resulted in sharp peaks and substantial peak-separation between the oxidation and reduction of the first redox couple. We attributed this to low degrees of solvation to the neutral polymers. This "solubility effect" was not apparent in the case of poly(**9**) and poly(**11**). We suspect that macrocyclic side chains and shape-persistent structures create an additional free space inside the polymer, which allows for more facile solvent and electrolyte diffusion into the polymer film as compared to the linear counterparts.

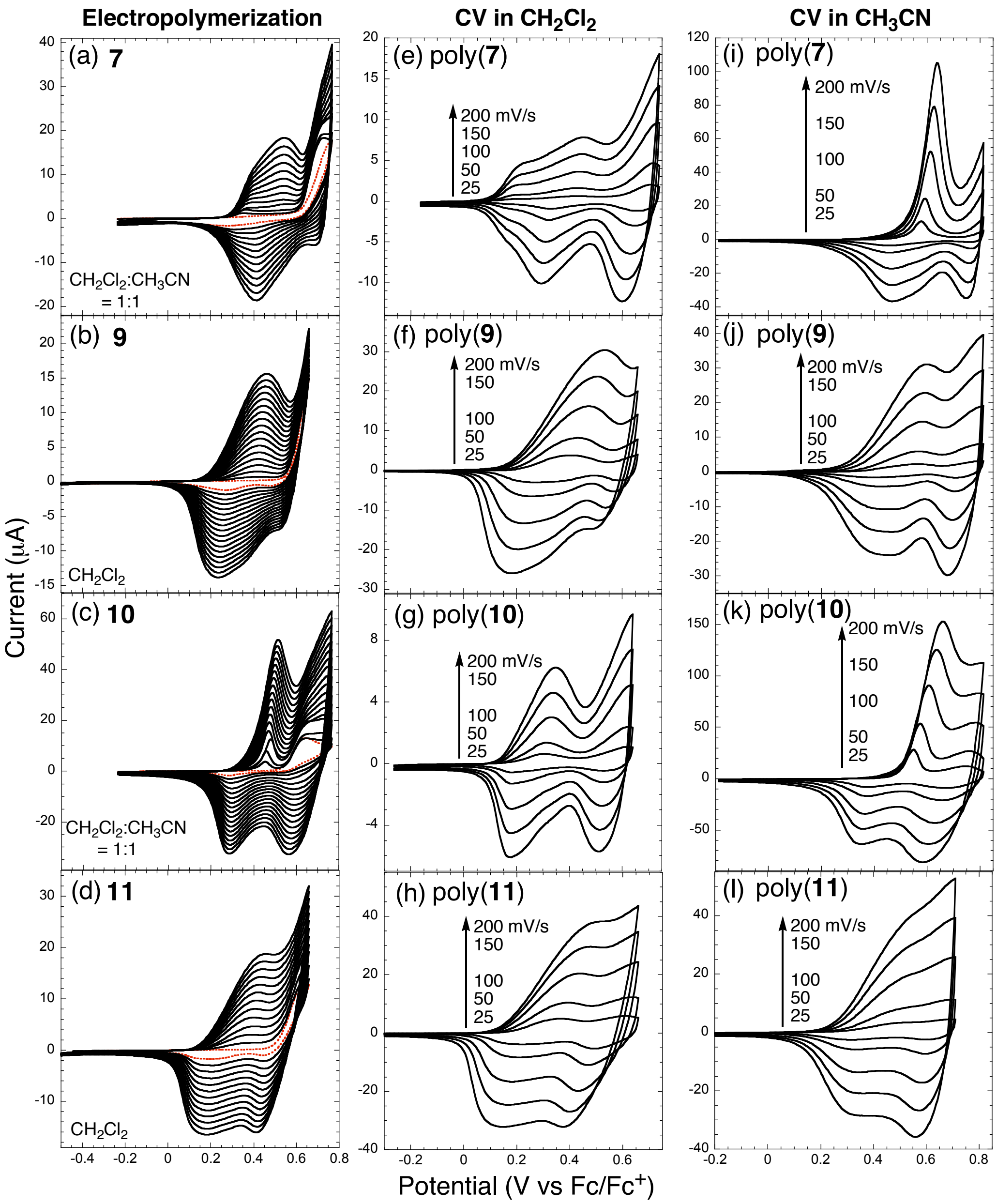

Figure 12. Electropolymerizations of **7** (a), **9** (b), **10** (c), and **11** (d) (all ~1.2 mM) on Pt button electrodes in the solvents indicated with 0.1 M $TBAPF_6$ as a supporting electrolyte. Dotted lines represent the first scan. CVs of corresponding polymer films at different scan rates in CH_2Cl_2 (e–h) and in CH_3CN (i–l) were presented in parallel.

The most striking feature in the CV was found for poly(**7**) in CH_2Cl_2 where the first redox couple was split. This was not found in CH_3CN or for any other polymers. The peak splitting was most evident when the film was thin, as shown in the first few scans at the electropolymerization (Figure 13a). In this case, we observed for poly(**7**) split oxidation peaks at 0.36 V and 0.54 V, and reduction peaks at 0.31 V and 0.40 V. In contrast, only one oxidation (0.46 V) and one reduction (0.29 V, all vs Fc/Fc$^+$) peak were observed in poly(**10**). In thicker films of poly(**7**), however, only one peak was observed.

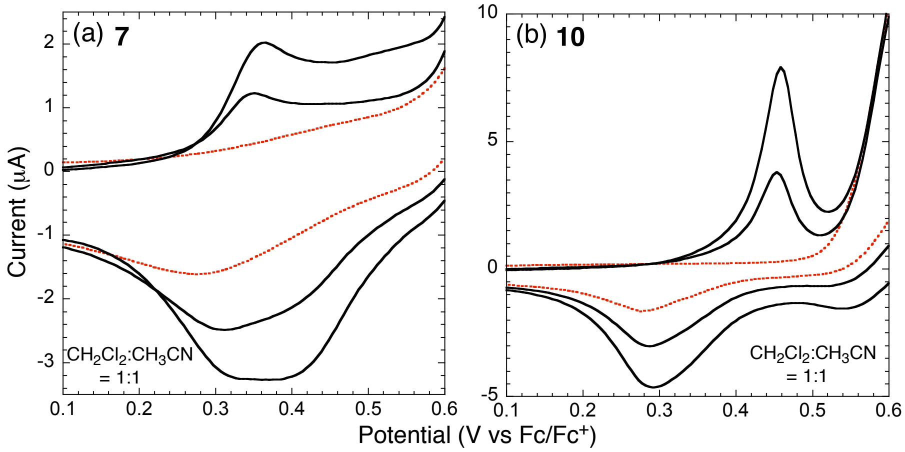

Figure 13. First three scans in the electropolymerization of **7** (a) and **10** (b) on Pt button electrodes in the 1:1 mixture of CH_2Cl_2 and CH_3CN with 0.1 M $TBAPF_6$ as a supporting electrolyte.

We speculate that in the case of poly(**7**), a mixed-valence π-complex between the radical cation and the neutral species was generated during the first oxidation. The stabilization by the mixed-valence complex leads to the shift of the onset potential of the first oxidation in the CVs: 0.1 V for poly(**7**) versus 0.2 V for poly(**9**) (Figure 14, all in CH_2Cl_2, vs. Fc/Fc$^+$). It is interesting that only the new monomer with 7,7'-substituents (**7**) showed such interaction, and that the side chains greatly affected its behavior. However, this mixed-valence complex is destabilized in the thick films, which implies that entangled and geometrically constrained structures may prevent its formation. We propose that highly-ordered structures are necessary to take advantage of this type of interaction.

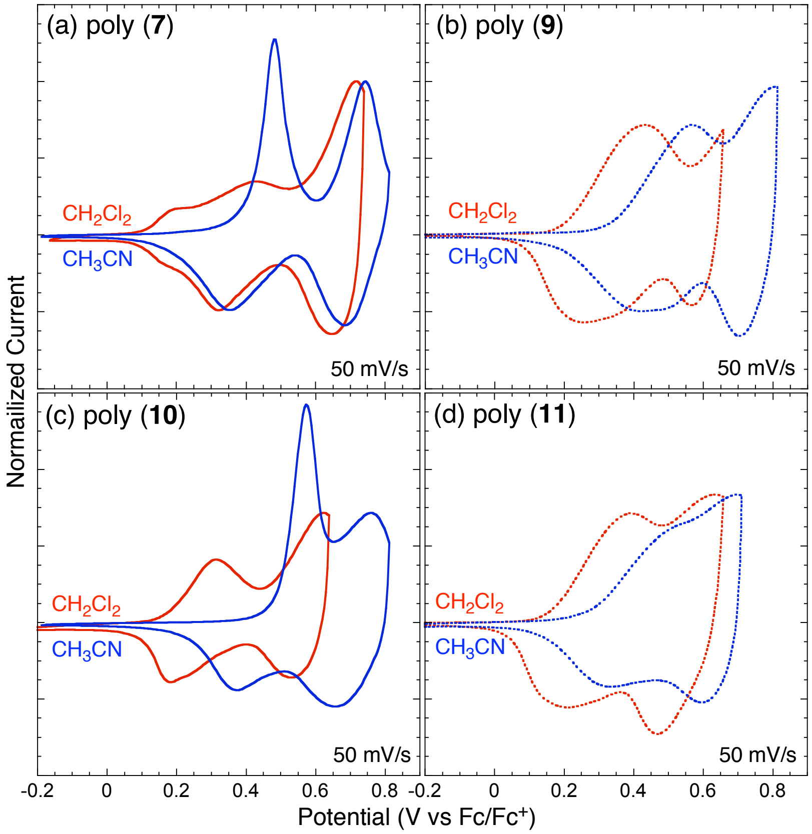

Figure 14. CVs of films of poly(**7**) (a), poly(**9**) (b), poly(**10**) (c), and poly(**11**) (d) on Pt button electrodes in CH_2Cl_2 (red line) and CH_3CN (blue line) with 0.1 M $TBAPF_6$ as a supporting electrolyte.

It should be noted here that upon alkylation we did not observe any signature of degradation or chemical transformation even at the very high oxidation levels. Indeed, all of the polymers (poly(**7**), poly(**9**), poly(**10**), and poly(**11**)) were remarkably stable at high oxidation states. This observation supports our proposal that reactions take place at the phenolic oxygens. Although highly stable redox systems are obtained by protecting the phenolic oxygens, the stability gain in these cases is at the expense of the conductivity. We found that the maximum conductivities of the alkylated systems were more than an order of magnitude lower than those of the free phenolic systems.

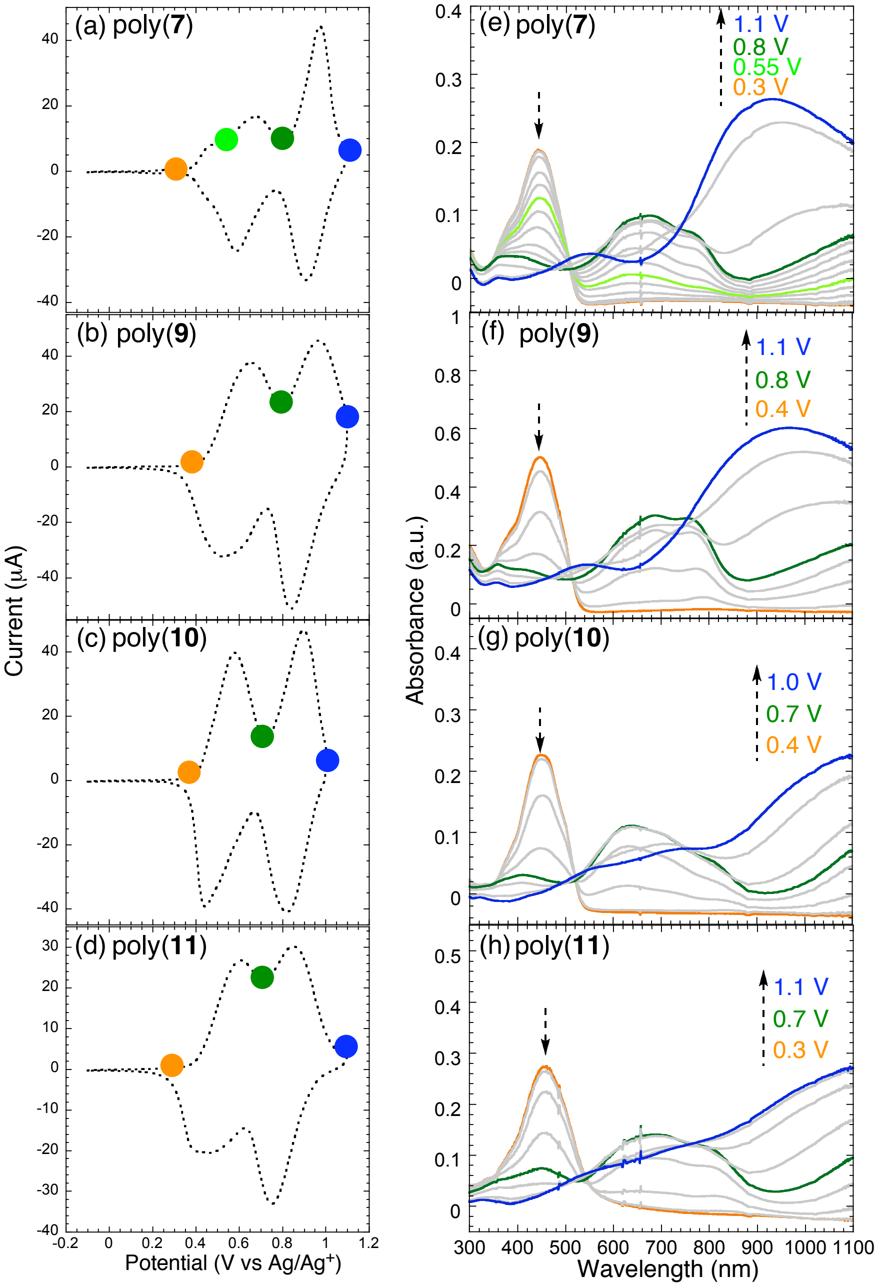

Figure 15. Electronic absorption spectra in CH_2Cl_2 of poly(**7**) (e), poly(**9**) (f), poly(**10**) (g), and poly(**11**) (h) on ITO-coated glass electrodes with 0.1 M $TBAPF_6$ as a supporting electrolyte, as a function of oxidation potential vs. Ag/Ag^+ (0.01 M). Roughly, orange, green, and blue lines represent their neutral, polaronic (radical cation), and bipolaronic (dication) states, respectively. CVs of the corresponding polymer films (a–d) were presented in parallel.

We measured *in situ* UV-vis absorptions as a function of oxidation levels by varying the applied voltages. The polymers were deposited onto the ITO-coated glass electrodes and placed into a quartz cell equipped with a counter electrode and a reference electrode. Figure 15 shows the spectroelectrochemical measurements (e–h) in CH_2Cl_2 under ambient atmosphere with 0.1 M $TBAPF_6$ and the CVs (a–d) of the corresponding polymers. We clearly observed two 1-electron redox couples for all polymers with the splitting of the first redox couple in the case of poly(**7**).

Based upon the optical spectra, we can divide the oxidations into three levels: neutral, radical cation (polaron-like), and dication (bipolaron-like). At the neutral state (orange lines), the absorptions of the polymers were all very similar with small red-shifted onsets for poly(**10**) and poly(**11**) as compared to those of poly(**7**) and poly(**9**). The spectra of poly(**7**) and poly(**9**) were almost identical as were poly(**10**) and poly(**11**), which indicates that the position of alkoxy groups affects the electronic structures more than the conformation of the hinge. Similarly, the dication states (blue lines) of poly(**7**) and poly(**9**) were very similar, and we see parallel similarities for poly(**10**) and poly(**11**). The positions of the absorption maxima were slightly different, but the shapes were consistent with bipolaron-like absorptions.[14]

We were intrigued by the development of sub-gap transitions to the radical cation states (green lines). All four polymers showed the typical pattern of polaron-like absorptions with the neutral absorptions decreasing while the two sub-gap transitions (~700 nm and >1100 nm) increased. However, upon close examination the first polaron-like transitions (~700 nm) contain two kinds of absorptions with different ratios according to each polymer. For poly(**7**) and poly(**9**), two absorptions at around 660 nm and 780 nm were observed in different ratios (Figure 15e and f). The 660-nm absorption prevailed in the oxidation of poly(**7**), while the 780-nm absorption developed first for poly(**9**) but at higher potentials the two absorptions were equalized.

In the case of poly(**10**) and poly(**11**), the polaron-like transitions are approximately at 630 nm and 820 nm (Figure 15g and h). The 630-nm absorption was dominant in poly(**10**). In poly(**11**), the 820-nm absorption was most noticeable, although it was not dominant. To summarize the effects of the substitution patterns (7,7'- vs 6,6'-) and the alkoxy groups (linear vs macrocyclic), we note the following; in the two absorptions for radical cations, the shorter-wavelength absorption was more prevalent in the polymers with 6,6'-substituted binaphthols than those with the 7,7'-susbstitution (poly(**10**) vs poly(**7**), and poly(**11**) vs poly(**9**)). In addition, linear alkoxy chains appeared to promote the shorter-wavelength absorption (poly(**7**) vs poly(**9**), and poly(**10**) vs poly(**11**)).

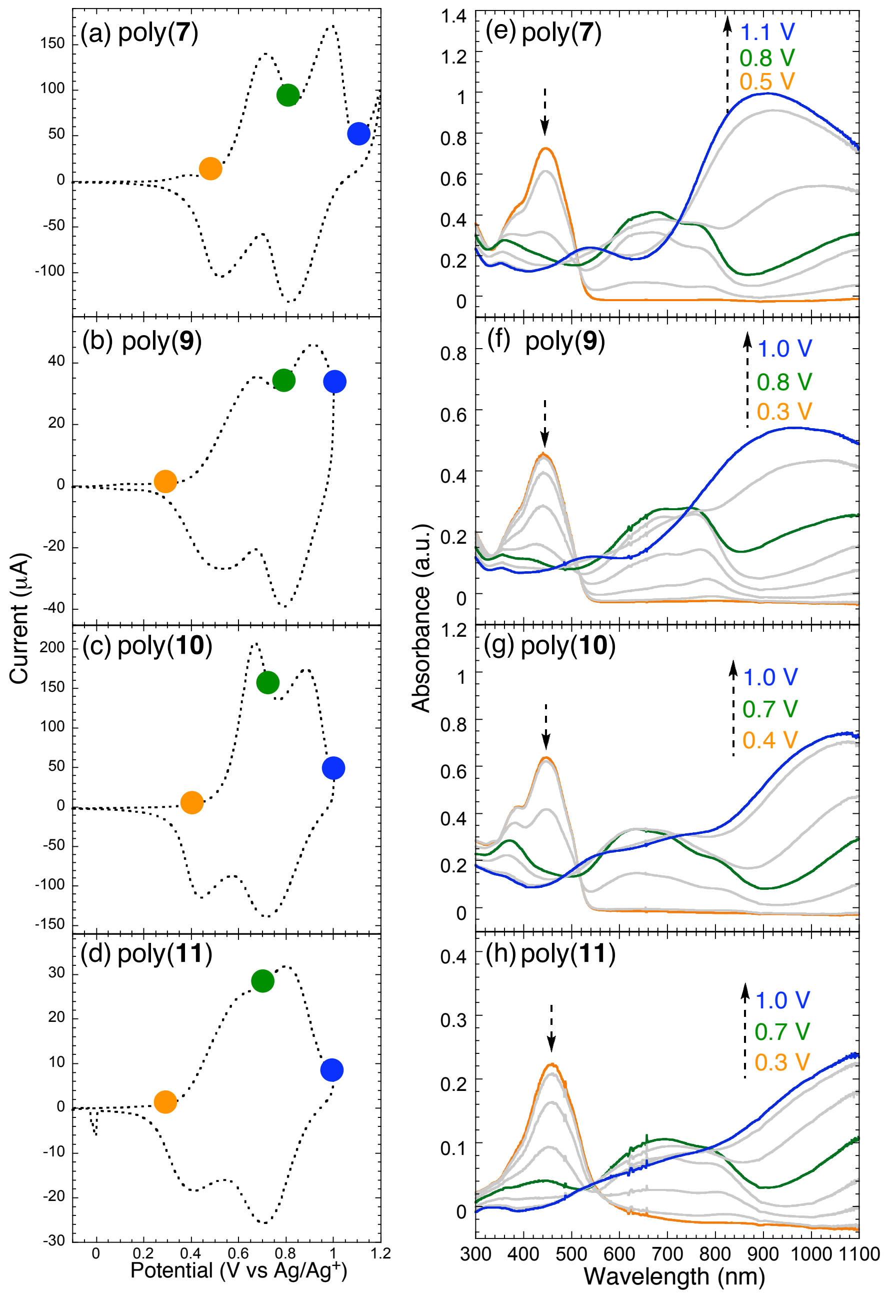

Figure 16. Electronic absorption spectra in CH_3CN of poly(**7**) (e), poly(**9**) (f), poly(**10**) (g), and poly(**11**) (h) on ITO-coated glass electrodes with 0.1 M $TBAPF_6$ as a supporting electrolyte, as a function of oxidation potential vs. Ag/Ag^+ (0.01 M). Roughly, orange, green, and blue lines represent their neutral, polaronic (radical cation), and bipolaronic (dication) states, respectively. CVs of the corresponding polymer films (a–d) were presented in parallel.

When we conducted the same measurements in CH_3CN (Figure 16), we were able to observe the same patterns for the development of polaron-like absorptions as in CH_2Cl_2, although the ratios varied slightly. Figure 17 summarizes the polaron-like absorptions of the polymers in both CH_2Cl_2 and CH_3CN. We[15] and others[16] found that in the small molecule systems, the polaron-like absorptions are blue-shifted when they form a π-dimer. We therefore assign the short wavelength peak as the π-dimer, and such interactions become stronger with linear alkoxy chains and 6,6'-substituted binaphthyls. However, we suspect that the interactions may rise from the *inter-chain* interactions, because the geometry with 7,7'-substituents should best promote an *intra-chain* interaction (Figure 13 and 14).

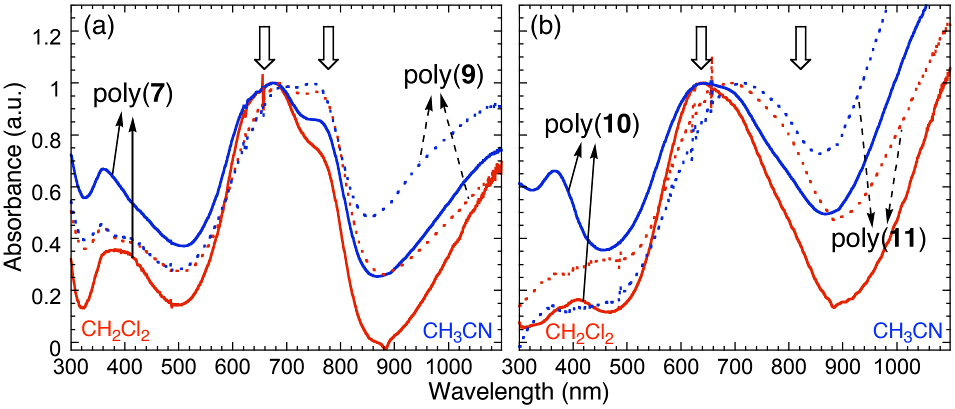

Figure 17. Electronic absorptions of poly (**7**) (a, solid lines), poly(**9**) (a, dotted lines), poly (**10**) (b, solid lines), and poly(**11**) (b, dotted lines) in CH_2Cl_2 (red lines) and CH_3CN (blue lines) at their radical cation states. Conditions were the same as in Figure 15 and 16.

Alignment of Polymers: Ring Opening Metathesis Polymerization

From our actuation studies, we believe that highly ordered polymer materials are necessary in order to translate the molecular dimensional changes into macroscopic movement. One method for aligning polymers or small molecules is to disperse them into ordered matrices, such as nematic liquid crystals, uniaxially stretched polymer films, etc.[17] The binaphthyl and its derivatives are known to align in these matrixes due to their aspect ratios and have been used to induce cholesteric mesophases in nematic liquid crystals (chirality transfer).[18] Thus, it is a reasonable approach that a mixture of a soluble binaphthyl polymer and an aligning matrix can be used to produce an aligned material. Incorporation of the binaphthyl moieties directly into the aligning matrix is another approach.

As a preliminary study, we tried to incorporate the binaphthyl moiety into the elastomeric matrix by using ring opening metathesis polymerization (ROMP, Scheme 5). ROMP is a well-controlled living polymerization method[19] and has been widely used to prepare a variety of materials.[20] As described earlier, we prepared macrocyclic binaphthyl monomers (**9** and **11**), however we find that they cannot be homopolymerized by the Ru catalysts developed by Grubbs. To create polymers, we employed a *cis*-cylcooctene (COE) comonomer at various ratios, and found that it gave the best results when the ratio of binaphthyl monomer:COE was 1:4.

Scheme 5.[a]

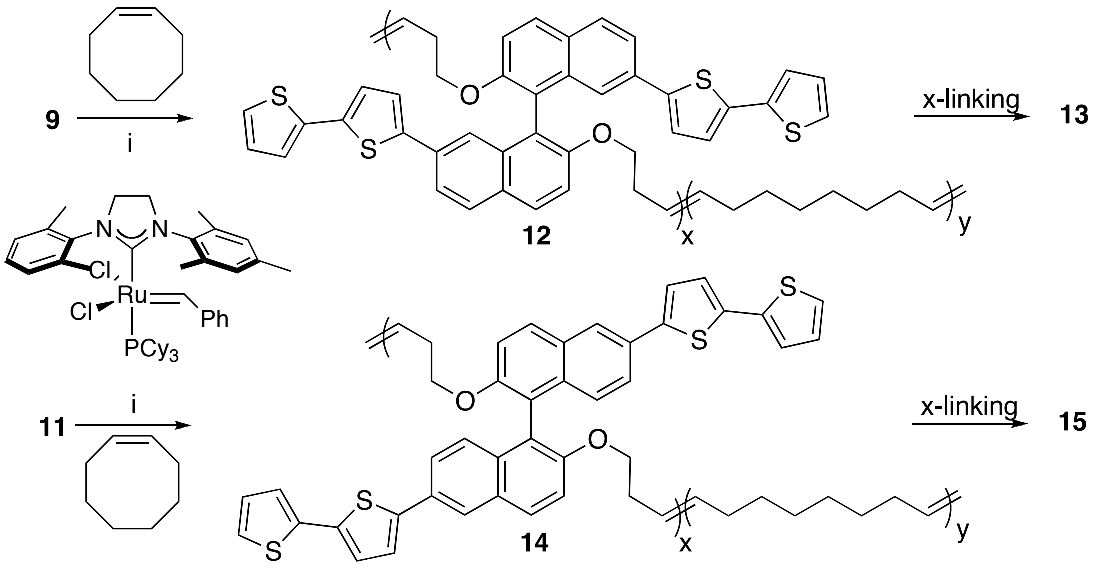

[a]Reagents: (i) CH_2Cl_2, 40 °C, 12 h, ~90%.

The molecular weight of polymer **12** and **14** were satisfactory. The M_n for **12** was 56,300 (PDI = 3.5), and M_n for **14** was 165,000 (PDI = 2.2). The polymers were soluble in $CHCl_3$ and high quality films could be obtained by drop-casting. Initially prepared films were highly fluorescent

(Figure 18a, bottom-right). However, we found that they slowly bleached in air (Figure 18a, bottom-left), probably as a result of oxidation. Storing the polymers in solution ($CHCl_3$) for a long period of time in air resulted in insoluble gel-like precipitates, which is probably due to oxidative cross-linking reactions between the thiophene groups.

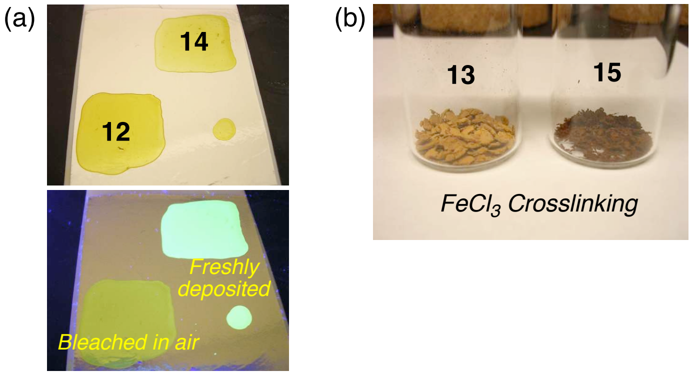

Figure 18. (a) Drop-cast polymers **12** and **14** (top) and their fluorescence under UV (~340nm) (bottom). Note that polymers were slowly bleached in air. (b) Cross-linked polymers **13** and **15** with $FeCl_3$.

To create conducting polymers from these copolymers, we investigated the oxidative cross-linking by $FeCl_3$ in $CHCl_3$. Not surprisingly, insoluble materials were obtained for both polymers (Figure 18b). We also found that the resulting polymers (**13** and **15**) lose their elastomeric properties and were brittle. To create conducting films, we also investigated solid-state oxidative cross-linking method (SOC)[21] by applying potentials to the drop-cast polymers on electrodes (Figure 19). As we swept the potentials, we observed the increasing current resulting from the extended oligothiophenes, but the current was soon saturated. As shown in the insets in Figure 19, the cross-linked polymers retained a green color even after the application of reducing potentials for an extended period of time. This suggests that not all the oxidized species have returned to their reduced (neutral) states, probably due to very low conductivity of the polymer films. We were not able to detect any conductivity in the *in situ* measurements.

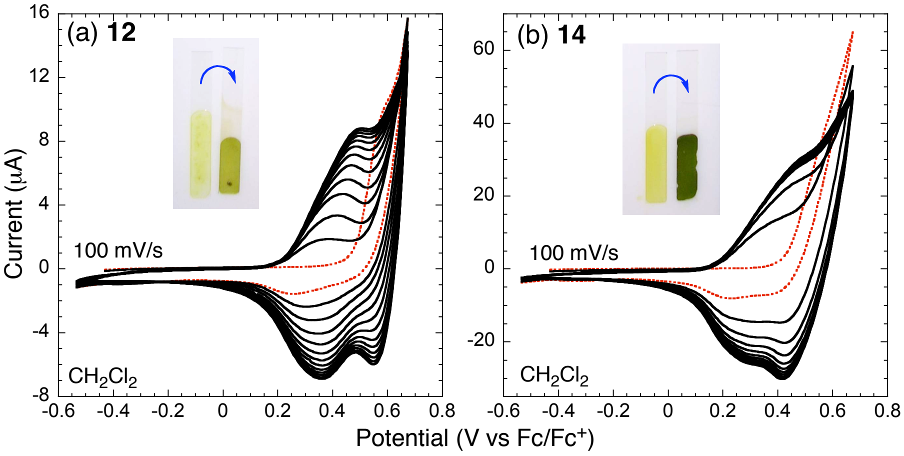

Figure 19. Solid-state oxidative crosslinking (SOC) of polymers **12** (a) and **14** (b) on ITO-coated glass electrodes in CH_2Cl_2 with 0.1 M $TBAPF_6$ as a supporting electrolyte. Insets show the polymer before and after SOC.

Because the conductivity seemed to limit the further cross-linking process, we went on to perform oxidative cross-linking with a chemical oxidant. Drop-cast films that were dipped into a CH_2Cl_2 solution of $SbCl_5$ turned deep green immediately. After washing with pure CH_2Cl_2, we dipped the films into a CH_2Cl_2 solution of N_2H_4 to reduce, which gave orange colors. We were able to repeat the above process many times (Figure 20). Although these films were highly chemo-chromic, the cross-linked orange films were rather brittle and lack the mechanical properties for stretching and actuation properties.

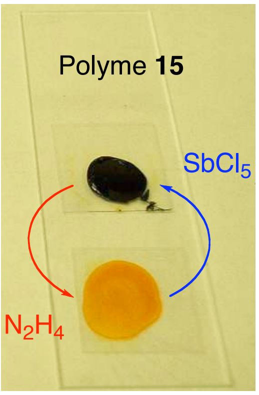

Figure 20. Chemo-chromic responses of polymer **15** to oxidant $SbCl_5$ and reductant N_2H_4.

Conclusion

We designed and synthesized several electropolymerizable monomers containing binaphthyl as molecular hinges and oligothiophenes as electroactive segments. The first generation (6,6'-substituted) polymer resulted in a conductive and thick film, however we were not able to observe any correlation between charges and stress or stain. The second generation (7,7'-substituted) polymer was synthesized and exhibited an interesting chemical transformation to other structures occurring at high oxidation states. The *O*-alkylated second generation polymers appeared to be highly stable. Furthermore, we found in these materials what we believe to be a mixed-valence interaction. In the spectroelectrochemial measurements of *O*-alkylated first and second generation polymers, we observed evidence for inter-chain π-interactions, which were more pronounced in the first generation polymers with linear alkyl chains. In an attempt to align polymers, we synthesized ROMP-polymerizable macrocylic monomers and successfully incorporated them into an elastomeric polymer matrix. However, thiophene-thiophene cross-linkings reduced the polymers' elasticity. Although the resulting polymer showed a very stable electrochemical chromicity, the conductivity of these systems is in need of improvements.

Experimental Section

General. NMR spectra were recorded on a Varian Mercury-300, Bruker Advance-400, or Varian Inova-500 spectrometer. Chemical shifts were reported in ppm and referenced to residual solvent peaks ($CDCl_3$: δ 7.27 ppm for ^1H, δ 77.23 ppm for ^{13}C, CD_2Cl_2: δ 5.32 ppm for ^1H, δ 54.00 ppm for ^{13}C). High-resolution mass spectra (HR-MS) were obtained on a Bruker Daltonics APEX II 3 Tesla FT-ICR-MS. UV-vis spectra were obtained using a HP 8453 diode array spectrometer. Electrochemical measurements were carried out using an Autolab PGSTAT 10 or PGSTAT 20 potentiostat (Eco Chemie) in a three-electrode cell configuration consisting of a quasi-internal Ag wire reference electrode (BioAnalytical Systems) submerged in 0.01 M $AgNO_3$ / 0.1 M tetrabutylammonium hexafluorophosphate ($TBAPF_6$) in anhydrous CH_3CN, a Pt button (1.6 mm in diameter) electrode, 5-μm interdigitated Pt micro-, or ITO-coated glass electrode as the working electrode, and a Pt coil or Pt gauze as the counter electrode. The ferrocene/ferrocenium (Fc/Fc^+) redox couple was used as an external reference. Half-wave potentials of Fc/Fc^+ were observed between 0.210~0.245 V vs Ag/Ag^+ in CH_2Cl_2 and 0.080~0.091 V in CH_3CN. All air and water sensitive synthetic manipulations were performed under an argon or nitrogen atmosphere using standard Schlenk techniques.

Materials. Spectroscopic grade CH_2Cl_2 was purchased from Aldrich for electrochemistry. $TBAPF_6$ was recrystallized in ethanol prior to use. Anhydrous DMF and NMP were purchased from Aldrich as Sure-Seal Bottles and used as received. Anhydrous CH_2Cl_2, THF, and toluene were purified by passing through two alumina columns of an Innovative Technologies purification system. *R*-, *S*-, and racemic 6,6’-dibromo-1,1’-bi-2,2’-naphthol (**1**) were purchased from TCI America. All other chemicals were of reagent grade and used as received. 5-

Tributylstannyl-2,2’-bithiophene was synthesized by a known procedure.[14] Typical Williamson ether synthesis furnished 6,6’-dibromo-2,2’-didecyloxy-1,1’-binaphthalene from **1**.

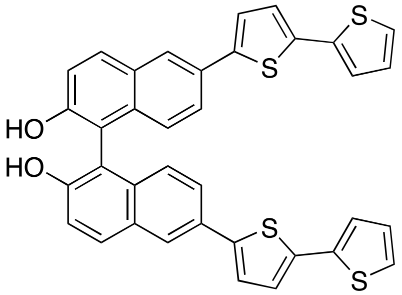

6,6’-Bis(2,2’-bithiophen-5-yl)-1,1’-bi-2,2’-naphthol (2). In a Schlenk tube equipped with a stir bar were combined 6,6’-dibromo-1,1’-bi-2,2’-naphthol (*racemic*-**1**) (0.133 g, 0.30 mmol), $Pd_2(dba)_3{\cdot}CHCl_3$ (9.3 mg, 3 mol %), *t*-Bu_3P (4.0 mg, 6.6 mol %), 5-tributylstannyl-2,2’-bithiophene (0.410 g, 0.90 mmol), KF (0.07 g, 1.2 mmol), and NMP (3 mL) in the glove box. The mixture was allowed to stir at 70 °C for 24 h, at which time it was cooled to room temperature. The mixture was filtered through a pad of celite and thoroughly washed with ethyl acetate. The filtrate was washed with brine (×2), dried over $MgSO_4$, and evaporated under reduced pressure. The crude product was purified by column chromatography (ethyl acetate:hexane = 1:1), and then recrystallization (dichloromethane/hexane). Yield: 0.112 g (61%) of yellow solid. ^1H NMR (400 MHz, $CDCl_3$) δ: 8.09 (d, 2H, *J* = 1.8 Hz), 7.99 (d, 2H, *J* = 9.0 Hz), 7.57 (dd, 2H, *J* = 8.8, 1.8 Hz), 7.43 (d, 2H, *J* = 9.0 Hz), 7.28 (d, 2H, *J* = 3.8 Hz), 7.23 (dd, 2H, *J* = 5.0, 1.1 Hz), 7.22 (dd, 2H, *J* = 3.7, 1.1 Hz), 7.18 (d, 2H, *J* = 8.8 Hz), 7.17 (d, 2H, *J* = 3.8 Hz), 7.04 (dd, 2H, *J* = 5.0, 3.7 Hz), 5.11 (s, 2H). ^{13}C NMR (100 MHz, $CDCl_3$) δ: 153.20, 143.04, 137.59, 136.92, 132.99, 131.67, 130.04, 129.79, 128.10, 125.72, 125.18, 124.90, 124.74, 124.62, 124.06, 123.85, 118.87, 111.40. HR-MS (ESI): calcd for $C_{36}H_{22}O_2S_2$ $[M–H]^-$, 613.0430; found, 613.0418.

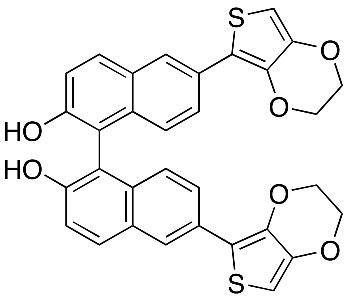

6,6’-Bis(3,4-ethylenedioxythiophen-2-yl)-1,1’-bi-2,2’-naphthol (3). In a Schlenk tube equipped with a stir bar were combined *racemic*-**1** (0.227 g, 0.50 mmol), $Pd_2(dba)_3{\cdot}CHCl_3$ (16 mg, 3 mol %), *t*-Bu_3P (6.7 mg, 6.6 mol %), 5-tributylstannyl-2,2’-bithiophene (0.648 g, 1.5 mmol), KF (0.116 g, 2.0 mmol), and NMP (10 mL) in the glove box. The mixture was allowed to stir at 70 °C for 36 h, at which time it was cooled to room temperature. The mixture was filtered through a pad of celite and thoroughly washed with ethyl acetate. The filtrate was washed with brine (×2), dried over $MgSO_4$, and evaporated under reduced pressure. The crude product was purified by column chromatography (ethyl acetate:hexane = 1:1), and then recrystallization (dichloromethane/hexane). Yield: 0.184 g (66%) of pale yellow solid. ^1H NMR (400 MHz, CD_2Cl_2) δ: 8.24 (d, 2H, *J* = 1.9 Hz), 7.99 (d, 2H, *J* = 8.9 Hz), 7.65 (d, 2H, *J* = 8.9, 1.9 Hz), 7.36 (d, 2H, *J* = 8.9 Hz), 7.11 (d, 2H, *J* = 8.9 Hz), 6.31 (s, 2H), 5.22 (s, 2H), 4.28 (m, 8H). ^{13}C NMR (125 MHz, CD_2Cl_2) δ: 153.26, 143.01, 139.01, 132.70, 131.92, 130.16, 129.53, 126.39, 125.32, 124.97, 118.76, 117.42, 111.68, 98.04, 65.42, 65.12. HR-MS (ESI): calcd for $C_{32}H_{22}O_6S_2$ $[M+Na]^+$, 589.0750; found, 589.0764.

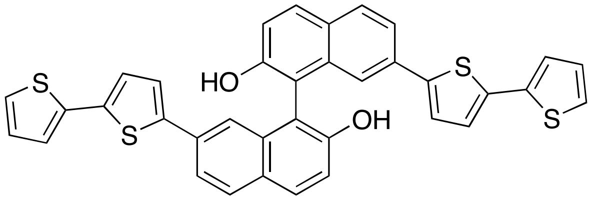

7,7'-Bis(2,2'-bithiophen-5-yl)-1,1'-bi-2,2'-naphthol (5). In a Schlenk tube equipped with a stir bar were combined 7,7'-dibromo-1,1'-bi-2,2'-naphthol (**4**) (0.045 g, 0.10 mmol), $PdCl_2(PPh_3)_2$ (3.6 mg, 5 mol %), and toluene (3 mL) under Ar. To the mixture was added 5-tributylstannyl-2,2'-bithiophene (0.137 g, 0.30 mmol), and the mixture was allowed to stir at 80 °C for 18 h. After being cooled to room temperature, the mixture was filtered through a pad of silica gel and thoroughly washed with ethyl acetate. The filtrate was evaporated under reduced pressure and purified by column chromatography (ethyl acetate:hexane = 1:2). Yield: 0.050 g (81%) of yellow solid. ^{1}H NMR (400 MHz, $CDCl_3$) δ: 8.92 (d, 2H, *J* = 8.9 Hz), 7.94 (d, 2H, *J* = 8.5 Hz), 7.64 (dd, 2H, *J* = 8.5, 1.8 Hz), 7.41 (d, 2H, *J* = 8.9 Hz), 7.38 (bs, 2H), 7.19 (dd, 2H, *J* = 5.1, 1.1 Hz), 7.12 (dd, 2H, *J* = 3.6, 1.1 Hz), 7.08 (d, 2H, *J* = 3.8 Hz), 7.04 (d, 2H, *J* = 3.8 Hz), 6.98 (dd, 2H, *J* = 5.1, 3.6 Hz), 5.25 (s, 2H). ^{13}C NMR (125 MHz, $CDCl_3$) δ: 153.69, 143.06, 137.48, 133.79, 133.47, 131.67, 129.54, 129.04, 128.55, 128.02, 124.80, 124.77, 124.66, 123.97, 122.78, 120.25, 118.07, 110.83. HR-MS (ESI): calcd for $C_{36}H_{22}O_2S_4$ $[M+Na]^+$, 637.0395; found, 637.0396.

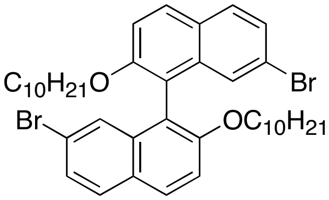

7,7'-dibromo-2,2'-didecyloxy-1,1'-binaphthalene (6a). In a round-bottom flask equipped with a stir bar and a refluxing condensor were combined **4** (1.36 g, 3.0 mmol), K_2CO_3 (2.90 g, 21 mmol), and acetone (30 mL). To the mixture was slowly added 1-bromodecane (3.18 mL, 15 mmol), and the mixture was allowed to reflux overnight. After most of acetone was evaporated under reduced pressure, the mixture was diluted with dichloromethane and washed with water and brine (×2). The filtrate was evaporated under reduced pressure and purified by recrystallization (dichloromethane/hexane). Yield: 1.87 g (86%) of white solid. ^{1}H NMR (400 MHz, $CDCl_3$) δ: 7.90 (d, 2H, *J* = 9.1 Hz), 7.72 (d, 2H, *J* = 8.6 Hz), 7.41 (d, 2H, *J* = 9.1 Hz), 7.39 (dd, 2H, *J* = 8.6, 1.9 Hz), 7.29 (d, 2H, *J* = 1.9 Hz), 3.96 (m, 4H), 1.40 (m, 4H), 1.35~1.01 (m, 28H), 0.90 (t, 6H, *J* = 6.8 Hz). ^{13}C NMR (100 MHz, $CDCl_3$) δ: 155.31, 135.52, 129.79, 129.59, 127.70, 127.47, 127.04, 121.06, 118.32, 115.62, 69.52, 53.64, 32.13, 29.67, 29.56, 29.46, 29.37, 25.82, 22.93, 14.36. HR-MS (ESI): calcd for $C_{40}H_{52}Br_2O_2$ $[M+Na]^+$, 745.2226; found, 745.2213.

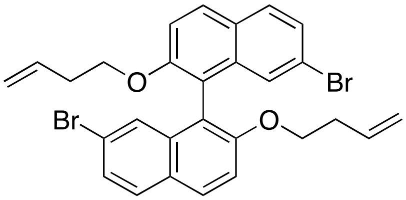

7,7'-dibromo-2,2'-di(3-butenyloxy)-1,1'-binaphthalene (6b). Similar to the preparation of **6a** except using 4-bromo-1-butene (0.305 mL, 3.0 mmol) instead of 1-bromodecane, starting with **4** (1.36 g, 3.0 mmol). Yield: 0.258 g (78%) of white solid. ^{1}H NMR (400 MHz, $CDCl_3$) δ: 7.92 (d, 2H, *J* = 9.0 Hz), 7.74 (d, 2H, *J* = 8.7 Hz), 7.44 (dd, 2H, *J* = 8.7, 1.8 Hz), 7.42 (d, 2H, *J* = 9.0 Hz), 7.37 (d, 2H, *J* = 1.8 Hz), 5.44 (m, 2H), 4.84 (m, 2H), 4.80 (m, 2H), 4.05 (m, 4H), 2.19 (m, 4H). ^{13}C NMR (100 MHz, $CDCl_3$) δ: 154.98, 135.41, 134.23, 129.82, 129.68, 127.73, 127.41, 127.11, 121.15, 118.77, 116.80, 115.44, 68.75, 33.88. HR-MS (ESI): calcd for $C_{28}H_{24}Br_2O_2$ $[M+Na]^+$, 573.0035; found, 573.0043.

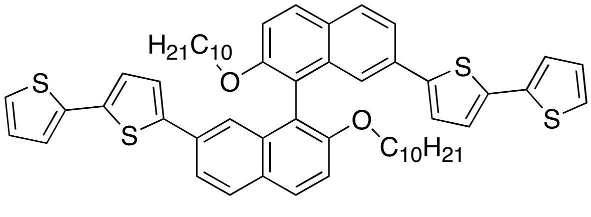

7,7’-Bis(2,2’-bithiophen-5-yl)-2,2’-didecyloxy-1,1’-binaphthalene (7). In a Schlenk tube equipped with a stir bar were combined **6a** (0.073 g, 0.099 mmol), $PdCl_2(PPh_3)_2$ (3.2 mg, 5 mol %), and DMF (2 mL) under Ar. To the mixture was added 5-tributylstannyl-2,2’-bithiophene (0.112 mL, 0.30 mmol), and the mixture was allowed to stir at 80 °C for 18 h. After being cooled to room temperature, the mixture was filtered through a pad of silica gel and thoroughly washed with ethyl acetate. The filtrate was washed with water and brine, dried over $MgSO_4$, and evaporated under reduced pressure. The crude product was purified by column chromatography (dichloromethane:hexane = 1:2). Yield: 0.062 g (70%) of yellow solid. ^1H NMR (400 MHz, $CDCl_3$) δ: 7.96 (d, 2H, J = 9.0 Hz), 7.89 (d, 2H, J = 8.5 Hz), 7.59 (dd, 2H, J = 8.5, 1.7 Hz), 7.48 (d, 2H, J = 1.7 Hz), 7.44 (d, 2H, J = 9.0 Hz), 7.17 (dd, 2H, J = 5.1, 1.1 Hz), 7.12 (d, 2H, J = 3.6, 1.1 Hz), 7.06 (d, 2H, J = 3.7 Hz), 7.04 (d, 2H, J = 3.7 Hz), 6.98 (dd, 2H, J = 5.1, 3.6 Hz), 4.01 (m, 4H), 1.42 (m, 4H), 1.35~1.09 (m, 28H), 0.91 (t, 6H, J = 7.2 Hz). ^{13}C NMR (125 MHz, $CDCl_3$) δ: 155.20, 144.01, 137.66, 136.68, 134.50, 131.73, 129.31, 128.82, 128.76, 127.92, 124.69, 124.35, 124.03, 123.68, 122.01, 121.92, 120.23, 115.45, 69.60, 32.13, 29.69, 29.68, 29.58, 29.57, 29.42, 25.83, 22.93, 14.39. HR-MS (ESI): calcd for $C_{56}H_{62}O_2S_4$ $[M]^+$, 894.3627; found, 894.3607.

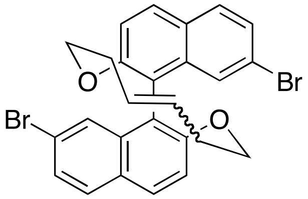

Compound 8. In a Schlenk flask equipped with a stir bar were placed **6b** (1.43 g, 2.5 mmol) and anhydrous CH_2Cl_2 (250 mL) was added under Ar. To the mixture was added a solution of Grubbs 1st generation catalyst (0.103 g, 5 mol%) in CH_2Cl_2 (10 mL), and the mixture was

allowed to stir at room temperature for 2 h, at which time ~1 mL of ethyl vinyl ether was added. After being stirred for 30 min more, the mixture was evaporated under reduced pressure and subjected to column chromatography (ethyl acetate:hexane = 1:10). The product was further purified by recrystallization (chloroform/hexane). Yield: 0.963 g (73%) of white solid with *cis*:*trans* = 91:9. ^{1}H NMR (*cis*, 400 MHz, CD_2Cl_2) δ: 7.98 (d, 2H, *J* = 9.0 Hz), 7.80 (d, 2H, *J* = 8.7 Hz), 7.50 (d, 2H, *J* = 9.0 Hz), 7.44 (dd, 2H, *J* = 8.7, 1.8 Hz), 7.27 (d, 2H, *J* = 1.8 Hz), 5.07 (*pseudo*-t, 2H, *J* = 3.4 Hz), 4.55 (ddd, 2H, *J* = 12, 5.2, 3.2 Hz), 4.06 (td, 2H, *J* = 12, 4.3 Hz), 2.52 (m, 2H), 2.20 (m, 2H). ^{13}C NMR (*cis*, 125 MHz, CD_2Cl_2) δ: 153.43, 136.29, 130.29, 129.67, 129.08, 127.89, 127.46, 127.32, 121.32, 119.50, 116.04, 66.71, 31.41.

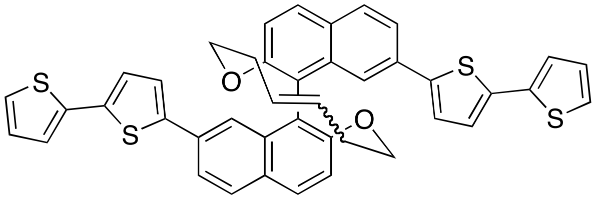

Compound 9. Using the same procedure for the synthesis of **7**, **6b** (0.55 g, 1.03 mmol) was treated with $PdCl_2(PPh_3)_2$ (43 mg, 6 mol %), DMF (10 mL), and 5-tributylstannyl-2,2'-bithiophene (1.16 mL, 3.09 mmol) under Ar. Yield: 0.484 g (67%) of yellow solid with *cis* >95%. ^{1}H NMR (*cis*, 400 MHz, $CDCl_3$) δ: 7.93 (d, 2H, *J* = 9.0 Hz), 7.88 (d, 2H, *J* = 8.5 Hz), 7.57 (dd, 2H, *J* = 8.5, 1.8 Hz), 7.42 (d, 2H, *J* = 9.0 Hz), 7.41 (d, 2H, *J* = 1.8 Hz), 7.17 (dd, 2H, *J* = 5.1, 1.1 Hz), 7.11 (dd, 2H, *J* = 3.6, 1.1 Hz), 7.04 (d, 2H, *J* = 3.8 Hz), 7.02 (d, 2H, *J* = 3.8 Hz), 6.97 (dd, 2H, *J* = 5.1, 3.6 Hz), 5.05 (*pseudo*-t, 2H, *J* = 3.3 Hz), 4.47 (ddd, 2H, *J* = 12, 4.5, 3.4 Hz), 4.02 (td, 2H, *J* = 12, 4.1 Hz), 2.49 (m, 2H), 2.13 (m, 2H). ^{13}C NMR (*cis*, 125 MHz, CD_2Cl_2) δ: 152.79, 144.07, 137.66, 136.72, 135.09, 131.81, 128.88, 128.82, 128.81, 128.51, 127.94,

124.69, 124.35, 124.21, 123.71, 122.05, 122.05, 120.75, 115.20, 66.22, 31.23. HR-MS (ESI): calcd for $C_{42}H_{30}O_2S_4$ $[M+Na]^+$, 717.1021; found, 717.1003.

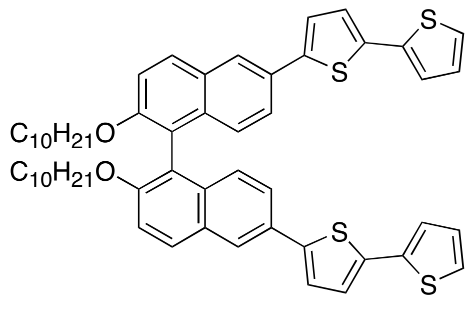

6,6'-Bis(2,2'-bithiophen-5-yl)-2,2'-didecyloxy-1,1'-binaphthalene (10). Using the same procedure for the synthesis of **7**, 6,6'-dibromo-2,2'-didecyloxy-1,1'-binaphthalene (0.034 g, 0.046 mmol) was treated with $PdCl_2(PPh_3)_2$ (1.6 mg, 5 mol %), DMF (1 mL), and 5-tributylstannyl-2,2'-bithiophene (0.052 mL, 0.138 mmol) under Ar. Yield: 0.031 g (75%) of yellow solid. ^1H NMR (400 MHz, $CDCl_3$) δ: 8.07 (d, 2H, *J* = 1.8 Hz), 7.96 (d, 2H, *J* = 9.0 Hz), 7.49 (dd, 2H, *J* = 8.9, 1.8 Hz), 7.44 (d, 2H, *J* = 9.0 Hz), 7.27 (d, 2H, *J* = 3.9 Hz), 7.23~7.21 (m, 4H), 7.20 (d, 2H, *J* = 8.9 Hz), 7.16 (d, 2H, *J* = 3.9 Hz), 7.04 (dd, 2H, *J* = 4.9, 3.8 Hz), 3.98 (m, 4H), 1.44 (m, 4H), 1.34–1.10 (m, 28H), 0.87 (t, 6H, *J* = 6.9 Hz). ^{13}C NMR (125 MHz, $CDCl_3$) δ: 155.05, 143.75, 137.80, 136.42, 133.73, 129.52, 129.45, 129.29, 128.04, 126.31, 124.82, 124.44, 124.40, 124.24, 123.65, 123.64, 120.58, 116.48, 69.84, 32.15, 29.78, 29.76, 29.58, 29.42, 25.93, 22.93, 14.36. HR-MS (ESI): calcd for $C_{56}H_{62}O_2S_4$ $[M]^+$, 894.3627; found, 894.3611.

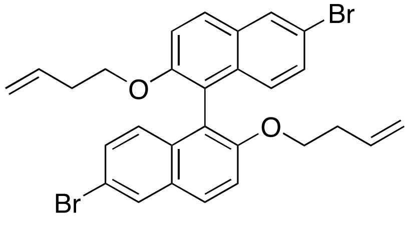

6,6'-dibromo-2,2'-di(3-butenyloxy)-1,1'-binaphthalene (A). Using the same procedure as for the preparation of **6a**, **1** (0.453 g, 1.0 mmol) was treated with K_2CO_3 (0.967 g, 7 mmol), acetone (10 mL), and 4-bromo-1-butene (0.508 mL, 5.0 mmol). Yield: 0.442 g (80%) of white solid. ^{1}H NMR (400 MHz, $CDCl_3$) δ: 8.04 (d, 2H, *J* = 2.0 Hz), 7.86 (d, 2H, *J* = 9.0 Hz), 7.43 (d, 2H, *J* = 9.0 Hz), 7.31 (dd, 2H, *J* = 9.0, 2.0 Hz), 7.03 (d, 2H, *J* = 9.0 Hz), 5.45 (m, 1H), 4.84 (m, 1H), 4.80 (m, 1H), 4.01 (m, 2H), 2.19 (q, 2H, *J* = 6.8 Hz). ^{13}C NMR (100 MHz, $CDCl_3$) δ: 154.65, 134.31, 132.70, 130.44, 129.97, 129.72, 128.67, 127.32, 120.14, 117.53, 116.80, 116.48, 69.01, 33.95. HR-MS (ESI): calcd for $C_{28}H_{24}Br_2O_2$ $[M+Na]^+$, 573.0035; found, 573.0050.

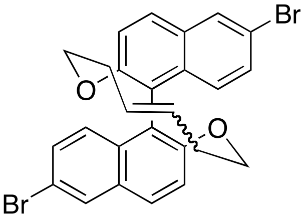

Compound B. Using the same procedure as for the preparation of **8**, **A** (1.66 g, 3.0 mmol) was treated with Grubbs 1st generation catalyst (0.123 g, 5 mol%) in anhydrous CH_2Cl_2 (300 mL). Yield: 1.38 g (88%) of white solid with *cis*:*trans* = 81:19. ^{1}H NMR (400 MHz, $CDCl_3$), for *cis*, δ: 8.02 (d, 2H, *J* = 2.0 Hz), 7.85 (d, 2H, *J* = 9.0 Hz), 7.42 (d, 2H, *J* = 9.0 Hz), 7.29 (dd, 2H, *J* = 9.0, 2.0 Hz), 7.00 (d, 2H, *J* = 9.0 Hz), 5.02 (*pseudo*-t, 2H, *J* = 4.0 Hz), 4.45 (ddd, 2H, *J* = 12, 6.0, 3.7 Hz), 4.03 (td, 2H, *J* = 11, 4.3 Hz), 2.48 (m, 2H), 2.15 (m, 2H). For *trans*, δ: 8.02 (d, 2H, *J* = 2.0 Hz), 7.85 (d, 2H, *J* = 9.0 Hz), 7.46 (d, 2H, *J* = 9.2 Hz), 7.27 (dd, 2H, *J* = 8.9, 2.0 Hz), 6.94 (d, 2H, *J* = 9.0 Hz), 5.28 (t, 2H, *J* = 5.1 Hz), 4.58 (ddd, 2H, *J* = 12, 7.2, 2.0 Hz), 3.96 (ddd, 2H, *J* = 12, 7.4, 2.4 Hz), 2.28 (m, 2H), 2.15 (m, 2H). ^{13}C NMR (100 MHz, $CDCl_3$), for *cis,* δ: 152.40, 133.20, 130.16, 129.95, 129.71, 128.74, 128.26, 127.40, 120.46, 117.48, 116.14, 66.40, 31.11.

For *trans*, δ: 153.61, 133.12, 130.02, 129.83, 129.38, 128.47, 127.26, 123.66, 120.28, 117.48, 115.28, 66.98, 28.41. HR-MS (ESI): calcd for $C_{26}H_{20}Br_2O_2$ $[M+Na]^+$, 544.9722; found, 544.9739.

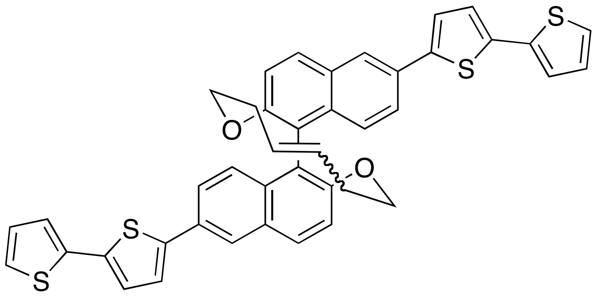

Compound 11. Using the same procedure for the synthesis of **7**, **B** (1.06 g, 2.0 mmol) was treated with $PdCl_2(PPh_3)_2$ (84 mg, 6 mol %), DMF (20 mL), and 5-tributylstannyl-2,2'-bithiophene (2.26 mL, 3.0 mmol) under Ar. Yield: 0.805 g (58%) of yellow solid with *cis*:*trans* = 75:25. ^1H NMR (300 MHz, $CDCl_3$), for *cis*, δ: 8.07 (d, 2H, *J* = 1.8 Hz), 7.97 (d, 2H, *J* = 9.0 Hz), 7.50 (dd, 2H, *J* = 9.0, 1.8 Hz), 7.45 (d, 2H, *J* = 9.0 Hz), 7.26 (d, 2H, *J* = 3.9 Hz), 7.23–7.22 (m, 4H), 7.18 (d, 2H, *J* = 9.0 Hz), 7.16 (d, 2H, *J* = 3.9 Hz), 7.04 (dd, 2H, *J* = 5.1, 3.9 Hz), 5.09 (*pseudo*-t, 2H, *J* = 3.3 Hz), 4.49 (ddd, 2H, *J* = 11, 4.5, 3.6 Hz), 4.06 (td, 2H, *J* = 11, 4.2 Hz), 2.51 (m, 2H), 2.18 (m, 2H). ^{13}C NMR (100 MHz, $CDCl_3$), for *cis*, δ: 152.57, 143.79, 137.79, 136.44, 134.19, 129.38, 129.23, 129.20, 128.84, 128.05, 126.29, 124.85, 124.65, 124.43, 124.35, 123.69, 120.70, 115.91, 66.54, 31.19. HR-MS (ESI): calcd for $C_{42}H_{30}O_2S_4$ $[M]^+$, 694.1123; found, 694.1147.

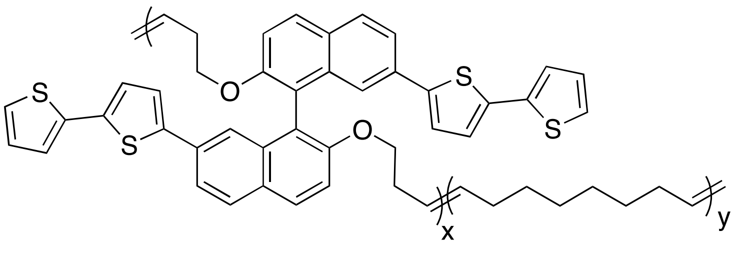

Polymer 12. In a Schlenk flask equipped with a stir bar were combined **9** (0.094 g, 0.13 mmol), cyclooctene (0.073 mL, 0.52 mmol), and anhydrous CH_2Cl_2 (1.2 mL) in a glove box. To the mixture was added a solution of Grubbs 2nd generation catalyst (0.00056 g, 0.1 mol % wrt total monomers) in CH_2Cl_2 (0.1 mL), and the mixture was allowed to stir at 40 °C for 12 h. To the mixture was added MeOH to precipitate out the caramel-like solid. The crude product was redissolved with $CHCl_3$ and precipitated again with hexane. The precipitation was repeated once more with $CHCl_3$ and acetone. Yield: 0.132 g (86%) of yellowish tacky solid (x:y = 1:6). GPC (polystyrene standard): M_n = 56,300, M_w = 196,000, PDI = 3.5. ^{1}H NMR (400 MHz, $CDCl_3$) δ: 7.94 (aromatic C-H), 7.88 (aromatic C-H), 7.59 (aromatic C-H), 7.46 (aromatic C-H), 7.44 (aromatic C-H), 7.27–6.97 (aromatic C-H), 5.39 (vinyl C-H), 5.15 (vinyl C-H), 4.98 (vinyl C-H), 4.04–3.96 (aliphatic C-H), 2.08–1.98 (aliphatic C-H), 1.70 (aliphatic C-H), 1.30–1.07 (aliphatic C-H).

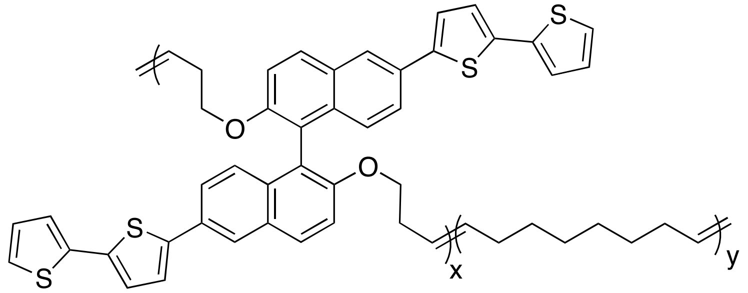

Polymer 14. Using the same procedure as for the synthesis of **12**, **11** (0.071 g, 0.1 mmol) was treated with cyclooctene (0.0548 mL, 0.4 mmol), Grubbs 2nd generation catalyst (0.00042 g, 0.1 mol % wrt total monomers), and anhydrous CH_2Cl_2 (1.0 mL). Yield: 0.132 g (86%) of yellowish tacky solid (x:y = 1:7). GPC (polystyrene standard): M_n = 165,000, M_w = 367,000, PDI = 2.23. ^{1}H NMR (400 MHz, $CDCl_3$) δ: 8.06 (aromatic C-H), 7.93 (aromatic C-H), 7.47 (aromatic C-H), 7.42 (aromatic C-H), 7.27–7.02 (aromatic C-H), 5.38 (vinyl C-H), 5.18 (vinyl C-H), 5.00 (vinyl

C-H), 3.97–3.93 (aliphatic C-H), 2.10–1.95 (aliphatic C-H), 1.72 (aliphatic C-H), 1.28–1.05 (aliphatic C-H)

References and Notes

(1) (a) Anquetil, P. A.; Yu, H. -h.; Madden, J. D.; Madden, P. G.; Swager, T. M.; Hunter, I. W. *Smart Structures and Materials 2002: EAPAD, Proc. Of SPIE* **2002,** *4695,* 424–434. (b) Yu, H. -h.; Xu, B.; Swager, T. M. *J. Am. Chem. Soc.* **2003,** *125,* 1142–1143. (c) Yu, H. -h.; Swager, T. M. *IEEE J. Oceanic Eng.* **2004,** *29,* 692–695.

(2) (a) Marsella, M. J. *Acc. Chem. Res.* **2002**, *35*, 944–951. (b) Marsella, M. J.; Reid, R. J.; Estassi, S.; Wang, L. -S. *J. Am. Chem. Soc.* **2002**, *124*, 12507–12510.

(3) Yu, H. –h. Ph.D. Thesis, Massachusetts Institute of Technology, 2003.

(4) Pu, L. *Chem. Rev.* **1998**, *98*, 2405–2494, and references therein.

(5) *Handbook of Conducting Polymers (Conjugated Polymers: Theory, Synthesis, Properties, and Characterization),* 3rd Ed; Skotheim, T. A., Reynolds, J. R., Eds.; CRC Press: New York, 2006.

(6) For polaron and bipolaron, see Chapter 2.

(7) (a) *Electroactive Polymer Electrochemistry*; Lyons, E. G., Ed.; Plenum Press: New York, 1994. (b) Cameron, C. G. Thesis, Califonia Institute of Technology, 2001.

(8) Yoon, M. –H.; DiBenedetto, S. A.; Facchetti, A.; Marks, T. J. *J. Am. Chem. Soc.* **2005,** *127,* 1348–1349.

(9) Vandesteeg, N. Ph.D. Thesis, Massachusetts Institute of Technology, 2006.

(10) Paul, E. W.; Ricco, A. J.; Wrighton, M. S. *J. Phys. Chem.* **1985,** *89,* 1441–1447.

(11) (a) Bandin, M.; Casolari, S.; Cozzi, P. G.; Proni, G.; Schmohel, E.; Spada, G. P.; Tagliavini, E.; Umani-Ronchi, A. *Eur. J. Org. Chem.* **2000**, 491–497. (b) Lustenberger, P.; Diederich, F. *Helv. Chim. Acta* **2000**, *83*, 2865–2883.

(12) Song, C.; Swager, T. M. *Macromolecules*, **2005**, *38*, 4569–4575.

(13) Nishinaga, T.; Wakamiya, A.; Yamazaki, D.; Komatsu, K. *J. Am. Chem. Soc.* **2004,** *126,* 3163–3174.

(14) Child, A. D.; Sankaran, B.; Larmat, F.; Reynolds, J. R. *Macromolecules* **1995**, *28*, 6571–6578.

(15) (a) Kingsbotough, R. P.; Swager, T. M. *J. Am. Chem. Soc.* **1999,** *121,* 8825–8834. (b) see Chapter 2.

(16) (a) Bäuerle, P.; Segelbacher, U.; Maier, A.; Mehring, M. *J. Am. Chem. Soc.* **1993,** *115,* 10217–10223. (b) Miller, L. L.; Mann, K. R. *Acc. Chem. Res.* **1996,** *29,* 417–423. (c) Graf, D. D.; Duan, R. G.; Campbell, J. P.; Miller, L. L.; Mann, K. R. *J. Am. Chem. Soc.* **1997,** *119,* 5888–5899. (d) Satou, T.; Sakai, T.; Kaikawa, T.; Takimiya, K.; Otsubo, T.; Aso, Y. *Org. Lett.* **2004,** *6,* 997–1000. (e) Sakai, T.; Satou, T.; Kaikawa, T.; Takimiya, K.; Otsubo, T.; Aso, Y. *J. Am. Chem. Soc.* **2005,** *127,* 8082–8089. (f) Knoblock, K. M.; Silvestri, C. J.; Collard, D. M. *J. Am. Chem. Soc.* **2006,** *128,* 13680–13681. (g) Yamazaki, D.; Nishinaga, T.; Tanino, N.; Komatsu, K. *J. Am. Chem. Soc.* **2006,** *128,* 14470–14471.

(17) (a) Thulstrup, E. W.; Michl, J.; Eggers, J. H. *J. Phys. Chem.* **1970**, *74*. 3868–3878. (b) Michl, J.; Thulstrup, E. W.; Eggers, J. H. *J. Phys. Chem.* **1970**, *74*. 3878–3884. (c) Long, T. M.; Swager, T. M. *Adv. Mater.* **2001**, *13*. 601–604. (d) Frackowiak, D.; Ptak, A.; Gryczynski, Z.; Gryczynski, I.; Targowski, P.; Zelent, B. *Photochem. Photobiol.* **2004**, *79*. 11–20.

(18) (a) Gottarelli, G.; Hibert, M.; Samori, B.; Solladié, G.; Spada, G. P.; Zimmermann, R. *J. Am. Chem. Soc.* **1983**, *105*, 7318–7321. (b) Gottarelli, G.; Spada, G. P. *J. Org. Chem.* **1986**, *51*, 589–592. (c) Deußen, H. –J.; Shibaev, P. V.; Vinokur, R.; Bjørnholm, T.;

Schaumburg, K.; Bechgaard, K.; Shibaev, V. P. *Liq. Cryst.* **1996**, *21*, 327–340. (d) Ferrarini, A.; Nordio, P. L.; Shibaev, P. V.; Shibaev, V. P. *Liq. Cryst.* **1998**, *24*, 219–227.

(19) ROMP is a polymerization method utilizing the olefin metathesis reaction and involves (strained) cyclic olefins. The relief of ring strains is the driving force for the polymerization.

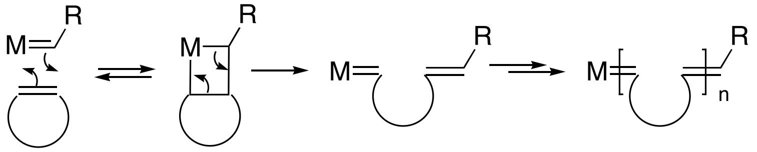

For more details, see *Olefin Metathesis and Metathesis Polymerization*; Ivin, K. J., Mol, J. C., Eds.; Academic Press: San Diego, 1997.

(20) Slugovc, C. *Macromol. Rapid Commun.* **2004**, *25*, 1283–1297.

(21) (a) Watson, K. J.; Wolfe, P. S.; Nguyen, S. T.; Zhu, J.; Mirkin, C. A. *Macromolecules* **2000**, *33*, 4628–4633. (b) Jang, S. –Y.; Sotzing, G. A. *Macromolecules* **2002**, *35*, 7293–7300. (c) Jang, S. –Y.; Marquez, M.; Sotzing, G. A. *J. Am. Chem. Soc.* **2004**, *126*, 9476–9477. (d) Jang, S. –Y.; Sotzing, G. A.; Marquez, M. *Macromolecules* **2004**, *37*, 4351–4359. (e) Stepp, B. R.; Nguyen, S. T. *Macromolecules* **2004**, *37*, 8222–8229.

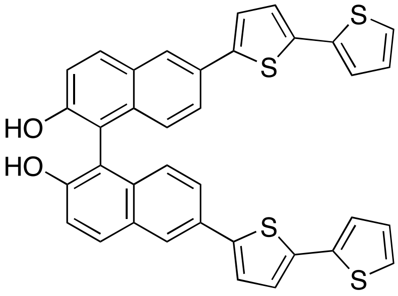

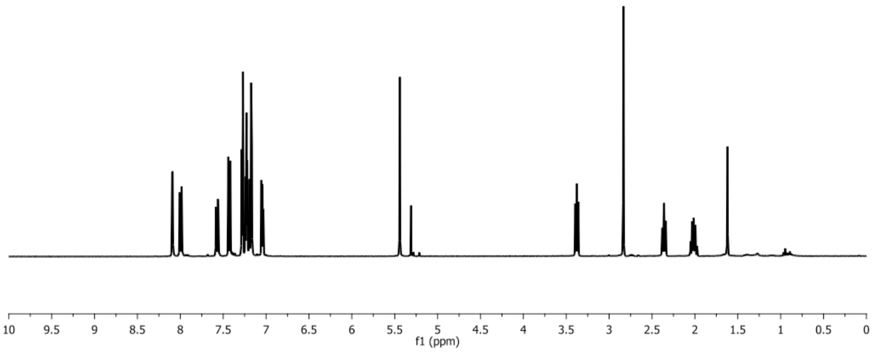

Spectrum 1. ^{1}H-NMR spectrum of **2** (400 MHz, $CDCl_3$).

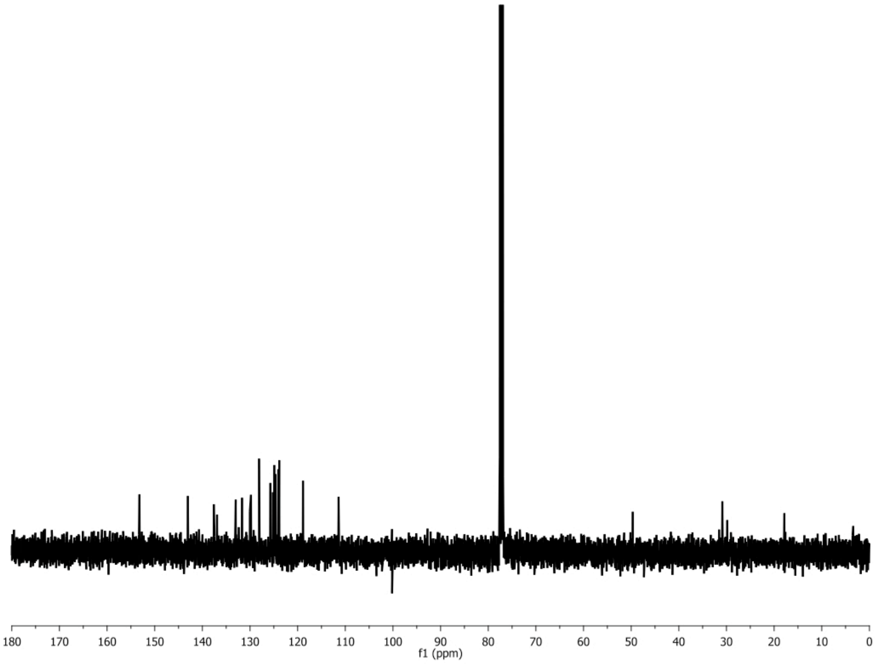

Spectrum 2. ^{13}C-NMR spectrum of **2** (100 MHz, $CDCl_3$).

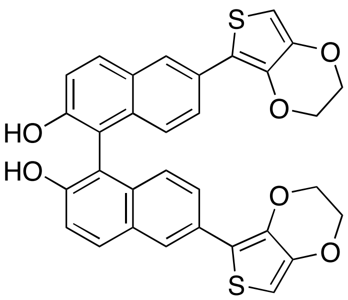

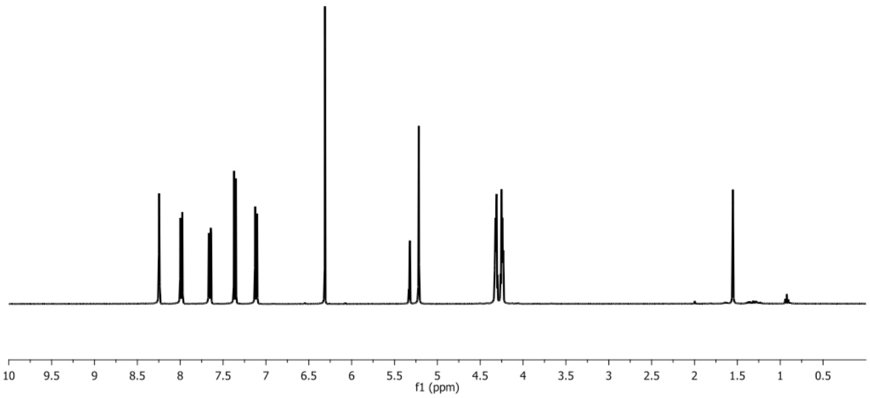

Spectrum 3. ^{1}H-NMR spectrum of **3** (400 MHz, CD_2Cl_2).

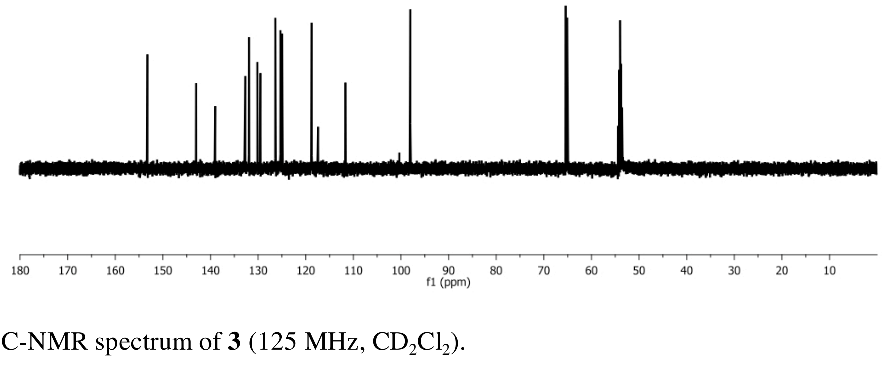

Spectrum 4. ^{13}C-NMR spectrum of **3** (125 MHz, CD_2Cl_2).

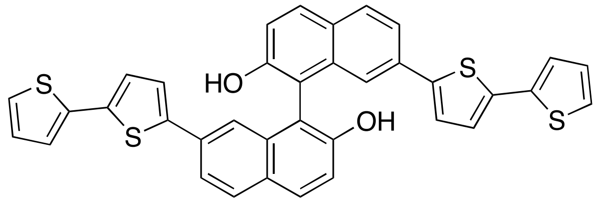

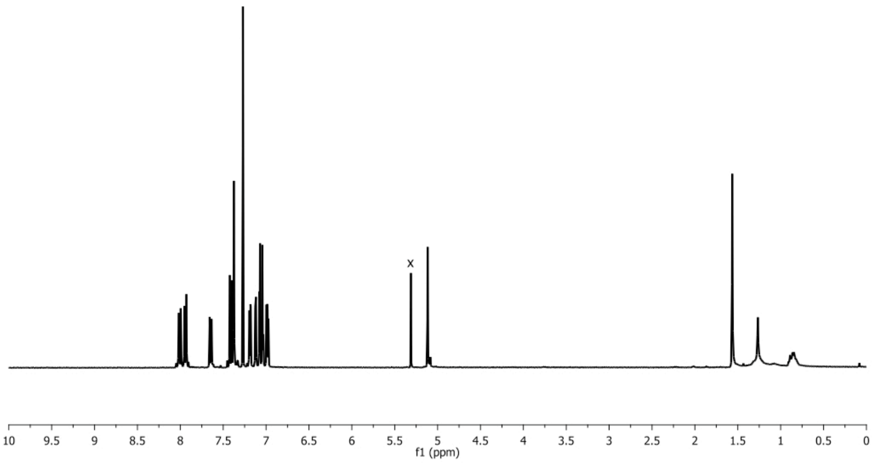

Spectrum 5. ^{1}H-NMR spectrum of **5** (400 MHz, CDCl$_3$).

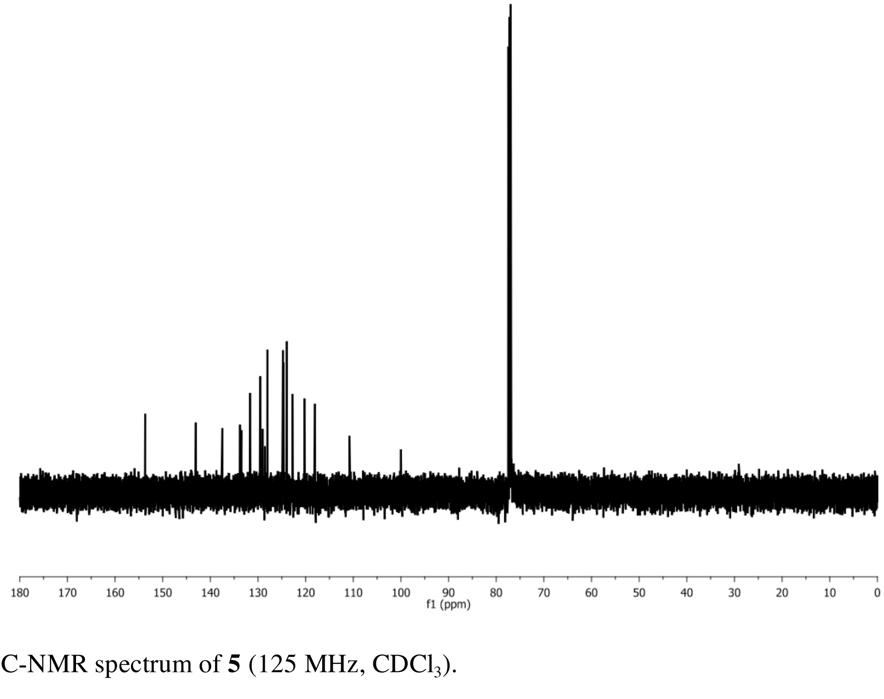

Spectrum 6. ^{13}C-NMR spectrum of **5** (125 MHz, CDCl$_3$).

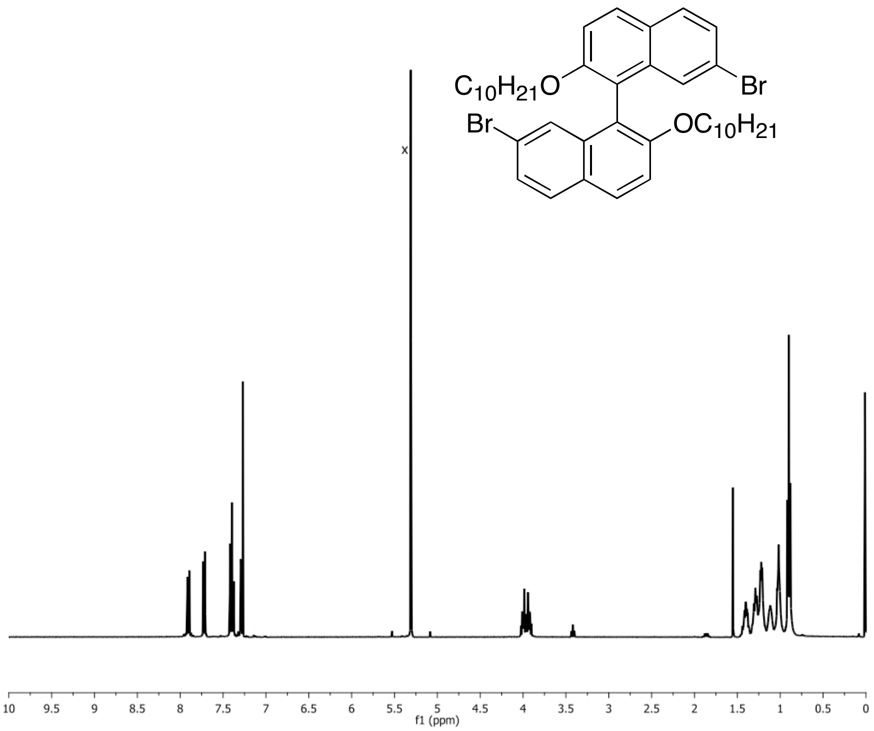

Spectrum 7. ^{1}H-NMR spectrum of **6a** (400 MHz, $CDCl_3$).

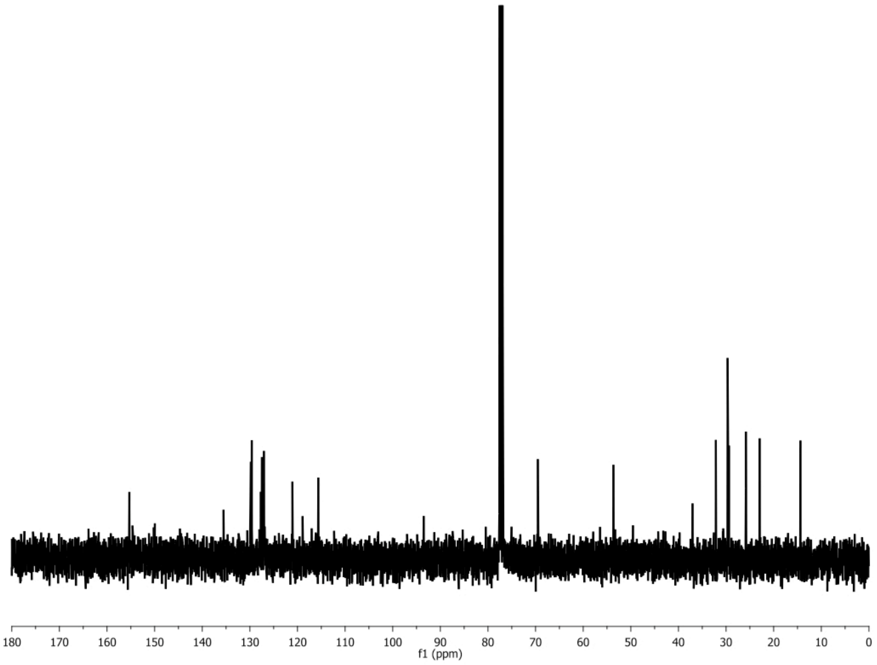

Spectrum 8. ^{13}C-NMR spectrum of **6a** (100 MHz, $CDCl_3$).

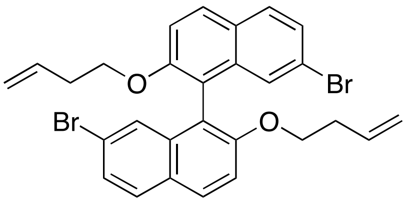

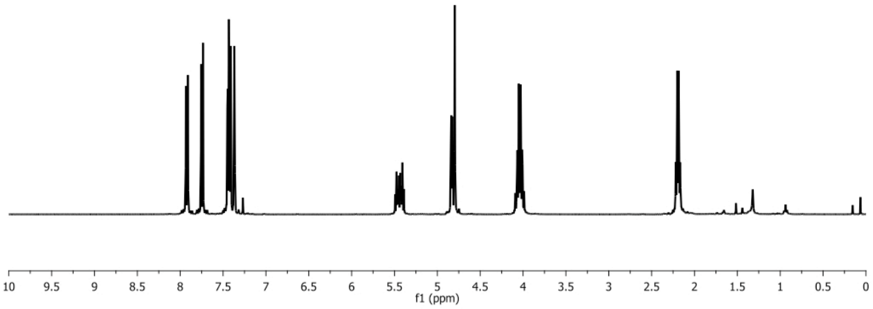

***Spectrum 9**.* ^{1}H-NMR spectrum of **6b** (400 MHz, $CDCl_3$).

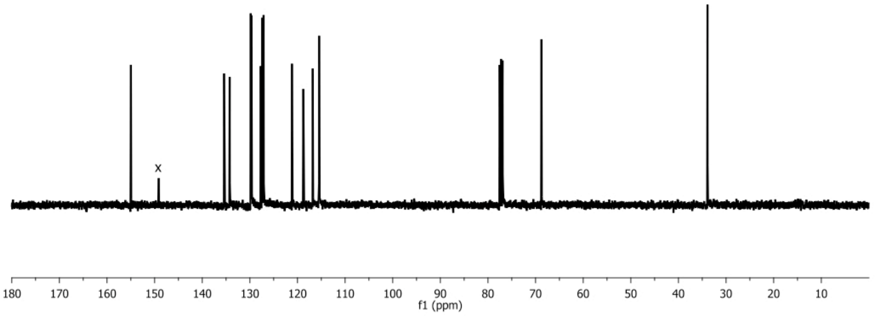

***Spectrum 10**.* ^{13}C-NMR spectrum of **6b** (100 MHz, $CDCl_3$).

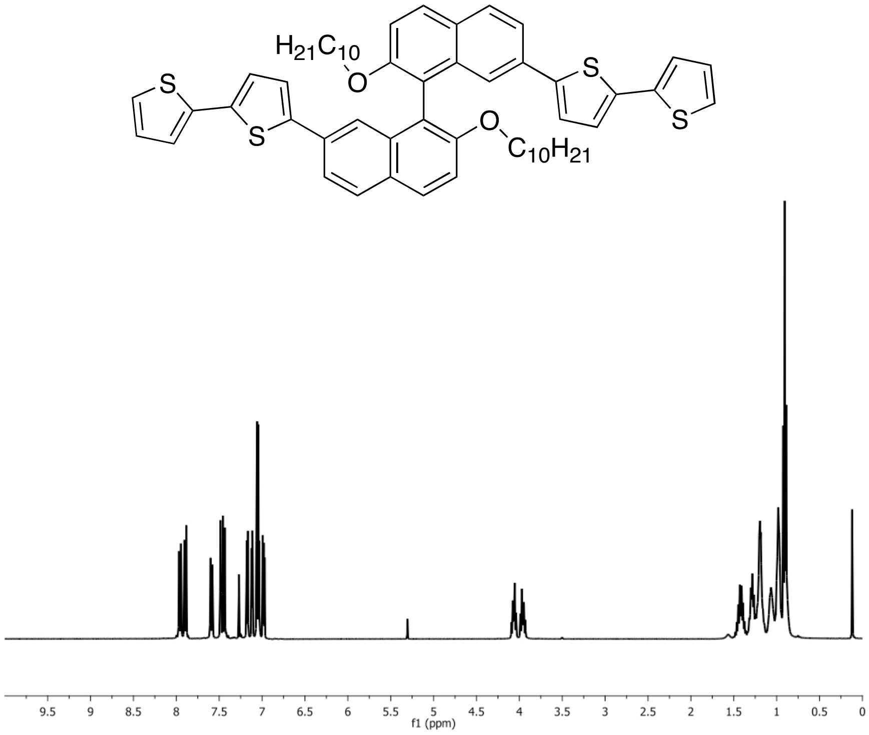

Spectrum 11. ^{1}H-NMR spectrum of **7** (400 MHz, $CDCl_3$).

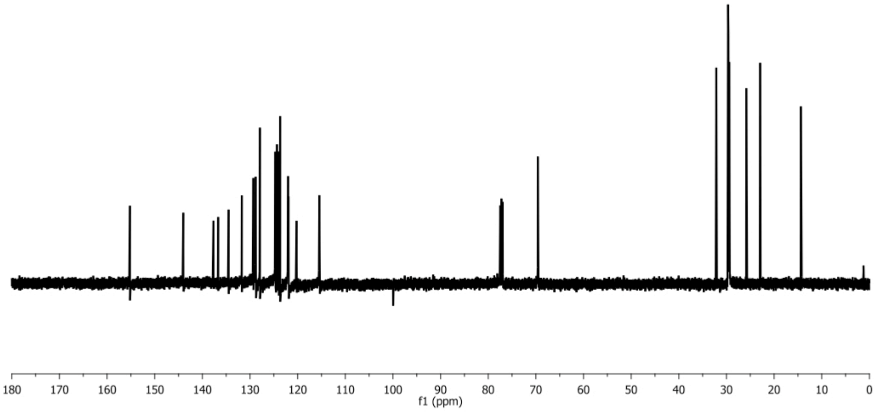

Spectrum 12. ^{13}C-NMR spectrum of **7** (125 MHz, $CDCl_3$).

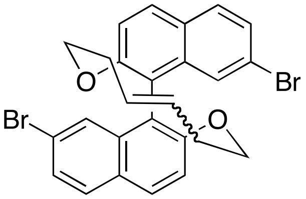

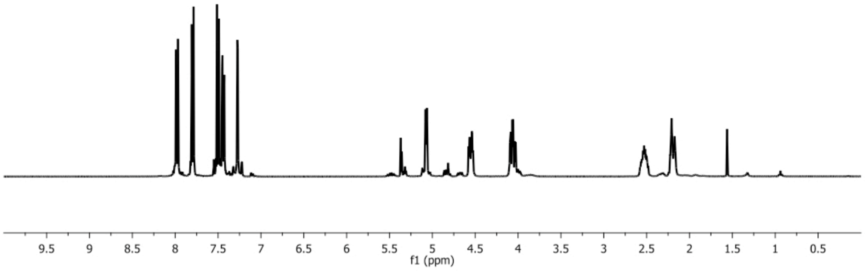

Spectrum 13. ^{1}H-NMR spectrum of **8** (400 MHz, CD_2Cl_2).

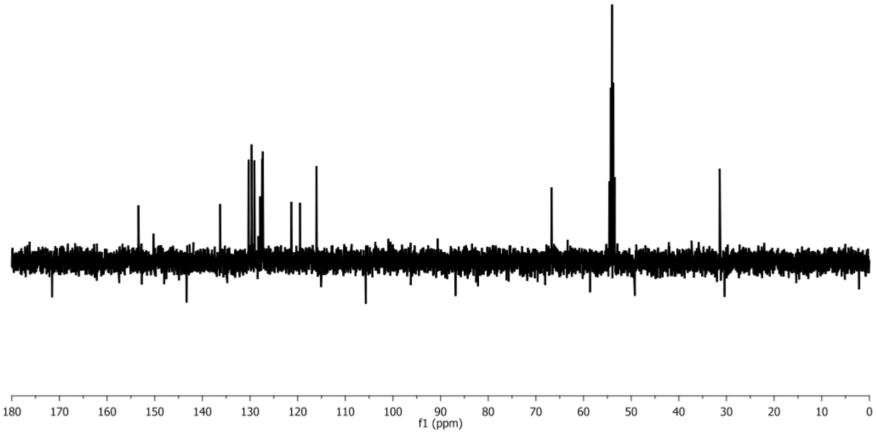

Spectrum 14. ^{13}C-NMR spectrum of **8** (100 MHz, CD_2Cl_2).

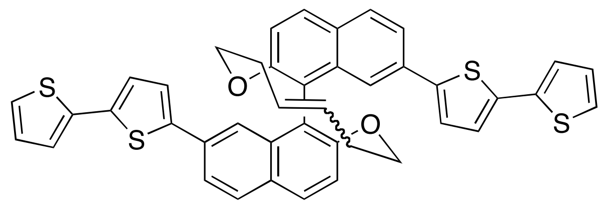

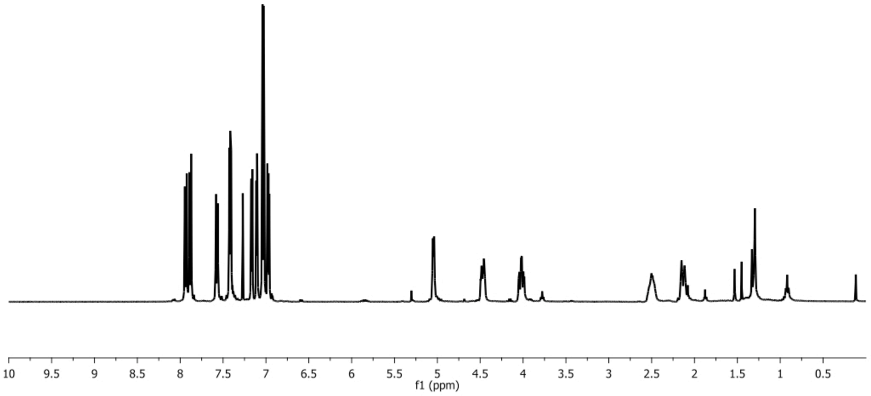

Spectrum 15. ^{1}H-NMR spectrum of **9** (400 MHz, CDCl$_3$).

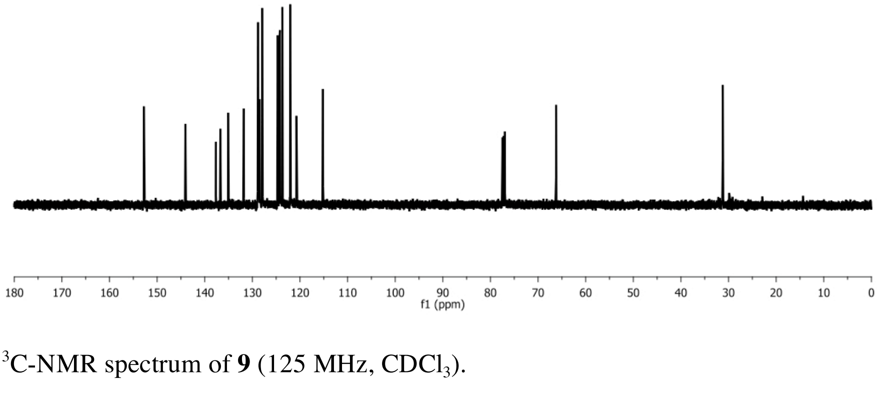

Spectrum 16. ^{13}C-NMR spectrum of **9** (125 MHz, CDCl$_3$).

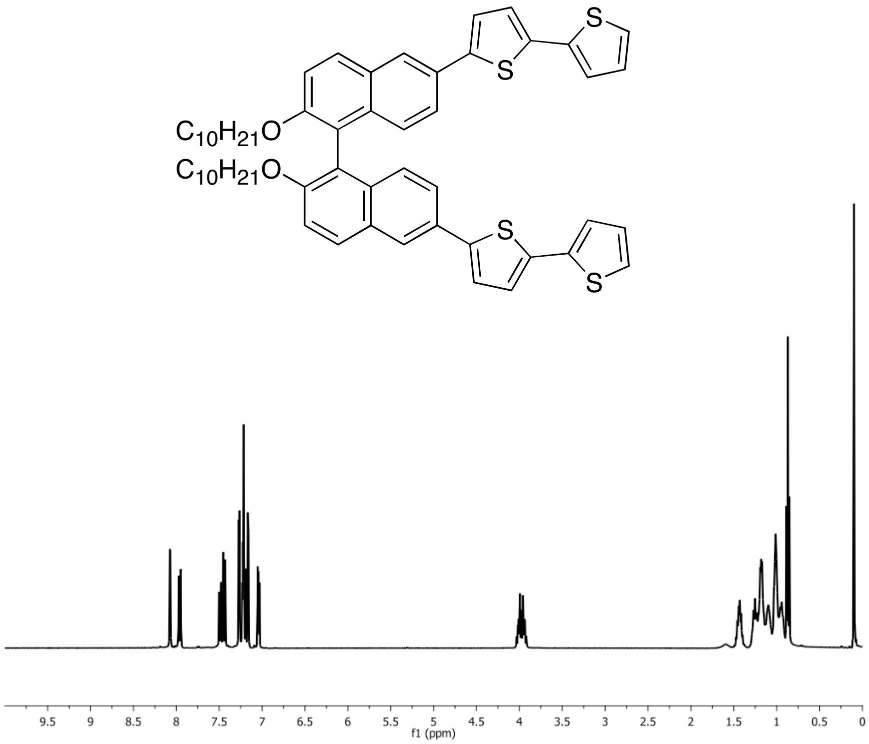

Spectrum 17. ^{1}H-NMR spectrum of **10** (400 MHz, $CDCl_3$).

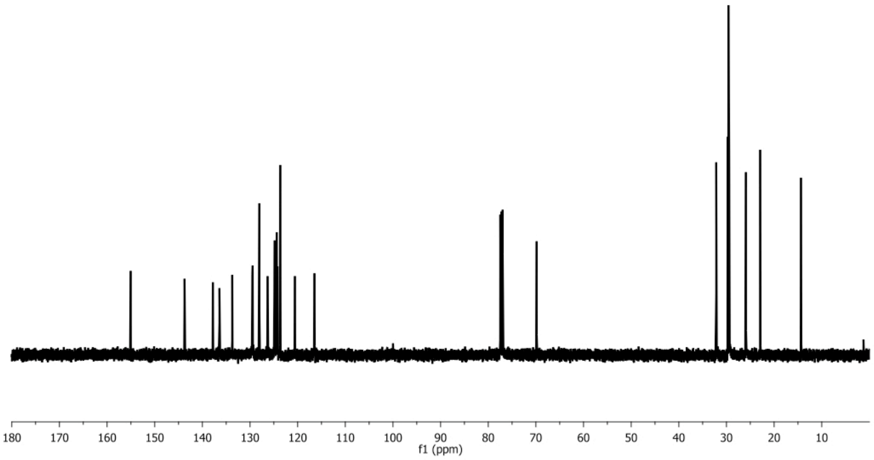

Spectrum 18. ^{13}C-NMR spectrum of **10** (125 MHz, $CDCl_3$).

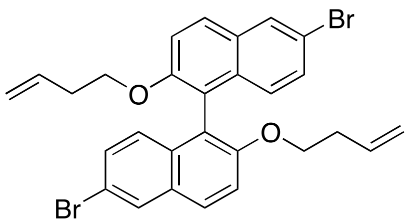

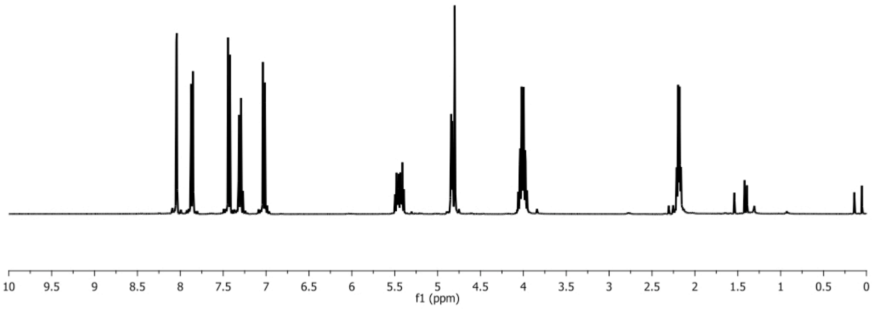

Spectrum 19. ^{1}H-NMR spectrum of **A** (400 MHz, $CDCl_3$).

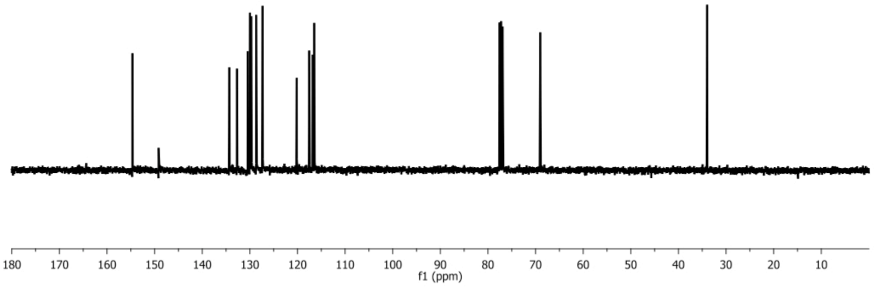

Spectrum 20. ^{13}C-NMR spectrum of **A** (100 MHz, $CDCl_3$).

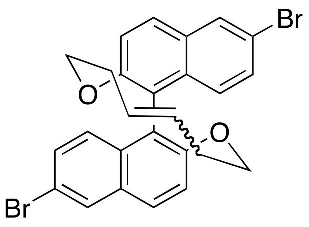

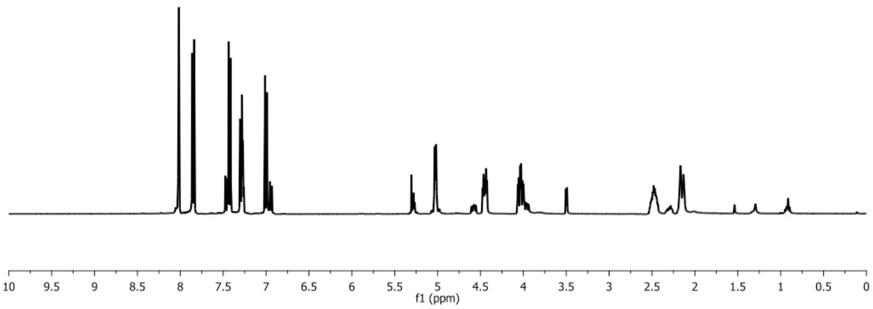

***Spectrum 21**.* ^{1}H-NMR spectrum of **B** (400 MHz, $CDCl_3$).

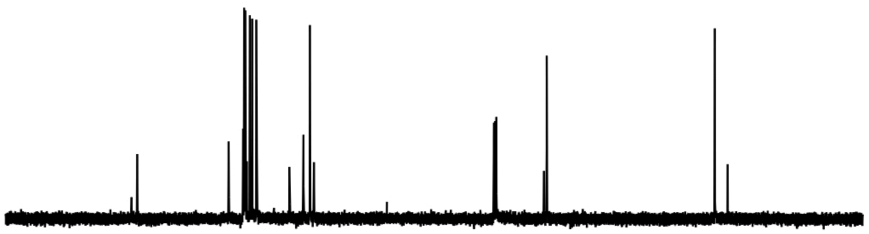

***Spectrum 22**.* ^{13}C-NMR spectrum of **B** (125 MHz, $CDCl_3$).

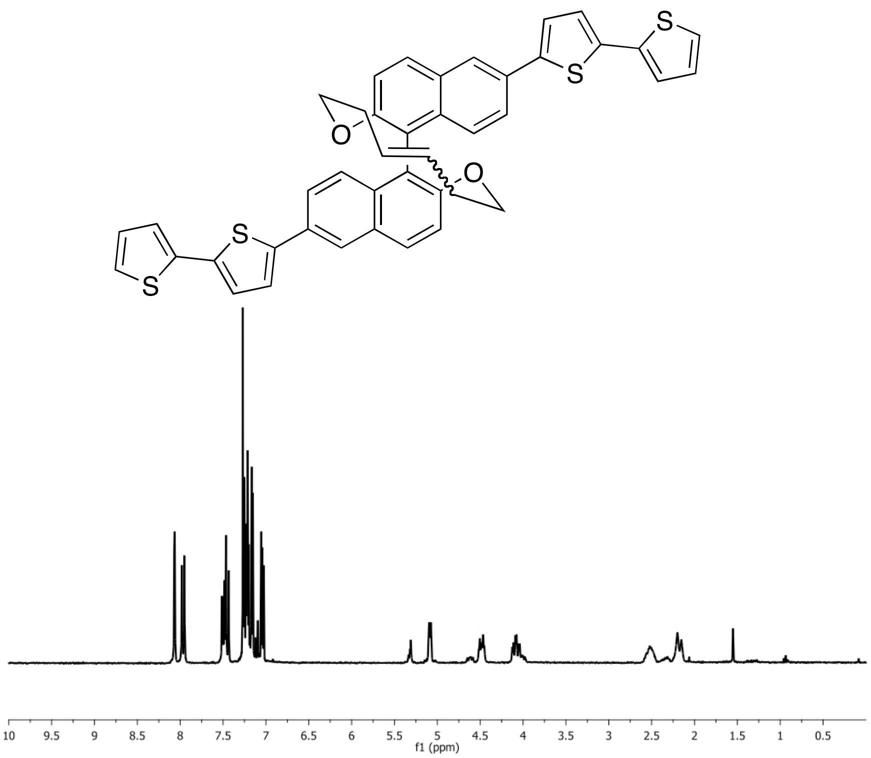

Spectrum 23. ^{1}H-NMR spectrum of **11** (300 MHz, $CDCl_3$).

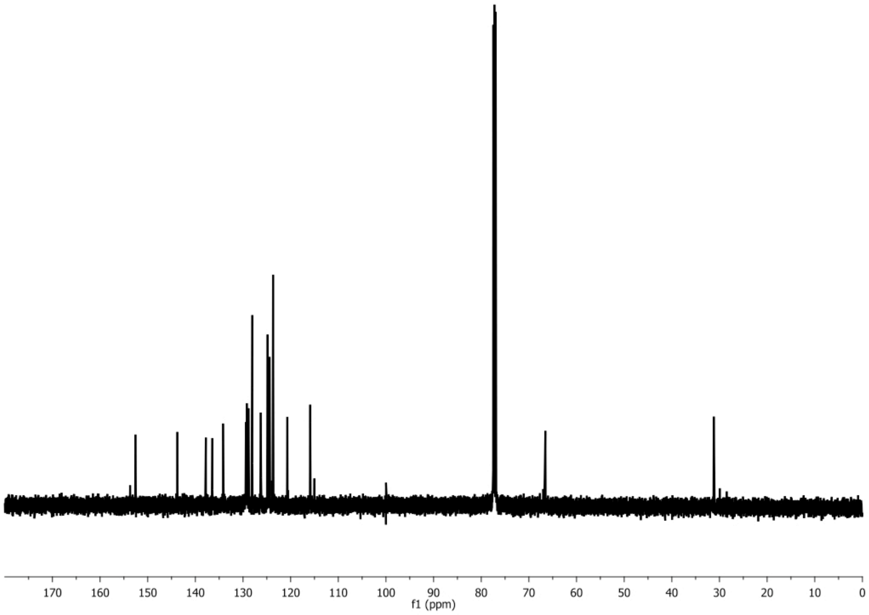

Spectrum 24. ^{13}C-NMR spectrum of **11** (125 MHz, $CDCl_3$).

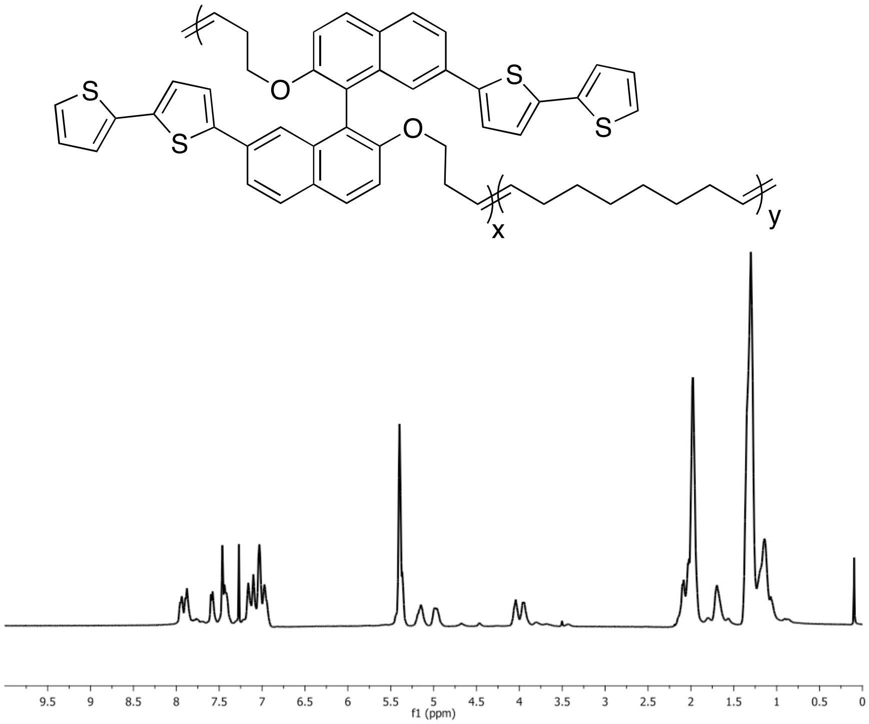

Spectrum 25*.* ^{1}H-NMR spectrum of **12** (400 MHz, $CDCl_3$).

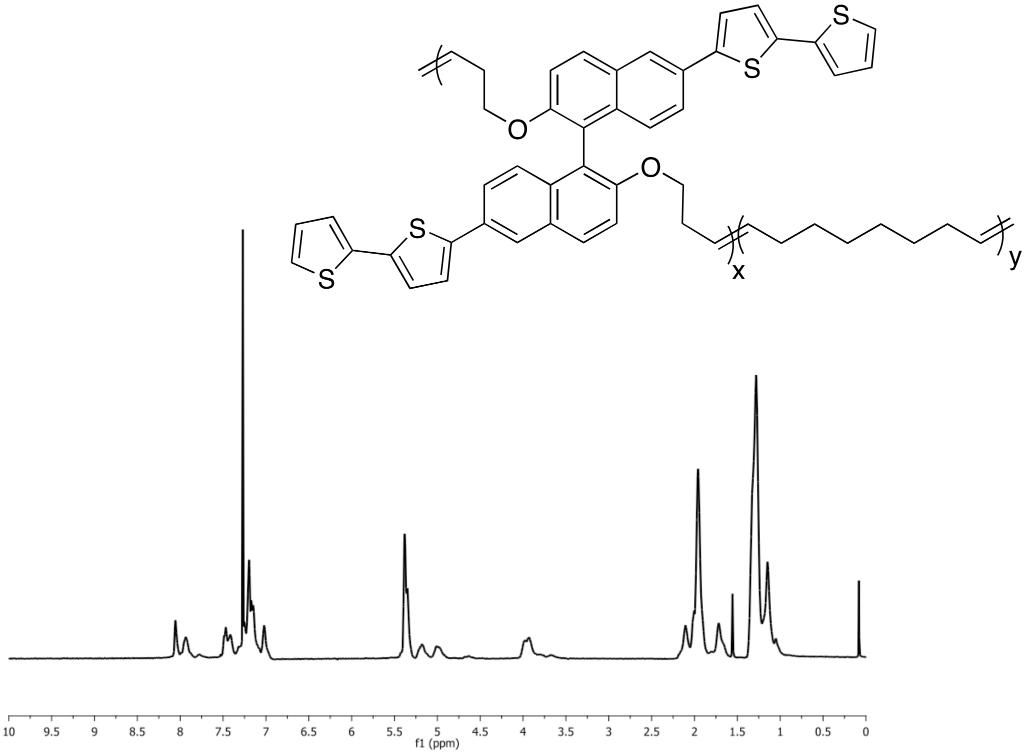

Spectrum 26*.* ^{1}H-NMR spectrum of **14** (400 MHz, $CDCl_3$).

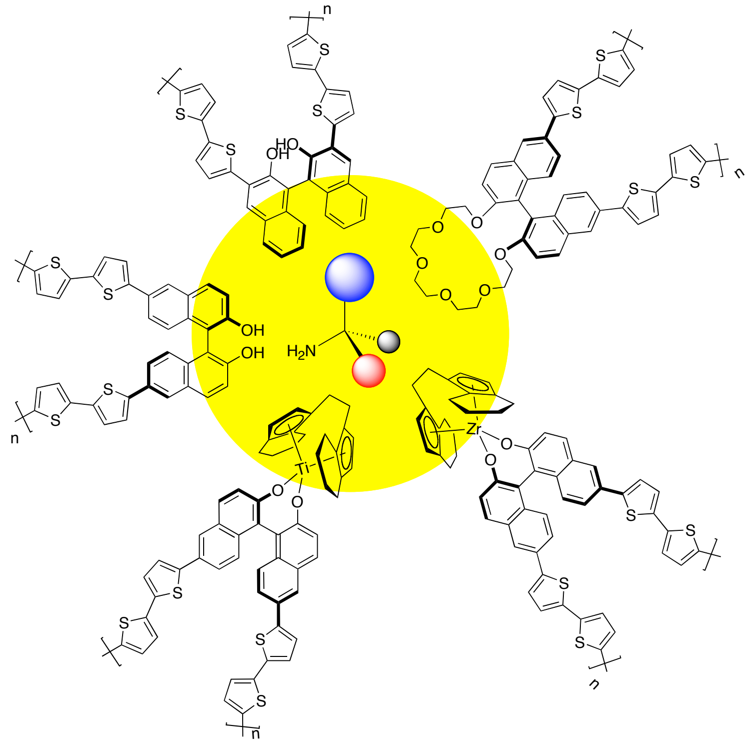
n
S
S
HO
OH
O
O
O
O
O
OH
OH
H2N
Ti
Zr
n
n
n
n

Chapter 4.

Electroactive Polymer Chiral Sensors

Introduction and Design Principles

Chiral conjugated (or conducting) polymers (CPs) have attracted interest due to their applications in selective gas or liquid permeation,[1] enatioselective sensing,[2] and (chromatographic) separation,[3] etc. Furthermore, supramolecular chirality from stimuli-induced aggregates of chiral CPs can be exploited for polarized photo- and electroluminescence.[4] We have been interested in enantioselective sensing utilizing chiral CPs due to the fact that their collective responses (e.g., resistivity) are very sensitive to even minor perturbations.[5] Generally, chiral CPs have been prepared by tethering a chiral moiety to a monomer, or by imprinting with a chiral molecule during polymerization. CPs with main-chain chirality, however, are more rare. Our aim is to develop highly sensitive chiral sensors by incorporating binaphthol moieties into the polymer main-chains. The 1,1'-bi-2,2'-naphthol group has two key features; its atropisomeric chirality and phenol functionality. Needless to say, 1,1'-binaphthyl is a privileged structure that has been widely used in chiral recognition and enantioselective catalysis.[6]

Conducting polymers with phenol groups have shown very interesting properties. For example, phenol groups can render conjugation-broken *meta*-linked polymers, which might be expected to be less conductive according to the conventional wisdom, to be as conductive as their *para*-linked isomers.[7] In other instances, phenols play a vital role in polymerization of calix[4]arene-based conducting polymers, as well as in the charge transporting mechanism.[8] The calix[4]arene-based system showed an intriguing proton-dopable property, which is reminiscent of polyaniline. Deprotonation of *p*-hydroquinone-like segments even by the weak basicity of the solvent CH_3CN resulted in a decrease in conductivity.

The proton-dopable property of the phenol-containing conducting polymers suggests that installation of a chiral discriminating factor would result in a new sensory material for chiral bases (e.g., amines). The binaphthyl scaffold, which has been widely used as a ligand for asymmetric catalysts and as a platform for chiral recognition, was chosen as the *chiral discriminator*. In fact, binaphthyl-based macrocyclic receptors have been used previously for chiral sensing utilizing fluorescent responses.[9]

Our design was to affix electroactive segments to a binaphthyl chiral discriminator, which also has phenol functional groups. We chose 1,1'-binaphth-2,2'-ol as the starting compound due to the availability of both enantiomers. As shown in Chart 1, we targeted polymers with 6,6'-substituted binaphthol (**1**) and with 3,3'-substituted binaphthol (**2**). Although the synthetic route to binaphthyl **2** requires additional steps, we hope 3,3'-substitution may increase the chiral discrimination when an analyte interacts with the polymer.

Chart 1. Candidate Polymer Structures for the Chiral Sensor

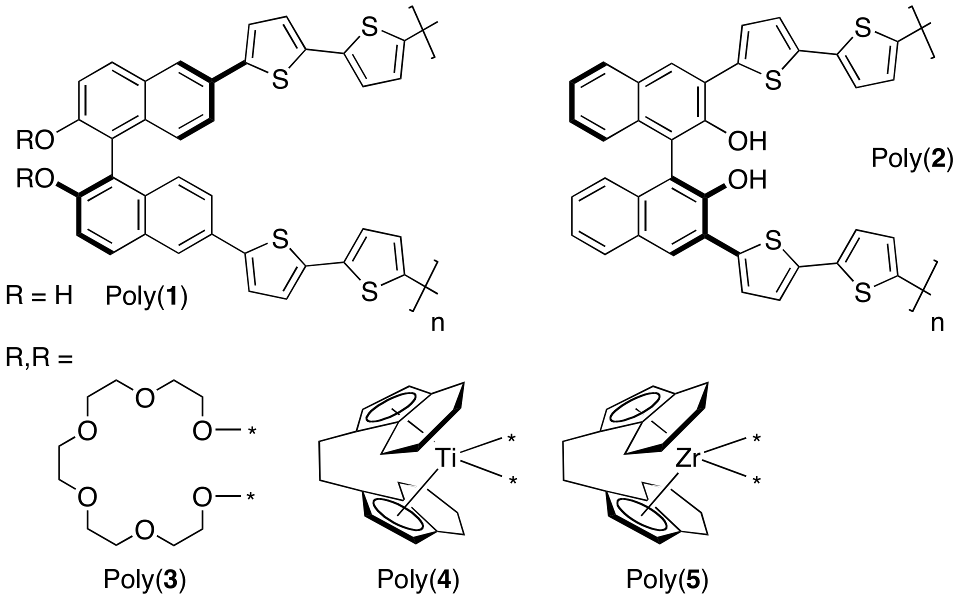

In this chapter, the syntheses of monomers and their electropolymerizations are described, followed by attempts to discriminate several chiral amines. To gain insight into the charge interaction, we also synthesized a monomer ligated to crown-6-ether (**3**) and transition metal compounds (**4** and **5**). Improvements in sensing responses will be discussed briefly at the end of this chapter.

Syntheses of Monomers

The synthesis of compound (*R*)-**1** is described in Chapter 3. Compound **2** was obtained from the MOM-protected 3,3'-iodo compound **6** (Scheme 1), which was prepared according to the literature procedures.[10] Stille cross coupling reaction of **6** with 5-tributylstannyl-2,2'-bithiophene furnished the compound **7**, which was then deprotected with an acid catalyst to yield the desired product **2**. Crown-ether precursor **8** was prepared in a good yield by alkylation to the dibromobinaphthol with tetraethylene glycol ditosylate. The desired monomer **3** was synthesized via a typical Stille cross coupling reaction.

Scheme 1.[a]

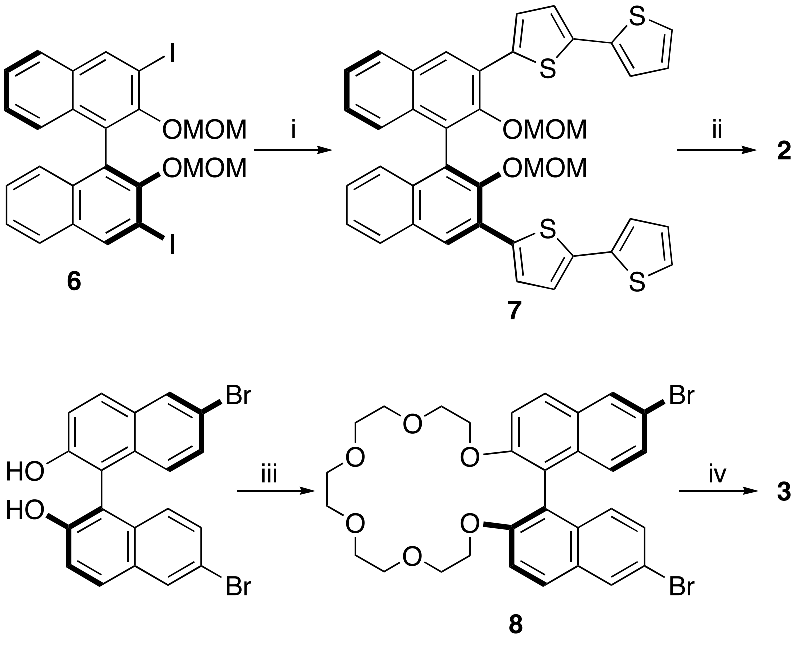

[a]Reagents: (i) $PdCl_2(PPh_3)_2$, 5-tributylstannyl-2,2'-bithiophene, toluene, 80 °C, 15 h, 74%. (ii) Amberlyst 15, THF/MeOH, reflux, 15 h, 96%. (iii) NaH, tetraethylene glycol ditosylate, THF, reflux, 24 h, 53%. (iv) $PdCl_2(PPh_3)_2$, 5-tributylstannyl-2,2'-bithiophene, DMF, 80 °C, 15 h, 71%.

The transition metal complexes **4** and **5** were synthesized from comound **1** and the respective metal precursors in the presence of base (Scheme 2). A relatively weak base, Et_3N, was sufficient for the preparation of ethylene-bis(tetrahydroindenyl) complexes **4** or **5**.

Scheme 2.[a]

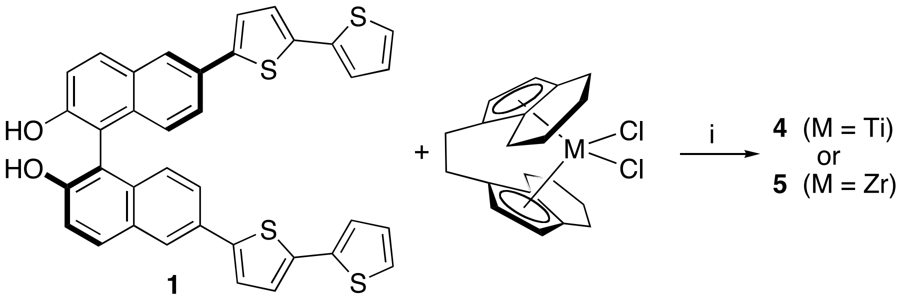

[a]Reagents: (i) Et_3N, CH_2Cl_2, dark, room temperature, 30 min, 85~93%.

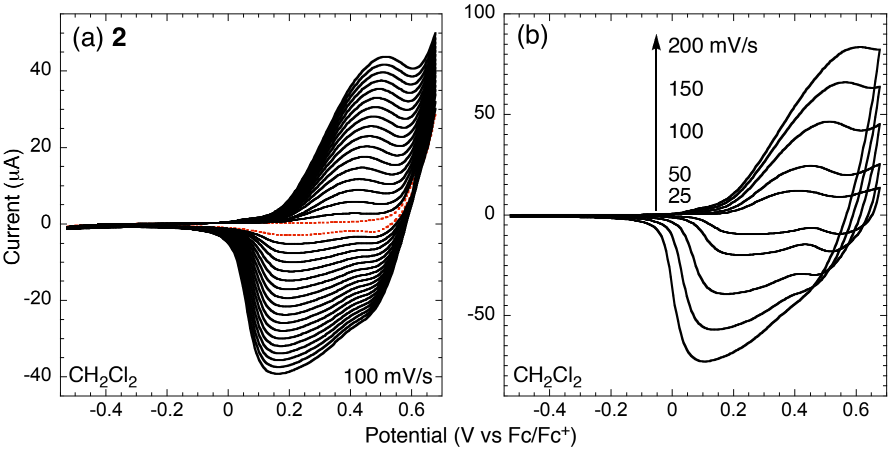

Figure 1. (a) Electropolymerization of **2** on a Pt button electrode. The dotted line represents the first scan. (b) CVs of a poly(**2**) film at different scan rates. All measurements were carried out in CH_2Cl_2 with 0.1 M $TBAPF_6$ as a supporting electrolyte.

Electropolymerization

The electropolymerization of 3,3'-substituted monomer **2** was performed to produce electrode-confined films in CH_2Cl_2 with 0.1 M $TBAPF_6$ as a supporting electrolyte under ambient conditions (Figure 1). The oxidatively coupled products were continually deposited as the potential sweeps were repeated. Similar to poly(**1**) (Chapter 3), we observed two 1-electron redox waves.

Poly(**3**) was prepared by electropolymerization in CH_3CN under similar conditions as above (Figure 2). The CVs of poly(**3**) were very similar to those of the other related polymers (macrocyclic poly(**11**) of Chapter 3). The peak potentials tended to shift in the thick films at higher scan rates (Figure 2c), probably due to the limited diffusion rates of ions in the polymer matrix. To test the effect of ion binding, we tried polymerization of **3** in the presence of K^+ under the same conditions (Figure 2b, red lines). We found that the oxidation onset for monomer **3** was slightly shifted to positive potentials (0.60 V from 0.57 V vs. Fc/Fc^+), and that the polymer growth rate (estimated by the current increase) was retarded.

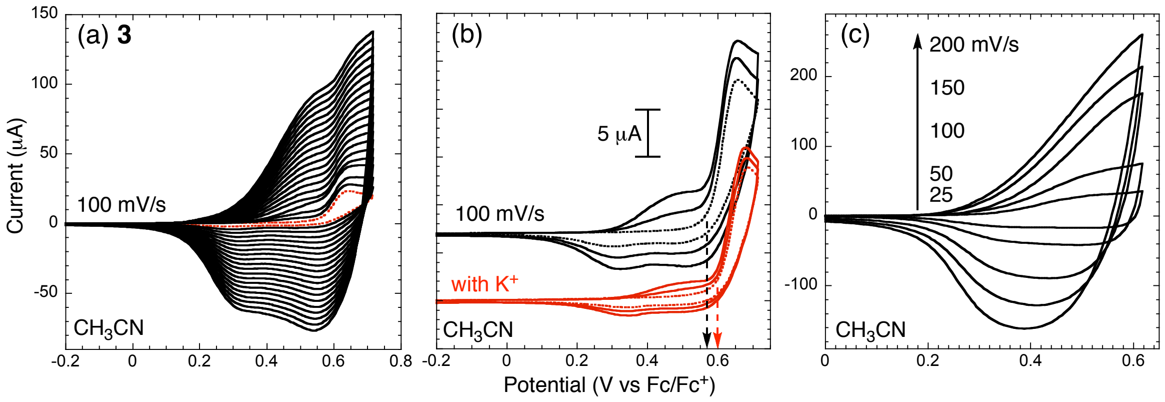

Figure 2. (a) Electropolymerization of **3** on a Pt button electrode. The dotted line represents the first scan. (b) The first three scans of electropolymerization of **3** with (red) or without (black) KPF_6 (0.01 M). (c) CVs of a poly(**2**) film at different scan rates. All measurements were carried out in CH_3CN with 0.1 M $TBAPF_6$ as a supporting electrolyte.

We believe that this retardation was due to the electrostatic repulsion between the potassium ion and the cationic intermediates generated during the electropolymerization. The potential shift, however, was not significant and the resulting polymers were almost identical in properties.

It appears that the binding of potassium ion was not strong enough to dramatically influence the film's properties, especially in the solid state as a deposited film.

The electropolymerizations of the metallo-monomers **4** and **5** are presented in Figure 3. In contrast to the other monomers, these metallo-monomers showed small redox waves right before the onset potential at which the polymerization occurred (Figure 3a and c). We found that cycling the potentials only up to these waves gave no polymer deposition. Interestingly, these small waves became insignificant compared to the polymers' electroactivity as the films became thicker.

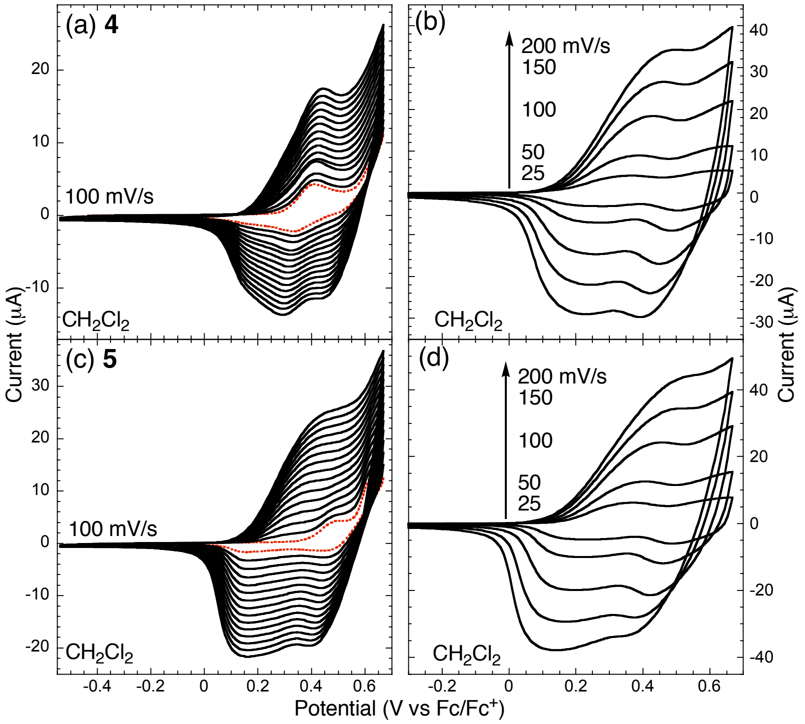

Figure 3. (left) Electropolymerization of **4** (a) and **5** (c) on Pt button electrodes. The dotted lines represent the first scans. (right) CVs of thin films of poly(**4**) (b) and poly(**5**) (d) at different scan rates. All measurements were carried out in CH_2Cl_2 with 0.1 M $TBAPF_6$ as a supporting electrolyte.

The CVs of the polymer films (Figure 3b and 3d) were very similar to each other, and to the CV of poly(**1**), a metal-free polymer. We consider that the detachment of metals during the polymerization should have resulted in extended *p*-quinone-like structures when oxidized, which is expected to give large differences in behavior. Given the similarities with the earlier polymers, we believe that the metal centers remain connected to the polymers.

Attempts for Chiral Sensing

We first examined if enantiospecific responses of poly(**1**) could be observed with a chiral hydroxy amine (Figure 4). We have tested various analytes including chiral amines shown in Chart 2. However, the polymers' responses were similar regardless of amines. Thus, only representative results were presented here.

Chart 2. Chiral Amines Tested in This Study

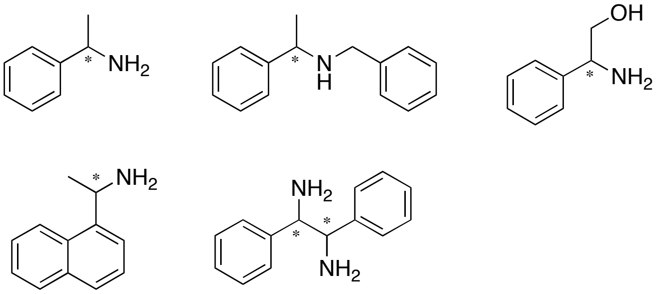

The polymer film's CV was measured repeatedly in the presence of the analyte (0.2 mM) in CH_2Cl_2. Upon exposure of the polymer to the analyte, the currents of the initial peaks were diminished, accompanying an emergence of a new redox wave. The new wave, which was at lower potential, was reminiscent of the behavior of a calix[4]arenecrown system in response to cation binding.[11] We attribute this base-specific response to the direct participation of naphthols in the electronic structures of radical cations, which is similar to the proton-dopable properties observed for a previously inverstigated calix[4]arene-based polymer.[8] The response to the (*R*)-amine, however, was very similar to that of the (*S*)-amine.

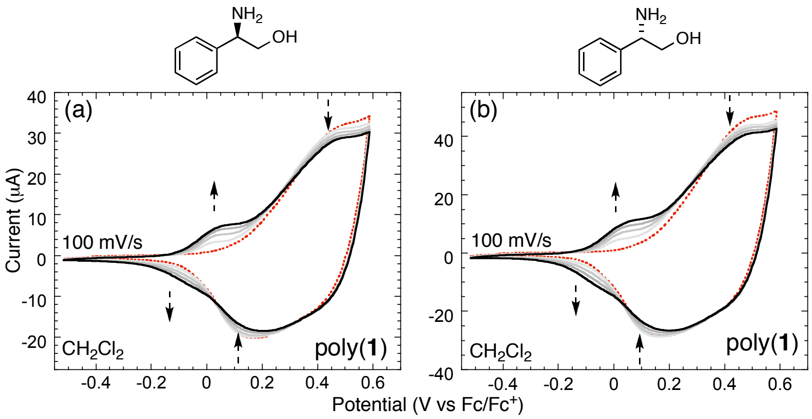

Figure 4. CVs of poly(**1**) films in the presence of (*R*)- (a) and (*S*)-2-phenylglycinol (b) (0.2 mM each) in CH_2Cl_2 with 0.1 M $TBAPF_6$ as a supporting electrolyte.

We also investigated potentiometric responses for a film of poly(**2**) toward naphthylethylamines (Figure 5). A freshly prepared film of poly(**2**) on the ITO-coated glass electrode was immersed in an electrolyte solution with a reference electrode ($Ag/AgNO_3$). We monitored the potential changes as we added more amine to the solution. As shown in Figure 5, the potentials relative to a reference electrode decreased as the concentration of amine increased. We attribute this to the development of negative charges on the polymer surface due to the acid-base interaction. The enantioselective responses, though measurable, were not substantial.

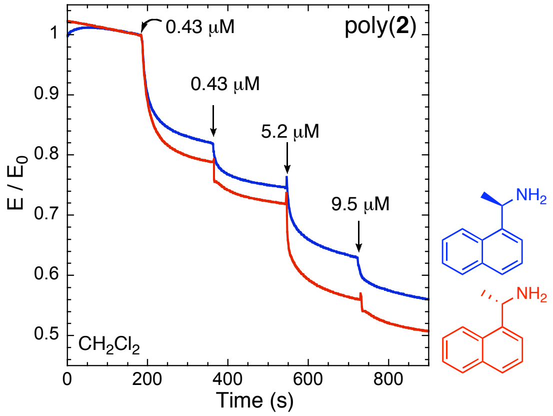

Figure 5. Potentiometric measurements (vs. $Ag/AgNO_3$) of a poly(**2**) film on a ITO-coated glass electrode in the presence of (*R*)- (blue line) and (*S*)-naphthylethylamine (red line) in CH_2Cl_2 with 0.1 M $TBAPF_6$ as a supporting electrolyte.

Interestingly, poly(**3**), which had no phenolic hydroxy group, showed a decrease in conductivity when exposed to the hydroxy amine. It turns out that the amine caused the degradation of poly(**3**), which was probably due to the nucleophilic attack on the radical cation species generated when oxidized.

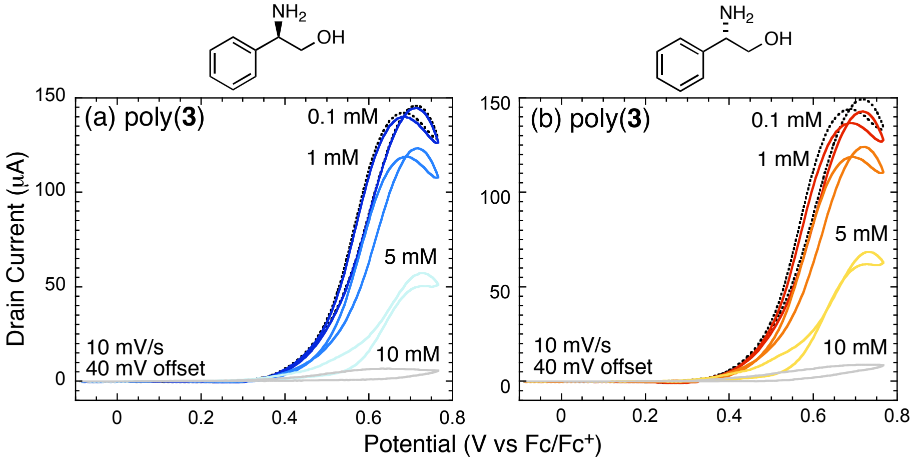

Figure 6. *In situ* drain current profiles ($\propto$ conductivity) of poly(**3**) films on 5-μm interdigitated microelectrodes in the presence of (*R*)- (a) and (*S*)-2-phenylglycinol (b) at different concentrations in CH_2Cl_2 with 0.1 M $TBAPF_6$ as a supporting electrolyte.

Our group previously showed that the conductivity of a calix[4]arene-linked polythiophene was dramatically influenced by the presence of sodium ions.[12] In this system, the calix[4]arene-based receptor was directly attached to the fully-conjugated polythiophene. We tested the ionoresistivity changes with poly(**3**) by measuring the *in situ* conductivity in the presence of ions of interest (Figure 7). With sodium (blue line) and lithium ions (green line), the conductivity profiles were similar to those obtained in the absence of analyte (dotted line), and displayed the same onset potentials. In the presence of lithium ions, the conductivity was slightly increased. In the presence of potassium ion (red line), however, the onset shifted to the positive potential and the maximum decreased slightly. As shown in the electropolymerization (Figure 2), it seems likely that the charge repulsion from bound potassium ions induces a decrease in conductivity. The effects are again small.

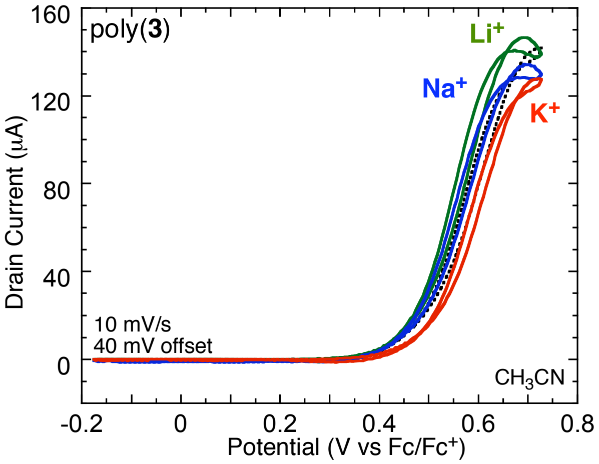

Figure 7. *In situ* drain current profiles of poly(**3**) films on 5-μm interdigitated microelectrodes in the presence 10 mM of $LiClO_4$ (green line), $NaPF_6$ (blue line), and KPF_6 (red line) in CH_3CN with 0.1 M $TBAPF_6$ as a supporting electrolyte.

We have also investigated the chiral responses of the metallo-polymers, poly(**4**) and poly(**5**). In these materials, we considered that the titanium or zirconium with the ethylene-bis(tetrahydroinden)-yl ligand would be equivalent to chiral protons and potentially one enantiomer of the amine would interact more strongly with the metal center than the other. We measured the CVs of a poly(**5**) film as a function of added chiral amines in CH_2Cl_2 at room temperature. As shown in Figure 8, the orginal peak currents were diminished as new ones developed. This same response was observed when we exposed the metallo-polymers to the presence of various chiral amines. We suspect that similar to deprotonation of poly(**1**), the amine binding to the metal center causes the dissociation of the metal and the binaphthol moieties (probably in the form of naphtoxide). Unfortunately, the poly(**5**) responded very similarly to both enantiomers.

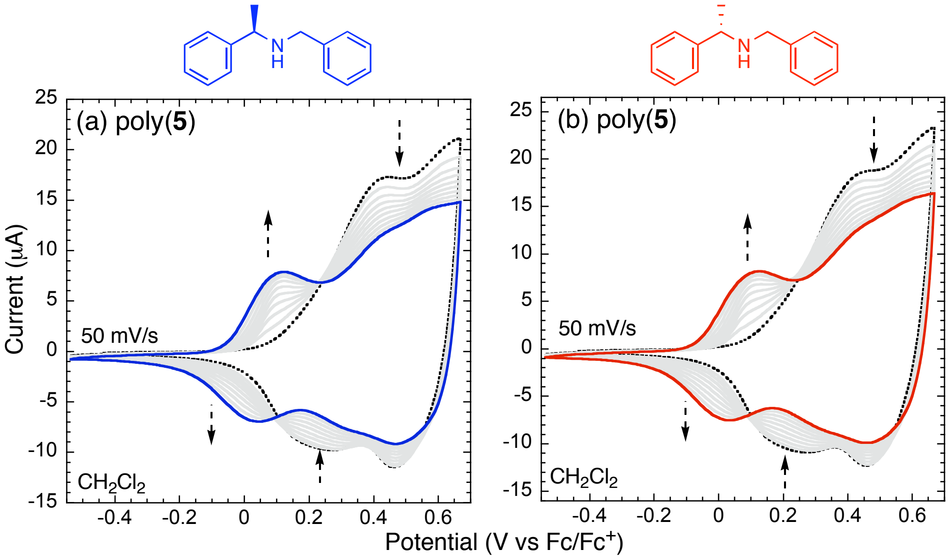

Figure 8. CVs of poly(**5**) films in the presence of (*R*)- (a) and (*S*)-*N*-benzyl-2-phenethylamine (b) (0.5 mM each) in CH_2Cl_2 with 0.1 M $TBAPF_6$ as a supporting electrolyte.

Discussion

We found in accordance with our proposal that the polymers with binaphthol moieties respond to bases. These results are similar to the proton-dopable properties of calix[4]arene-based conducting polymers developed in our group. Based on the fact that low-potential peaks developed at the expense of the original peaks,[11] we hypothesize (Scheme 3) that upon exposure to the base during the oxidation process, the protonated dihydroquinone-like structures (A–C) turn to quinone-like structures (D–F). The deprotonation is most facile at the dication state (C) where the pK_a of the polymer is lowered. We expect the oxidation of the phenoxide-containing structure (D or E) would occur at the lower potentials compared to that of the phenol-containing structure (A or B). This is likely responsible for the development of the low-potential peaks. The counter-cation M^+ in Scheme 3 could represent the protonated amine or tetrabutylammonium ion exchanged from the supporting electrolyte.

Scheme 3. Proposed equilibria of poly(**1**) with electrochemical processes and proton-ion exchanges

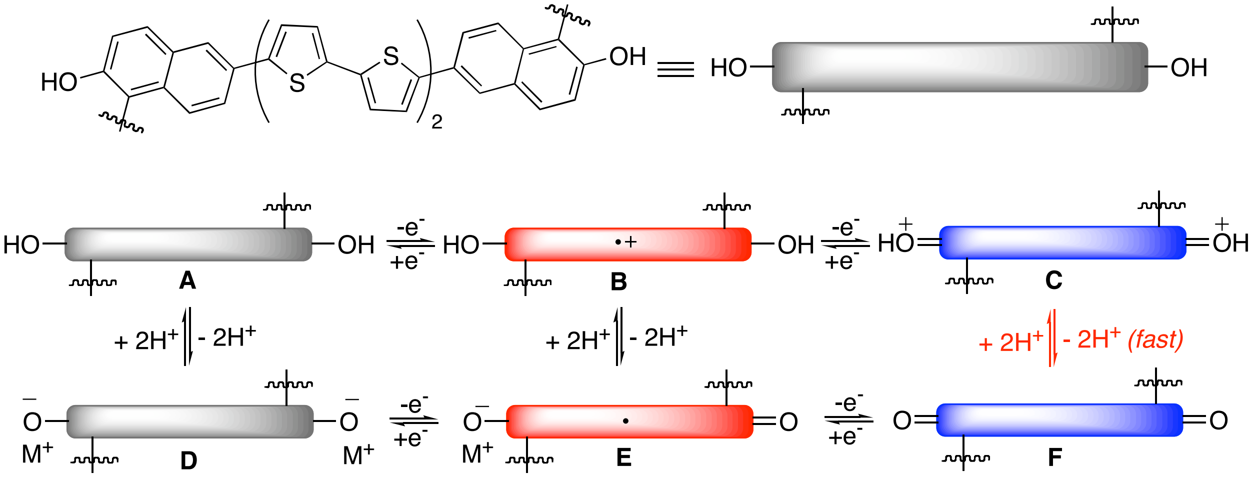

This effect of protonation/deprotonation is strong relative to their coulombic charge interactions. If the phenols are alkylated, the base has a minimal effect on the system. As shown in the case of poly(**3**) with the crown-ether binaphthols, the interaction with ions only slightly alters the electronic properties of the polymer. It appears that in the alkylated system, the wavefunctions for the radical cation are more localized to the oligothiophene portions. The charge-transporting properties are minimally affected by the coulombic interaction at the oxygens on the periphery.

Excess exposure to a base can be detrimental to polymer electrochemistry. Generally, the polymers investigated here are air stable and operate in solutions that have not been kept anhydrous. In the oxidized states, however, the charge can be prone to attacks by nucleophiles such as water, bases, oxygens, etc. This degradation will limit these types of materials as amine sensors.

We tried several methods to differentiate enantiomers using our schemes and the results were not satisfactory. To understand the lack of specific responses, we postulate a mechanism detailed in Figure 9. The chiral amines are first absorbed into the polymer matrix (k_{abs}). The electroactive segment in the polymer then forms a complex with the amines (complex I, k_{cx}), followed by the proton transfer reaction (k_p), resulting in the transient complex II. The protonated amine can be easily dissociated and diffused away, or displaced with the surrounding cations from the supporting electrolyte (k_d).

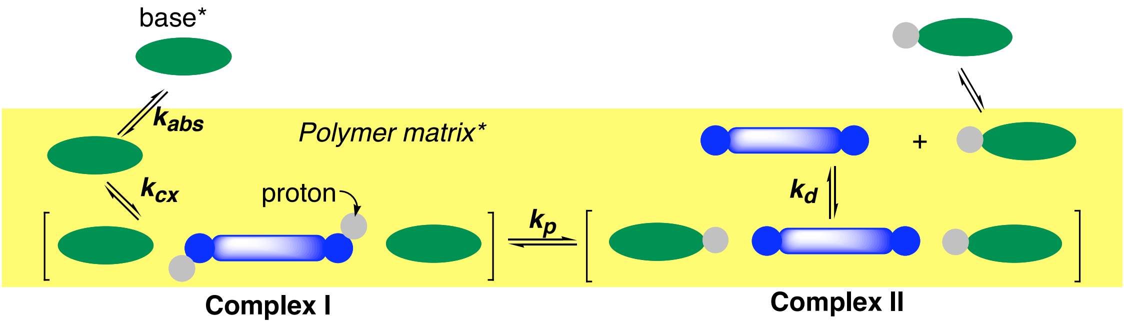

Figure 9. Schematic representation of equilibria in polymer-amine interactions.

All the measurements were performed on polymer films immersed in solution, which causes swelling and the subsequent softening of the polymer matrices. Therefore, we can expect the k_{abs} would be similar for each enantiomer, which may already be solvated.

Zhang *et al*. pointed out in their review[9a] the general principles of chiral recognition; (1) chiral receptors should form reasonably stable complexes with one enantiomer, (2) larger chiral barriers usually create better chiral recognition, and (3) conformational rigidity of receptors results in high degrees of recognition. Their principles suggest that, in order to obtain significant differentiation, binaphthyl polymers should form a stable complex (complex I or II) with only one of the enantimers. The acid-base reaction (k_p), however, is expected to be very fast because the polymer's acidity is significantly increased when oxidized. Hence, it may be hard to obtain recognition events that can compete with this lightly exothermal deprotonation event.

Another possibility is that there is a number of points of interaction between the polymer and the analyte, which enables the analyte to approach the polymer from many different directions without forming a stable complex. In order to obtain and strengthen the chiral differentiation a more defined chiral pocket should be designed.

In terms of conformational rigidity of the recptor, binaphthyls are known to exist as *cisoid* (less than 90° of dihedral angle along the 1,1' C-C bond) and *transoid* (over 90°) conformations. In the solid state, we can imagine that there are a number of conformations with varying dihedral angles. Tuning the dihedral angles to gain maximum interactions with an analyte would also lead to enhancement of the response of the poymer.

Lastly, if we can impart "chirality" on the proton, proton transfer (k_p) can be exploited as the differentiating factor. The (ebthi)Ti or (ebthi)Zr were found to be unsuitable to such end. Other types of metals and ligands, however, merit further investigation.

Conclusion

We proposed binaphthol-containing electroactive polymers for chiral amine sensors utilizing the proton-dopable properties and chirality of these materials. We synthesized polymers with chiral binaphthol moieties, poly(**1**)–poly(**5**), via electropolymerization. However, the enantioselective responses toward chiral amines were not substantial. Designs for improving enantioselective sensing responses were suggested, including more defined chiral receptors and affixed dihedral angles.

Experimental Section

General. NMR spectra were recorded on a Varian Mercury-300, Bruker Advance-400, or Varian Inova-500 spectrometer. Chemical shifts were reported in ppm and referenced to residual solvent peaks ($CDCl_3$: δ 7.27 ppm for ^{1}H, δ 77.23 ppm for ^{13}C). High-resolution mass spectra (HR-MS) were obtained on a Bruker Daltonics APEX II 3 Tesla FT-ICR-MS. Electrochemical measurements were carried out using an Autolab PGSTAT 10 or PGSTAT 20 potentiostat (Eco Chemie) in a three-electrode cell configuration consisting of a quasi-internal Ag wire reference electrode (BioAnalytical Systems) submerged in 0.01 M $AgNO_3$ / 0.1 M tetrabutylammonium hexafluorophosphate ($TBAPF_6$) in anhydrous CH_3CN, a Pt button (1.6 mm in diameter) or 5-μm interdigitated Pt micro-electrodes as the working electrode, and a Pt coil or Pt gauze as the counter electrode. The ferrocene/ferrocenium (Fc/Fc^+) redox couple was used as an external reference. Half-wave potentials of Fc/Fc^+ were observed between 0.210-0.245 V vs Ag/Ag^+ in CH_2Cl_2, and between 0.080-0.091 V vs Ag/Ag^+ in CH_3CN. All air and water sensitive synthetic manipulations were performed under an argon or nitrogen atmosphere using standard Schlenk techniques.

Materials. Spectroscopic grade CH_2Cl_2 was purchased from Aldrich for electrochemistry. $TBAPF_6$ was recrystallized in ethanol prior to use. Anhydrous DMF was purchased from Aldrich as Sure-Seal Bottles and used as received. THF was purified by passage through two alumina columns of an Innovative Technologies purification system. All other chemicals were of reagent grade and used as received. Synthesis of compound **1** was described in Chapter 2. Compounds **6**[13] and **8**[14] were prepared by literature methods. 5-Tributylstannyl-2,2'-bithiophene was synthesized by a known procedure.[15]

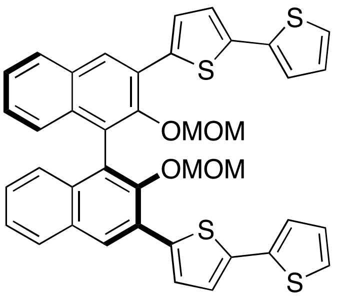

(*S*)-3,3'-Bis(2,2'-bithiophen-5-yl)-2,2'-bis(methyloxymethoxy)-1,1'-binaphthalene (7). In a Schlenk tube equipped with a stir bar were combined MOM-protected diiodobinaphthol **6** (0.063 g, 0.10 mmol), $PdCl_2(PPh_3)_2$ (7 mg, 10 mol %), and toluene (2 mL) under Ar. To the mixture was added 5-tributylstannyl-2,2'-bithiophene (0.113 mL, 0.30 mmol), and the mixture was allowed to stir at 80 °C for 15 h. After being cooled to room temperature, the mixture was filtered through a pad of silica gel and thoroughly washed with ethyl acetate. The filtrate was evaporated under reduced pressure and purified by column chromatography (dichloromethane:hexane = 1:1). Yield: 0.052 g (74%) of bright yellow solid. ^{1}H NMR (300 MHz, $CDCl_3$) δ: 8.20 (s, 2H), 7.92 (d, 2H, *J* = 8.4 Hz), 7.60 (d, 2H, *J* = 3.9 Hz), 7.45 (ddd, 2H, *J* = 8.1, 6.3, 1.8 Hz), 7.33–7.25 (m, 8H), 7.24 (d, 2H, *J* = 3.9 Hz), 7.06 (dd, 2H, *J* = 5.1, 3.9 Hz), 4.73 (d, 2H, *J* = 5.4 Hz), 4.55 (d, 2H, *J* = 5.4 Hz), 2.52 (s, 6H). ^{13}C NMR (125 MHz, $CDCl_3$) δ: 150.46, 138.81, 138.29, 137.59, 133.75, 131.00, 129.34, 128.19, 128.12, 128.11, 127.80, 126.93, 126.87, 126.65, 125.81, 124.66, 124.33, 123.92, 98.79, 56.50. HR-MS (ESI): calcd for $C_{40}H_{30}O_4S_4$ $[M]^+$, 702.1021; found, 702.1004.

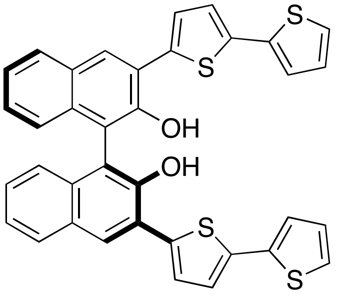

(*S*)-3,3'-Bis(2,2'-bithiophen-5-yl)-1,1'-bi-2-naphthol (2). In a flask equipped with a stir bar were combined **8** (0.019 g, 0.027 mmol), Amberlyst 15 resin (0.027 g) in THF/MeOH (1:1). After being stirred at reflux for 15 h, the cooled-down mixture was filtered off to remove the resin, and the filtrate was evaporated under reduced pressure. The crude mixture was purified by column chromatography (ethyl acette:hexane = 1:3). Yield: 0.016 g (96%) of yellow solid. ^{1}H NMR (300 MHz, $CDCl_3$) δ: 8.33 (s, 2H), 7.95 (bd, 2H, *J* = 8.1 Hz), 7.67 (d, 2H, *J* = 3.9 Hz), 7.42 (ddd, 2H, *J* = 8.1, 6.9, 1.2 Hz), 7.32 (ddd, 2H, *J* = 8.4, 6.9, 1.5 Hz), 7.26–7.25 (*m*, 4H), 7.24 (d, 2H, *J* = 3.9 Hz), 7.16 (bd, 2H, *J* = 8.1 Hz), 7.06 (dd, 2H, *J* = 4.5, 4.2 Hz), 5.64 (s, 2H). ^{13}C NMR (125 MHz, $CDCl_3$) δ: 149.81, 138.11, 137.93, 137.57, 132.60, 129.61, 129.40, 128.69, 128.14, 128.10, 127.94, 125.04, 124.77, 124.43, 124.28, 123.96, 123.40, 112.07. HR-MS (ESI): calcd for $C_{36}H_{22}O_2S_4$ $[M+H]^+$, 615.0575; found, 615.0566.

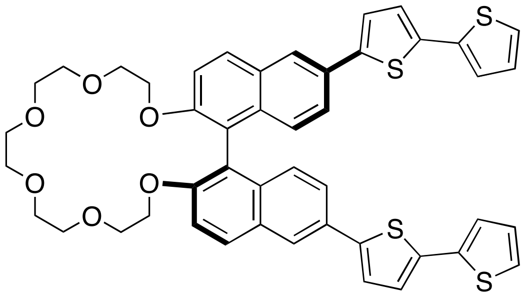

(*R*)-6,6'-Bis(2,2'-bithiophen-5-yl)-2,2'-(pentaethylene glycol)-1,1'-binaphthalene (3). In a Schlenk tube equipped with a stir bar were combined crown-6-type dibromobinaphthyl **8** (0.066 g, 0.10 mmol), $PdCl_2(PPh_3)_2$ (3.5 mg, 5 mol %), and DMF (2 mL) under Ar. To the mixture was added 5-tributylstannyl-2,2'-bithiophene (0.113 mL, 0.30 mmol), and the mixture was allowed to stir at 80 °C for 15 h. After being cooled to room temperature, the mixture was filtered through a pad of silica gel and thoroughly washed with ethyl acetate. The filtrate was washed successively with saturated NH_4Cl (aq), NaF (aq) (×2), and NH_4Cl (aq) again. The organic layer was dried over $MgSO_4$ and evaporated under reduced pressure. The crude mixture was purified by column chromatography (ethyl acetate only). Yield: 0.058 g (71%) of yellow solid. ^{1}H NMR (400 MHz, $CDCl_3$) δ: 8.07 (d, 2H, J = 1.8 Hz), 7.97 (d, 2H, J = 9.0 Hz), 7.50 (d, 2H, J = 9.0 Hz), 7.49 (dd, 2H, J = 8.9, 1.8 Hz), 7.26 (d, 2H, J = 3.8 Hz), 7.23–7.21 (m, 4H), 7.18 (d, 2H, J = 8.9 Hz), 7.16 (d, 2H, J = 3.8 Hz), 7.04 (dd, 2H, J = 4.9, 3.8 Hz), 4.26 (m, 2H), 4.10 (m, 2H), 3.64 (m, 4H), 3.56 (m, 8H), 3.42 (m, 4H). ^{13}C NMR (125 MHz, $CDCl_3$) δ: 154.98, 143.54, 137.72, 136.60, 133.60, 129.68, 129.65, 129.56, 128.07, 126.29, 124.86, 124.67, 124.50, 124.25, 123.81, 123.74, 120.46, 116.80, 71.06, 70.85, 70.79, 69.98, 69.97. HR-MS (ESI): calcd for $C_{46}H_{40}O_6S_4$ $[M+Na]^+$, 839.1600; found, 839.1575.

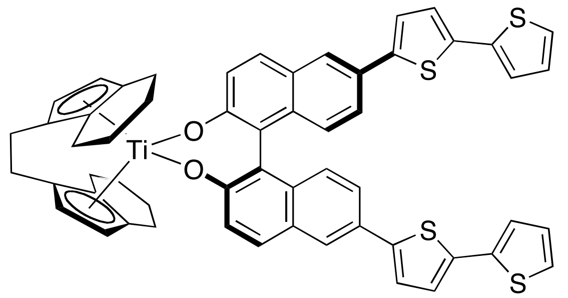

(R,R)-Ethylene-1,2-bis(η^5-4,5,6,7-tetrahydro-1-indenyl)-titanium (R)- 6,6'-Bis(2,2'-bithiophen-5-yl)-1,1'-binaphth-2-olate (4). To a mixture of (R,R)-ethylene-1,2-bis(η^5-4,5,6,7-tetrahydro-1-indenyl)-titanium dichloride (0.027 g, 0.07 mmol) and (R)-binaphthol **1** (0.043 g, 0.07 mmol) in CH_2Cl_2(1 mL) was added triethylamine (0.030 mL, 0.21 mmol). The reaction flask was wrapped in aluminum foil and stirred at room temperature for 30 min. The mixture was filtered through a short pad of alumina and evaporated under reduced pressure. The crude product was purified by recrystallization (dichloromethane/hexane). Yield: 0.055 g (85%) of orange-red solid. ^{1}H NMR (400 MHz, $CDCl_3$) δ: 8.01 (d, 2H, J = 1.9 Hz), 7.84 (d, 2H, J = 8.7 Hz), 7.33 (dd, 2H, J = 8.9, 1.9 Hz), 7.24 (d, 2H, J = 3.9 Hz), 7.22–7.20 (m, 4H), 7.16 (*pseudo*-s, 2H), 7.14 (d, 2H, *J* = 3.9 Hz), 7.04 (dd, 2H, *J* = 4.6, 4.1 Hz), 6.96 (d, 2H, *J* = 8.9 Hz), 3.38 (m, 2H), 3.13 (m, 2H), 2.58 (m, 4H), 1.75 (m, 6H), 1.53 (m, 4H), 1.24 (m, 2H). ^{13}C NMR (125 MHz, $CDCl_3$) δ: 166.38, 144.14, 138.00, 137.45, 135.89, 134.26, 133.39, 128.85, 128.79, 128.03, 127.66, 127.62, 125.82, 124.82, 124.23, 124.20, 123.50, 123.44, 123.17, 122.44, 118.12, 116.44, 106.79, 27.64, 24.10, 23.39, 22.23, 21.96.

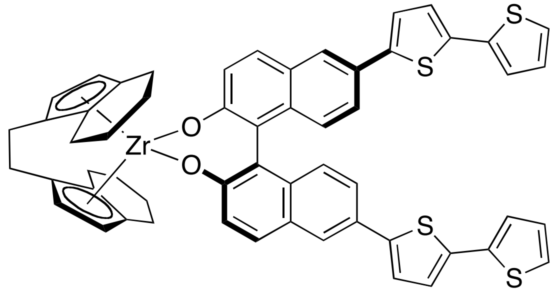

(*R*,*R*)-Ethylene-1,2-bis(η^5-4,5,6,7-tetrahydro-1-indenyl)-zirconium (*R*)- 6,6'-Bis(2,2'-bithiophen-5-yl)-1,1'-binaphth-2-olate (5). Similar to the prepartion of 5 except using (*R*,*R*)-ethylene-1,2-bis(η^5-4,5,6,7-tetrahydro-1-indenyl)-zirconium dichloride (0.030 g, 0.07 mmol). Yield: 0.063 g (93%) of orange-brown solid. ^{1}H NMR (300 MHz, $CDCl_3$) δ: 8.01 (d, 2H, *J* = 2.0 Hz), 7.87 (d, 2H, *J* = 8.7 Hz), 7.34 (dd, 2H, *J* = 9.0, 2.0 Hz), 7.24 (d, 2H, *J* = 3.9 Hz), 7.22–7.20 (m, 6H), 7.15 (d, 2H, *J* = 3.9 Hz), 7.03 (dd, 2H, *J* = 4.8, 3.9 Hz), 6.91 (d, 2H, *J* = 9.0 Hz), 5.72 (d, 2H, *J* = 3.0 Hz), 5.60 (d, 2H, *J* = 3.0 Hz), 3.22 (m, 4H), 2.62 (m, 4H), 1.79 (m, 6H), 1.62 (m, 4H), 1.27 (m, 2H). ^{13}C NMR (125 MHz, $CDCl_3$) δ: 160.72, 144.02, 137.95, 135.99, 134.47, 132.63, 130.91, 129.43, 128.83, 128.03, 127.92, 127.44, 124.83, 124.26, 124.23, 123.67, 123.59, 123.54, 123.27, 123.06, 117.36, 114.14, 106.24, 27.82, 23.87, 22.89, 22.56, 22.31.

References and Notes

(1) Kaner, R. B. *Synth. Met.* **2002,** *125,* 65-71.

(2) Huang, J.; Egan, V. M.; Guo, H.; Yoon, J. –Y.; Briseno, A. L.; Rauda, I. E.; Garrell, R. L.; Knobler, C. M.; Zhou, F.; Kaner, R. B. *Adv. Mater.* **2003,** *15,* 1158-1161.

(3) Mwongela, S. M.; Numan, A.; Gill, N. L.; Agbaria, R. A.; Warner, I. M. *Anal. Chem.* **2003,** *75,* 6098-6096.

(4) (a) Goto, H.; Yashima, E. *J. Am. Chem. Soc.* **2002,** *124,* 7943-7949. (b) Satrijo, A.; Meskers, S. C. J.; Swager, T. M. *J. Am. Chem. Soc.* **2006,** *128,* 9030-9031.

(5) (a) Swager, T. M. *Acc. Chem. Res.* **1998,** *31,* 201-207. (b) McQaude, D. T.; Pullen, A. E.; Swager, T. M. *Chem. Rev.* **2000,** *100,* 2537-2574.

(6) Pu, L. *Chem. Rev.* **1998**, *98*, 2405-2494.

(7) Song, C.; Swager, T. M. *Macromolecules*, **2005**, *38*, 4569-4575.

(8) Yu, H. -h.; Xu, B.; Swager, T. M. *J. Am. Chem. Soc.* **2003,** *125,* 1142-1143.

(9) (a) Zhang, X. X.; Bradshaw, J. S.; Izatt, R. M. *Chem. Rev.* **1997**, *97*, 3313-3361. (b) Kubo, Y. *Synlett* **1999,** 161-174. (c) Lin, J.; Zhang, H. –C.; Pu. L. *Org. Lett.* **2002**, *4*, 3297-3300.

(10) Wu, T. R.; Shen, L.; Chong, J. M. *Org. Lett.* **2004**, *6,* 2701-2704.

(11) Yu, H. -h.; Pullen, A. E.; Büschel, M G.; Swager, T. M. *Angew. Chem. Int. Ed.* **2004,** *43,* 3700-3703.

(12) Marsella, M. J.; Newland, R. J.; Carroll, P. J.; Swager, T. M. *J. Am. Chem. Soc.* **1995,** *117,* 9842-9848.

(13) Wu, T. R.; Shen, L.; Chong, J. M. *J. Org. Chem.* **2004,** *6,* 2701-2704.

(14) Cui, Y.; Lee, S. J.; Lin, W. *J. Am. Chem. Soc.* **2003,** *125,* 6014-6015.

(15) Zhu, S. S.; Swager, T. M. *J. Am. Chem. Soc.* **1997,** *119,* 12568-12577.

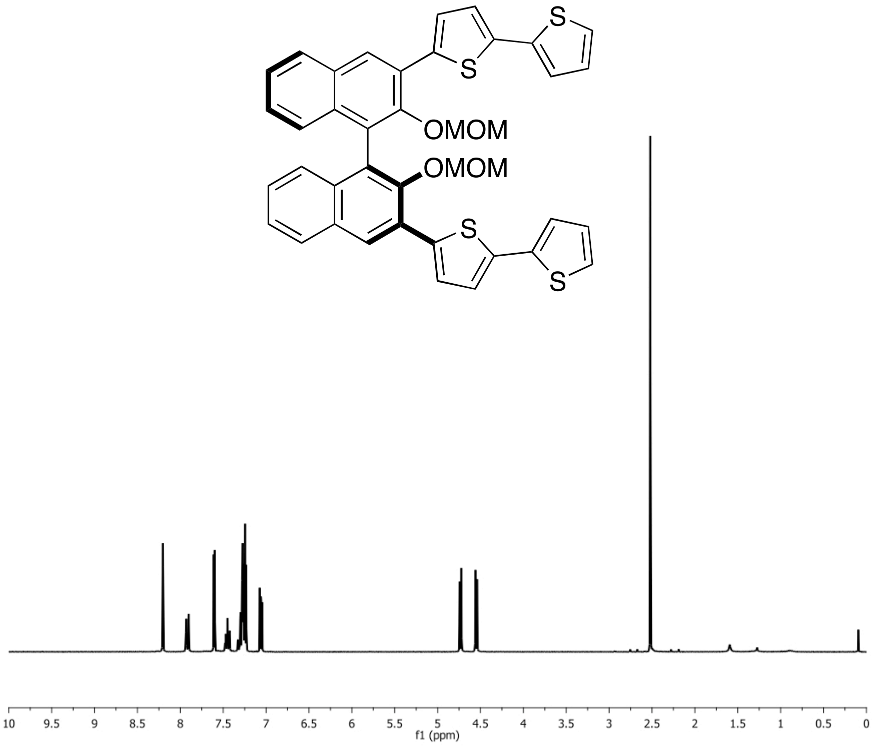

Spectrum 1. ^{1}H-NMR spectrum of **7** (300 MHz, $CDCl_3$).

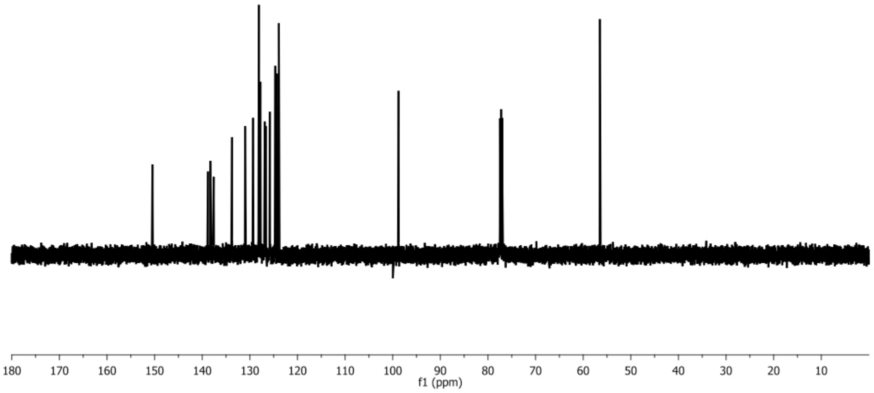

Spectrum 2. ^{13}C-NMR spectrum of **7** (125 MHz, $CDCl_3$).

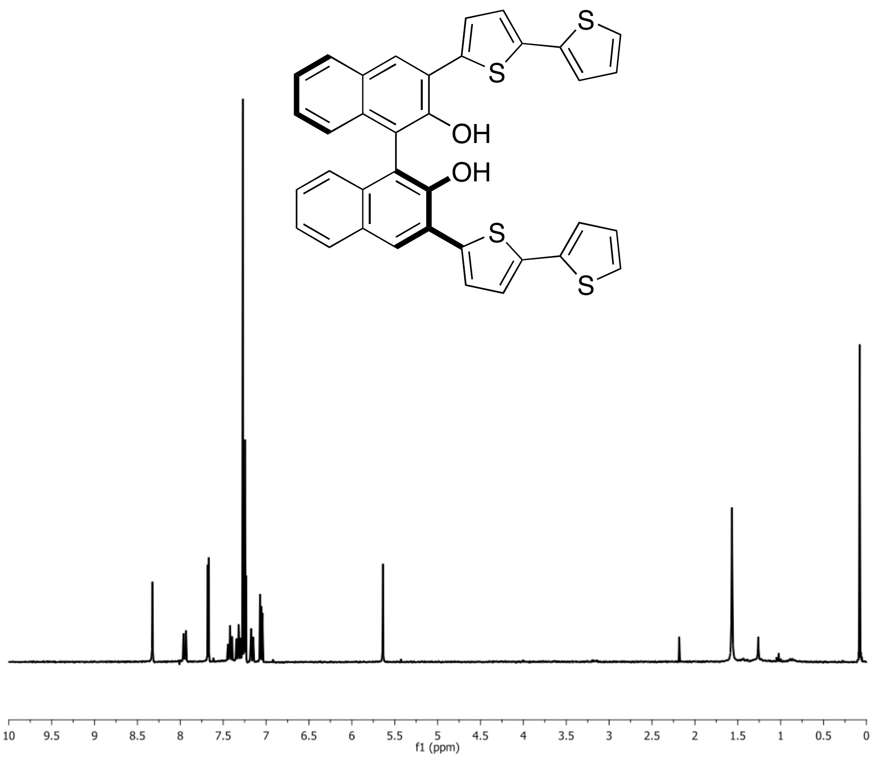

Spectrum 3. ^{1}H-NMR spectrum of **2** (300 MHz, $CDCl_3$).

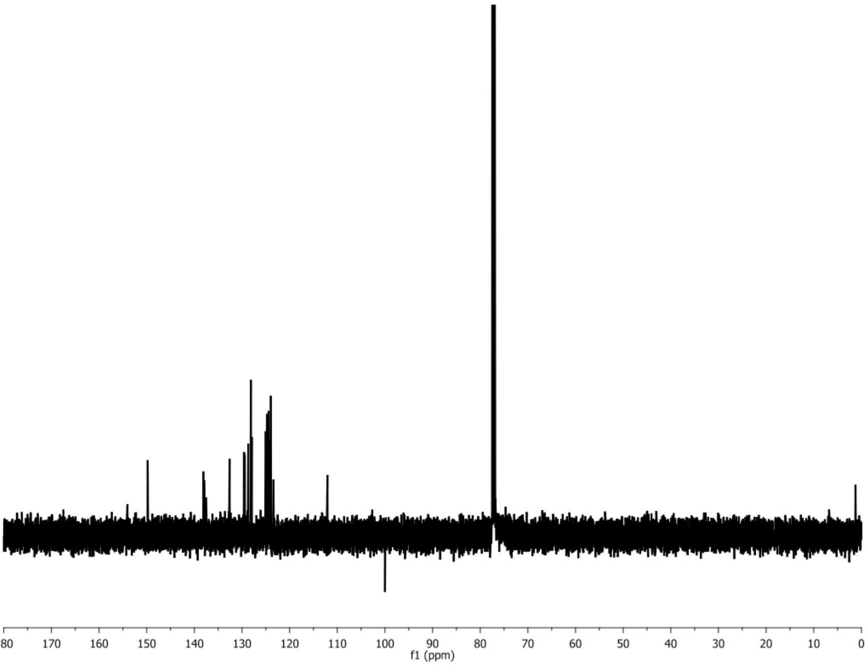

Spectrum 4. ^{13}C-NMR spectrum of **2** (125 MHz, $CDCl_3$).

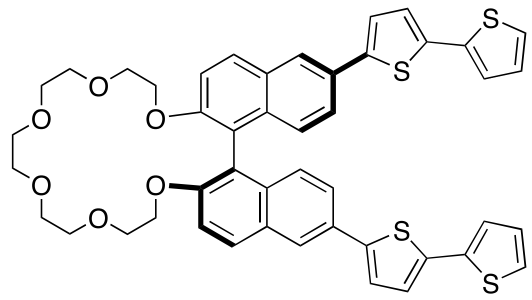

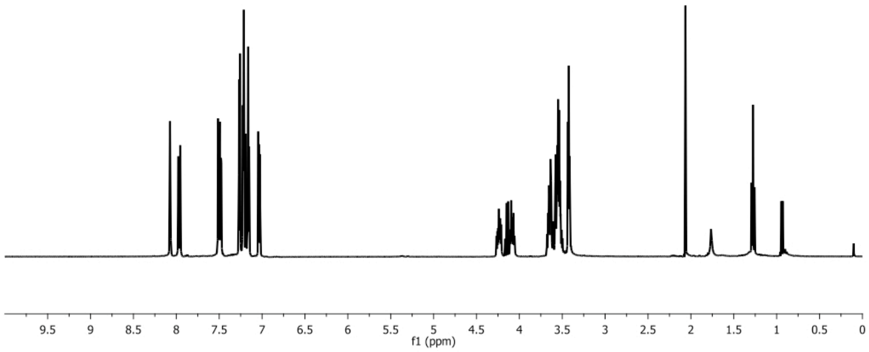

Spectrum 5. ^{1}H-NMR spectrum of **3** (400 MHz, $CDCl_3$).

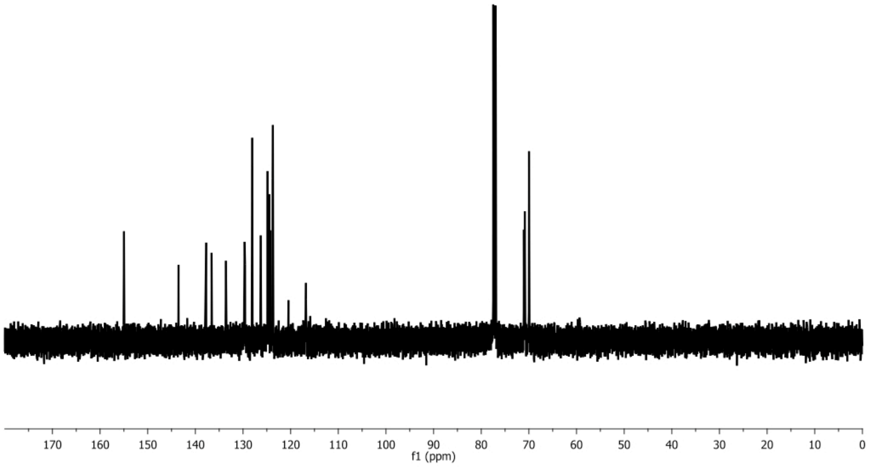

Spectrum 6. ^{13}C-NMR spectrum of **3** (125 MHz, $CDCl_3$).

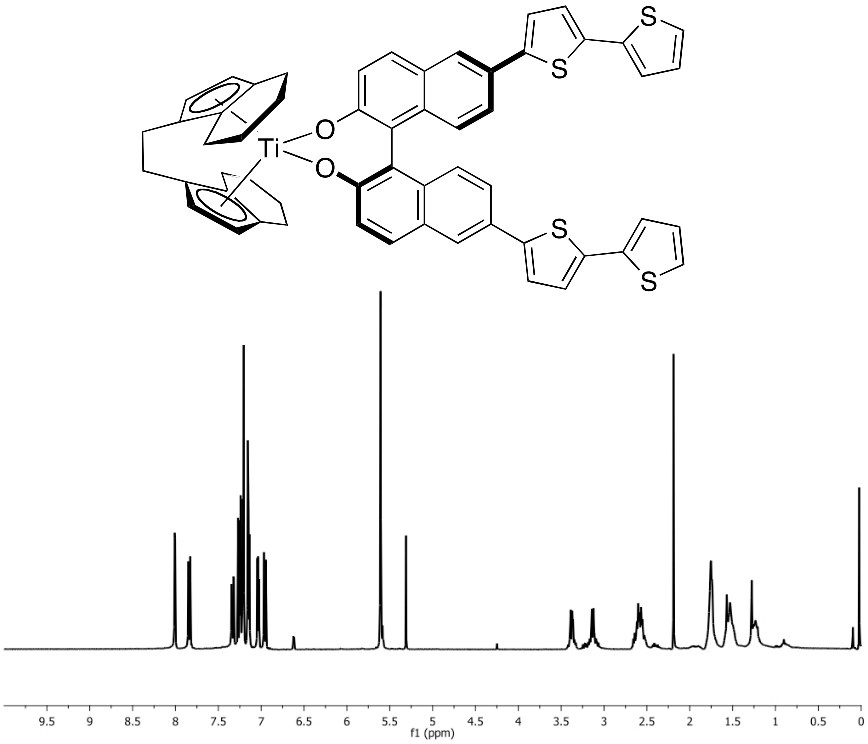

Spectrum 7. ^{1}H-NMR spectrum of **4** (400 MHz, $CDCl_3$).

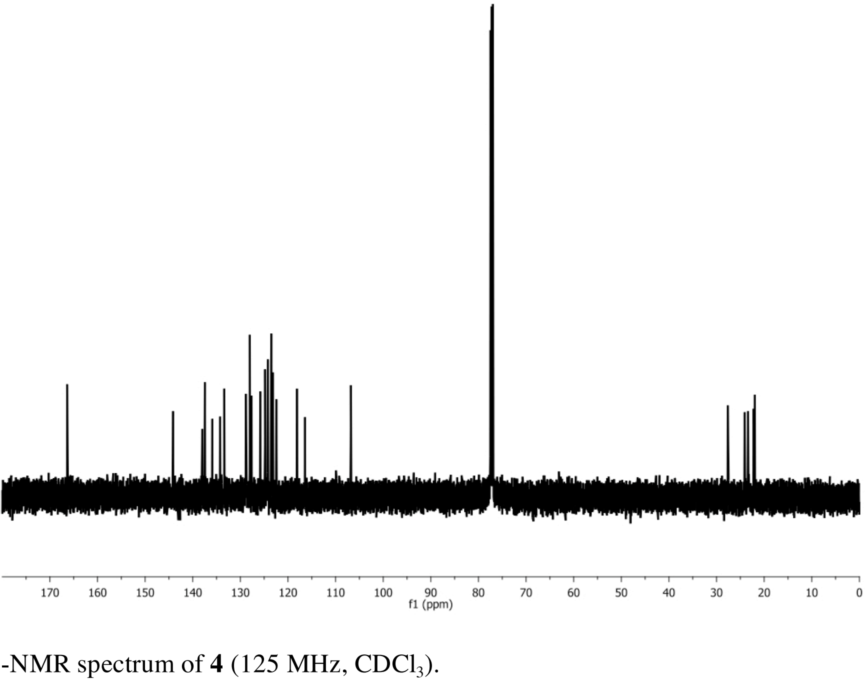

Spectrum 8. ^{13}C-NMR spectrum of **4** (125 MHz, $CDCl_3$).

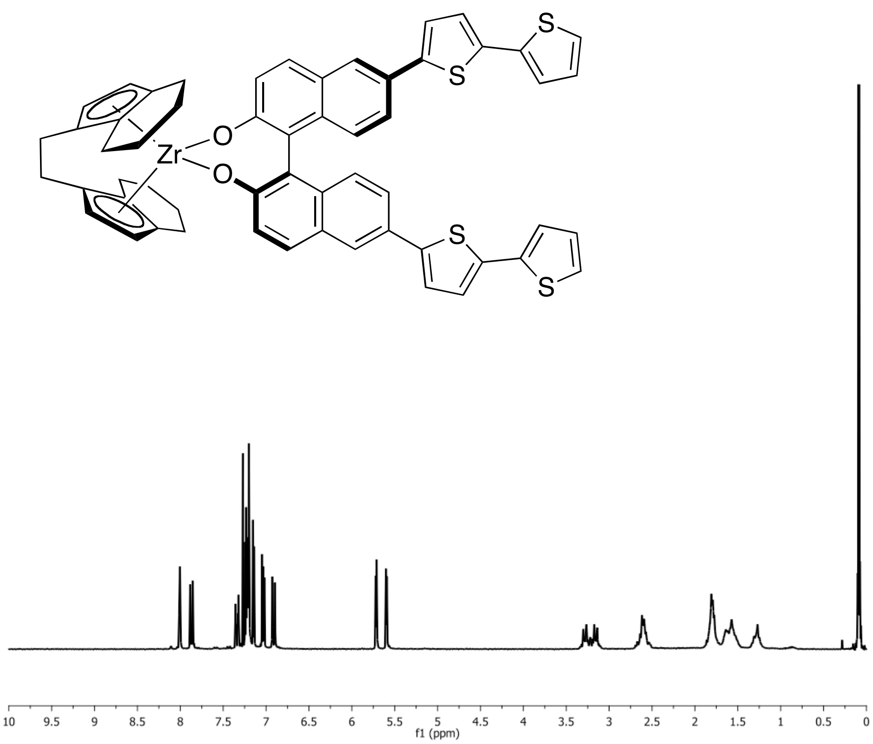

Spectrum 9. ^{1}H-NMR spectrum of **5** (300 MHz, $CDCl_3$).

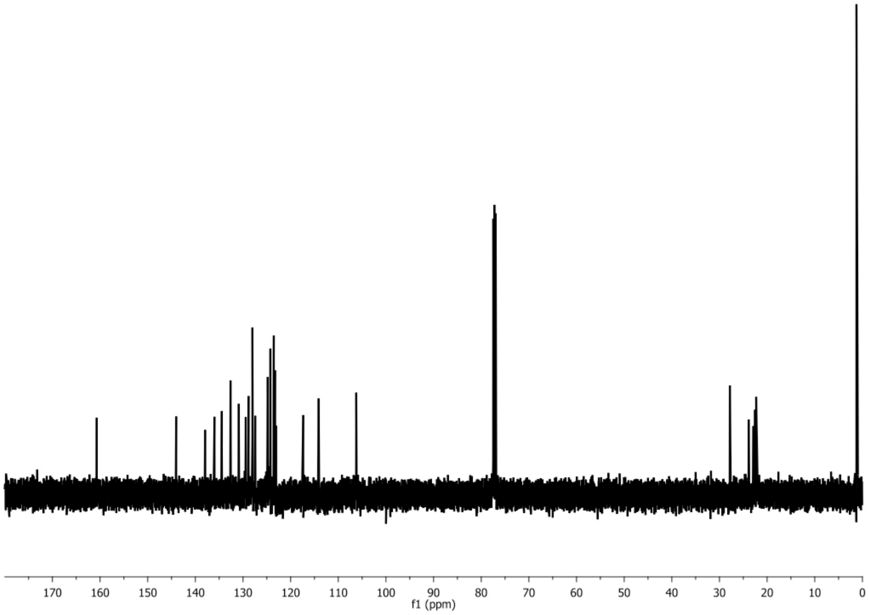

Spectrum 10. ^{13}C-NMR spectrum of **5** (125 MHz, $CDCl_3$).

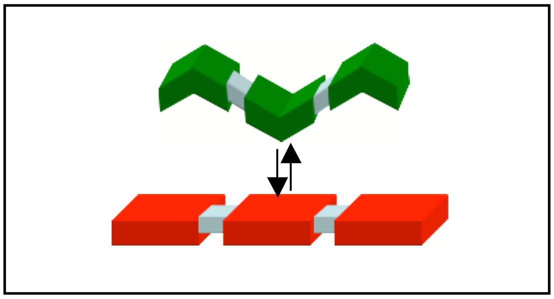

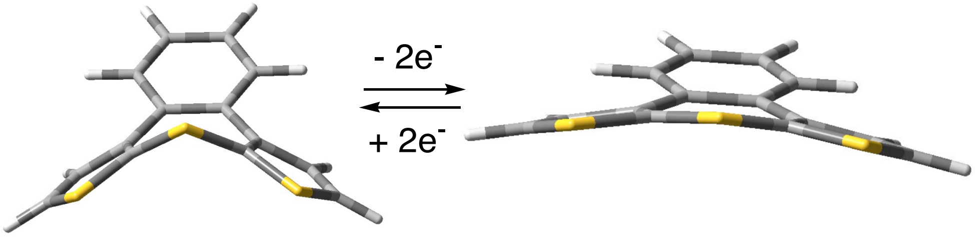

Chapter 5.

Annulated Thiepins as Building Blocks for Actuating and Sensory Materials

Introduction

Conducting polymer (CP) actuators convert the electrochemical energy input to a mechanical output (e.g., volume change) by utilizing the ingress and release of counterions to maintain charge neutrality (swelling mechanism).[1] In most cases, the polymer is oxidized (positively doped) to incorporate counter-anions and associated solvents. When oxidized, the individual chains of CPs do not need to undergo large conformational variations. The dimensional change represents a bulk swelling process.

We proposed the new concept of actuation based upon molecular mechanisms as an alternative to the swelling mechanism. These new mechanisms utilitze the conformational changes within a single polymer chain which can be triggered by electrochemical stimuli. We are interested in developing molecular building blocks with such properties and incorporating them into polymer materials.

One of the candidates suitable for realizing molecular actuation is a molecular scaffold that has a bent geometry in the neutral state, but is a planarized structure when oxidized or reduced (expanding model). One driving force for such a conformational change is the aromatization (*4n±2* π-electrons) energy gained from molecules with *4n* π-electrons, which initially prefer a bent geometry due to antiaromatization. Cyclooctatetraene- and thianthrene-based building bocks have been proposed for this purpose.[2]

Chart 1. Heteroepines

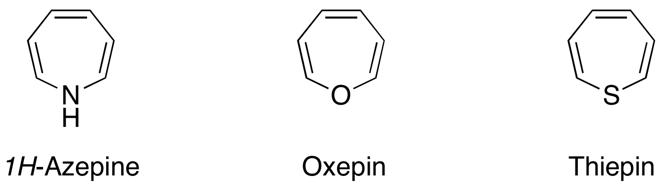

1H-Azepine Oxepin Thiepin

We are interested in conjugated seven-membered ring systems that have a heteroatom with a lone pair of electrons: heteroepines (Chart 1). With the lone pair electrons on the heteroatoms, heteroepines can be considered to be 8 π-electron heteroannulenes, which are antiaromatic according to Hückel's rule. Thus, heteroepines are possible candidates for molecular actuators using "bent-to-planar" transformations under redox control. The chemistries of azepine and oxepin have been well documented,[3] but the thiepin's chemistry is relatively rare due to thermal instability of the parent molecule.[4]

Thermal Stability of Thiepins and Design of the Molecular Scaffold

Compared to azepine and oxepin, thiepin is notoriously unstable and the parent molecule (without any substituent) has not been detected so far. It easily loses the sulfur atom and furnishes a benzenoid product. Sulfur extrusion is believed to occur by valence isomerization to the corresponding thianorcaradiene, followed by the cheletropic loss of sulfur (Scheme 1).[4,5] The pronounced instablility is the result of the low activation energy of the sulfur extrusion step.

Scheme 1. Sulfur Extrusion of Thiepin

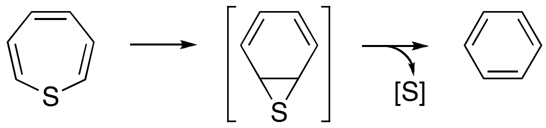

Stable thiepins have been prepared by adding annulation and steric effects (Chart 2). When bulky groups are introduced at the 2- and 7-positions, steric repulsion disfavors the thianorcaradiene intermediate, and the molecules are thermally stable. If aromatic rings are annulated to thiepin, there should be a substantial resonance energy loss in order to be valenceisomerized. Increasing the number of annulated benzene rings results in higher thermal stability of thiepins.[4]

Chart 2. Thiepins

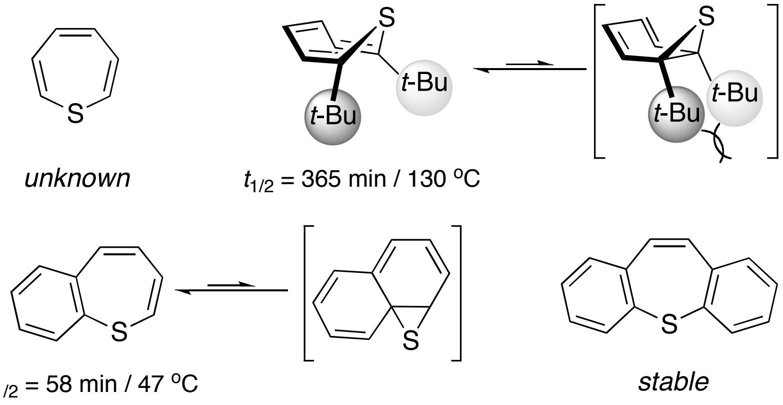
S
unknown
S
t-Bu
t-Bu
$t_{1/2}$ = 365 min / 130 °C
S
t-Bu
t-Bu
S
$t_{1/2}$ = 58 min / 47 °C
S
S
stable

Our design of the molecular building block for actuating material is to annulate aromatic rings to the thiepin system with two thiophenes and one benzene ring (Figure 1a). We chose thiophene due to its electrochemical stability and ease of synthetic modification. Solubilizing groups could also be easily attached to the benzene moiety. We expect further functionalization through α-position of the annulated thiophenes (C3 and C10).

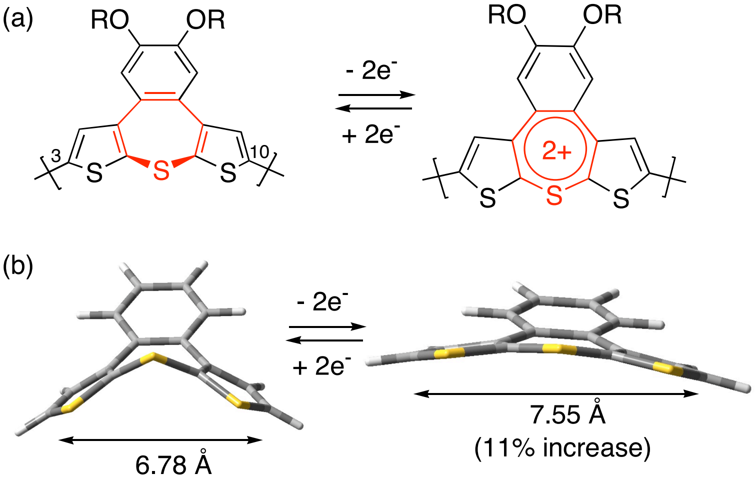
(a)
RO
OR
3
S
S
S
10
- 2e⁻
+ 2e⁻
RO
OR
2+
S
S
S
(b)
- 2e⁻
+ 2e⁻
6.78 Å
7.55 Å
(11% increase)

Figure 1. (a) Design of a annulated thiepin polymer. (b) Geometry optimized (B3LYP, 3-21g) structures of dithieno[*b*,*f*]benzo[*d*]thiepin in its neutral (left) and doubly-oxidized states (right).

We calculated the optimal geometry (B3LYP, 3-21G) of the simple dithieno[*b*,*f*]benzo[*d*]thiepin (Figure 1b). As expected, the molecule of the neutral state adopts a bent geometry. The distance between the outmost carbons (from C3 to C10) is ~6.8 Å. Optimized geometry of the doubly oxidized molecule is nearly planar presumably due to the energy gain from its aromatic electronic structure. The distance between the outmost carbons in the planar conformation is ~7.6 Å which is an 11% increase from the neutral state.

Synthesis of Thiophene-Annulated Thiepins

Yasuike *et al.* reported the synthesis of dithieno[*b*,*f*]thiepins via dilithium intermediates, but did not investigate any applications (Scheme 2).[6] Traditionally, annulated thiepins have been prepared by condensation, elimination, ring expansion or rearrangement, etc.[4] However, Yasuike's approach is modular and they were able to prepare dithienoheteroepines containing group 14, 15, and 16 elements, including thiepins. This "dilithio" method has been applied to the preparation of other heteroepins,[7] annulated thiophenes,[8] and various aromatic thioethers.[9] The typical source of sulfur is sulfur dichloride or bis(phenylsulfonyl) sulfide ($(PhSO_2)_2S$). However, the drawback is the generally low yields, typically ~30% for cyclic products.

Scheme 2. Dilithio Route to Dithienoheteroepines[6]

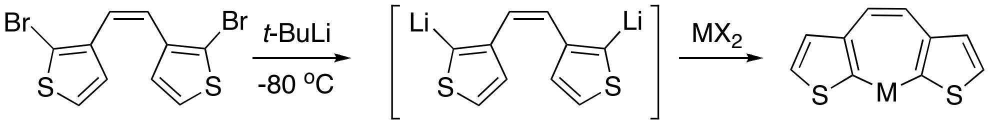

MX_2 = $S(PhSO_2)_2$, $Se(PhSO_2)_2$, Cl_2TeCl_2, $PhPCl_2$, $PhAsCl_2$, $PhSbCl_2$, $PhBiBr_2$
Me_2SiCl_2, Me_2GeCl_2, Me_2SnCl_2

We first followed the same "dilithio" method starting with bis(bromothienyl)benzene derivatives **3a–c**, which were prepared by bromination of compounds **2a–c** (Scheme 3).

Compounds **2a–c** were synthesized starting from catechol according to known procedures that were optimized in our group.[10] Bromination of compounds **2a–c** with NBS were high yielding and highly selective for 2-positions. The dibromides **3a–c** were subjected to lithiation, followed by substitution with sulfur sources. We were able to isolate the desired thiepin products **4a–c**, but the yields were less than 30%. Attempts to improve the yield by varying the solvent or temperature were not successful.

Scheme 3.[a]

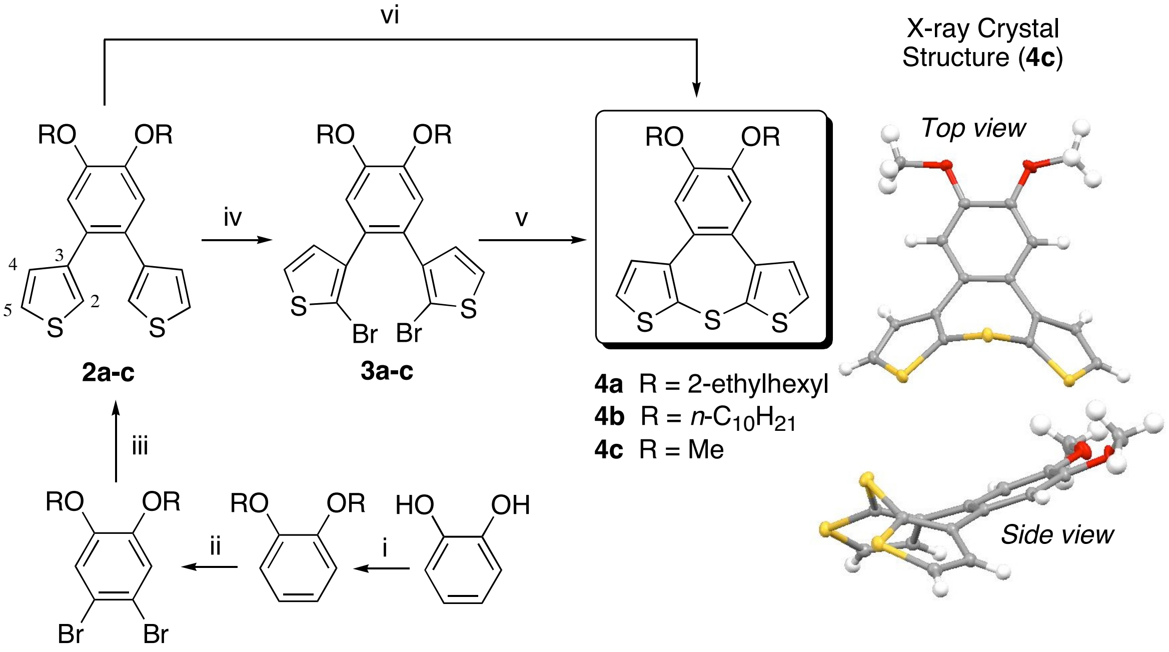

[a]Reagents: (i) K_2CO_3, 1-bromodecane, acetone, reflux, 1 d, 93%. (ii) Br_2, CH_2Cl_2, room temperature, 2 h, 96%. (iii) 3-thiophene boronic acid, Na_2CO_3, $Pd(PPh_3)_4$, toluene, EtOH, H_2O, reflux, 18 h, 94%. (iv) NBS, $CHCl_3$, acetic acid, room temperature, 89%. (v) t-BuLi, Et_2O or THF, then $(PhSO_2)_2S$ or SCl_2, –78 °C → room temperature, <30%. (vi) SCl_2, CH_2Cl_2, –40 °C, 80%.

Noticing that sulfur dichloride could be a good electrophile in the aromatic electrophilic substitution, we tried a direct cyclization with compounds **2a–c**. This route was inspired by the preparation of 3,3'-dipyrrolyl sulfides using sulfur dichloride starting from substituted pyrroles.[11] In addition, the 2-position of thiophene is highly selective over 5-position in other electrophilic reactions (e.g., bromination). Fortunately, we were able to obtain the desired thiepins in good yields. It should be noted that sulfur dichloride needs to be freshly distilled right before use because it tends to decompose to sulfur monochloride (S_2Cl_2) and chlorine.

Thiepins **4a–c** were pale yellow, crystalline powders even with the highly disordering 2-ethylhexyloxy side chains. The X-ray crystal structure of the methoxy derivative **4c** clearly shows the bent geometry at its neutral state. The distance between the outmost carbons (6.85 Å) is in good agreement with the value from the DFT calculation.

In order to examine the effect of the substitution pattern, we synthesized dithieno[3,2-*b*;2',3'-*f*]benzo[*d*]thiepin **7**, which is isomeric to **4b** (Scheme 4). To incorporate bromines into the 3- and 3'-positions, **2b'** was first tetrabrominated and then debrominated to compound **6**. This route was necessary because bromination occurs at the 5-positions first, however lithium-bromine exchange also favors the less sterically hindered 5-positions. Following the standard "dilithio" procedure, we were able to obtain isomeric thiepin **7**, albeit in a low yield.

Scheme 4.[a]

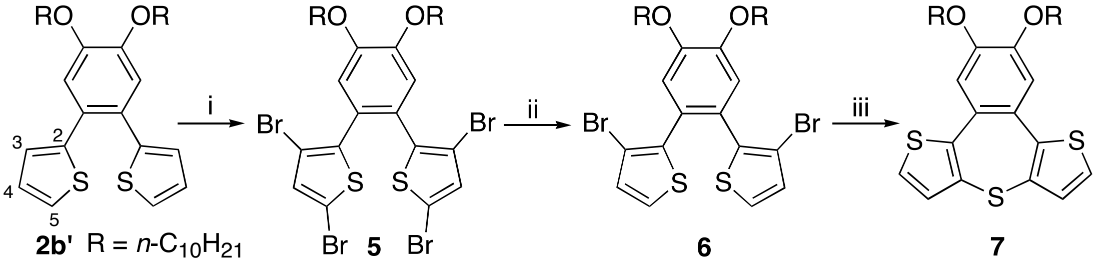

[a]Reagents: (i) NBS (4 equiv), $CHCl_3$, acetic acid, room temperature, 97%. (ii) *n*-BuLi, THF, -78 °C, 30 min, then MeOH, 90%. (iii) *t*-BuLi, Et_2O, $(PhSO_2)_2S$, -78 °C → room temperature, 15 h, 31%.

Cyclic Voltammograms of Annulated Thiepins

Figure 2 shows the cyclic voltammograms (CVs) of compounds **4c** and **7**. The CVs were taken in CH_2Cl_2 with 0.1 M $TBAPF_6$ as a supporting electrolyte on a Pt button electrode with a standard 3-electrode configuration under ambient conditions.

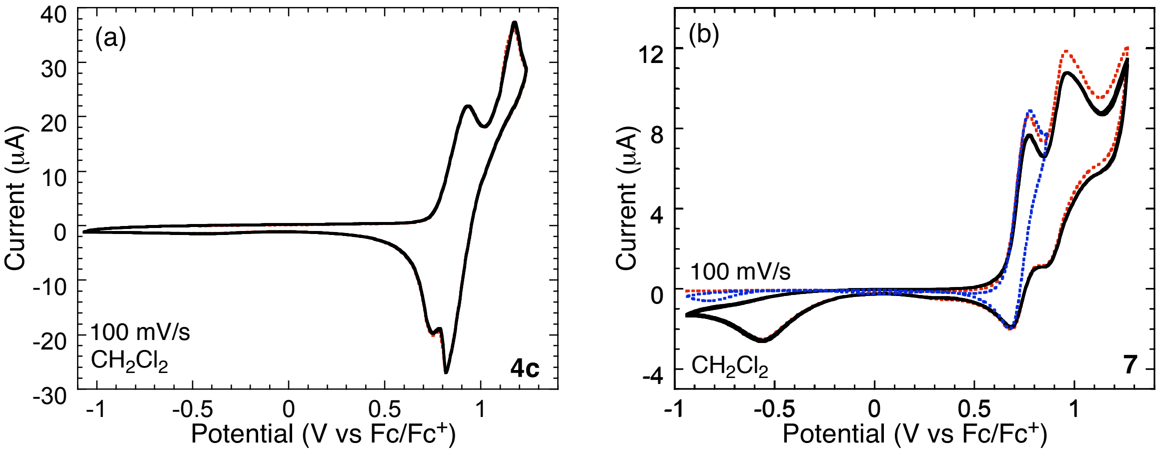

Figure 2. CVs of **4c** (a) and **7** (b) in CH_2Cl_2 with 0.1 M $TBAPF_6$ as a supporting electrolyte. The red dotted lines represent the first scans. The blue dotted line (b) is the scan up to the first oxidation.

Both CVs showed two 1-electron oxidation waves, which could imply the oxidation of the thiepin π-systems from 8 to 6 π-electrons. Oxidation of **7** (0.73 V) occurred at a lower potential than **4c** (0.82 V vs. Fc/Fc^+, the first half potentials). Although more experiments are needed, this difference can be rationalized by the positions where electrons or charges reside, when drawing the stable canonical resonance forms (Scheme 4).

If we assume that the radical prefers the benzyl position, the radical in $\mathbf{7}^{\bullet+}$ is then in the α-position of the thiophene, while the radical in $\mathbf{4c}^{\bullet+}$ is at the β-position. Note that in 5-membered heterocycles (thiophene, pyrrole, and furan), charges prefer being at the α-position, and are susceptible to various chemical reactions (e.g., substitutions, radical-radical couplings, etc.). Moreover, the charge is more delocalized in $\mathbf{7}^{\bullet+}$.

Scheme 4. Proposed Charge Delocalization of **4c**$^{\bullet+}$ and **7**$^{\bullet+}$.

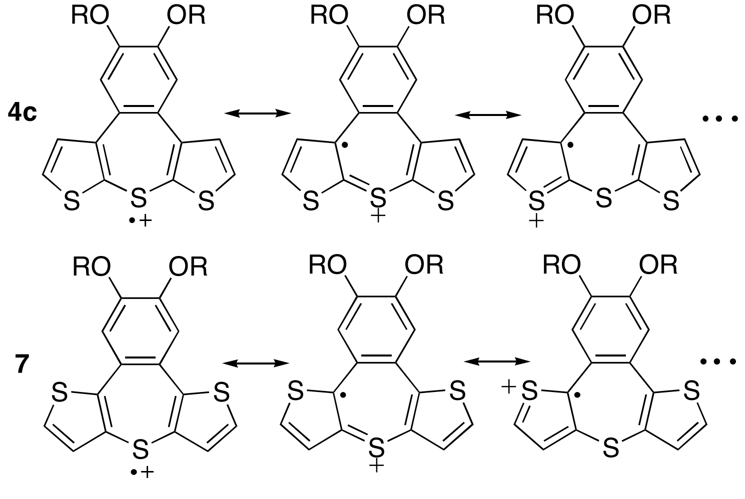

- radical on benzyl and β to sulfur

- radical on benzyl and α to sulfur
- charge is more delocalized

The reduction waves of **4c** and **7** are quite different. The reduction from **4c**$^{2+}$ to **4c**$^{\bullet+}$ appears as a sharp peak, which is at a lower potential than expected. We attribute this to the aromatic energy gained after the second oxidation (8 to 6 π-electrons). In other words, the dication **4c**$^{2+}$ is stabilized by planarization and it takes an over-potential to re-reduce the molecule. The reduction for **7**$^{2+}$ is peculiar and not understood. The reduction was not complete, but an additional reduction peak appeared at the lower potential (~ –0.5 V vs. Fc/Fc^{+}). This strange reduction occurred only from the **7**$^{2+}$, not from **7**$^{\bullet+}$. When we cycled the potentials up to the first oxidation, we did not observe this effect (Figure 2b, blue dotted line).

In short, both thiepin **4c** and **7** showed two 1-electron redox events, which are reproducible under the above conditions. The annulation pattern influences the molecule's oxidation potentials. The sharp reduction from **4c**$^{2+}$ to **4c**$^{\bullet+}$ supports our proposal of planarization by aromatic energy gains.

Electropolymerization of Extended Thiepins

We focused on the **4**-types of thiepins ([2,3-*b*]-annulation). We synthesized electropolymerizable thiepins **9** and **10** by bromination of **4a**, followed by Stille coupling reactions (Scheme 6).

Scheme 6.[a]

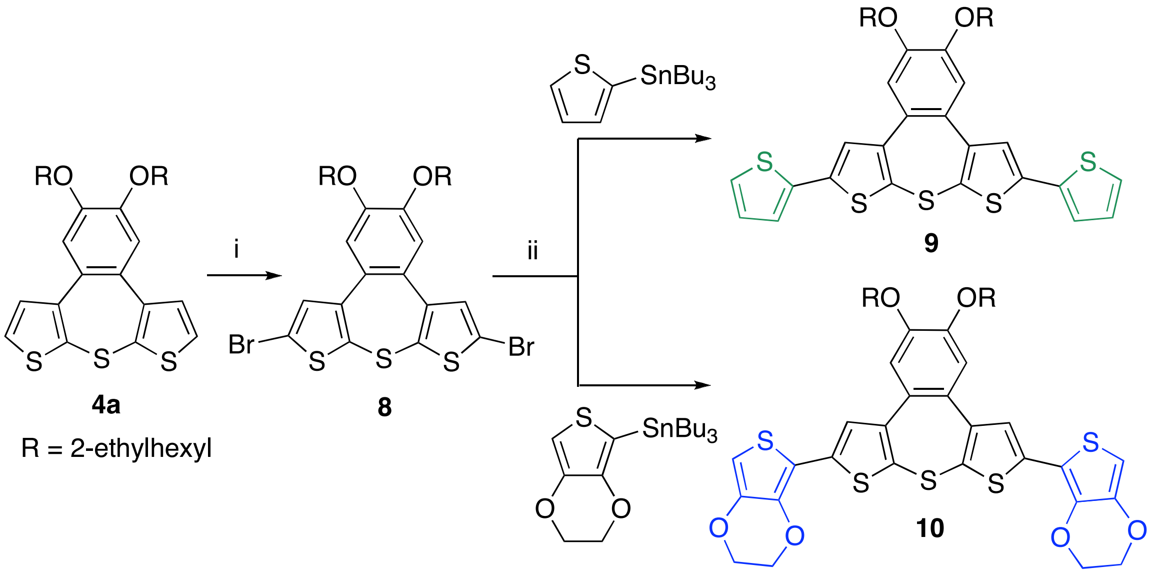

[a]Reagents: (i) NBS, $CHCl_3$, acetic acid, room temperature, 76%. (ii) $PdCl_2(PPh_3)_2$, DMF, 80 °, 15 h, 78-80%.

Electropolymerizations were attempted with monomer solutions in 1:1 mixture of CH_2Cl_2 and CH_3CN with 0.1 M $TBAPF_6$ as a supporting electrolyte under swept potential conditions (Figure 3a and b). In CH_2Cl_2 only, we obtained a similar polymer growth, but the resulting polymers were not irreversibly deposited onto the electrodes to form good films.

Both monomers **9** and **10** were electropolymerized and displayed a linear growth of redox currents. Both poly(**9**) and poly(**10**) have very similar properties as shown in the standard characterization measurements. Scan-rate dependences on the thin polymer films in the monomer-free solution (CH_3CN) are linear, but the shape of the CVs suggests a limited ion diffustion as the films grow thicker (Figure 3c and d). *In situ* conductivity measurements revealed the maximum conductivities were around 60–70 S/cm for both poly(**9**) and poly(**10**) (Figure 4). Spectroelectrochemical measurements show very delocalized electronic structures, especially at high doping levels (Figure 5).

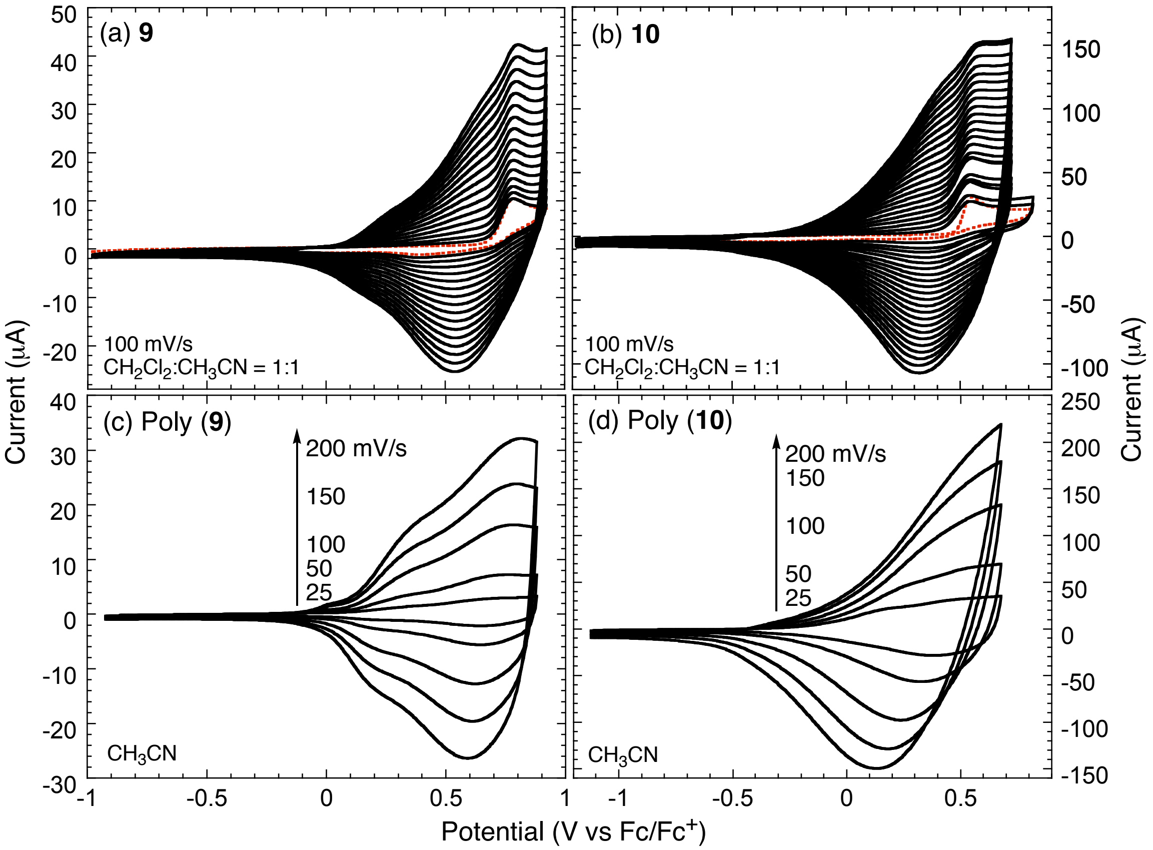

Figure 3. (top) Electropolymerization of **9** (a) and **10** (b) on Pt button electrodes in 1:1 mixture of CH_2Cl_2 and CH_3CN with 0.1 M $TBAPF_6$ as a supporting electrolyte. The red dotted lines represent the first scans. (bottom) CVs of films of poly(**9**) (c) and poly(**10**) (d) at different scan rates.

We found with repeated electrochemical sweeps that the initially red polymers were getting darker, which was more pronounced for electron-rich poly(**10**). We also noticed in the CVs that the redox couple at the low potentials (~0.2 V for poly(**9**) and ~ –0.1V for poly(**10**), all vs. Fc/Fc$^+$) is very similar to that of poly(dithienonaphthalene)s, which were reported earlier in our group by using a tandem cyclization and polymerization mechanism.[10,12] The molecular structure of dithienonaphthalene is identical to the structure obtained if the sulfur is extruded in the thiepins. Moreover, vibrational fine structure was evident in the absorption of poly(**10**) at the neutral state, which is unusual for this type of (flexible) polymers. This implies that the polymer had some rigid molecular frames. The above observations lead to the possibility of sulfur extrusion in the polymers.

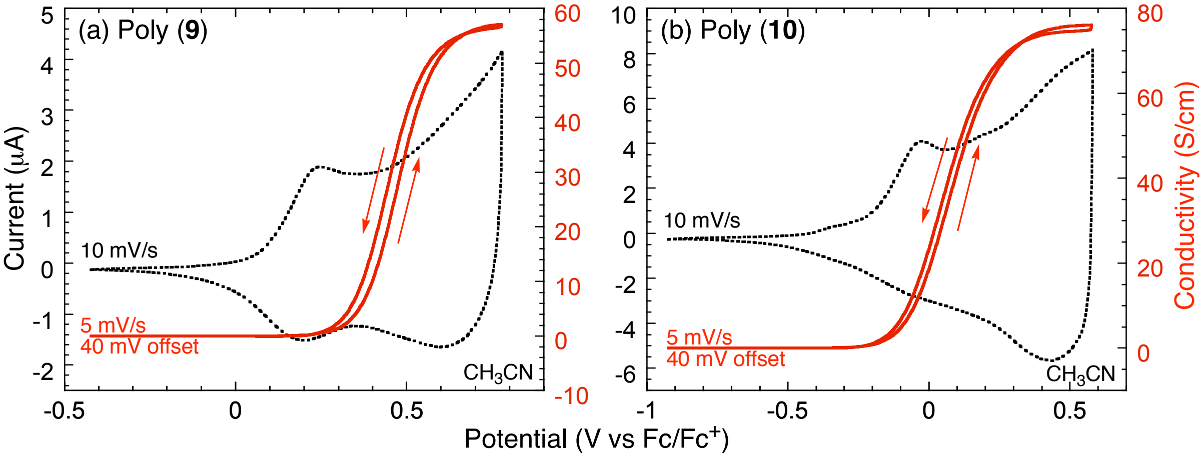

Figure 4. CVs (dotted lines) and *in situ* conductivity measurements (solid lines) of films of poly(**9**) (a) and poly(**10**) (b) on 5-μm interdigitated Pt microelectrodes in CH_3CN with 0.1 M $TBAPF_6$ as a supporting electrolyte.

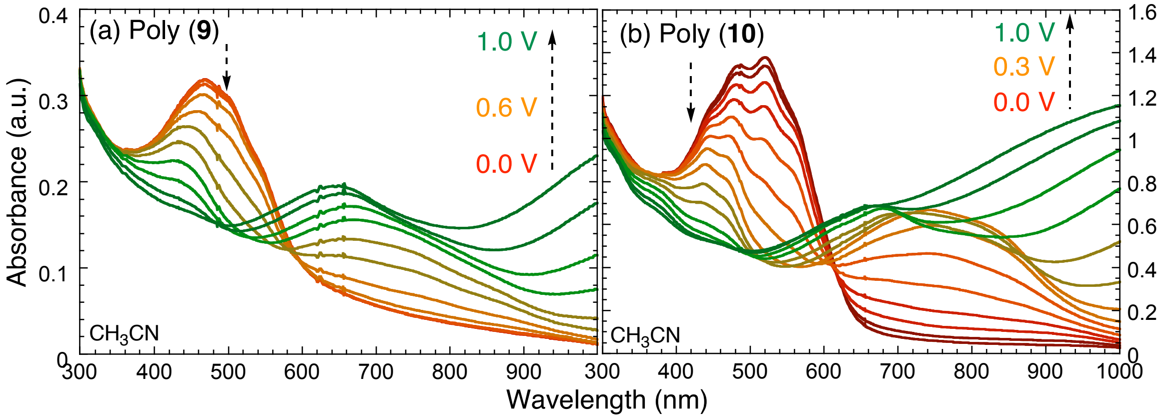

Figure 5. Electronic absorption spectra of films of poly(**9**) (a) and poly(**10**) (b) on ITO-coated glass electrodes in CH_3CN with 0.1 M $TBAPF_6$ as a supporting electrolyte, as a function of oxidation potential from 0.0 V to 1.0 V vs. Ag/Ag^+.

To test this sulfur extrusion hypothesis, we synthesized the thiepin polymers **11** and **12** via cross coupling chemistry (Scheme 7). Polymer **11** consists of only thiophene-annelated thiepins while polymer **12** has alternating structure of thiepins and oligothiophenes. For polymer **11**, we tried an *in situ* stannylation and Stille coupling polymerization[13] to provide the desired polymer of a bright red solid. Although we conducted an extensive screening of reaction conditions, we were only able to get polymer **11** with low molecular weights (6.2 kDa). Copolymer **12** was obtained as an orange-red powder by Stille coupling polymerization with bis(trimethylstannyl)bithiophene, giving a low molecular weight of 8.0 kDa.

Scheme 7.

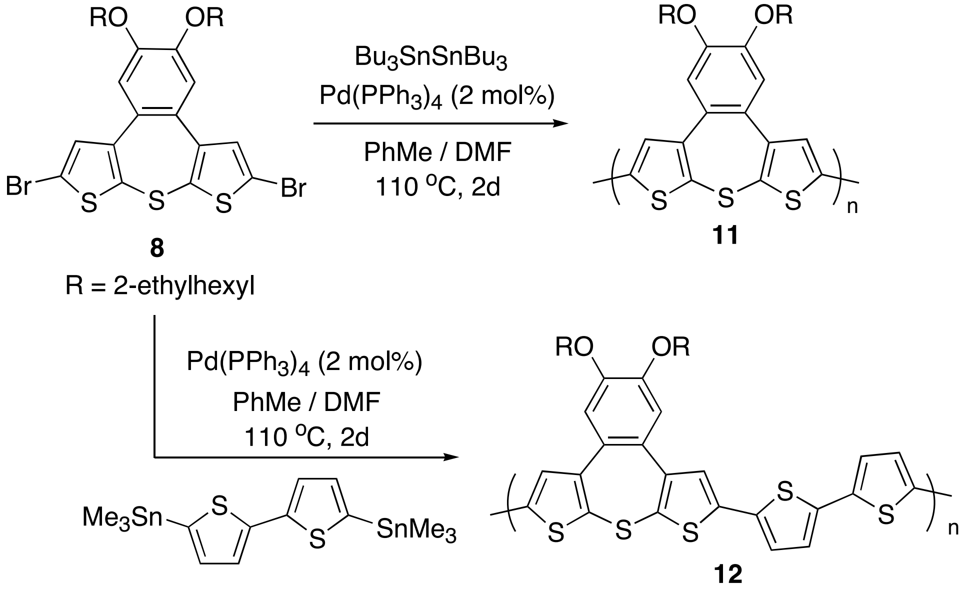

A CH_2Cl_2 solution of polymer **12** with a supporting electrolyte (0.1 M $TBAPF_6$) was subjected to the swept potential conditions (Figure 6). Interestingly, the current gradually increased as the crimson polymer was deposited onto the electrode. The scan-rate dependence in the monomer-free solution shows very good linear proportionality between the peak currents and the scan rates. The peak potentials scarcely moved both for the oxidation and reduction currents, implying exceptional electrochemical kinetics. However, it should be noted that the CVs are similar to those of poly(dithienonaphthalene)s.[12] The polymer could grow either by end-group couplings between oxidized species, or by the solubility changes caused by sulfur extrusion. Indeed, there should be great a difference in solubility from the bent and flexible thiepin structure to the rigid dithienonaphthalenes.

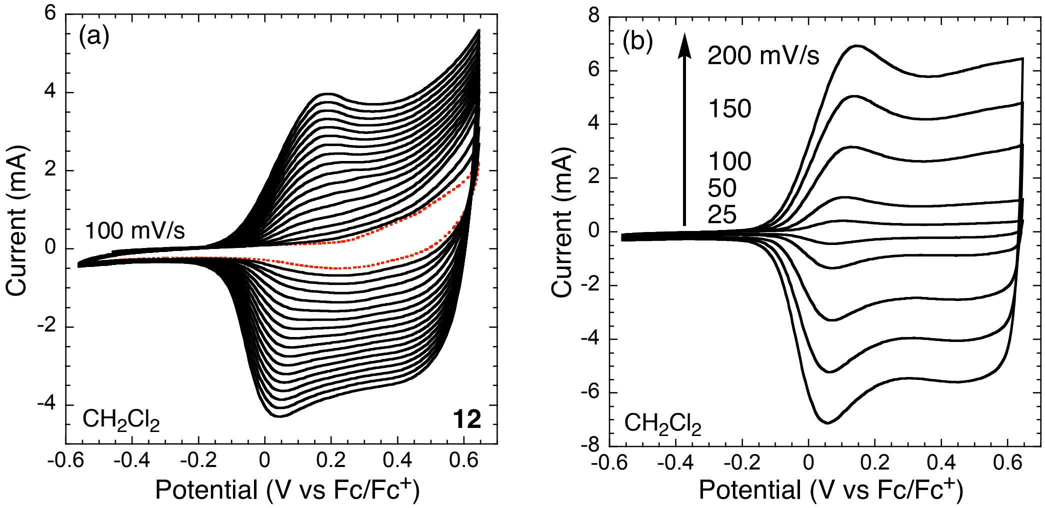

Figure 6. (a) Electrodeposition onto a Pt button electrode from a CH_2Cl_2 solution of polymer **12**. (b) CVs of the resulting polymer at different scan rates. All measurements were with 0.1 M $TBAPF_6$ as a supporting electrolyte.

We subsequently measuered the electroactivity of a drop-cast film of polymer **11**. The onset of the first scan was ~0.9 V, but it shifted to lower potentials (~0.3 V, all vs. Fc/Fc$^+$) with subsequent scans. Furthermore, upon reversing of the high potential in the first scan, the current in its return crossed over that of the first positive sweep, which strongly suggests some irreversible reactions occurred to create materials with lower oxidation potentials. The profiles of successive scans resembled those of poly(dithienonaphthalene)s, which can be produced by the sulfur extrusion.

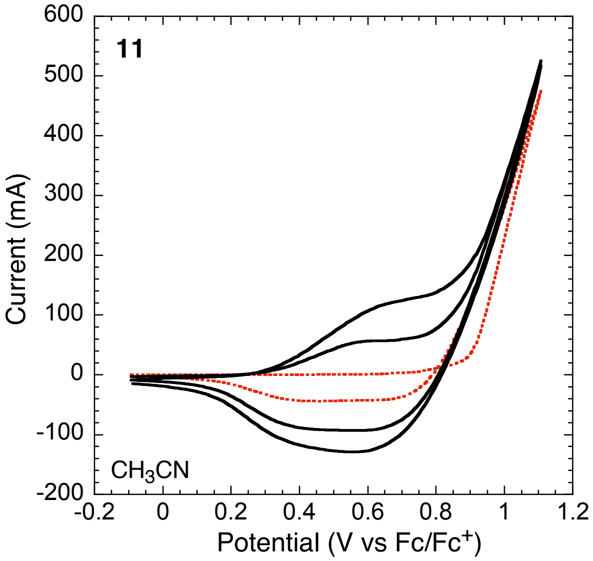

Figure 7. CVs of a drop-cast film of polymer **11** on an ITO-coated glass electrode in CH_3CN with 0.1 M $TBAPF_6$ as a supporting electrolyte. The dotted line represents the first scan.

We conclude that oxidized thiophene-annulated thiepins are unstable and prone to sulfur extrusion (Scheme 8). However, as Figure 2 shows, thiophene-annulated thiepins are electrochemically stable if there is no substitution at 2,2'-positions.

Scheme 8. Sulfur Extrusion of Thiepin Polymer

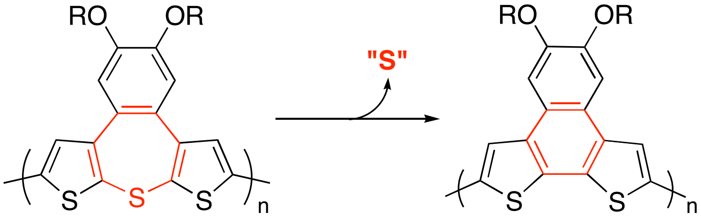

We demonstrated that the substituted thiepins undergo sulfur extrusion with an oxidation and reduction cycle (Scheme 9). Compound **13** was subjected to oxidation by nitrosonium ion in CH_2Cl_2, followed by reduction with methanol. The isolated product was the sulfur-extruded **14**, which was confirmed by NMR and mass spectroscopies. In contrast, when non-substituted **4c** was subjected to the same conditions, the starting material was recovered in a 40% yield, along with the thiepin 1-oxide **15** in a 60% yield. One plausible explanation is that oxidation increases the quinoid character of the annulating thiophenes, which can substantially decrease the activation barrier for the valence isomerization. Note that annulation of aromatic rings successfully increases the thermal stability of thiepins. We expect that any substituent capable of stabilizing the quinoid structure of the oxidized thiophenes may cause the sulfur extrusion.

Scheme 9.

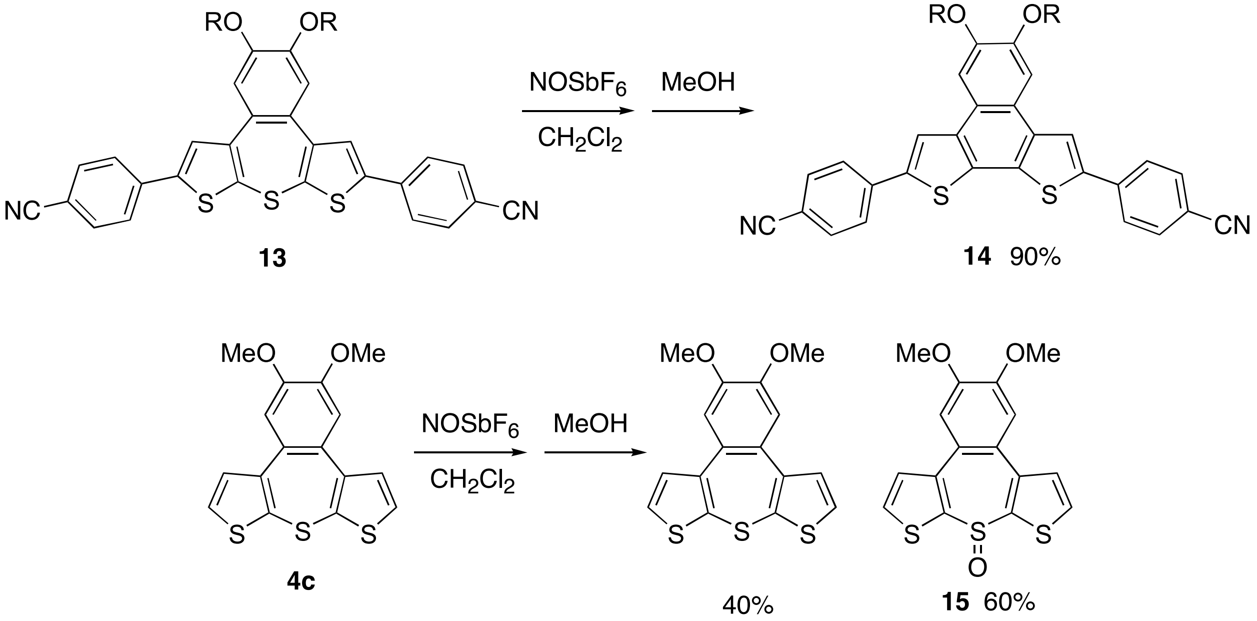

13

14 90%

4c

40%

15 60%

Properties of Thiepin 1-Oxide (Sulfoxide)

Contrary to our proposal, the annulated thiepins with substitutions become labile when oxidized, which is discouraging for use in electrochemical applications. However, we can take advantage of such properties for other applications. Because the sulfur extrusion from the annulated thiepins produces dithienonaphthalenes, which are very rigid and robust in structure, we can expect the photoluminescence would be greatly increased. Note that the annulated thiepin adopts a bent and non-delocalized structure.

It has been known that thiepin 1-oxides (sulfoxide) are less thermally stable than thiepins.[14] Even thiepin 1-oxides from the sterically or electronically stabilized thiepins are easily converted to the benzenoid compounds, presumably through the same valence isomerization and sulfur extrusion mechanism. It should be noted here that unlike thiepin 1-oxides, thiepin 1,1-dioxides (sulfones) are known to be thermally very stable. In fact, the parent thiepin 1,1-dioxide has been isolated as a stable compound at room temperature.[4,15]

The above discussion indicates that if initially non- or weakly-emissive thiepin molecules encounter a peroxide, a portion of the thiepins can be converted to thiepin 1-oxide, which will then transform to a highly fluorescent benzenoid compound. Organic peroxides have been used in explosives (e.g., tricycloacetone peroxides or TCAP) and their detection is of increasing importance. Thus, we decided to investigate the potential of the annulated thiepins as peroxide sensors.

We first synthesized the thiepin 1-oxide **15** from thiepin **4c** by reaction with *m*-chloroperoxybenzoic acid in CH_2Cl_2 at low temperature (Scheme 10). With 1 equivalent of peroxide, thiepin 1,1-dioxide was also formed as a byproduct in a ~15% yield. We were able to isolate the thiepin 1-oxide **15** as a crystalline solid, but it slowly decomposed at room temperature. However, it was stable enough to be characterized, and fortunately we could obtain a single crystal at –20 °C.

The molecular structure of thiepin 1-oxide **15** is similar to that of thiepin **4c** with a slight increase of the distance between the outmost carbons (6.897 vs 6.853 Å). In the ^{1}H-NMR spectrum, there were two sets of signals in a roughly 3:1 ratio, indicating two isomers are present. We obtained the X-ray crystal structure with the oxygen in the *endo*(axial)-position. However, thiepin 1-oxide with the oxygen in the *exo*(equatorial)-position is another possible structure. X-ray structure of a related benzothiepin 1-oxide with sulfoxide oxygen's *exo*-position was previously reported.[16]

Scheme 10.

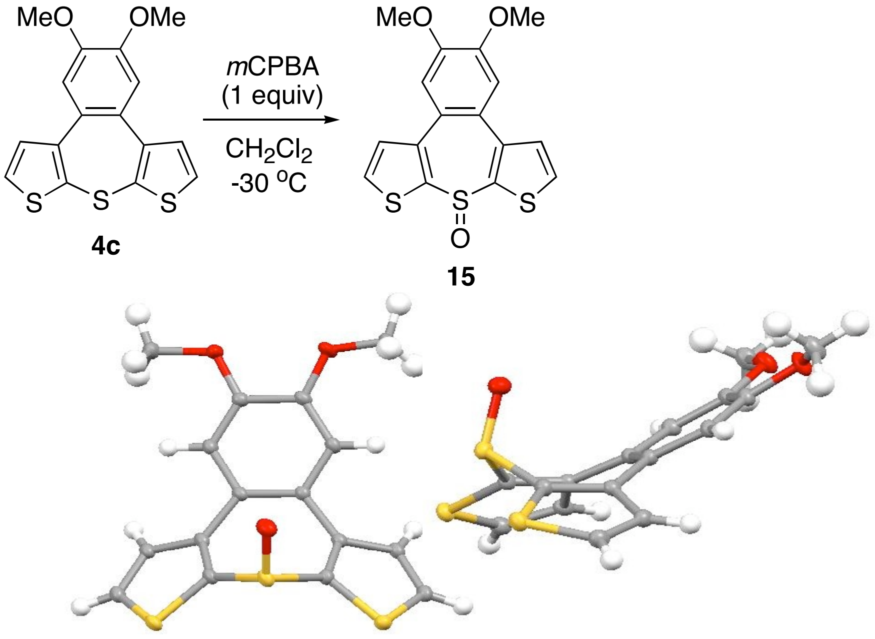
MeO
OMe
S
4c
*m*CPBA
(1 equiv)
CH2Cl2
-30 °C
MeO
OMe
S
O
15

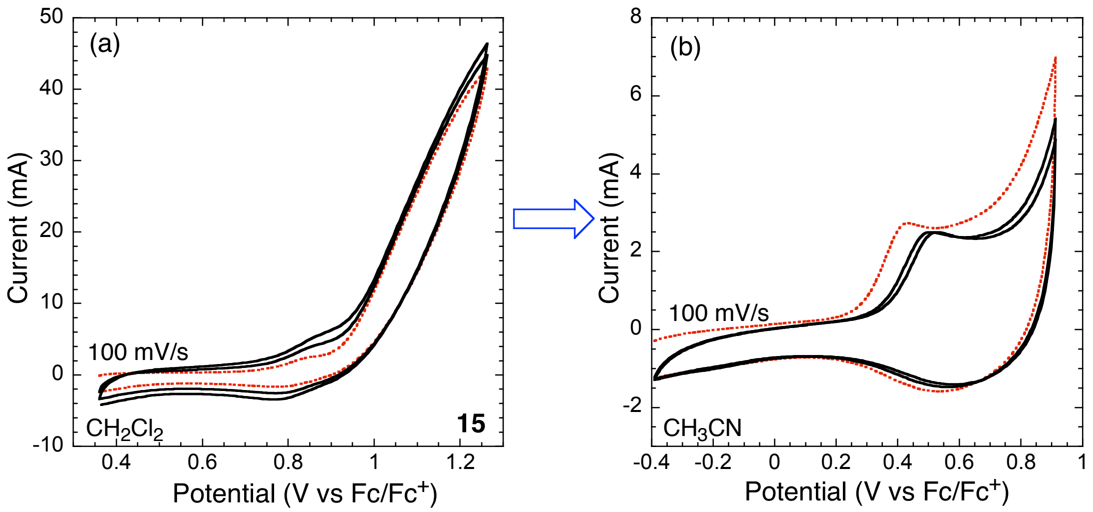

Figure 8. (a) CVs of thiepin 1-oxide **15** in CH_2Cl_2 with 0.1 M $TBAPF_6$ as a supporting electrolyte. (b) CVs of the material that was deposited on the electrode during the CV measurement of **15** (a). The dotted lines represent the first scans.

Cyclic voltammograms measured in CH_2Cl_2 solution revealed the instability of thiepin 1-oxide **15** (Figure 8). While thiepin **4c** showed reproducible and quasi-reversible waves (Figure 2), oxidation of thiepin 1-oxide was completely irreversible under the conditions. Interestingly, we found a dark brown material deposited on the electrode after the CV measurements. The CV of the material measured in acetonitrile solution resembled that of poly(dithienonaphthalene)s, suggesting the sulfoxide (SO) was extruded.

We utilized compounds **9** and **10** as the sensory materials because they could produce well-extended, highly emissive chromophores. We synthesized thiepin 1-oxide **16** and dithienonaphthalene **18** in order to compare the photophysical properties (Scheme 11). Thiepin 1-oxide **16** was prepared using similar conditions for the preparation of **15**. Dithienonaphthalene **18** was prepared by Stille coupling reaction with compound **17**, which was prepared by following the literature procedure.[10]

Scheme 11.[a]

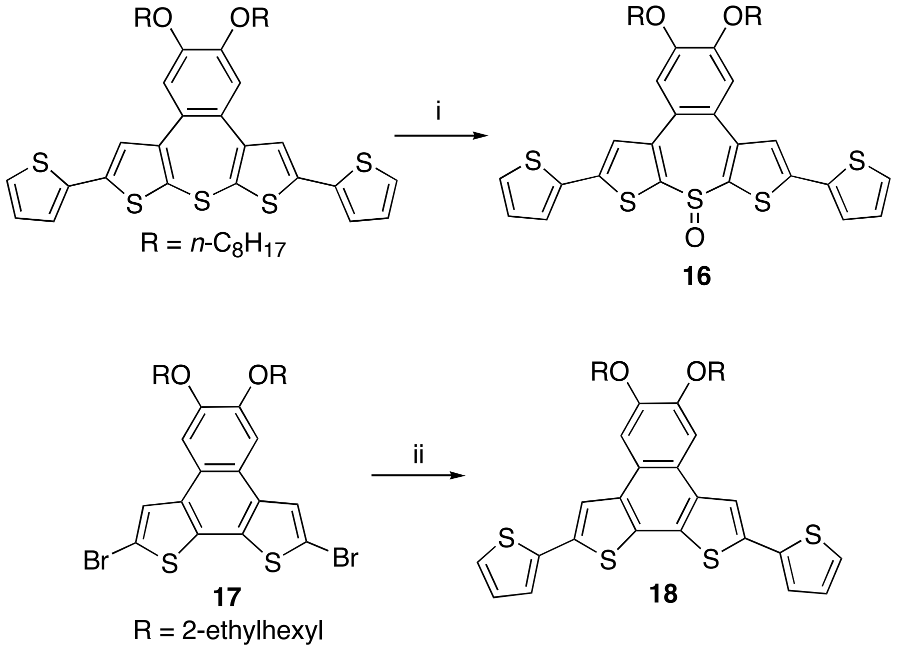

[a]Reagents: (i) *m*-chloroperoxybenzoic acid, CH_2Cl_2, -20 °C, 1 h, 55%. (ii) 2-Tributylstannylthiophene, $PdCl_2(PPh_3)_2$, DMF, 80 °C, 15 h, 70%.

Figure 9 shows UV-vis absorbance and fluorescence spectra of thiepin 1-oxide **16** and dithienonaphthalene **18** measured in CH_2Cl_2 solution under air. As expected, dithienonaphthalene **18** was highly fluorescent and gave an emissive band with vibronic structure (Figure 9c). The maximum fluorescent intensity of **18** was observed at 433 nm and the UV-vis absorption maximum was at 396 nm. The UV-vis spectrum of thiepin 1-oxide **16** contained a tail at around 400 nm. From the shape of the spectrum, it appears that the dithienonaphthalene **18** was already generated in the mixture.

The fluorescence spectrum of **16** showed the shoulder around 400 nm in addition to a well-resolved vibronic structure. The latter can be well matched to the spectrum of dithienonaphthalene **18**, so we can conclude the sample contained a mixture of **16** and **18**. Excitation spectra clearly demonstrated that there were two emitting chromophores in the sample (Figure 9b). The excitation spectrum of the 399-nm emission is well matched with the **16**'s absorption. On the other hand, the excitation spectra of the 432- and 458-nm emissions resemble the absorption spectrum of **18**. Furthermore, when the fluorescence was measured again with the same sample, we observed the shoulder's intensity was decreased whereas peaks common with **16** increased (Figure 9a). The above data confirm that the thiepin 1-oxide **16** was converted to dithienonaphthalene **18**.

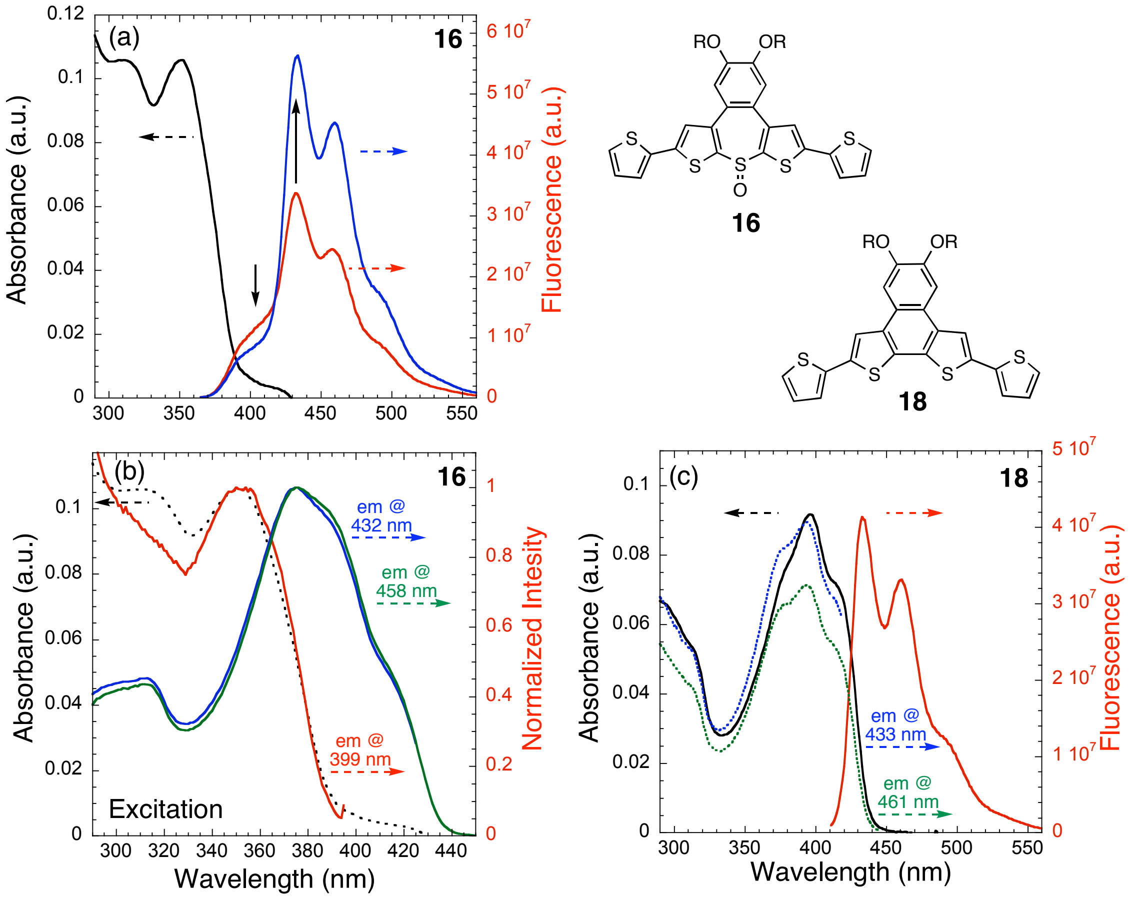

Figure 9. (a) Absorption and emission spectra for **16**. For emission, red line represents the first measurement, and blue line the second. (b) Excitation spectra of **16** for emissions at indicated wavelengths. The absorption spectrum from 'a' were plotted as a dotted line for comparison. (c) Absorption and emission spectra for **18**, with excitation spectra in dotted lines. All spectra were acquired at room temperature in CH_2Cl_2.

We subsequently examined the fluorescence changes when **9** and **10** were exposed to a peroxide. In a cuvette containing a CH_2Cl_2 solution of **9** or **10**, we added one drop of a CH_2Cl_2 solution containing *m*-chloroperoxybenzoic acid (~0.05 M, excess) and monitored the fluorescence intensities as time progressed. Thiepin **9** (Figure 10a) displayed emissions that are very similar to Figure 9a. Therefore, it is reasonable to conclude that the mixture contained thiepin 1-oxide **16** and dithienonaphthalene **18**. The fluorescence at 400 nm, which is from the thiepin 1-oxide **16**, increased, followed by increase of dithienonaphthalene **18**'s fluorescence. The trend is conserved for EDOT-containing **10**, except a ~10-nm red-shift in the fluorescence maxima (Figure 10b). However, in the case of **10**, the time evolution was much faster when compared to **9**, presumably due to the electron-rich character of **10**.

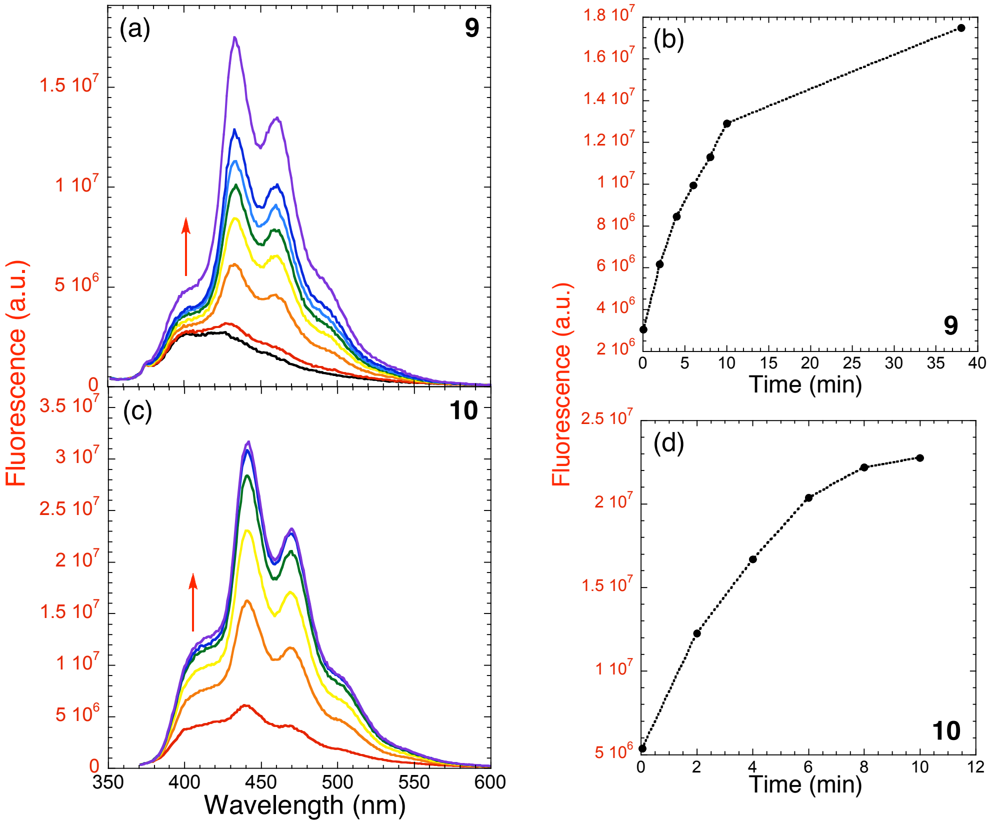

Figure 10. Time evolution of emission spectra for **9** (a) and **10** (c) in the presence of *m*-chloroperoxybenzoic acid (excess) at room temperature in CH_2Cl_2. Emission maxima were plotted as a function of elapsed time (c and d).

The fact that the emission from dithienonaphthalenes developed and we also observed the emission from thiepin 1-oxides suggests that de-sulfoxidation (k_2) (Scheme 12) is the rate-limiting step. If this thiepin system is to be used for a peroxide sensor, the substituents need to be tuned in order to increase the de-sulfoxidation rate. In this way, we can prevent double oxidation to sulfone, which is known to be very stable.

Scheme 12.

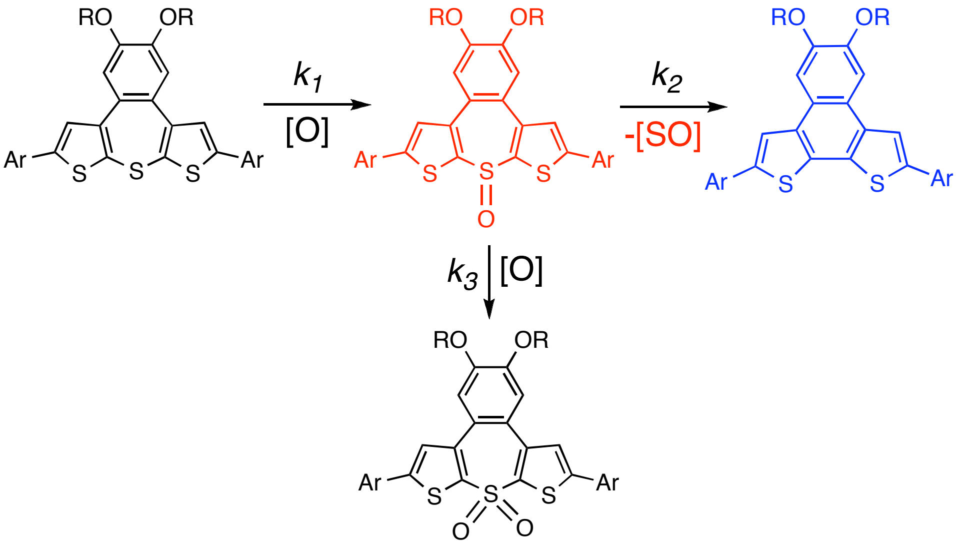

Conclusions

We have designed and synthesized annulated thiepin systems, which would undergo bent-to-planar transformation driven by aromatization under electrochemical control. In the cyclic voltammetry, dithienobenzothiepin **4c** showed a very interesting sharp peak for the reduction of dication **4c**$^{2+}$, which supports aromatic energy gains in the doubly oxidized thiepin. However, in spite of the thermal stability in the neutral state, extended thiepin systems were unstable when oxidized, probably due to the non-aromatic character in the oxidized molecules and polymers. The effort for developing new heteroepine systems has been continued with azepines (Chapter 6). Although sulfur extrusion was not suitable for actuating applications, such a property was tested as a peroxide sensor, exploiting the fact that sulfoxide has an even lower extrusion barrier than sulfur. Preliminary studies exhibited the increased fluorescence originated from the extrusion products. Fine-tuning of substituents is needed to accelerate the extrusion reaction.

Experimental Section

General. NMR spectra were recorded on a Varian Mercury-300, Bruker Advance-400, or Varian Inova-500 spectrometer. Chemical shifts are reported in ppm and referenced to residual solvent peaks ($CDCl_3$: δ 7.27 ppm for ^1H, δ 77.23 ppm for ^{13}C). High-resolution mass spectra (HR-MS) were obtained on a Bruker Daltonics APEX II 3 Tesla FT-ICR-MS. UV-vis spectra were obtained using a HP 8453 diode array spectrometer. Electrochemical measurements were carried out using an Autolab PGSTAT 10 or PGSTAT 20 potentiostat (Eco Chemie) in a three-electrode cell configuration consisting of a quasi-internal Ag wire reference electrode (BioAnalytical Systems) submerged in 0.01 $AgNO_3$ / 0.1 M tetrabutylammonium hexafluorophosphate ($TBAPF_6$) in anhydrous CH_3CN, a Pt button (1.6 mm in diameter) electrode, 5-μm interdigitated Pt microelectrode, or ITO-coated glass electrode as the working electrode, and a Pt coil or Pt gauze as the counter electrode. The ferrocene/ferrocenium (Fc/Fc^+) redox couple was used as an external reference. Half-wave potentials of Fc/Fc^+ were observed between 210-245 mV vs Ag/Ag^+ in CH_2Cl_2, and between 80-91 mV vs Ag/Ag^+ in CH_3CN. EPR spectra were obtained using a Bruker Model EMX Electron Paramagnetic Resonance Spectrometer operating as the X-band with 100 kHz modulation at room temperature. All air and water sensitive synthetic manipulations were performed under an argon or nitrogen atmosphere using standard Schlenk techniques.

Materials. SCl_2 was synthesized from S_2Cl_2 with Cl_2 according to the literature method[17] and freshly distilled with a few drops of PCl_3 prior to use. Spectroscopic grade CH_2Cl_2 was purchased from Aldrich for electrochemistry. $TBAPF_6$ was recrystallized in ethanol prior to use. Anhydrous DMF was purchased from Aldrich as Sure-Seal Bottles and used as received. THF, anhydrous CH_2Cl_2, and toluene were purified by passage through two alumina columns of an

Innovative Technologies purification system. All other chemicals were of reagent grade and used as received.

Compounds **2a–c**, **3a–c**, **3b'**, and **17** were prepared by literature methods.[10,12] 5,5'-Bis(trimethylstannyl)-2,2'-bithiophene was synthesized by reported procedures.[18] The structure of benzo[*d*]-dithieno[2,3-*b*;3',2'-*f*]-thiepin and its numbering are shown as follow.

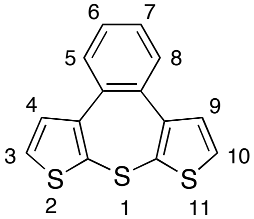

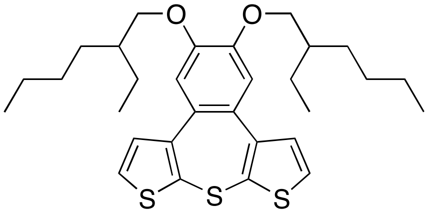

6,7-Di(2-ethylhexyloxy)-benzo[*d*]-dithieno[2,3-*b*;3',2'-*f*]-thiepin (4a). A freshly distilled SCl_2 (2.1 mL, 16.5 mmol) in CH_2Cl_2 (100 mL) was added dropwise to a CH_2Cl_2 (450 mL) solution of compound **2a** (7.48 g, 15 mmol) at –40 °C under Ar. The mixture was slowly warmed to room temperature and stirred for 15 h, at which time the mixture was poured into 10% aqueous $NaHCO_3$. The organic layer was washed with brine, dried over $MgSO_4$, and evaporated under reduced pressure. The crude mixture was subjected to column chromatography (dichloromethane:hexane = 1:10). The product was further purified by recrystallization (dichloromethane/methanol). Yield: 6.04 g (76%) of lightly yellow solid. ^1H NMR (500 MHz, $CDCl_3$) δ: 7.25 (d, 2H, $J = 5.5$ Hz), 7.13 (d, 2H, $J = 5.5$ Hz), 7.05 (s, 2H), 3.96 (m, 4H), 1.82 (m, 2H), 1.57–1.34 (m, 16H), 0.94 (m, 12H). ^{13}C NMR (125 MHz, $CDCl_3$) δ: 148.90, 145.33, 130.71, 129.44, 127.95, 126.44, 114.13, 71.72, 39.75, 30.82, 29.34, 24.16, 23.31, 14.33, 11.44. HR-MS (ESI): calcd for $C_{30}H_{40}O_2S_3$ $[M+Na]^+$, 551.2083; found, 551.2077.

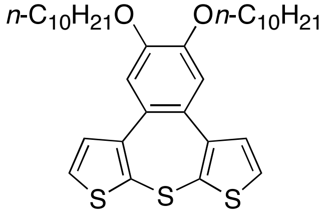

6,7-Di(decyloxy)-benzo[*d*]-dithieno[2,3-*b*;3',2'-*f*]-thiepin (4b). Using the same procedure for the preparation of **4a**, compound **2b** (1.31 g, 2.36 mmol) in CH_2Cl_2 (100 mL) was treated with SCl_2 (0.3 mL, 2.36 mmol) in CH_2Cl_2 (50 mL). Yield: 1.03 g (75%) of lightly yellow solid. ^1H NMR (400 MHz, $CDCl_3$) δ: 7.24 (d, 2H, J = 5.4 Hz), 7.11 (d, 2H, J = 5.4 Hz), 7.06 (s, 2H), 4.09 (m, 4H), 1.87 (m, 4H), 1.52–1.28 (m, 28H), 0.90 (t, 6H, J = 7.0 Hz). ^{13}C NMR (125 MHz, $CDCl_3$) δ: 148.56, 145.24, 130.76, 129.40, 128.13, 126.47, 114.57, 69.55, 32.13, 29.86, 29.81, 29.63, 29.58, 29.46, 26.26, 22.91, 14.35. HR-MS (ESI): calcd for $C_{34}H_{48}O_2S_3$ $[M+Na]^+$, 607.2709; found, 607.2722.

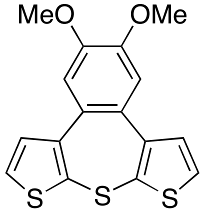

6,7-Dimethoxy-benzo[*d*]-dithieno[2,3-*b*;3',2'-*f*]-thiepin (4c). Using the same procedure for the preparation of **4a**, compound **2c** (1.51 g, 5 mmol) in CH_2Cl_2 (30 mL) was treated with SCl_2 (0.635 mL, 5 mmol) in CH_2Cl_2 (15 mL). Yield: 1.26 g (76%) of lightly yellow solid. ^1H NMR (500 MHz, $CDCl_3$) δ: 7.26 (d, 2H, J = 5.4 Hz), 7.13 (d, 2H, J = 5.4 Hz), 7.06 (s, 2H), 3.98 (s, 6H). ^{13}C NMR (125 MHz, CDCl$_3$) δ: 148.39, 145.10, 131.08, 129.30, 128.15, 126.65, 112.25, 56.24. HR-MS (ESI): calcd for $C_{16}H_{12}O_2S_3$ [M+Na]$^+$, 354.9892; found, 354.9893.

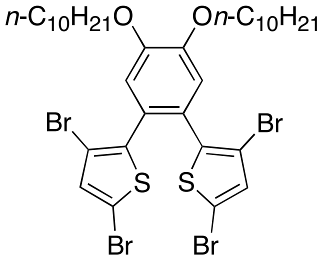

1,2-Di(decyloxy)-4,5-bis(3,5-dibromothiophen-2-yl)benzene (5). To the mixture of compound **3b'** (2.07 g, 3.7 mmol), CHCl$_3$ (40 mL), and AcOH (40 mL) was added NBS (2.72 g, 15.2 mmol) in portions. After being stirred at room temperature for 6 h, the mixture was diluted with CHCl$_3$. The organic layer was washed with water and brine, dried over MgSO$_4$, and evaporated under reduced pressure. The crude mixture was subjected to column chromatography (ethyl acetate:hexane = 1:15). Yield: 3.12 g (97%) of white solid. ^{1}H NMR (400 MHz, CDCl$_3$) δ: 6.97 (s, 2H), 6.94 (s, 2H), 4.07 (m, 4H), 1.87 (m, 4H), 1.51 (m, 4H), 1.39–1.28 (m, 24H), 0.91 (t, 6H, J = 6.6 Hz). ^{13}C NMR (100 MHz, CDCl$_3$) δ: 149.41, 138.62, 132.45, 124.40, 116.14, 112.87, 110.01, 69.31, 32.10, 29.81, 29.76, 29.58, 29.54, 29.25, 26.18, 22.89, 14.34. HR-MS (ESI): calcd for $C_{34}H_{46}Br_4O_2S_2$ [M]$^+$, 869.9640; found, 869.9646.

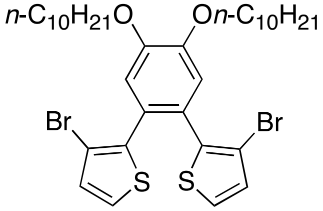

1,2-Di(decyloxy)-4,5-Bis(3-bromothien-2-yl)benzene (6). To a THF (12 mL) solution of compound **5** (1.06 g, 1.2 mmol) was added dropwise n-BuLi (1.6 M in hexane, 1.54 mL, 2.46

mmol) at –78 °C under Ar. After being stirred for 30 min, methanol (1 mL) was added to quench and the mixture was warmed to room temperature. The mixture was diluted with diethyl ether and washed with water and brine. The organic layer was dried over $MgSO_4$, evaporated under reduced pressure, and subjected to column chromatography (dichloromethane:hexane 1:4). The product was further purified by recrystallization (dichloromethane/methanol) at –20 °C. Yield: 0.773 g (90%) of white solid. ^{1}H NMR (400 MHz, $CDCl_3$) δ: 7.20 (d, 2H, *J* = 5.3 Hz), 7.00 (s, 2H), 6.93 (d, 2H, *J* = 5.3 Hz), 4.08 (m, 4H), 1.88 (m, 4H), 1.64 (m, 4H), 1.50–1.30 (m, 24H), 0.90 (t, 6H, *J* = 6.2 Hz). ^{13}C NMR (125 MHz, $CDCl_3$) δ: 149.05, 137.34, 130.15, 126.22, 125.26, 116.38, 110.73, 69.32, 32.10, 29.82, 29.77, 29.60, 29.55, 29.31, 26.21, 22.88, 14.33. HR-MS (ESI): calcd for $C_{34}H_{48}Br_2O_2S_2$ $[M]^+$, 712.1449; found, 712.1436.

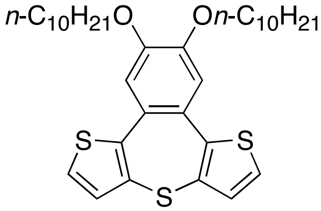

6,7-Di(decyloxy)-benzo[*d*]-dithieno[3,2-*b*;2’,3’-*f*]-thiepin (7). To a cooled (–78 °C) Et_2O (50 mL) solution of compound **6** (0.713 g, 1 mmol) was added dropwise *t*-BuLi (1.7 M in hexane, 2.41 mL, 4.1 mmol). The initially cloudy mixture became clear as lithiation proceeded. After the mixture was stirred at –78 °C for 10 min, $(PhSO_2)_2S$ was added in portions. The mixture was allowed to stir at –78 °C for 3 h, and then at room temperature for another 12 h. After being diluted with diethyl ether, the mixture was washed with 10% aqueous $NaHCO_3$ and brine. The organic layer was dried over $MgSO_4$, and evaporated under reduced pressure. The crude mixture was subjected to column chromatography (chloroform:hexane = 1:7). Yield: 0.181g (31%) of light yellow solid. ^{1}H NMR (400 MHz, $CDCl_3$) δ: 7.29 (d, 2H, *J* = 5.2 Hz), 7.10 (s, 2H), 6.93 (d, 2H, *J* = 5.2 Hz), 4.09 (m, 4H), 1.87 (m, 4H), 1.50 (m, 4H), 1.40–1.28 (m, 24H), 0.89 (t, 6H, *J* = 6.8 Hz). ^{13}C NMR (125 MHz, CDCl$_3$) δ: 149.18, 143.17, 131.49, 130.70, 125.86, 125.76, 115.38, 69.54, 32.14, 29.86, 29.81, 29.62, 29.58, 29.36, 26.23, 22.92, 14.36. HR-MS (ESI): calcd for $C_{34}H_{48}O_2S_3$ [M+Na]$^+$, 607.2709; found, 607.2711.

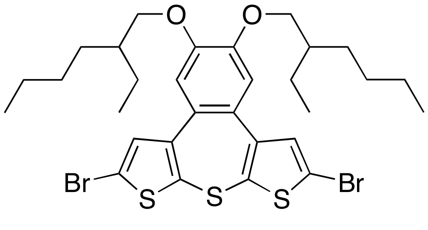

3,10-Dibromo-6,7-di(2-ethylhexyloxy)-benzo[*d*]-dithieno[2,3-*b*;3',2'-*f*]-thiepin (8). To the mixture of compound **4a** (1.74 g, 3.3 mmol), CHCl$_3$ (20 mL), and AcOH (20 mL) was added NBS (1.24 g, 6.9 mmol) in portions. After being stirred at room temperature for 15 h, the mixture was diluted with CHCl$_3$. The organic layer was washed with water and brine, dried over MgSO$_4$, and evaporated under reduced pressure. The crude mixture was subjected to column chromatography (dichloromethane:hexane = 1:10). Yield: 1.73 g (76%) of white solid. ^{1}H NMR (400 MHz, CDCl$_3$) δ: 7.11 (s, 2H), 6.97 (s, 2H), 3.95 (m, 4H), 1.82 (m, 2H), 1.57–1.34 (m, 16H), 0.99–0.91 (m, 12H). ^{13}C NMR (125 MHz, CDCl$_3$) δ: 149.23, 145.69, 132.18, 130.06, 127.12, 113.57, 112.48, 71.68, 39.75, 30.82, 29.35, 24.17, 23.30, 14.33, 11.45. HR-MS (ESI): calcd for $C_{30}H_{38}Br_2O_2S_3$ [M+Na]$^+$, 707.0293; found, 707.0293.

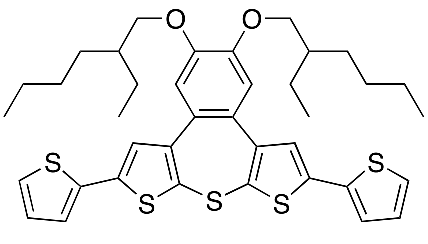

6,7-Di(2-ethylhexyloxy)-3,10-bis(thiophen-2-yl)-benzo[*d*]-dithieno[2,3-*b*;3',2'-*f*]-thiepin (9). To a degassed solution of DMF (5 mL) of compound **8** (0.350 g, 0.5 mmol) were added 2-tributylstannyl thiophene (0.368 mL, 1.1 mmol) and $PdCl_2(PPh_3)_2$ (18 mg, 5 mol %). The mixture was allowed to stir at 80 °C for 15 h, at which time the mixture was cooled to room temperature. Ethyl aceate was added to the mixture, and the organic layer was washed with saturated aqueous NH_4Cl, KF, and NH_4Cl again. After being dried over $MgSO_4$, the organic layer was evaporated under reduced pressure and subjected to column chromatography (dichloromethane:hexane = 1:3). The product was further purified by recrystallization (dichloromethane/methanol). Yield: 0.270 g (78%) of pale yellow solid. ^1H NMR (400 MHz, $CDCl_3$) δ: 7.24 (dd, 2H, *J* = 5.1, 1.0 Hz), 7.18 (s, 2H), 7.16 (dd, 2H, *J* = 3.6, 1.0 Hz), 7.10 (s, 2H), 7.12 (dd, 2H, *J* = 5.1, 3.6 Hz), 3.95 (m, 4H), 1.82 (m, 2H), 1.57–1.34 (m, 16H), 0.99–0.91 (m, 12H). ^{13}C NMR (125 MHz, $CDCl_3$) δ: 149.11, 145.98, 138.08, 136.86, 128.94, 128.12, 127.87, 125.69, 125.18, 124.46, 113.94, 71.81, 39.79, 30.84, 29.36, 24.17, 23.32, 14.34, 11.47. HR-MS (ESI): calcd for $C_{38}H_{44}O_2S_5$ $[M+Na]^+$, 715.1837; found, 715.1869.

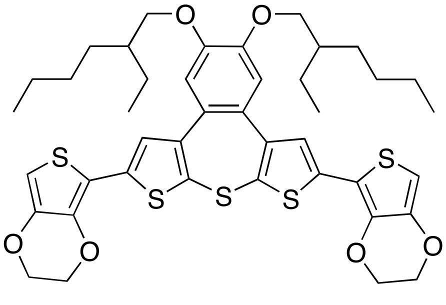

3,10-Bis(3,4-ethylenedioxythiophen-2-yl)-6,7-di(2-ethylhexyloxy)-benzo[*d*]-dithieno[2,3-*b*;3',2'-*f*]-thiepin (10). Using the same procedure for the synthesis of **9**, compound **8** (0.350 g, 0.5 mmol) was treated with 2-tributylstannyl-3,4-ethylenedioxythiophene (0.473 mL, 1.25 mmol) and $PdCl_2(PPh_3)_2$ (18 mg, 5 mol %) in DMF (5 mL). Yield: 0.330 g (80%) of pale yellow solid. ^{1}H NMR (400 MHz, CDCl$_3$) δ: 7.17 (s, 2H), 7.07 (s, 2H), 6.24 (s, 2H), 4.34 (m, 4H), 4.25 (m, 4H), 3.97 (m, 4H), 1.83 (m, 2H), 1.57–1.35 (m, 16H), 0.99–0.91 (m, 12H). ^{13}C NMR (125 MHz, CDCl$_3$) δ: 148.98, 145.17, 141.97, 138.18, 135.41, 128.85, 128.05, 124.48, 114.22, 111.79, 97.67, 71.89, 65.24, 64.77, 39.78, 30.82, 29.35, 24.15, 23.32, 14.35, 11.46. HR-MS (ESI): calcd for $C_{42}H_{48}O_6S_5$ [M+Na]$^+$, 831.1941; found, 831.1963.

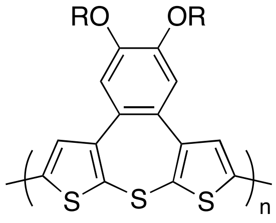

Polymer 11. Compound **8** (0.069 g, 0.1 mmol) and hexabutylditin (0.058 mL, 0.11 mmol) were dissolved in toluene (1.5 mL) and DMF (1.5 mL). The mixture was degassed with Ar for 40 min and Pd(PPh$_3$)$_4$ (2.4 mg, 2 mol %) was added under gentle Ar stream. The mixture was allowed to stir at 110 ºC for 2 d, at which time the mixture was cooled to room temperature and methanol was added to precipitate. The filtered solid was re-dissolved in CHCl$_3$ and added to acetone to precipitate again. The product was filtered and dried under air. Yield: 0.041 g (78%) of crimson solid. GPC (polystyrene standard): M_n = 6170, M_w = 7790, PDI = 1.26. ^{1}H NMR (300 MHz, CDCl$_3$) δ: 7.15 (aromatic C-H), 7.03 (aromatic C-H), 3.95 (aliphatic C-H), 1.84–0.92 (aliphatic C-H).

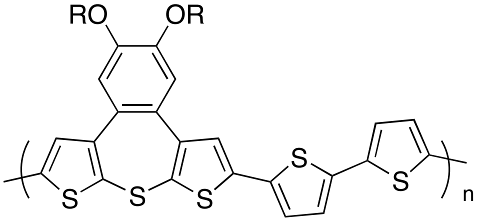

Polymer 12. Compound **8** (0.035 g, 0.05 mmol) and 5,5'-bis(trimethylstannyl)-2,2'-bithiophene (0.025 g, 0.05 mmol) were dissolved in toluene (0.5 mL) and DMF (0.5 mL). The mixture was degassed with Ar for 40 min and $Pd(PPh_3)_4$ (2.4 mg, 2 mol %) was added under gentle Ar stream. The mixture was allowed to stir at 110 ºC for 2 d, at which time the mixture was cooled to room temperature and methanol was added to precipitate. The filtered solid was re-dissolved in $CHCl_3$ and added to methanol to precipitate again. The product was filtered and dried under air. Yield: 0.023 g (67%) of crimson solid. GPC (polystyrene standard): M_n = 3560, M_w = 7970, PDI = 2.24. ^{1}H NMR (300 MHz, $CDCl_3$) δ: 7.18 (aromatic C-H), 7.08 (aromatic C-H), 3.98 (aliphatic C-H), 1.82 (aliphatic C-H), 1.57–0.93(aliphatic C-H).

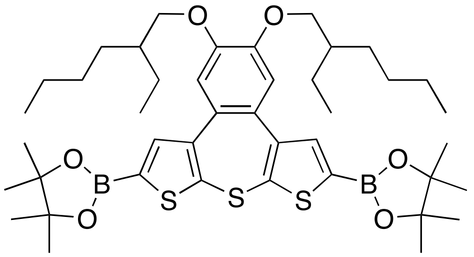

Compound A. To a THF (40 mL) solution of compound **4a** (2.12 g, 4 mmol) was added dropwise *n*-BuLi (1.6 M in hexane, 5.25 mL, 8.4 mmol) at –78 °C (dry ice/acetone). Upon completion, the cooling bath was removed and the mixture was allowed to stir at room temperature for 1 h. The mixture was cooled to –40 °C and 2-isopropoxy-4,4,5,5-tetramethyl-1,3,2-dioxaborolane (2.5 mL, 12 mmol) was added dropwise. After being warmed to room temperature, the mixture was allowed to stir for 15 h, at which time most THF had evaporated. The residue was diluted with dichloromethane and washed with water and brine. The organic layer was dried over $MgSO_4$ and evaporated under reduced pressure. The crude product was purified by recrystallization (dichloromethane/hexane). Yield: 2.85 g (90%) of pale gray solid. ^{1}H

NMR (400 MHz, CDCl$_3$) δ: 7.62 (s, 2H), 7.07 (s, 2H), 3.95 (m, 4H), 1.82 (m, 2H), 1.57–1.35 (m, 16H), 1.34 (s, 12H), 1.33 (s, 12H), 0.99–0.90 (m, 12H). ^{13}C NMR (125 MHz, CDCl$_3$) δ: 148.91, 146.64, 138.75, 137.65, 127.50, 113.85, 84.55, 71.70, 39.83, 30.82, 29.37, 25.03, 24.79, 24.20, 23.32, 14.34, 11.46. HR-MS (ESI): calcd for $C_{42}H_{62}B_2O_6S_3$ [M+H]$^+$, 781.3994; found, 781.4028.

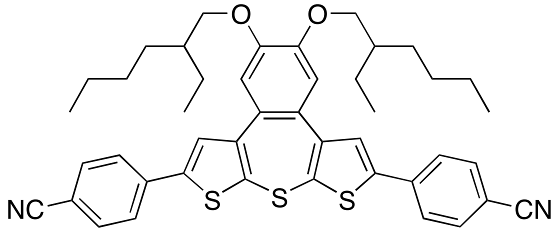

3,10-Bis(4-cyanophenyl)-6,7-di(2-ethylhexyloxy)-benzo[*d*]-dithieno[2,3-*b*;3’,2’-*f*]-thiepin (13). To a THF (1.2 mL) solution of compound **A** (0.096 g, 0.12 mmol) and 4-bromobenzonitrile (0.049 g, 0.264 mmol) were added 1 M K_2CO_3 (aq) (degassed for 2 h, 0.6 mL) and Pd(PPh$_3$)$_4$ (7 mg, 5 mol %). The mixture was allowed to stir at reflux for 15 h, at which time the mixture was cooled to room temperature and diluted with ethyl aceate. The organic layer was washed with water and brine, dried over MgSO$_4$, and evaporated under reduced pressure. The crude product was purified by column chromatography (dichloromethane:hexane = 1:1). Yield: 0.061 g (70%) of orange solid. ^{1}H NMR (400 MHz, CDCl$_3$) δ: 7.66 (s, 8H), 7.44 (s, 2H), 7.09 (s, 2H), 3.98 (m, 4H), 1.84 (m, 2H), 1.59–1.35 (m, 16H), 1.00–0.91 (m, 12H). ^{13}C NMR (125 MHz, CDCl$_3$) δ: 148.38, 146.61, 142.65, 138.13, 133.05, 131.72, 127.61, 126.97, 126.12, 118.84, 113.80, 111.36, 71.78, 39.80, 30.83, 29.36, 24.17, 23.29, 14.33, 11.47.

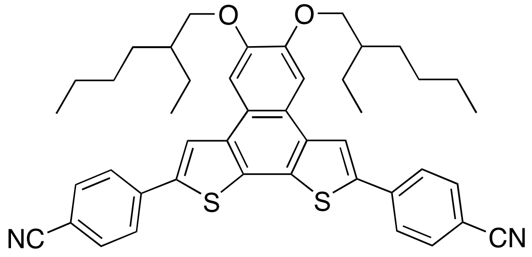

2,9-Bis(4-cyanophenyl)-5,6-di(2-ethylhexyloxy)-dithieno[3,2-*a*;2',3'-*c*]naphthalene (14) (byproduct from crystallization of oxidized **13**). In a Schlenk flask were combined compund **13** (0.014 g, 0.019 mmol) and $NOSbF_6$ (0.005 g, 0.019 mmol). After cooling to –78 °C, CH_2Cl_2 (1 mL) was vapor-transferred to the flask via a cannula. The vacuum valve was closed, and the cooling bath was removed in order to promote the reaction (NO gas evolution). After 30 min, the mixture was cooled in a liquid nitrogen bath, and hexane (3 mL) was vapor-transferred (layered on the CH_2Cl_2). The layered solution was left at room temperature for 7 d. Methanol (2 mL) was added to the mixture, which was then diluted with dichloromethane. The organic layer was washed with water and brine, dried over MgSO4, and evaporated under reduced pressure. The crude product was purified by column chromatography (dichloromethane:hexane = 1:1). Yield: 0.012 g (90%) of red solid. ^1H NMR (400 MHz, $CDCl_3$) δ: 8.18 (s, 2H), 7.44 (*pseudo*-d, 4H, *J* = 8.4 Hz), 7.73 (*pseudo*-d, 4H, *J* = 8.4 Hz), 7.65 (s, 2H), 4.12 (m, 4H), 1.92 (m, 2H), 1.68–1.39 (m, 16H), 1.03 (t, 6H, *J* = 7.5 Hz), 0.95 (t, 6H, *J* = 7.2 Hz). ^{13}C NMR (125 MHz, $CDCl_3$) δ: 150.01, 140.06, 138.53, 135.64, 132.97, 130.42, 126.50, 122.84, 120.60, 118.95, 111.25, 106.06, 71.69, 39.87, 30.93, 29.48, 24.25, 23.34, 14.39, 11.57.

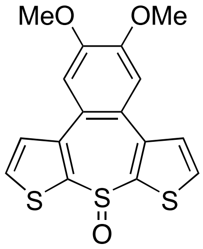

6,7-Dimethoxy-benzo[*d*]-dithieno[2,3-*b*;3',2'-*f*]-thiepin 1-oxide (15). To a CH_2Cl_2 (1 mL) solution of **4c** (0.033 g, 0.1 mmol) was added *m*-chloroperoxybenzoic acid (assumed as 72% purity, 0.024 g, 0.1 mmol) in CH_2Cl_2 (0.5 mL) at –20 °C, and the mixture was allowed to stir for 1 h. After being warmed to room temperature, the mixture was diluted with CH_2Cl_2, and washed with saturated $NaHCO_3$ and brine. The organic layer was dried over $MgSO_4$, evaporated under reduced pressure, subjected to column chromatography (ethyl acetate:hexane = 1:2 and ethyl acetate only). Yield: 0.019 g (55%) of white solid. ^{1}H NMR (300 MHz, $CDCl_3$) for *endo* (*axial*), δ: 7.51 (d, 2H, *J* = 6.8 Hz), 7.48 (d, 2H, *J* = 6.8 Hz), 7.32 (s, 2H), 4.01 (s, 6H). For *exo* (*equatorial*), δ: 7.53 (d, 2H, *J* = 6.8 Hz), 7.26 (d, 2H, *J* = 6.8 Hz), 7.08 (s, 2H), 3.99 (s, 6H). ^{13}C NMR (125 MHz, $CDCl_3$) δ: 149.06, 140.94, 138.64, 131.10, 130.06, 127.76, 111.97, 56.26. HR-MS (ESI): calcd for $C_{16}H_{12}O_3S_3$ $[M+H]^+$, 349.0021; found, 349.0018.

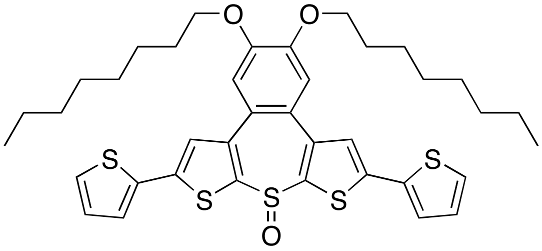

6,7-Di(2-ethylhexyloxy)-3,10-bis(thiophen-2-yl)-benzo[*d*]-dithieno[2,3-*b*;3',2'-*f*]-thiepin 1-oxide (16). Using the similar procedure to the preparation of **15**, 6,7-di(*n*-octyloxy)-3,10-bis(thiophen-2-yl)-benzo[*d*]-dithieno[2,3-*b*;3',2'-*f*]-thiepin (0.029 g, 0.042 mmol) in CH_2Cl_2 (1 mL) was treated with *m*-chloroperoxybenzoic acid (0.010 g, 0.042 mmol) in CH_2Cl_2 (0.5 mL). The crude product was purified by column chromatography (ethyl acetate:hexane:chloroform = 1:7:1). Yield: 0.015 g (51%) of pale yellow solid. ^{1}H NMR (400 MHz, $CDCl_3$) for *endo* (*axial*), δ: 7.47 (s, 2H), 7.33 (dd, 2H, *J* = 5.1, 1.0 Hz), 7.33 (s, 2H), 7.29 (dd, 2H, *J* = 3.6, 1.0 Hz), 7.08 (dd, 2H, *J* = 5.1, 3.6 Hz), 4.16 (m, 4H), 1.90 (m, 4H), 1.53–1.27 (m, 20H), 0.90 (t, 6H, *J* = 6.8

Hz). For *exo* (*equatorial*), δ: 7.28 (dd, 2H, *J* = 5.1, 1.0 Hz), 7.26 (s, 2H), 7.23 (dd, 2H, *J* = 3.6, 1.0 Hz), 7.10 (s, 2H), 7.05 (dd, 2H, *J* = 5.1, 3.6 Hz), 4.16 (m, 4H), 1.90 (m, 4H), 1.53–1.27 (m, 20H), 0.90 (t, 6H, *J* = 6.8 Hz). ^{13}C NMR (125 MHz, $CDCl_3$) for *endo* (*axial*), δ: 149.44, 141.67, 139.29, 136.26, 135.66, 128.41, 127.14, 126.53, 125.85, 125.42, 113.95, 69.62, 32.04, 29.58, 29.51, 29.45, 26.26, 22.89, 14.34. For *exo* (*equatorial*), δ: 149.22, 139.71, 139.58, 135.24, 134.81, 128.26, 126.25, 125.88, 124.82, 118.81, 113.77, 69.62, 32.04, 29.58, 29.51, 29.45, 26.26, 22.89, 14.34. HR-MS (ESI): calcd for $C_{38}H_{44}O_3S_5$ [M+H]$^+$, 709.1967; found, 709.1979.

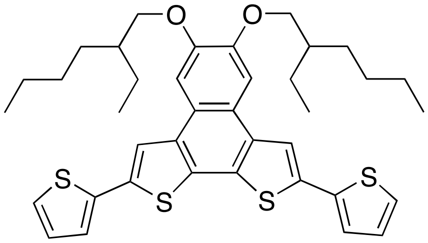

2,9-Bis(thiophen-2-yl)-5,6-di(2-ethylhexyloxy)-dithieno[3,2-*a*;2’,3’-*c*]naphthalene (18). Using the same procedure for the synthesis of **9**, compound **17** (0.033 g, 0.05 mmol) was treated with 2-tributylstannylthiophene (0.037 mL, 0.125 mmol) and $PdCl_2(PPh_3)_2$ (1.8 mg, 5 mol %) in DMF (1 mL). Yield: 0.023 g (70%) of yellow solid. ^{1}H NMR (300 MHz, $CDCl_3$) δ: 7.84 (s, 2H), 7.56 (s, 2H), 7.34 (dd, 2H, *J* = 3.6, 1.2 Hz), 7.32 (dd, 2H, *J* = 5.1, 1.2 Hz), 7.10 (dd, 2H, *J* = 5.1, 3.6 Hz), 4.10 (m, 4H), 1.92 (m, 2H), 1.67–1.37 (m, 16H), 1.03 (t, 6H, *J* = 7.5 Hz), 0.96 (t, 6H, *J* = 6.9 Hz). ^{13}C NMR (125 MHz, $CDCl_3$) δ: 149.60, 137.76, 135.14, 134.82, 128.97, 128.27, 125.24, 124.80, 122.68, 118.84, 106.23, 71.66, 39.85, 30.95, 29.47, 24.27, 23.35, 14.39, 11.57. HR-MS (ESI): calcd for $C_{38}H_{44}O_2S_4$ [M+Na]$^+$, 683.2116; found, 683.2139.

References and Notes

(1) Baughman, R. *Synth. Met.* **1996,** *78,* 339–353.

(2) (a) Marsella, M. J. *Acc. Chem. Res.* **2002**, *35*, 944–951. (b) Yu, H. -h.; Swager, T. M. *IEEE J. Oceanic Eng.* **2004,** *29,* 692–695.

(3) (a) Vogel, E.; Günther, H. *Angew. Chem. Int. Ed.* **1967**, *6*, 385–401. (b) Dewar, M. J. S.; Trinajstic, N. *Tetrahedron* **1970,** *26,* 4269–4267. (c) Paquette, L. A. *Angew. Chem. Int. Ed.* **1971**, *10*, 11–20.

(4) Murata, I.; Nakasuji, K. *Top. Curr. Chem.* **1981**, *97*, 33–70.

(5) Gleiter, R.; Krennrich, G.; Cremer, D.; Yamamoto, K.; Murata, I. *J. Am. Chem. Soc.* **1985**, *107*, 6874–6879.

(6) Yasuike, S.; Nakashima, F.; Kurita, J.; Tsuchiya, T. *Heterocycles* **1997,** *45,* 1899–1902.

(7) (a) Yasuike, S.; Ohta, H.; Shiratori, S.; Kurita, J.; Tsuchiya, T. *J. Chem. Soc., Chem. Commun.* **1993,** 1817–1819. (b) Yasuike, S.; Shiratori, S. –i.; Kurita, J.; Tsuchiya, T. *Chem. Pharm. Bull.* **1999,** *47,* 1108–1114. (c) Yasuike, S.; Kiharada, T.; Tsuchiya, T.; Kurita, J. *Chem. Pharm. Bull.* **2003,** *51,* 1283–1288.

(8) (a) Nenajdenko, V. G. et al. *Synthesis* **2003,** 124–128. (b) Nenajdenko, V. G.; Sumerin, V. V.; Chernichenko, K. Y.; Balenkova, E. S. *Org. Lett.* **2004,** *6,* 3437–3439. (c) Rajca, A.; Miyasaka, M.; Pink, M.; Wang, H.; Rajca, S. *J. Am. Chem. Soc.* **2004**, *126*, 15211–15222.

(9) (a) Nakayama, J.; Katano, N.; Shimura, Y.; Sugihara, Y.; Ishii, A. *J. Org. Chem.* **1996**, *61*, 7608–7610. (b) Chahma, M.; Hicks, R. G.; Myles, D. J. T. *Macromolecules* **2004**, *37*, 2010–2012. (c) Chahma, M.; Myles, D. J. T.; Hicks, R. G. *Chem. Mater.* **2005**, *17*, 2672–2678.

(10) Tova, J. D.; Rose, A.; Swager, T. M. *J. Am. Chem. Soc.* **2002**, *124*, 7762–7769.

(11) Chen, Q.; Dolphin, D. *Synthesis* **2001,** 40–42.

(12) Tova, J. D.; Swager, T. M. *Adv. Mater.* **2001**, *13*, 1775–1780.

(13) Kelly, T. R.; Li, Q.; Bhushan, V. *Tetrahedron Lett.* **1990**, *31*, 161–164.

(14) (a) Schlessinger, R. H.; Ponticello, G. S. *Tetrahedron Lett.* **1968**, *9*, 3017–3020. (b) Hofmann, H.; Gaube, H. *Angew. Chem. Int. Ed.* **1975**, *14*, 812–813. (c) Yamazaki, S.; Isokawa, A.; Yamamoto, K.; Murata, I. *J. Chem. Soc., Perkin Trans. 1* **1994,** 2631–2635.

(15) Mock, W. L. *J. Am. Chem. Soc.* **1967**, *89*, 1281–1283.

(16) Hofmann, H.; Böhme, R.; Wilhelm, E. *Chem. Ber.* **1978**, *111*, 309.

(17) Schmeisser, M. In *Handbook of Preparative Inorganic Chemistry*, 2nd ed.; Bauer, G., Ed.; Academic: New York, 1963.

(18) Kilbinger, A. F. M.; Feast, W. J. *J. Mater. Chem.* **2000,** *10,* 1777–1784.

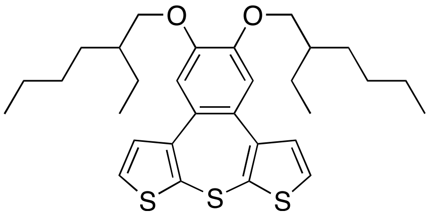

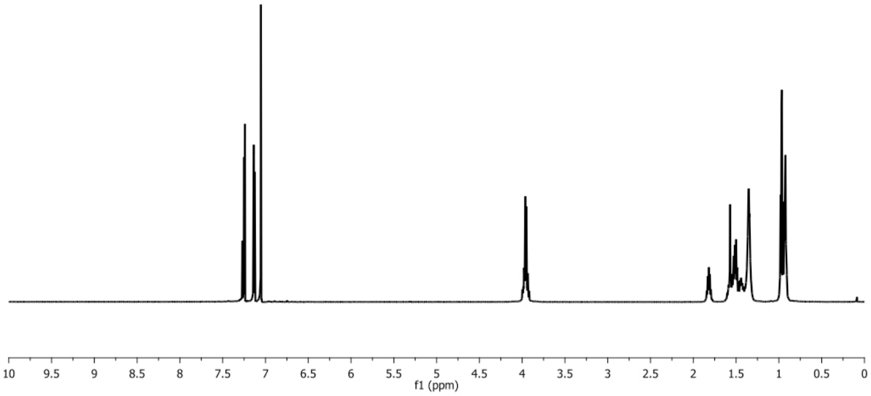

Spectrum 1. ^{1}H-NMR spectrum of **4a** (500 MHz, $CDCl_3$).

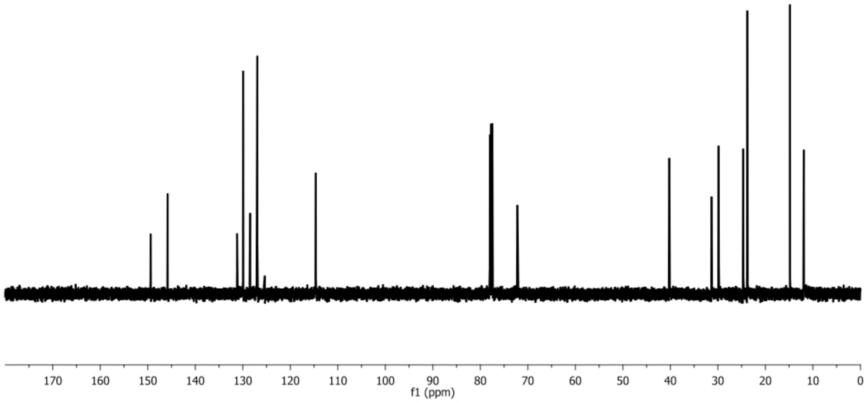

Spectrum 2. ^{13}C-NMR spectrum of **4a** (125 MHz, $CDCl_3$).

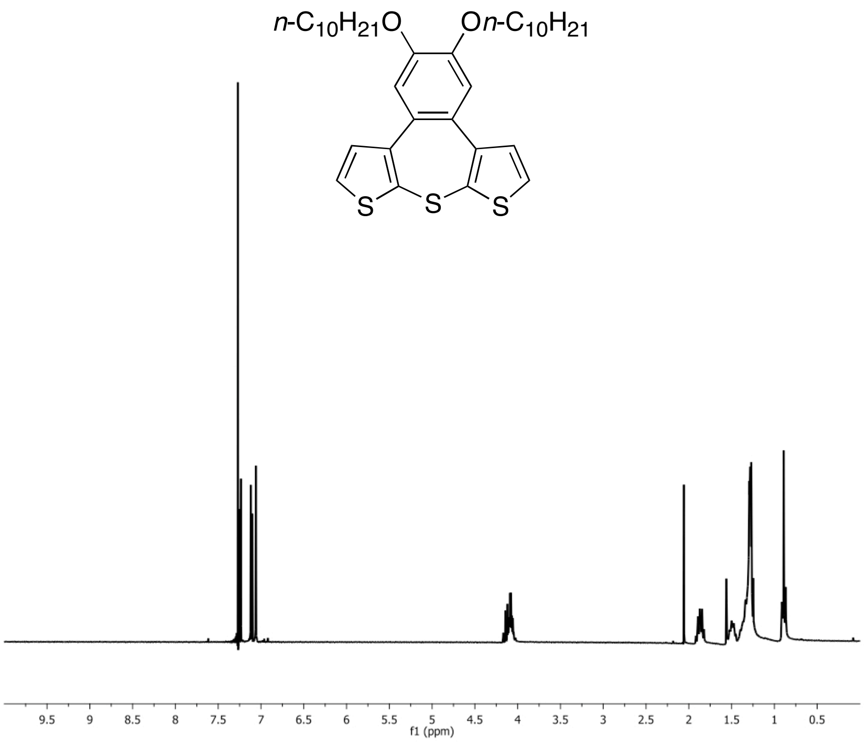

Spectrum 3. ^{1}H-NMR spectrum of **4b** (300 MHz, $CDCl_3$).

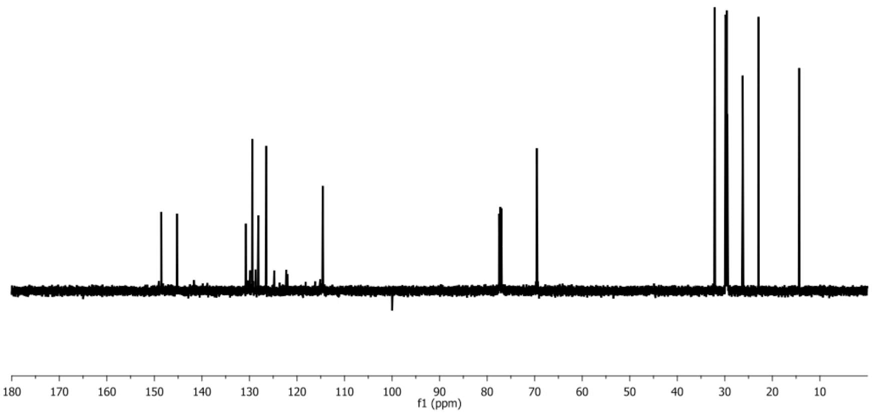

Spectrum 4. ^{13}C-NMR spectrum of **4b** (125 MHz, $CDCl_3$).

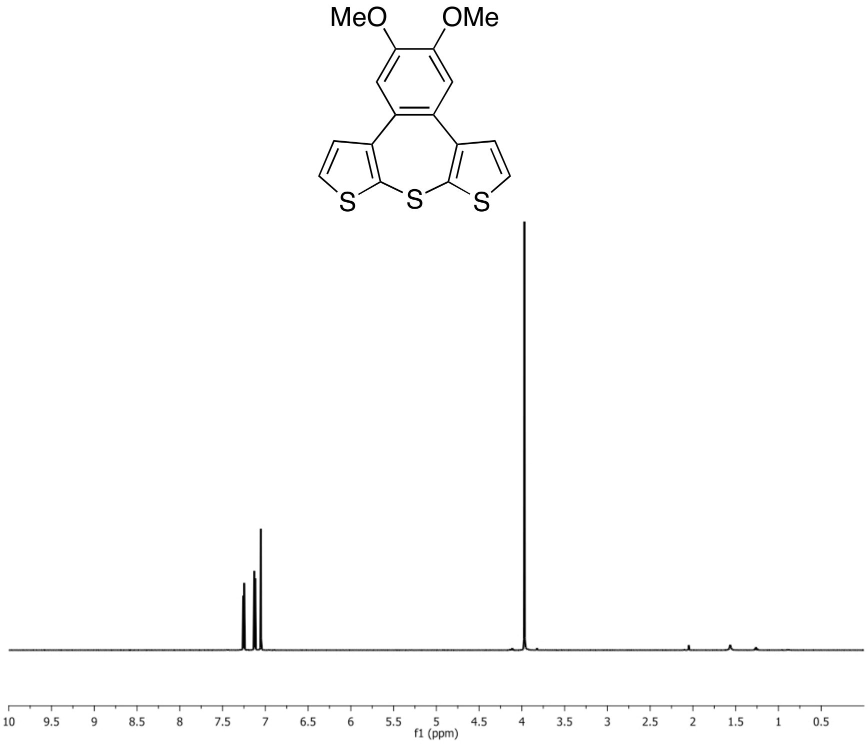

***Spectrum 5**.* ^{1}H-NMR spectrum of **4c** (500 MHz, $CDCl_3$).

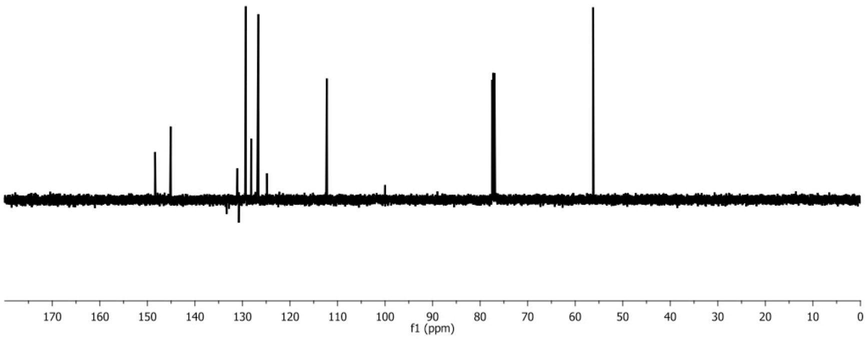

***Spectrum 6**.* ^{13}C-NMR spectrum of **4c** (125 MHz, $CDCl_3$).

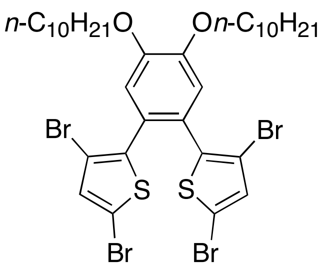
n-C10H21O
On-C10H21
Br
Br
S
S
Br
Br

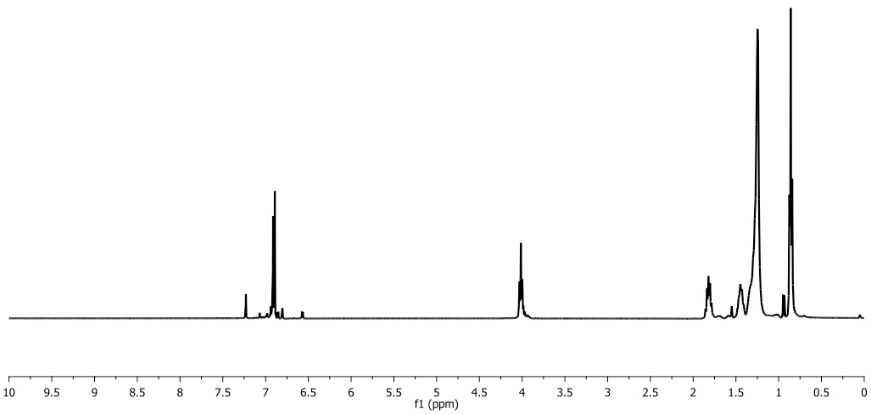

Spectrum 7. ^{1}H-NMR spectrum of **5** (400 MHz, $CDCl_3$).

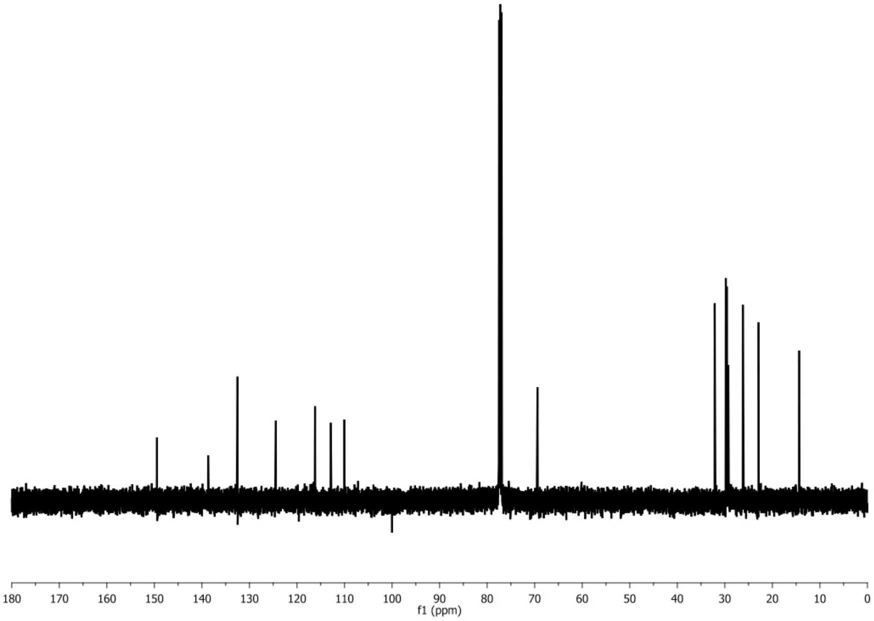

Spectrum 8. ^{13}C-NMR spectrum of **5** (125 MHz, $CDCl_3$).

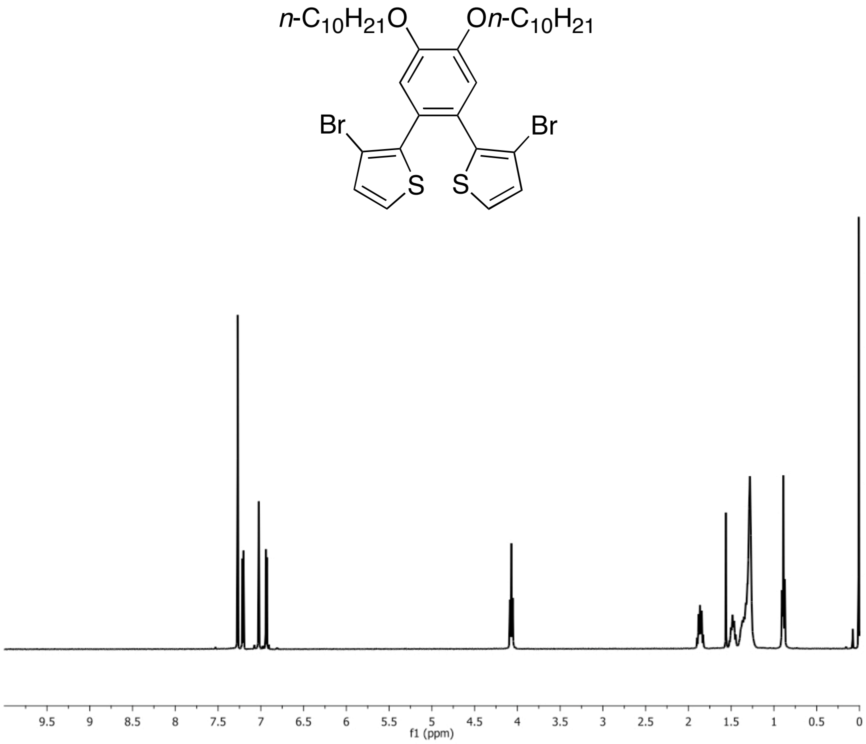

Spectrum 9. ^{1}H-NMR spectrum of **6** (400 MHz, $CDCl_3$).

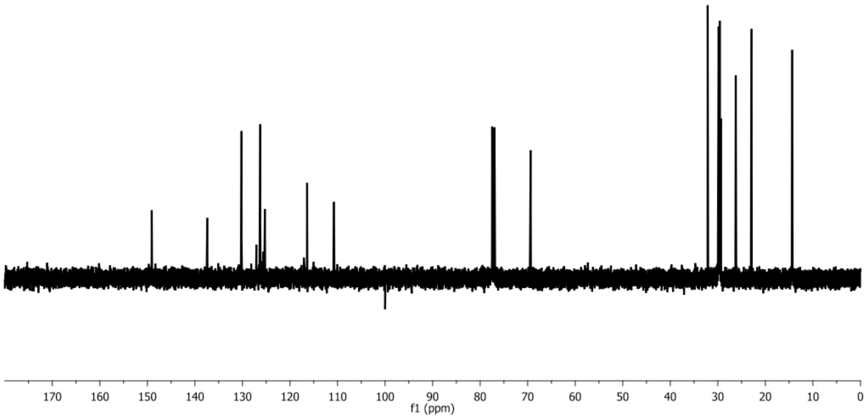

Spectrum 10. ^{13}C-NMR spectrum of **6** (125 MHz, $CDCl_3$).

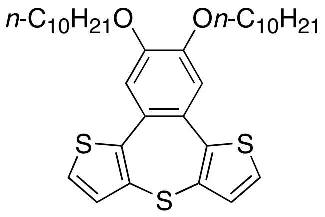
n-C10H21O
On-C10H21
S
S
S

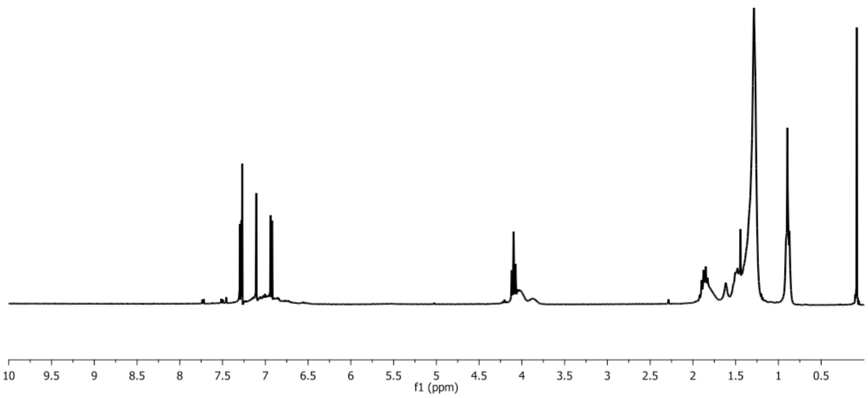

Spectrum 11. ^{1}H-NMR spectrum of **7** (300 MHz, $CDCl_3$).

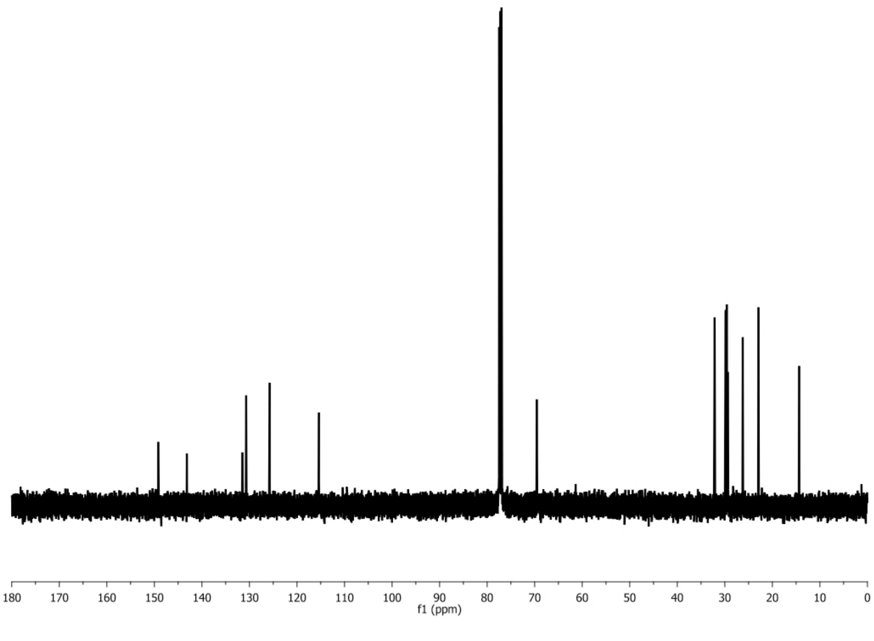

Spectrum 12. ^{13}C-NMR spectrum of **7** (125 MHz, $CDCl_3$).

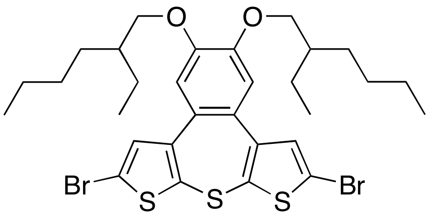

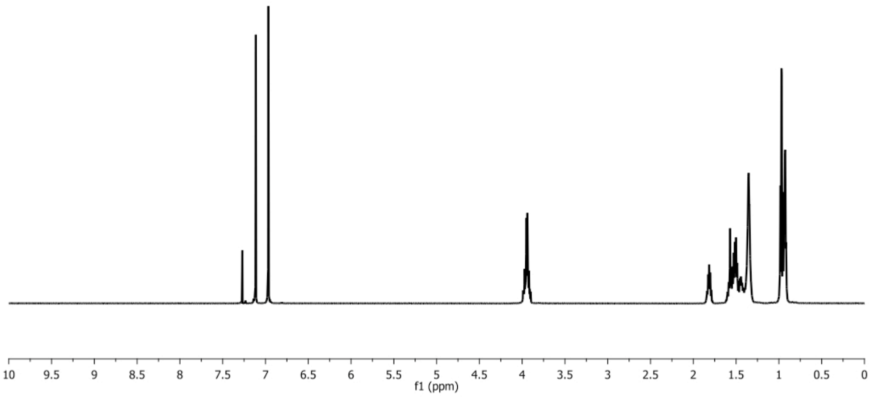

Spectrum 13. ^{1}H-NMR spectrum of **8** (500 MHz, $CDCl_3$).

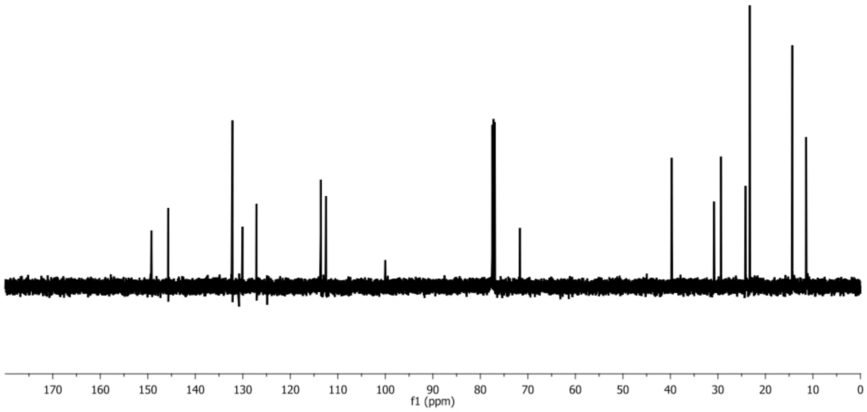

Spectrum 14. ^{13}C-NMR spectrum of **8** (125 MHz, $CDCl_3$).

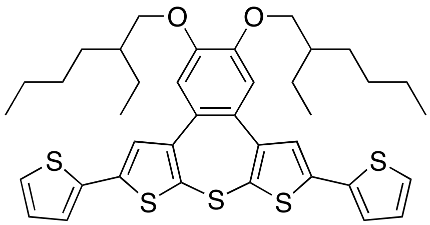

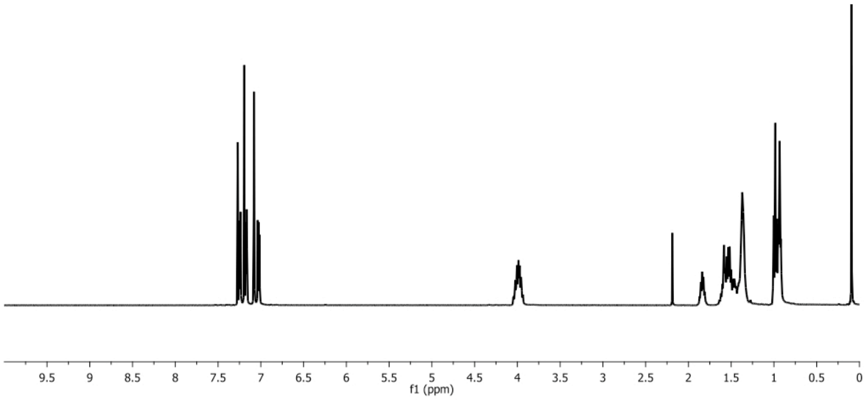

Spectrum 15. ^{1}H-NMR spectrum of **9** (400 MHz, $CDCl_3$).

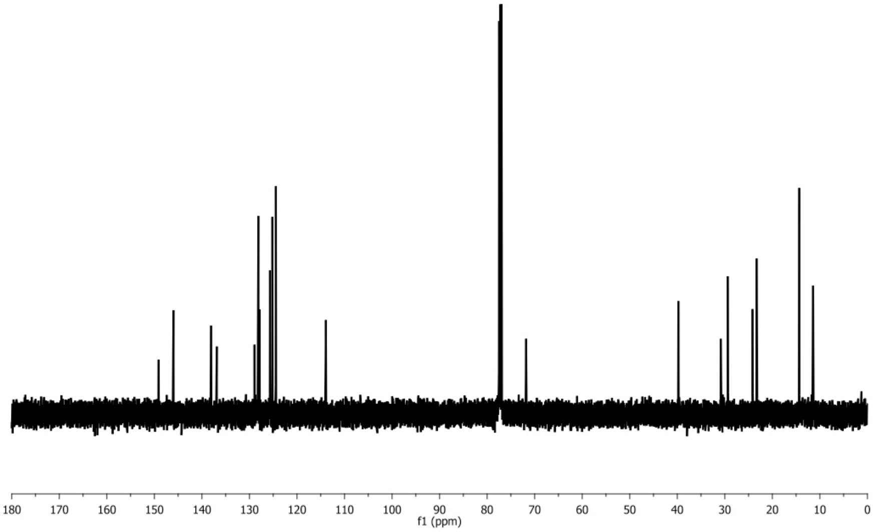

Spectrum 16. ^{13}C-NMR spectrum of **9** (125 MHz, $CDCl_3$).

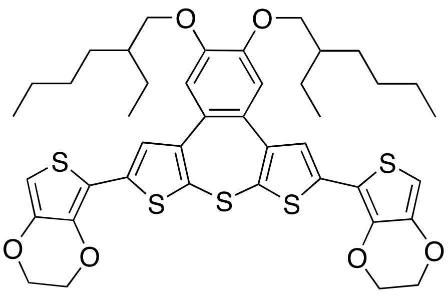

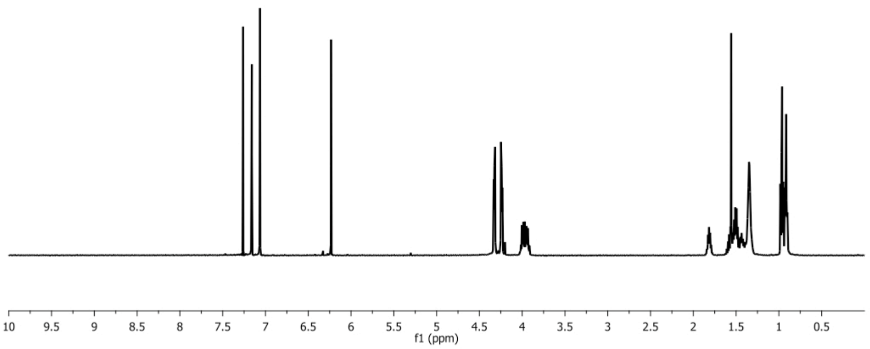

Spectrum 17. ^{1}H-NMR spectrum of **10** (500 MHz, $CDCl_3$).

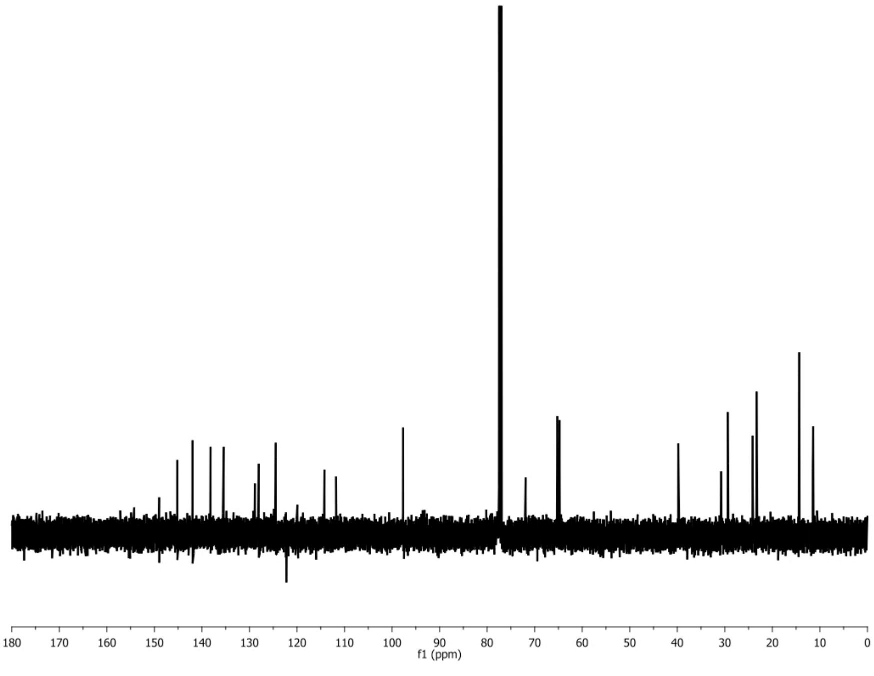

Spectrum 18. ^{13}C-NMR spectrum of **10** (125 MHz, $CDCl_3$).

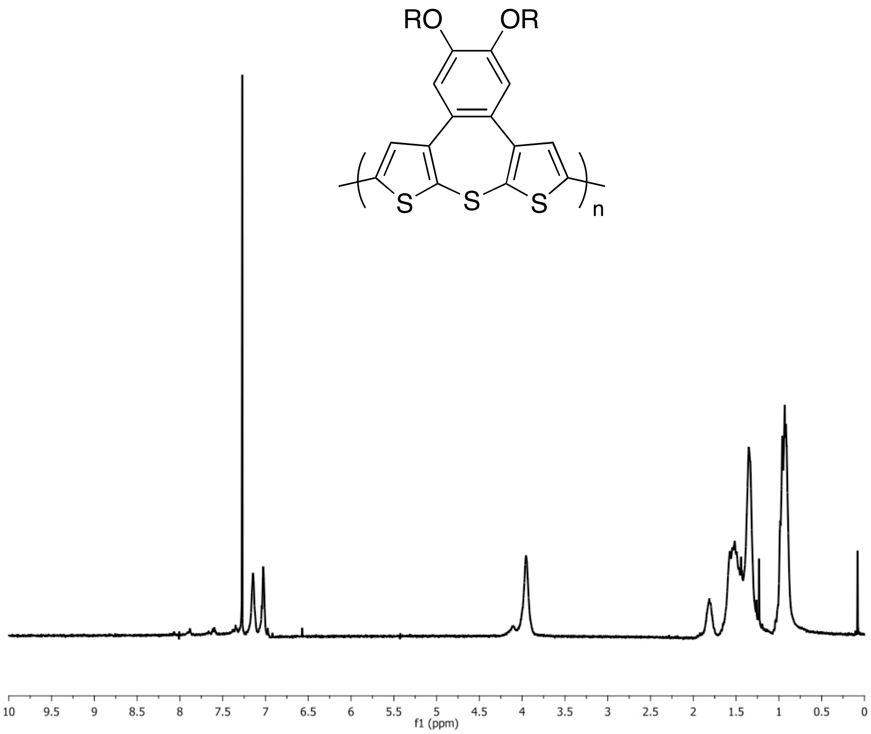

***Spectrum 19**.* ^{1}H-NMR spectrum of **11** (300 MHz, $CDCl_3$).

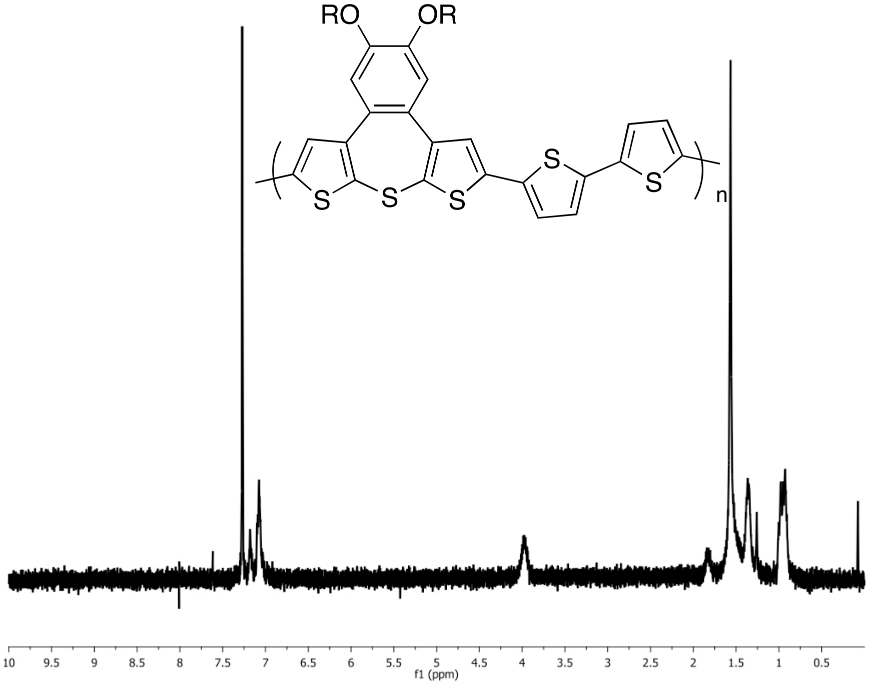

***Spectrum 20**.* ^{1}H-NMR spectrum of **12** (300 MHz, $CDCl_3$).

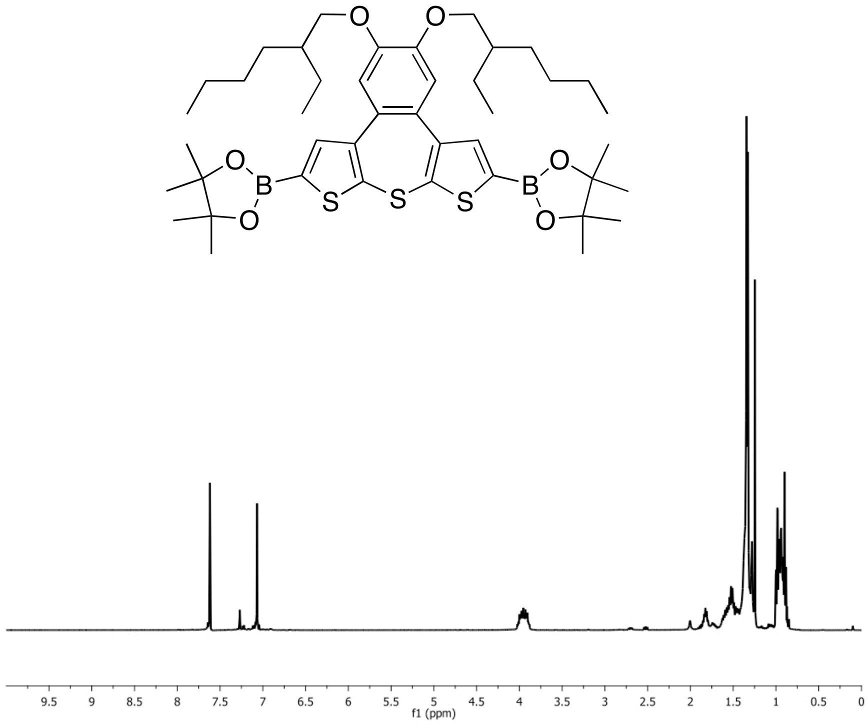

Spectrum 21. ^{1}H-NMR spectrum of **A** (400 MHz, $CDCl_3$).

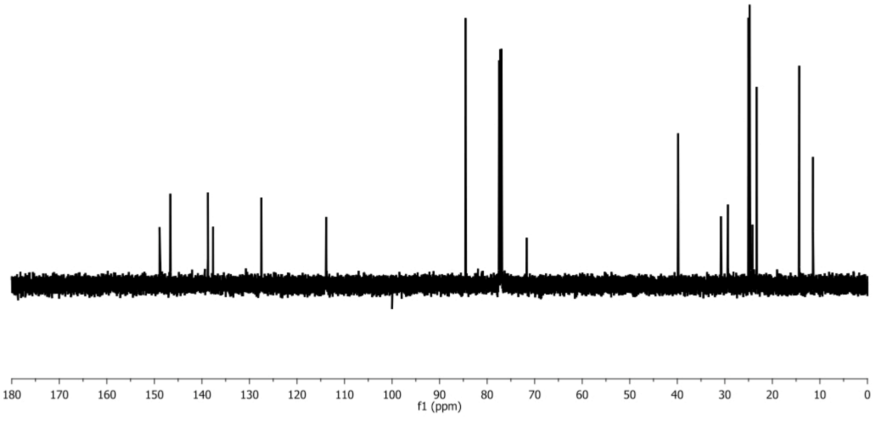

Spectrum 22. ^{13}C-NMR spectrum of **A** (125 MHz, $CDCl_3$).

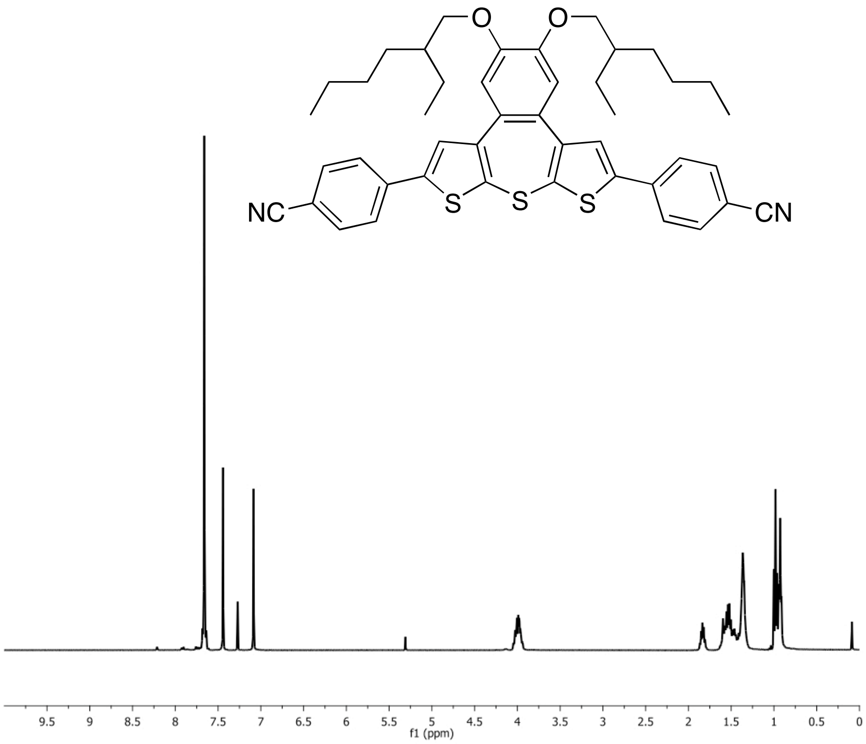

Spectrum 23. ^{1}H-NMR spectrum of **13** (400 MHz, $CDCl_3$).

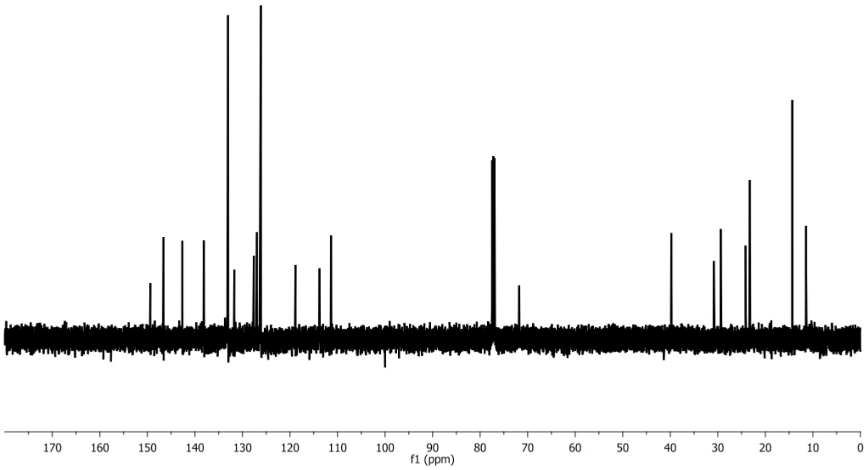

Spectrum 24. ^{13}C-NMR spectrum of **13** (125 MHz, $CDCl_3$).

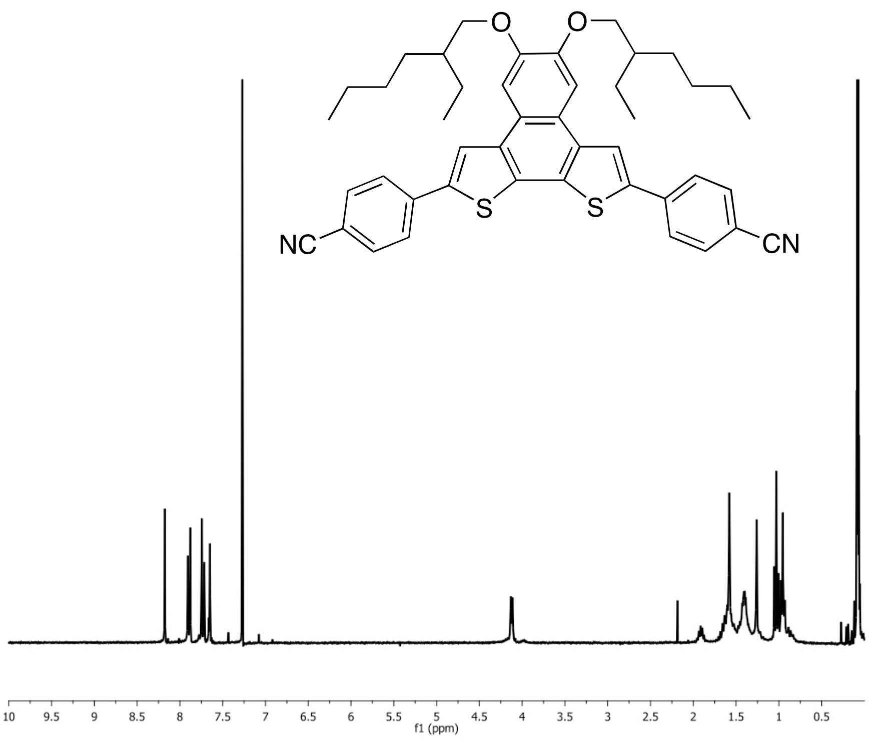

Spectrum 25. ^{1}H-NMR spectrum of **14** (300 MHz, $CDCl_3$).

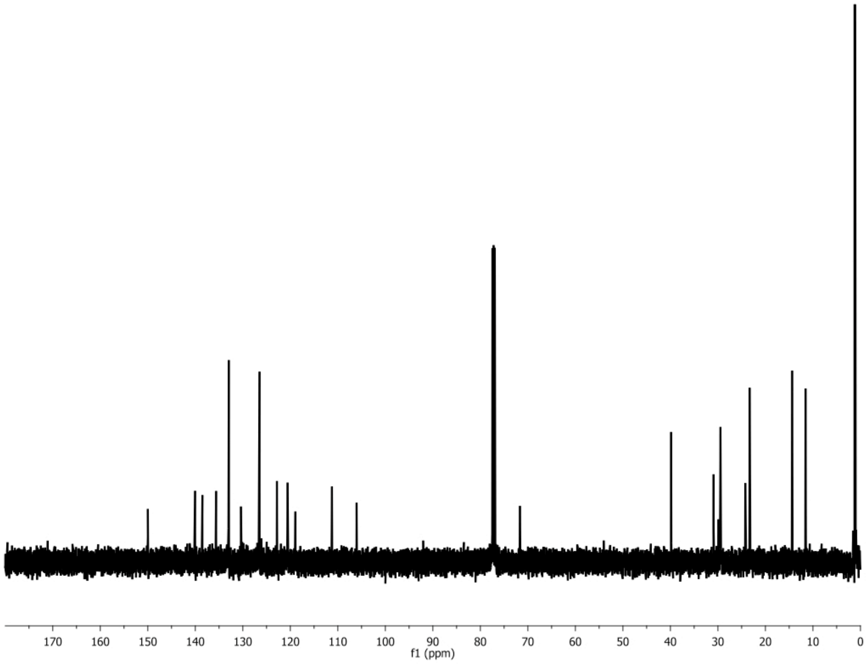

Spectrum 26. ^{13}C-NMR spectrum of **14** (125 MHz, $CDCl_3$).

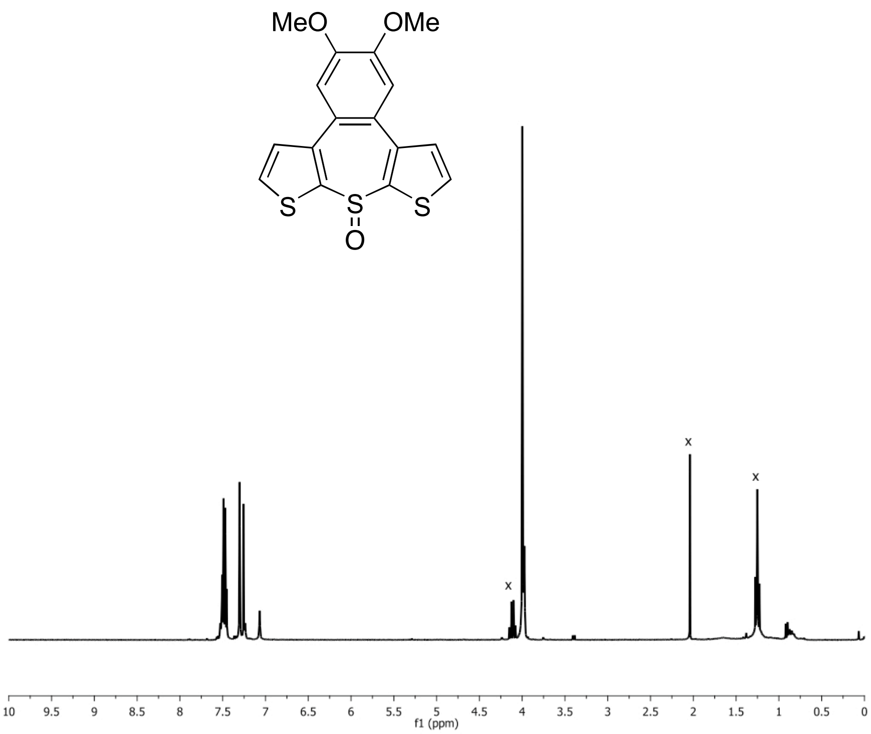

Spectrum 27. ^{1}H-NMR spectrum of **15** (300 MHz, $CDCl_3$).

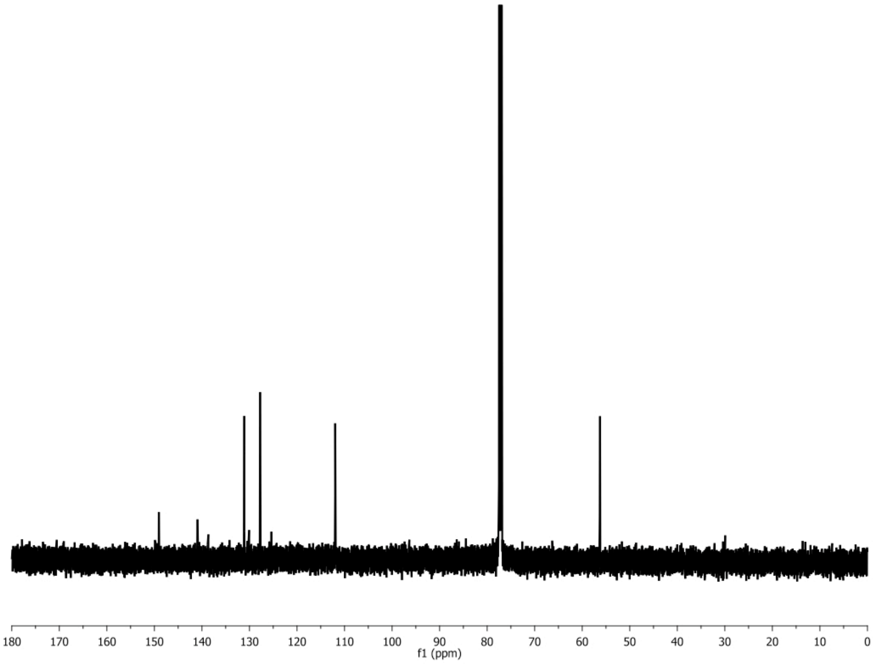

Spectrum 28. ^{13}C-NMR spectrum of **15** (125 MHz, $CDCl_3$).

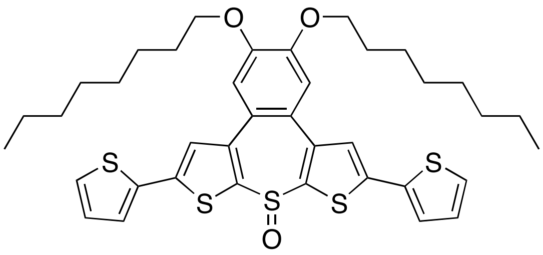

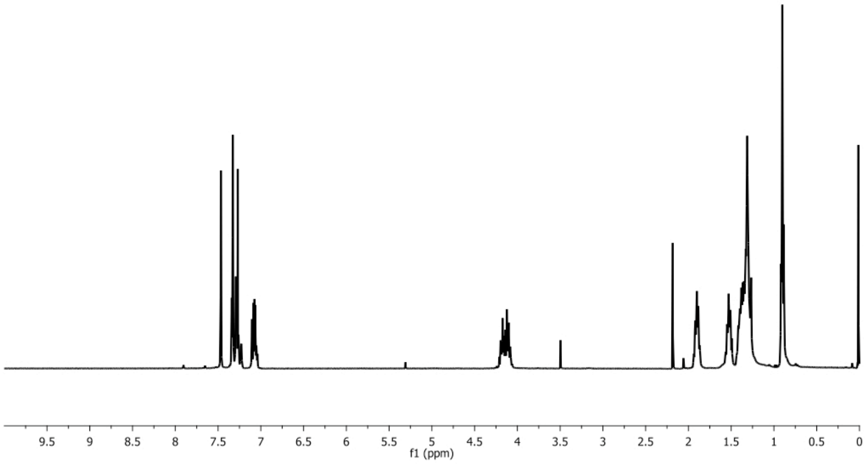

Spectrum 29. ^{1}H-NMR spectrum of **16** (400 MHz, $CDCl_3$).

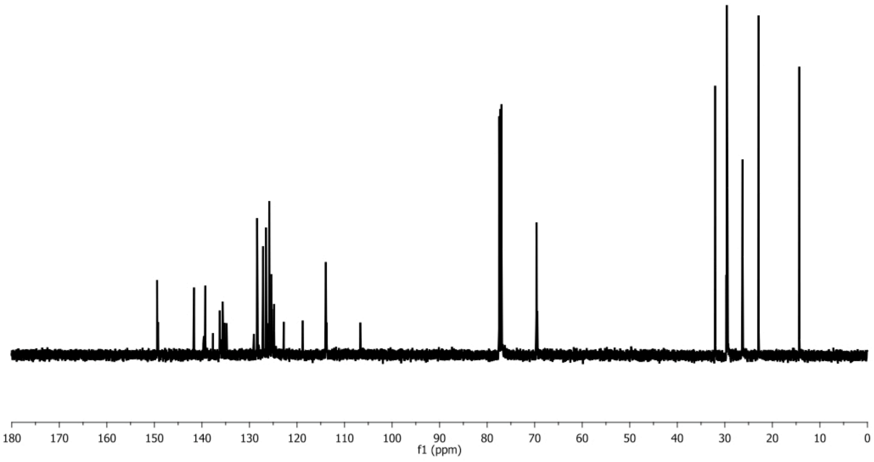

Spectrum 30. ^{13}C-NMR spectrum of **16** (125 MHz, $CDCl_3$).

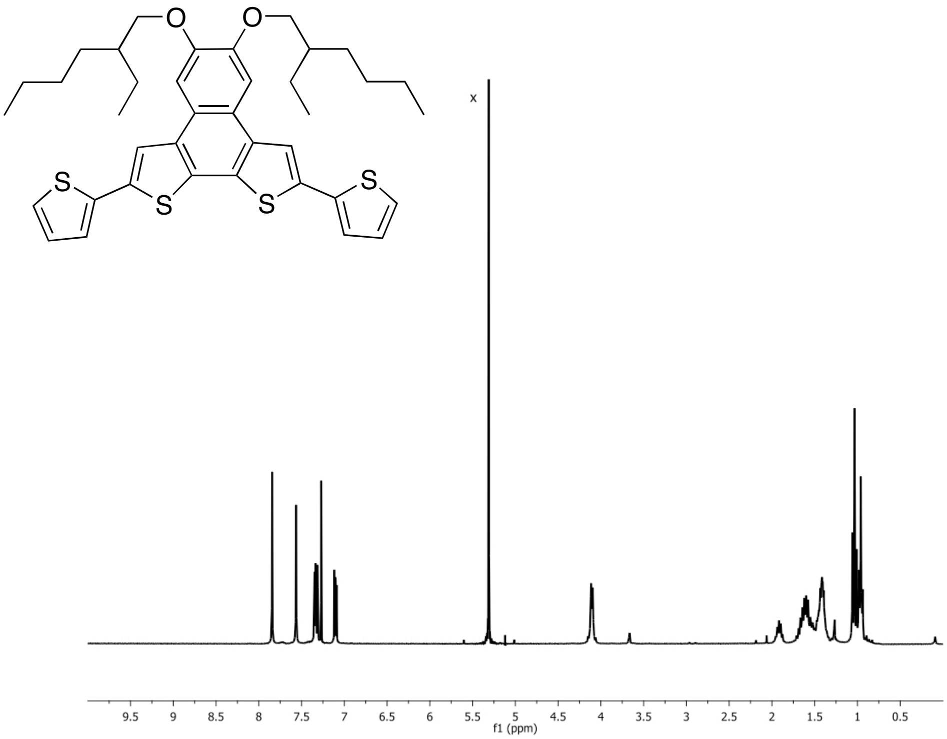

***Spectrum 31**.* ^{1}H-NMR spectrum of **18** (300 MHz, $CDCl_3$).

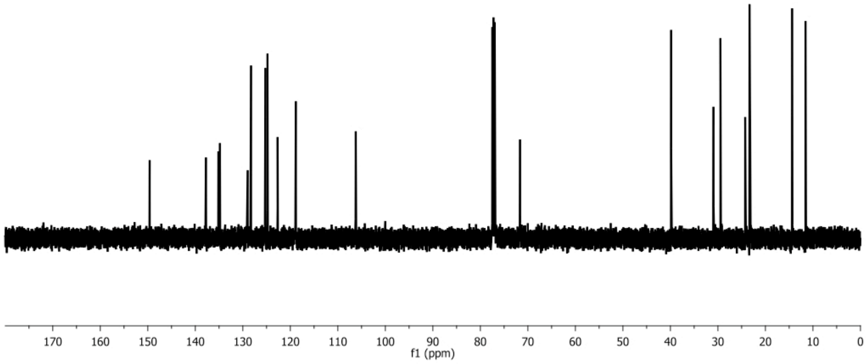

***Spectrum 32**.* ^{13}C-NMR spectrum of **18** (125 MHz, $CDCl_3$).

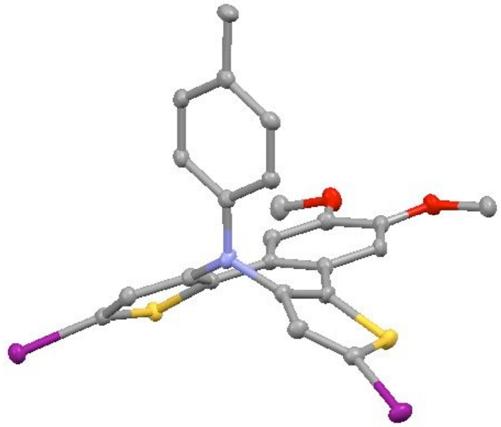

Chapter 6.

Polymers Incorporating Azepines:
Redox Stable Materials For Actuation

Introduction

We have developed annulated thiepin systems with the goal of using them as molecular actuators that would operate through bent-to-planar transformations driven by redox-induced aromatization (Chapter 5). However, due to the instability of the substituted thiepins in their oxidized form, we have turned our attention to other heteroepine structures. Of the iso-electronic systems, we chose the nitrogen-containing *azepine* as a target for the following reasons. Firstly, heteroepine systems with heavier atoms than sulfur (e.g., Se and Te) are expected to have even lower extrusion barriers. Secondly, heteroepines of group 15 (P, As, Bi, except N) are easily oxidized to 1-oxides, which are no longer iso-electronic. Lastly, the incorporation of nitrogen is synthetically more facile than that of oxygen, and we can prepare materials in a modular fashion, thanks to the recent development of palladium-catalyzed amination reactions.

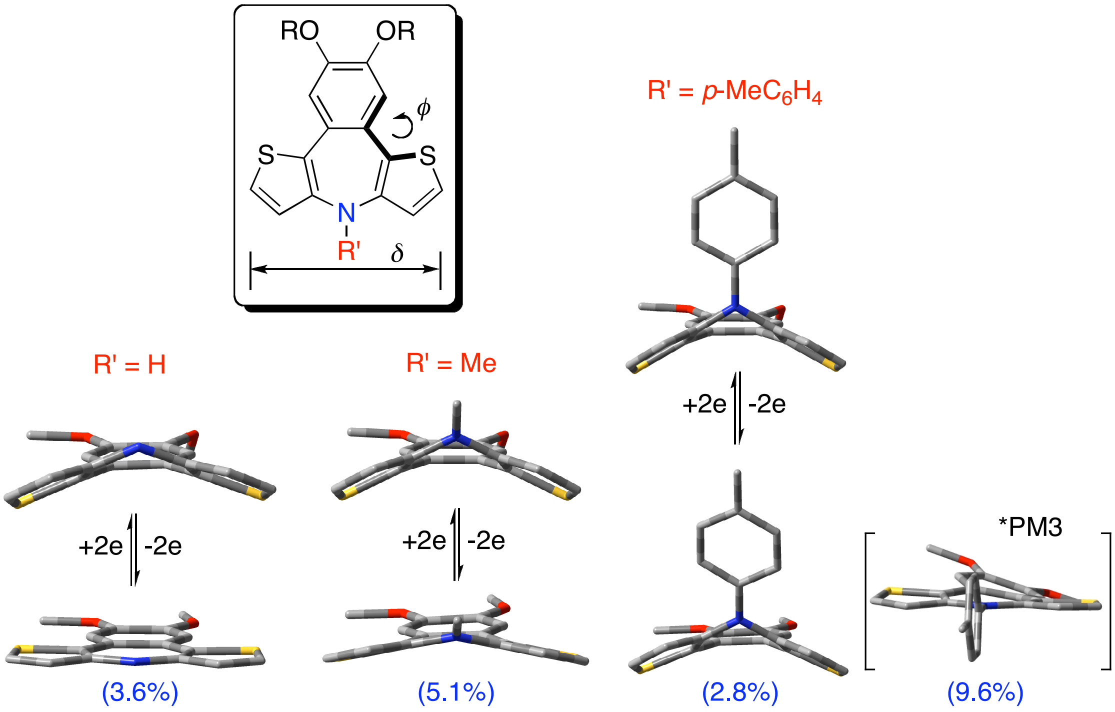

Figure 1. DFT optimizations (B3LYP, 6-31g) of dithieno[*b*,*f*]benzo[*d*]azepines in their neutral and oxidized states. Percent increases of δ in doubly oxidized states are presented in parentheses.

To confirm the potential of dithieno[*b*,*f*]benzo[*d*]azepines for the actuating system, we conducted DFT calculations (B3LYP, 6-31g) to see how the conformations change upon oxidation. Figure 1 shows the optimized structures in their neutral and doubly oxidized states according to the R' groups.

All of the azepines adapted a bent form in the neutral state but the degree of bent geometry depended on the *N*-substituents: the more demanding the steric effects, the more bent the structures. The distance between the outmost carbons (δ in Figure 1) decreased (more bent) from the smallest hydrogen (H) to the largest *p*-tolyl group (Table 1). The substituent effect was also found on the optimized geometries of doubly oxidized azepines. When R'=H, the oxidized azepine appears to have a completely flat conformation. If R' group is more sterically demanding than hydrogen (e.g., methyl), the geometry is distorted from the planar conformation.

Table 1. Distance (δ) and Dihedral Angle (ϕ) from Optimized Geometries (Figure 1)

	R' = H		**R' = Me**		**R' = *p*-Tolyl**	
	Neutral	Oxidized (2+)	Neutral	Oxidized (2+)	Neutral	Oxidized (2+)
Distance δ (A)	6.89	7.14	6.73	7.07	6.49	6.67
Dihedral Angle ϕ (°)	24.3	0.0	28.7	12.5	32.3	24.3

In case of the *p*-tolyl group, positioning the tolyl group in the same plane as the azepine ring creates large steric repulsions, and B3LYP (6-31g) suggests that it remains in the bent structure with a slight tortion of the tolyl group. Interestingly, the PM3 calculation with the same molecule produced a different result, wherein the tolyl group rotates and bissects the azepine's plane in such a way that they are perpendicular with each other. In this conformation (the tolyl group in normal to azepine), steric demands of the R' group are less than the methyl group, so that azepine becomes planar. It seems that the steric and electronic effects are competing in the case of the oxidized azepines.

In this chapter, we describe the syntheses of annelated azepines and their electrochemical properties. We also synthesized the azepin-incorporated polymers. Initial investigations reveal that azepines are very promising candidates for actuators and other related applications.

Synthesis of Annelated Azepines via Buchwald-Hartwig Amination

We initially tried to synthesize the annulated azepine **2**, which is analogous to the thiepins in Chapter 5, via a *double* amination strategy. The palladium-catalyzed C-N bond formation is a research area of great interest,[1] and since Buchwald and Hartwig independently reported the first general procedures for various amination reations,[2] the substrate scope and reaction efficiency have been greatly increased.[3] The "double" amination strategy has been applied to prepare dithienopyrrole derivatives,[4] but azepine-type compounds have not been prepared previously by this method.

Scheme 1.

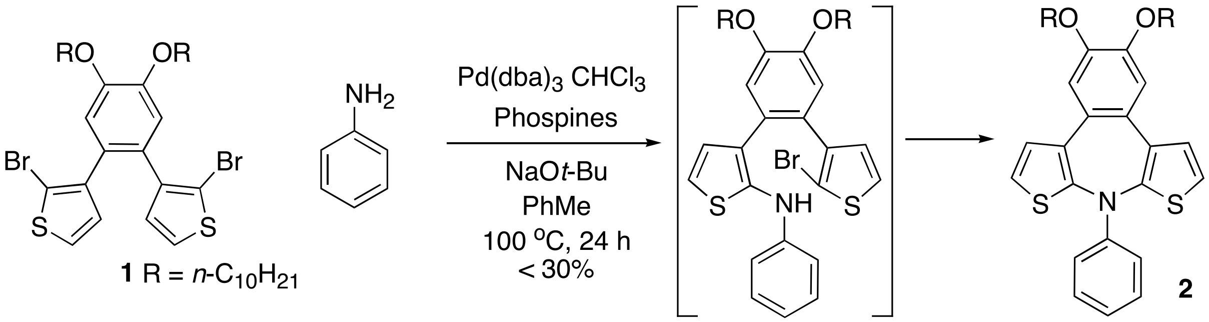

Starting from dibromide **1**, we first applied the recently reported method by Buchwald for the amination of a wide range of heteroaryl halides[3c] (Scheme 1). However, we were not able to isolate any of the desired product even when using a bulky electron-rich biaryl phosphine (e.g.

SPhos) in the catalysis. Instead, we observed significant amounts of byproducts that gave streaks on the TLC plate with almost no desired product. When a BINAP ligand[5] was utilized instead of the biaryl phosphine, the similar result was obtained.

We suspected that the ring-closing C-N bond formation (the second amination) between "2-bromothiophene" and "diarylamine" was problematic. This is consistent with the findings of Hartwig and coworkers that indicate (1) diarylamines react slowly when compared to *N*-methylaniline (the fastest) and aniline; (2) 3-bromothiophene reacts well with aniline but 2-bromothiophene does not; and (3) methyl substitution on the 3-position further reduces the reactivity of 2-bromothiophene.[3a] Hence, according to their findings, the second amination in Scheme 1 is expected to be challenging. In their subsequent study, they proposed that the amination of five-membered heteroaryl halides is dominated by the effectiveness of the reductive elimination step, which is unproductive in the case of the thiophen-2-yl-palladium amido complex.[3b]

Nevertheless, using *t*-Bu$_3$P as a ligand, we were able to isolate the desired product, albeit in a low yield. We suspect the intramolecular reaction condition facilitated the second amination and reduced side reactions, thus mitigating some of the above undesirable effects.

Considering the fact that 3-bromothiophene is a better substrate than 2-bromothiophene, we modified our plans and targeted **4**, which has [3,2-*b*;2',3'-*f*]annulation of thiophenes rather than [2,3-*b*;3',2'-*f*]. The double aminations of 3,3'-dibromide **3a–b** with several anilines were now very effective, providing the desired products **4a–c** in good yields.

Scheme 2.

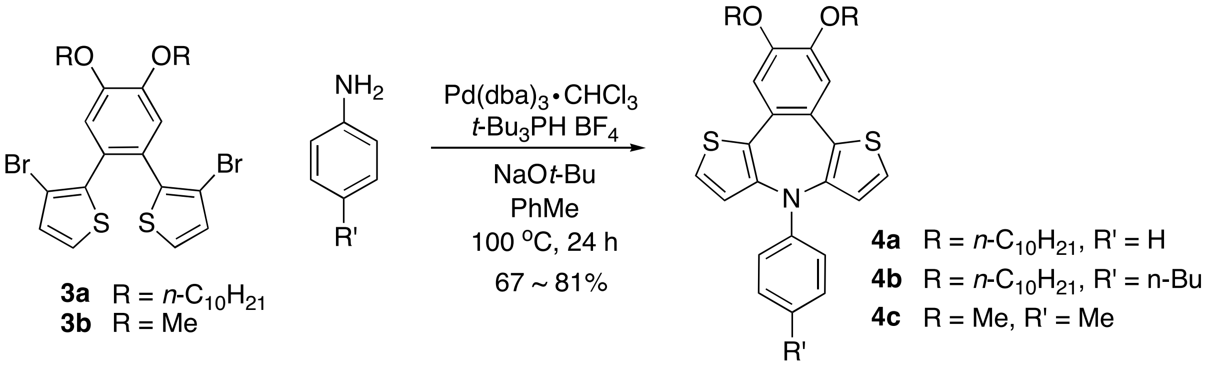
RO
OR
Br
Br
S
S
NH2
R'
Pd(dba)3•CHCl3
t-Bu3PH BF4
NaOt-Bu
PhMe
100 °C, 24 h
67 ~ 81%
RO
OR
S
S
N
R'

3a R = n-$C_{10}H_{21}$
3b R = Me

4a R = n-$C_{10}H_{21}$, R' = H
4b R = n-$C_{10}H_{21}$, R' = n-Bu
4c R = Me, R' = Me

With *N*-aryl azepines at hand, we next tried to synthesize *N*-alkyl azepines (**5**, for example). It is known that β-hydride elimination is a competing side reaction with alkyl amines and the process can lead to dehalogenated products.[5a] The undesired β-hydride elimination can be suppressed by the use of bidentate ligands, such as BINAP, dppf, etc. In fact, we were not able to obtain the desired product with a monodentate ligand *t*-Bu_3P, and switching to the BINAP ligand furnished the desired *N*-benzyl azepin **5** (Scheme 3). In this case, however, the yield was not satisfactory, presumably due to reduced reactivity of the first amination product. It appears that while the bidentate ligands successfully suppress the undesired β-hydride elimination, the catalyst complex is not active enough for cyclization (the second amination).

Scheme 3.

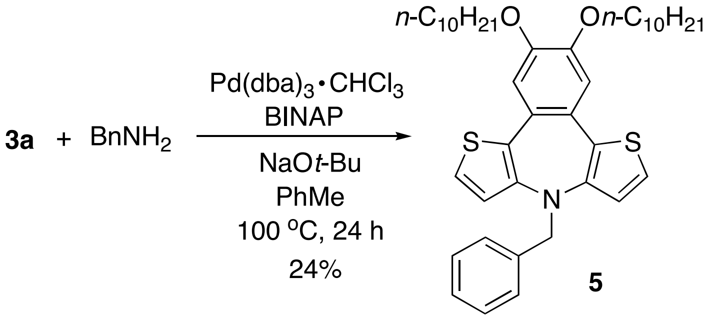
3a + BnNH2
Pd(dba)3•CHCl3
BINAP
NaOt-Bu
PhMe
100 °C, 24 h
24%
n-C10H21O
On-C10H21
S
S
N

5

Scheme 4.[a]

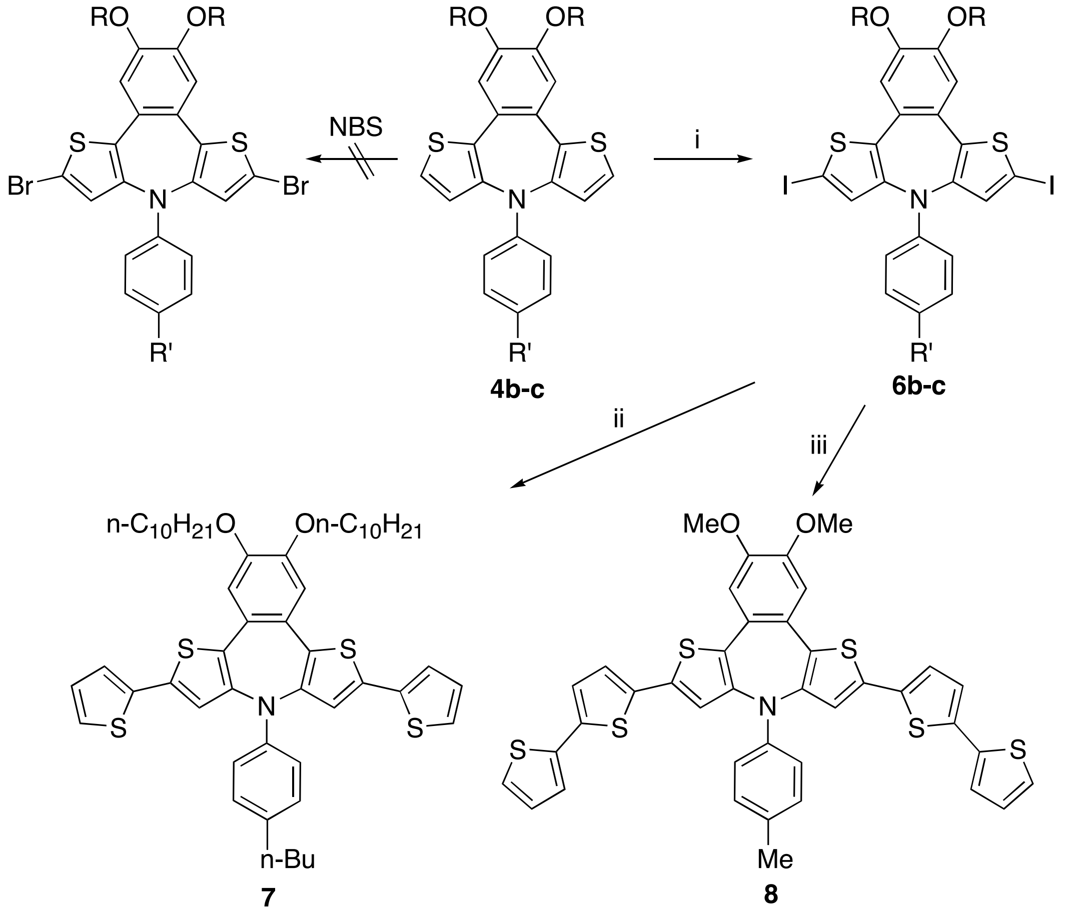

[a]Reagents: (i) *n*-BuLi, THF, -78 ºC; then I_2, room temperature, 58-91%. (ii) $PdCl_2(PPh_3)_2$, 2-tributylstannylthiophene, DMF, 80 ºC, 55%. (iii) $PdCl_2(PPh_3)_2$, 5-tributylstannyl-2,2'-bithiophene, DMF, 80 ºC, 85%.

Functionalization of Annulated Azepines

To further functionalize the azepine monomers, we tried to synthesize the dibromide employing standard bromination reagents, such as NBS. However, the reaction mixture turned dark brown immediately, and the reaction did not proceed. The color change was found to stem from the acid generated in the reaction, and the protonated azepins interfered with bromination. As an alternative strategy, we attempted a lithiation and electrophile quenching sequence. As shown in Scheme 4, diiodides **6b–c** were furnished by this approach in good yields. Among them, **6c** was characterized by X-ray crystallography (Figure 2), and its structure is in good agreement with our calculations (Figure 1).

Starting from diiodide **6**, bis(monothiophene)- and bis(bithiophene)-incorporated azepines, **7** and **8**, respectively, were synthesized via Stille coupling reactions using corresponding tributylstannyl thiophenes.

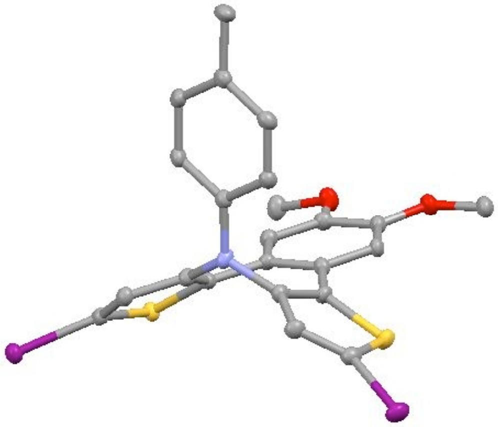

Figure 2. X-ray crystal structure of **6c** with 50% probability ellipsoids. Hydrogen atoms are omitted for clarity.

Azepine-incorporated polymers were also synthesized. A Stille coupling polymerization reaction between diiodide **6b** and distannes **9** resulted in a low molecular weight polymer **10** (M_n = 6,530 with PDI = 1.87) with a bright orange-red solid. In addition, Sonogashira polymerization of **6b** and diacetylene **11** produced a poly(phenyleneethylene)-type azepine polymer **12**, with a moderate molecular weight (M_n = 16,900 with PDI = 1.57).

Scheme 5.

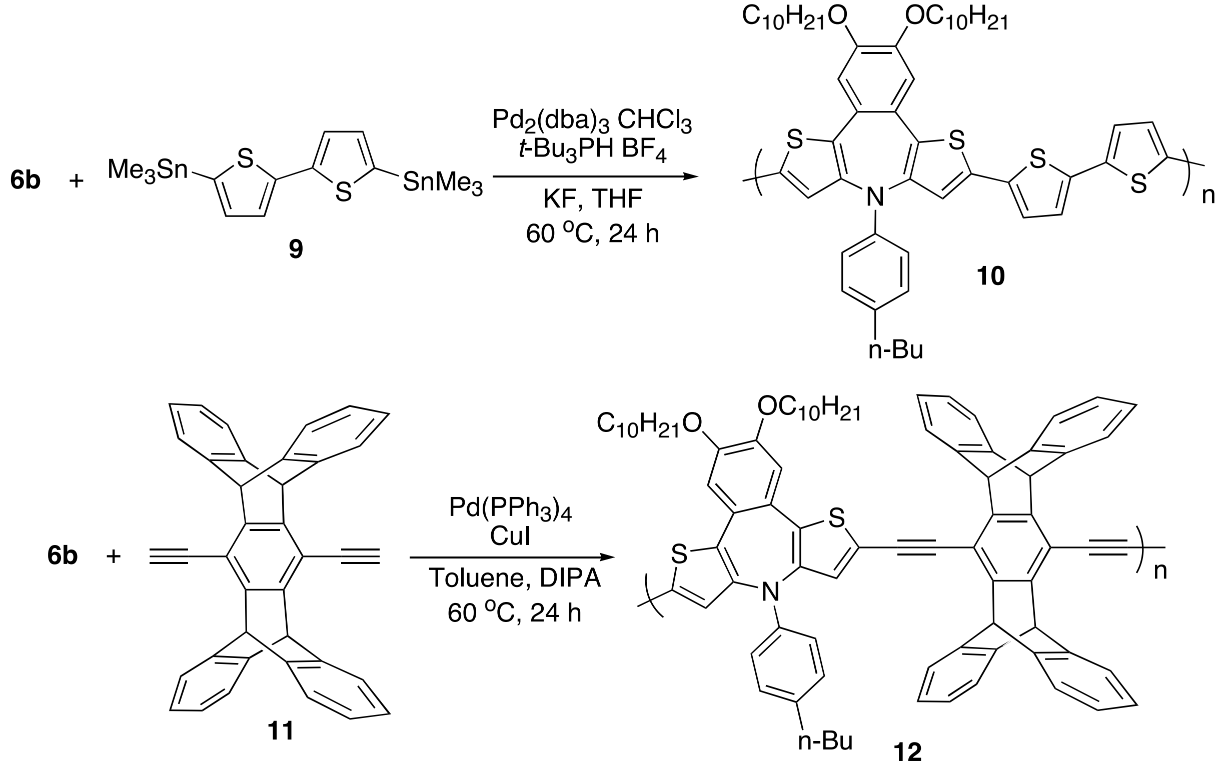
6b
+
Me3Sn
S
S
SnMe3
9
Pd2(dba)3 CHCl3
t-Bu3PH BF4
KF, THF
60 °C, 24 h
C10H21O
OC10H21
S
S
N
S
S
n
n-Bu
10
6b
+
11
Pd(PPh3)4
CuI
Toluene, DIPA
60 °C, 24 h
C10H21O
OC10H21
S
S
N
n
n-Bu
12

Cyclic Voltammetry

The cyclic voltammograms (CVs) of azepines **2**, **4a**, and **5** were measured from a standard 3-electrode apparatus in CH_2Cl_2 with 0.1 M $TBAPF_6$ as a supporting electrolyte. All measurements were carried out under ambient conditions, and they all produced very reproducible CVs (Figure 3).

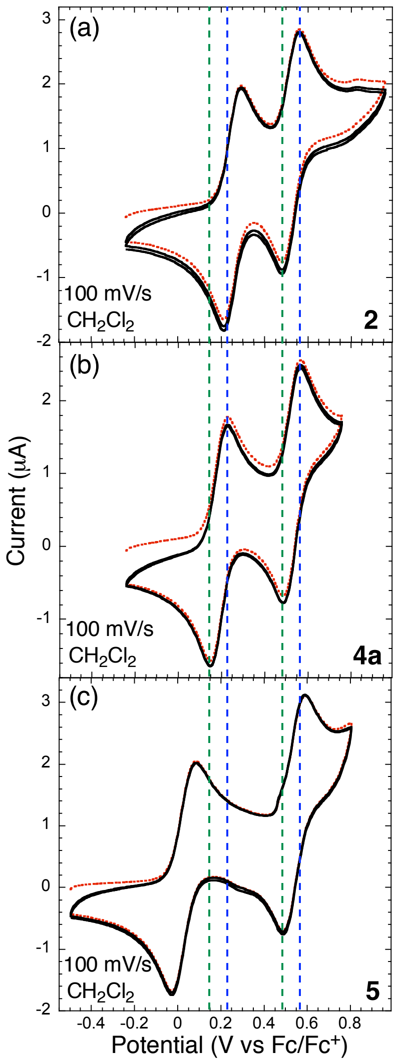

Figure 3. CVs of azepines **2** (a), **4a** (b), and **5** (c) measured on Pt button electrodes in CH_2Cl_2 with 0.1 M $TBAPF_6$ as a supporting electrolyte.

All the CVs showed two quasi-reversible one-electron redox waves but the oxidation potentials were slightly different, especially for the first oxidations. The half potential for the first redox couple ($E_{1/2}^1$) of azepin **2** (0.25 V) was slightly higher than that of azepine **4a** (0.19 V vs. Fc/Fc^+). This trend was also observed for related thiepins (Chapter 5) with analogous patterns of annulation. We suspect that the **4a**-type annulation more stabilizes the oxidized compound. Interestingly, however, the second oxidations occurred at very similar potentials ($E_{1/2}^2$ = 0.53 V vs. Fc/Fc$^+$). In the case of the *N*-alkyl azepine **5**, the first half potential $E_{1/2}{}^1$ shifted further to the negative potentials (0.03 V), while the second redox couple occurred at very similar potentials as other azepines (0.54 V vs. Fc/Fc$^+$). We suspect that this difference is due to the inductive effect of the alkyl group relative to the aryl group. More electron-donating *N*-alkyl groups reduce oxidation potentials when compared to the aryl group. Remarkably, however, all the second oxidations occur at the same potential, which is not fully understood at this time.

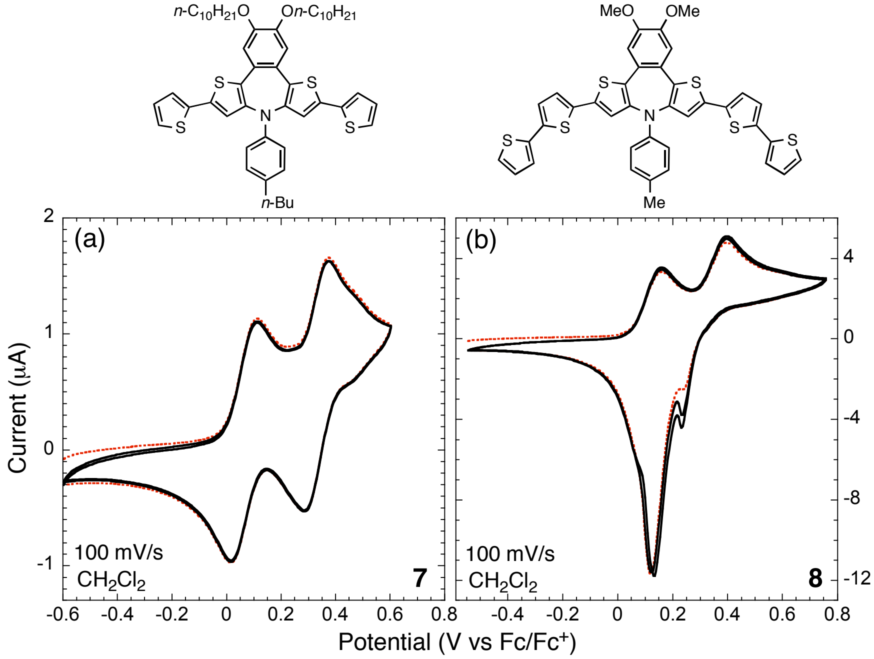

Figure 4. CVs of azepines **7** (a) and **8** (b) measured on Pt button electrodes in CH_2Cl_2 with 0.1 M $TBAPF_6$ as a supporting electrolyte.

Figure 4 shows the CVs of compounds **7** and **8**, which have extended thiophenes. Initially, we expected that the extended thiophenes on **7** and **8** would help electropolymerization and the polymers would be deposited on the electrode surface. However, no polymer was observed from either **7** or **8**. Instead, fairly reproducible CVs were obtained. The CV measurements were performed in similar conditions under air. When compared to the results from azepine **4a**, the first and second oxidations/reductions happen at the lower potentials. This is not surprising due to the extended conjugations.

The CVs of compound **8** showed very interesting shapes. In the forward scan, we observed two typical 1-electron oxidations similar to the other azepines. However, in the backward scan the two reductions combined and happened at the same potential; it appears that the reduction of dication $\mathbf{8}^{2+}$ to radical cation $\mathbf{8}^{\bullet+}$ requires an overpotential. One possible reason for this barrier is that the dication $\mathbf{8}^{2+}$ deposits as a stabilized solid on the electrode surface and thus gives complicated reduction kinetics.

Electrochemistry of Azepine-Incorporated Polymers

We measured the electrochemical properties of the films of polymers **10** and **12** on the electrodes. The films were prepared by drop-casting $CHCl_3$ solutions and drying in air. Figure 5 represents the CVs measured on Pt button electrodes in CH_3CN, which is a poor solvent for both of the polymers. Similar to the CVs of the monomeric compounds (Figure 3 and 4), we observed two redox waves. The second redox couple has larger integrated currents, which is most apparent for polymer **10**. In addition, the first oxidation peak was abnormally sharp, which implies that the solvent CH_3CN did not swell the neutral polymer and thus impeded the diffusion of ions and accompanying solvent molecules. Once charged, the polymer was more solvated by CH_3CN and ions diffused more readily into and out of the polymer. The electrochemical responses then had a more typical shape.

Interestingly, the first scan was also very different from the successive scans; the onset potential was higher and the amount of the integrated current was bigger. One reason might be the re-organization of the polymer's microstructure caused by the solvent uptake and release during the first redox cycle. However, the difference in the amount of the integrated current at the forward scan suggests the occurrence of some irreversible reactions. We suspect that oxidative couplings between the reactive end groups (or at the other positions) occurred. It is not likely that nitrogen extrusion occurs during the oxidation because the scaffold was found stable in all of the forms (Figure 3 and 4), and because the CV did not resemble those of poly(dithienonaphthalene)s.[6]

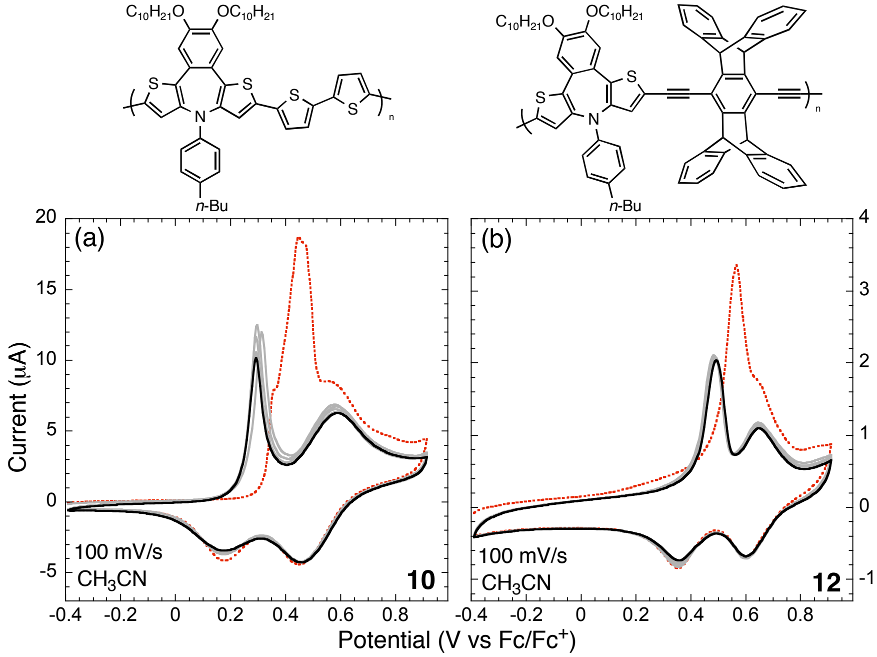

Figure 5. CVs of polymers **10** (a) and **12** (b) on Pt button electrodes (drop-cast from $CHCl_3$ solution) in CH_3CN with 0.1 M $TBAPF_6$ as a supporting electrolyte. The dotted lines represent the first scans.

To measure spectroelectrochemical properties, we drop-cast the azepine polymers on indium-tin-oxide (ITO) coated glass electrodes. Figure 6 illustrates the *in situ* measurements of UV-vis spectra following the increased oxidation levels in CH_3CN. The top pictures (a and b) show the CV profiles of polymers **10** and **12** used in the spectroelectrochemical measurements. Due to the greater thickness needed in order to ensure a sufficient amount of optical absorption, the first oxidation peak was not as sharp as observed in Figure 5, and this was especially apparent for polymer **10**. The bottom pictures (c and d) exhibit the absorption changes; the black line represents the absorption at 0 V, the red line at 0.6 V, and the blue line at 1.0 V (all vs. Ag/Ag$^+$).

There are two regimes in the potential-dependent optical spectra that reveal the development of sub-gap absorptions. One is from 0 V to 0.6 V, and the other is from 0.6 V to 1.0 V (all vs. Ag/Ag$^+$), and these are roughly matched with the first and second oxidations, respectively. For polymer **10**, in the first regime, the original bandgap absorption decreased and new absorption increased in the sub-gap region. The new absorptions were broad and feature-less, which implies that the polymer has a very delocalized electronic structure. However, the absorptions became more distinct in the second oxidation regime. It is an interesting feature that the original bandgap region retains a considerable amount of absorption while most polythiophene derivatives show almost complete depletion of these absorptions with increased oxidation levels.[7]

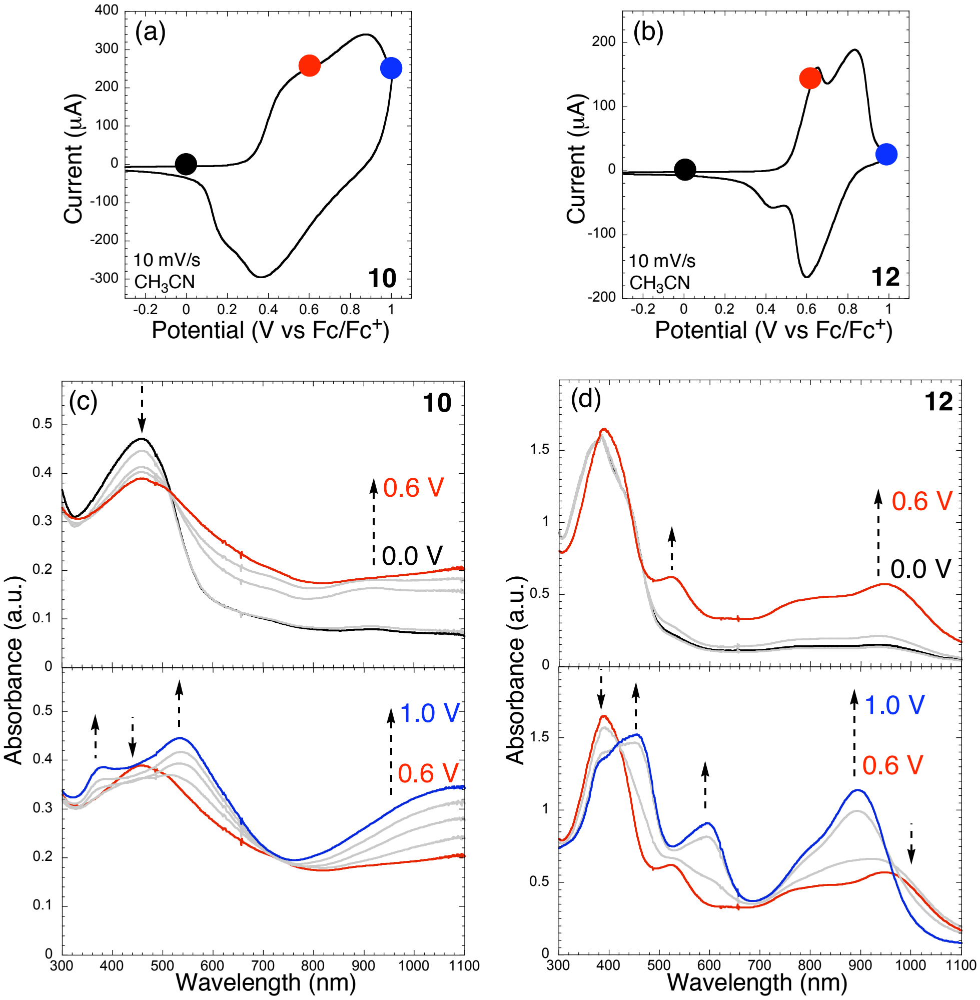

Figure 6. Electronic absorption spectra of polymers **10** (c) and **12** (d) on ITO-coated glass electrodes in CH$_3$CN with 0.1 M TBAPF$_6$ as a supporting electrolyte, as a function of oxidation potential from 0.0 V to 1.0 V vs. Ag/Ag$^+$. CVs of the same polymers **10** (a) and **12** (b) were presented for comparison.

Polymer **12**'s UV-vis absorption showed similar characteristics to that of polymer **10**. However, the electronic structure of polymer **12** appeared more localized (higher energy) as compared to polymer **10**.

We attempted to measure *in situ* conductivities from the azepine-incorporated polymers **10** and **12** by drop-casting the polymer on interdigitated microelectrodes. However, we were not able to detect any drain current signals, probably due to low conductivity and high contact resistance with the electrode. Instead, interestingly enough, we could measure the *in situ* conductivity of poly(**8**), which was prepared by $FeCl_3$-mediated polymerization. Due to the short alkyl chains, poly(**8**) showed poor solubility in common organic solvents, and was intractable for further characterization. Nevertheless, a drop-cast slurry of poly(**8**) in $CHCl_3$ on an interdigitated microelectrode produced a functional device.

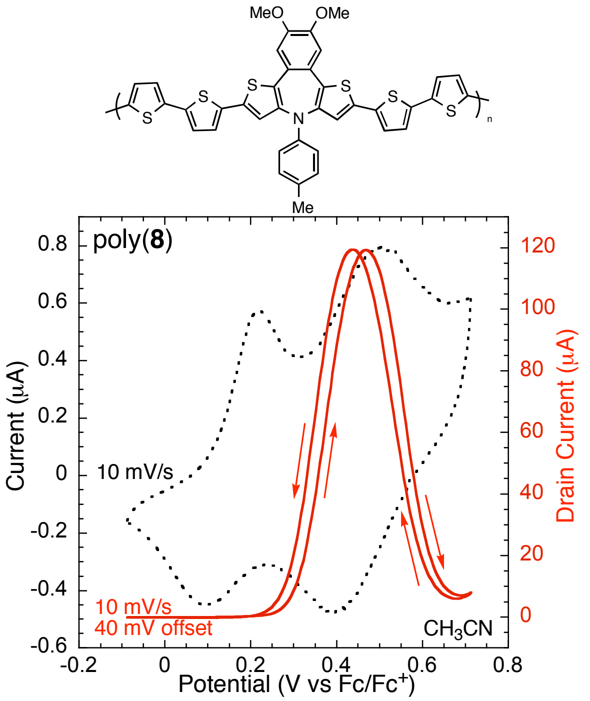

Figure 7. CVs (dotted lines) and *in situ* conductivity measurements (drain current, solid lines) of poly(**8**) on a 5-μm interdigitated Pt microelectrode in CH_3CN with 0.1 M $TBAPF_6$ as a supporting electrolyte.

As shown in Figure 7, the CV showed two redox peaks, the second of which was slightly larger than the first. The drain current, which is proportional to conductivity, started to increase as the second oxidation occurred. It is very intriguing that the drain current profile had a bell-shape, which was very reversible and reproducible. In general, the bell-shaped profile can be found in the segmented (not fully conjugated) polymers.[8] Thus, poly(**8**) performs as though it is a segmented polymer when oxidized. We suspect this is due to the charge barriers developed in the azepine-moieties, which is reminiscent of a tropone-containing polymer[9] reported earlier by our group. In the tropone polymer, when the charges are introduced by addition of an acid, they appear to reduce the conductivity of the system because the charge carriers' mobility is decreased. Likewise in poly(**8**), by the first oxidation, charges are developed and localized on the azepine moieties. At the second oxidation, the oligothiophene portions start to be oxidized as indicated by the larger currents, and the conductivity increases. However, the charge carriers cannot move readily along the polymer chain because of the barrier on the azepine moieties. They can only transport the charges by hopping between the chains.

Conclusion

Azepines, which are potential bent-to-planar molecular actuators, were designed and successfully synthesized via a Pd-catalyzed double amination strategy. Contrary to thiepins and other heteroepine systems, azepines were very stable even in highly oxidized states. The CVs displayed two 1-electron redox peaks that were reversible and reproducible, even with extended thiophenes. The azepine-incorporated polymers showed two oxidation regimes, involving the azepine moiety only at low potentials and the whole polymer at higher potentials. The polymer's conductivity did not increase until oxidized in the second regime. Judging from the bell-shaped conductivity profile, it appears that the charge carriers move readily by hopping between the polymer chains. Due to their high electrochemical stability, azepines are promising candidates for actuators and other related applications.

Experimental Section

General. NMR spectra were recorded on a Varian Mercury-300, Bruker Advance-400, or Varian Inova-500 spectrometer. Chemical shifts were reported in ppm and referenced to residual solvent peaks ($CDCl_3$: δ 7.27 ppm for ^{1}H, δ 77.23 ppm for ^{13}C). High-resolution mass spectra (HR-MS) were obtained on a Bruker Daltonics APEX II 3 Tesla FT-ICR-MS. UV-vis spectra were obtained using a HP 8453 diode array spectrometer. Electrochemical measurements were carried out using an Autolab PGSTAT 10 or PGSTAT 20 potentiostat (Eco Chemie) in a three-electrode cell configuration consisting of a quasi-internal Ag wire reference electrode (BioAnalytical Systems) submerged in 0.01 $AgNO_3$ / 0.1 M tetrabutylammonium hexafluorophosphate ($TBAPF_6$) in anhydrous CH_3CN, a Pt button (1.6 mm in diameter), 5-μm interdigitated micro-, or ITO-coated glass electrodes as the working electrode, and a Pt coil or Pt gauze as the counter electrode. The ferrocene/ferrocenium (Fc/Fc^+) redox couple was used as an external reference. Half-wave potentials of Fc/Fc^+ were observed between 88–95 mV in CH_3CN and 210-245 mV (all vs. Ag/Ag^+) in CH_2Cl_2. All air and water sensitive synthetic manipulations were performed under an argon or nitrogen atmosphere using standard Schlenk techniques.

Materials. Spectroscopic grade CH_2Cl_2 was purchased from Aldrich for electrochemistry. $TBAPF_6$ was recrystallized in ethanol prior to use. Anhydrous DMF was purchased from Aldrich as Sure-Seal Bottles and used as received. THF was purified by passage through two alumina columns of an Innovative Technologies purification system. All other chemicals were of reagent grade and used as received. Compounds **1** was prepared by literature methods.[9] Synthesis of **3a-b** was described in Chapter 5. 5-Tributylstannyl-2,2'-bithiophene[10] and 5,5'-trimethylstannyl-2,2'-bithiophene (**9**) [11] were synthesized by known procedures.

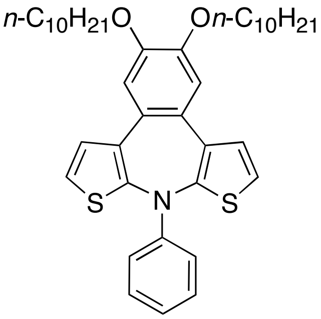

6,7-Di(decyloxy)-1-phenyl-dithieno[2,3-*b*;3’,2’-*f*]-benzo[*d*]-azepine (2). In a Schlenk equipped with a stir bar were combined compound **1** (0.143 g, 0.2 mmol), $Pd_2(dba)_3$•$CHCl_3$, (6 mg, 3 mol %), (*t*-$Bu_3PH)BF_4$ (7 mg, 12 mol %), and the tube was evacuated and backfilled with Ar two times. Under a gentle stream of Ar, NaO*t*-Bu (0.054 g, 5.6 mmol) was added, and the tube was evacuated and backfilled with Ar two times more. To the mixture was added aniline (0.018 mL, 0.2 mmol) and toluene (2 mL), and the mixture was allowed to stir at 100 °C for 20 h. After being cooled to room temperature, the mixture was filtered through a pad of celite and washed with ethyl acetate. The filtrate was concentrated under reduced pressure and subjected to a column chromatography (chloroform:hexane = 1:3). Yield: 0.037 g (29%) of white solid. ^{1}H NMR (300 MHz, $CDCl_3$) δ: 7.22 (d, 2H, *J* = 6.0 Hz), 7.17–7.12 (m, 2H), 7.14 (d, 2H, *J* = 6.0 Hz), 7.08 (s, 2H), 7.08–7.04 (m, 2H), 6.83 (tt, 1H, *J* = 7.2, 1.2 Hz), 4.04 (t, 4H, *J* = 6.6 Hz), 1.84 (m, 4H), 1.48–1.28 (m, 28H), 0.89 (t, 6H, *J* = 6.9 Hz). ^{13}C NMR (125 MHz, $CDCl_3$) δ: 148.50, 148.30, 142.42, 136.44, 128.86, 126.84, 126.02, 122.69, 120.20, 114.43, 113.31, 69.54, 32.13, 29.85, 29.80, 29.62, 29.58, 29.48, 26.25, 22.91, 14.35. HR-MS (ESI): calcd for $C_{40}H_{53}NO_2S_2$ $[M+H]^+$, 644.3590; found, 644.3615.

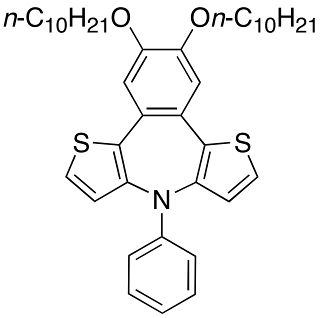

6,7-Di(decyloxy)-1-phenyl-dithieno[3,2-*b*;2',3'-*f*]-benzo[*d*]-azepine (4a). Using the same procedure for the preparation of **2**, compound **3a** (0.028 g, 0.039 mmol) was treated with $Pd_2(dba)_3$•$CHCl_3$, (2 mg, 5 mol %), (*t*-$Bu_3PH)BF_4$ (1.4 mg, 12 mol %), NaO*t*-Bu (0.009 g, 0.094 mmol), aniline (0.0036 mL, 0.039 mmol), and toluene (0.5 mL). The eluent for the column chromatography was dichloromethane:hexane = 1:2. Yield: 0.008 g (32%) of white solid. ^{1}H NMR (400 MHz, $CDCl_3$) δ: 7.39 (d, 2H, *J* = 5.3 Hz), 7.11 (m, 2H), 7.08 (d, 2H, *J* = 5.3 Hz), 7.06 (s, 2H), 6.80 (m, 2H), 6.75 (tt, 1H, *J* = 7.2, 1.2 Hz), 4.05 (t, 4H, *J* = 6.6 Hz), 1.84 (m, 4H), 1.46–1.28 (m, 28H), 0.90 (t, 6H, *J* = 6.6 Hz). ^{13}C NMR (125 MHz, $CDCl_3$) δ: 149.05, 147.79, 141.48, 136.13, 129.06, 127.93, 125.17, 124.01, 118.64, 113.60, 112.45, 69.54, 32.14, 29.85, 29.80, 29.61, 29.58, 29.37, 26.22, 22.92, 14.36. HR-MS (ESI): calcd for $C_{40}H_{53}NO_2S_2$ $[M+H]^+$, 644.3590; found, 644.3593.

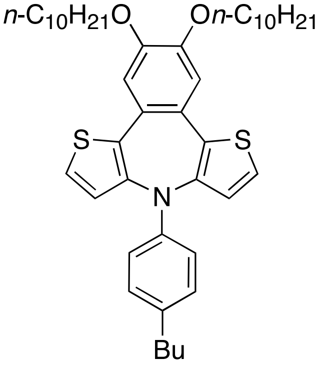

1-(4-Butylphenyl)-6,7-di(decyloxy)-dithieno[3,2-*b*;2',3'-*f*]-benzo[*d*]-azepine (4b). Using the same procedure for the preparation of **2**, compound **3a** (0.094 g, 0.13 mmol) was treated with $Pd_2(dba)_3$•$CHCl_3$, (6.7 mg, 5 mol %), (*t*-$Bu_3PH)BF_4$ (4.5 mg, 12 mol %), NaO*t*-Bu (0.030 g, 0.31 mmol), 4-butylaniline (0.025 mL, 0.156 mmol), and toluene (1.5 mL). Yield: 0.008 g (32%) of white solid. ^1H NMR (400 MHz, $CDCl_3$) δ: 7.39 (d, 2H, *J* = 5.3 Hz), 7.10 (d, 2H, *J* = 5.3 Hz), 7.09 (s, 2H), 6.95 (*pseudo*-d, 2H, *J* = 8.7 Hz), 6.75 (*pseudo*-d, 2H, *J* = 8.7 Hz), 4.07 (t, 4H, *J* = 6.6 Hz), 2.49(t, 2H, *J* = 7.8 Hz), 1.86 (m, 4H), 1.52 (m, 6H), 1.40–1.28 (m, 26H), 0.90 (t, 9H, *J* = 7.0 Hz). ^{13}C NMR (100 MHz, $CDCl_3$) δ: 148.98, 145.68, 141.83, 135.96, 133.07, 128.93, 128.02, 125.07, 124.12, 113.62, 112.36, 69.51, 34.82, 34.17, 32.13, 29.84, 29.79, 29.60, 29.57, 29.36, 26.21, 22.91, 22.56, 14.35, 14.17. HR-MS (ESI): calcd for $C_{44}H_{61}NO_2S_2$ $[M+H]^+$, 700.4216; found, 700.4194.

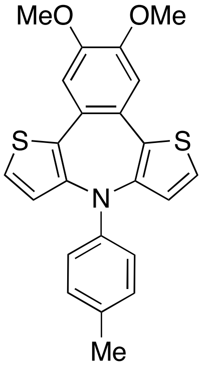

6,7-Dimethoxy-1-(4-tolyl)-dithieno[3,2-*b*;2',3'-*f*]-benzo[*d*]-azepine (4c). Using the same procedure for the preparation of **2**, compound **3b** (0.845 g, 1.8 mmol) was treated with *p*-toluidine (0.195 g, 1.8 mmol), $Pd_2(dba)_3$•$CHCl_3$, (93 mg, 5 mol %), (*t*-$Bu_3PH)BF_4$ (63 mg, 12 mol %), NaO*t*-Bu (0.415 g, 4.32 mmol), and toluene (18 mL). The eluent for the column chromatography was ethyl acetate:hexane = 1:5. Yield: 0.640 g (87%) of white solid. ^1H NMR (300 MHz, $CDCl_3$) δ: 7.41 (d, 2H, *J* = 5.4 Hz), 7.10 (d, 2H, *J* = 5.4 Hz), 7.08 (s, 2H), 6.95

(*pseudo*-d, 2H, *J* = 8.7 Hz), 6.74 (*pseudo*-d, 2H, *J* = 8.7 Hz), 3.95 (s, 6H), 2.24 (s, 3H). ^{13}C NMR (125 MHz, $CDCl_3$) δ: 148.79, 145.53, 142.11, 135.81, 129.52, 128.07, 127.91, 125.26, 124.02, 112.44, 111.35, 56.17, 20.46. HR-MS (ESI): calcd for $C_{23}H_{19}NO_2S_2$ [M+H]$^+$, 406.0930; found, 406.0938.

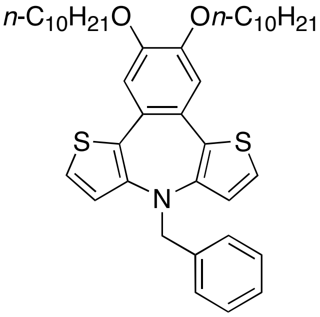

1-Benzyl-6,7-di(decyloxy)-dithieno[3,2-*b*;2’,3’-*f*]-benzo[*d*]-azepine (5). Using the same procedure for the preparation of **2**, compound **3a** (0.032 g, 0.045 mmol) was treated with $Pd_2(dba)_3$•$CHCl_3$, (2.3 mg, 5 mol %), BINAP (5.6 mg, 20 mol %), NaO*t*-Bu (0.010 g, 0.108 mmol), benzylamine (0.005 mL, 0.045 mmol), and toluene (1 mL). The eluent for the column chromatography was dichloromethane:hexane = 1:3. Yield: 0.007 g (24%) of white solid. ^{1}H NMR (300 MHz, $CDCl_3$) δ: 7.39 (*pseudo*-d, 2H, *J* = 7.2 Hz), 6.80 (*pseudo*-t, 2H, *J* = 7.2 Hz), 7.19 (tt, 1H, *J* = 7.2, 1.2 Hz), 7.11 (d, 2H, *J* = 5.4 Hz), 6.91 (s, 2H), 6.64 (d, 2H, *J* = 5.4 Hz), 4.69 (s, 2H), 4.06 (t, 4H, *J* = 6.6 Hz), 1.86 (m, 4H), 1.56–1.28 (m, 28H), 0.89 (t, 6H, *J* = 7.2 Hz). ^{13}C NMR (125 MHz, $CDCl_3$) δ: 149.28, 148.62, 138.23, 128.56, 128.10, 127.77, 127.15, 126.28, 124.46, 122.06, 113.93, 69.57, 55.95, 32.15, 29.87, 29.82, 29.67, 29.59, 29.48, 26.27, 22.92, 14.36. HR-MS (ESI): calcd for $C_{41}H_{55}NO_2S_2$ [M+H]$^+$, 658.3747; found, 658.3752.

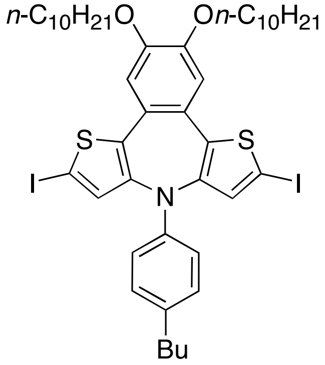

1-(4-Butylphenyl)-6,7-di(decyloxy)-3,10-diiodo-dithieno[3,2-*b*;2’,3’-*f*]-benzo[*d*]-azepine (6b). To a THF (2 mL) solution of compound **4b** (0.157 g, 0.22 mmol) was added *n*-BuLi (1.6 M in hexane, 0.290 mL, 0.462 mmol) at –40 ºC. The mixture was taken out of the cooling bath and allowed to stir at room temperature for 1 h, at which time the mixture was cooled to –40 ºC again and iodine (0.123 g, 0.462 mmol) was added to the mixture. After being allowed to stir at room temperature for 15 h, the mixture was diluted with diethyl ether and washed with saturated $Na_2S_2O_3$ (aq) and brine. The organic layer was dried over $MgSO_4$, evaporated under reduced pressure, and subjected to column chromatography (chloroform:hexane = 1:3). Yield: 0.191 g (91%) of pale yellow solid. ^{1}H NMR (400 MHz, $CDCl_3$) δ: 7.21 (s, 2H), 6.95 (*pseudo*-d, 2H, *J* = 8.7 Hz), 6.93 (s, 2H), 6.70 (*pseudo*-d, 2H, *J* = 8.7 Hz), 4.02 (t, 4H, *J* = 6.6 Hz), 2.48 (t, 2H, *J* = 7.2 Hz), 1.83 (m, 4H), 1.49 (m, 6H), 1.40–1.28 (m, 26H), 0.90 (t, 3H, *J* = 7.3 Hz), 0.89 (t, 6H, *J* = 6.7 Hz). ^{13}C NMR (125 MHz, $CDCl_3$) δ: 149.35, 144.80, 141.75, 141.52, 136.92, 133.92, 129.05, 123.21, 113.11, 112.53, 72.96, 69.49, 34.81, 34.13, 32.13, 29.83, 29.79, 29.57, 29.57, 29.27, 26.17, 22.91, 22.53, 14.36, 14.17. HR-MS (ESI): calcd for $C_{44}H_{59}I_2NO_2S_2$ $[M+H]^+$, 952.2149; found, 952.2120.

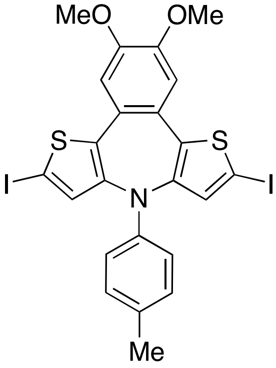

3,10-Diiodo-6,7-dimethoxy-1-(4-tolyl)-dithieno[3,2-*b*;2',3'-*f*]-benzo[*d*]-azepine (6c). Using the same procedure for the preparation of **6b**, compound **4c** (0.124 g, 0.3 mmol) was treated with *n*-BuLi (1.6 M in hexane, 0.394 mL, 0.63 mmol) and iodine (0.168 g, 0.66 mmol) in THF (3 mL). The eluent for the column chromatography was ethyl acetate:hexane = 1:4. Yield: 0.115 g (58%) of pale yellow solid. ^{1}H NMR (300 MHz, CDCl$_3$) δ: 7.21 (s, 2H), 6.94 (*pseudo*-d, 2H, *J* = 8.7 Hz), 6.94 (s, 2H), 6.67 (*pseudo*-d, 2H, *J* = 8.7 Hz), 3.91 (s, 6H), 2.22 (s, 3H). ^{13}C NMR (125 MHz, CDCl$_3$) δ: 149.23, 144.70, 142.11, 141.39, 137.01, 129.67, 128.80, 123.23, 112.65, 111.06, 73.22, 56.25, 20.53. HR-MS (ESI): calcd for $C_{23}H_{17}I_2NO_2S_2$ [M]$^+$, 656.8785; found, 656.8785.

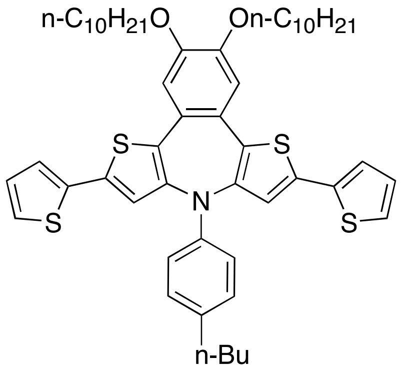

1-(4-Butylphenyl)-6,7-di(decyloxy)-3,10-bis(thiophen-2-yl)-dithieno[3,2-*b*;2',3'-*f*]-benzo[*d*]-azepine (7). To a degassed solution of DMF (0.5 mL) of compound **6b** (0.020 g, 0.023

mmol) were added 2-tributylstannyl thiophene (0.018 mL, 0.053 mmol) and $PdCl_2(PPh_3)_2$ (0.8 mg, 5 mol %). The mixture was allowed to stir at 80 °C for 15 h, at which time the mixture was cooled to room temperature. Ethyl acetate was added to the mixture, and the organic layer was washed with saturated aqueous NH_4Cl, KF, and NH_4Cl again. After being dried over $MgSO_4$, the organic layer was evaporated under reduced pressure and subjected to column chromatography (chloroform:hexane = 1:4). Yield: 0.011 g (55%) of yellow solid. ^{1}H NMR (300 MHz, $CDCl_3$) δ: 7.26 (dd, 2H, *J* = 5.1, 1.2 Hz), 7.22 (dd, 2H, *J* = 3.6, 1.2 Hz), 7.19 (s, 2H), 7.06 (dd, 2H, *J* = 5.1, 3.6 Hz), 7.04 (s, 2H), 6.95 (*pseudo*-d, 2H, *J* = 8.7 Hz), 6.82 (*pseudo*-d, 2H, *J* = 8.7 Hz), 4.07 (t, 4H, *J* = 6.6 Hz), 2.48 (t, 2H, *J* = 7.5 Hz), 1.86 (m, 4H), 1.51 (m, 6H), 1.38–1.27 (m, 26H), 0.89 (t, 3H, *J* = 7.5 Hz), 0.89 (t, 6H, *J* = 6.6 Hz). ^{13}C NMR (125 MHz, $CDCl_3$) δ: 149.14, 145.29, 141.26, 137.62, 136.60, 135.06, 133.54, 129.04, 128.16, 125.04, 124.22, 124.01, 123.66, 113.22, 112.56, 69.53, 34.85, 34.17, 32.15, 29.87, 29.82, 29.62, 29.59, 29.36, 26.23, 22.92, 22.57, 14.36, 14.19. HR-MS (ESI): calcd for $C_{52}H_{65}NO_2S_4$ $[M+H]^+$, 864.3971; found, 864.3994.

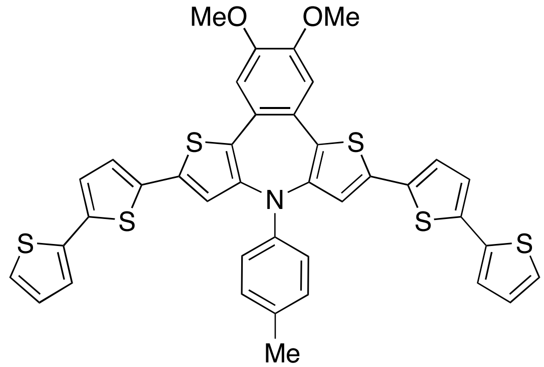

3,10-bis(2,2'-bithiophen-5-yl)-6,7-dimethoxy-1-(4-tolyl)-dithieno[3,2-*b*;2',3'-*f*]-benzo[*d*]-azepine (8). Using the same procedure for the synthesis of **7**, compound **6c** (0.073 g, 0.11 mmol) was treated with 5-tributylstannyl-2,2'-bithiophene (0.109 mL, 0.27 mmol) and $PdCl_2(PPh_3)_2$ (4 mg, 5 mol %) in DMF (1 mL). Yield: 0.069 g (85%) of orange solid. ^{1}H NMR (400 MHz,

$CDCl_3$) δ: 7.25 (dd, 2H, *J* = 5.1, 1.2 Hz), 7.20 (dd, 2H, *J* = 3.6, 1.2 Hz), 7.19 (s, 2H), 7.14 (d, 2H, *J* = 3.8 Hz), 7.12 (d, 2H, *J* = 3.8 Hz), 7.04 (dd, 2H, *J* = 5.1, 3.6 Hz), 7.04 (s, 2H), 6.96 (*pseudo*-d, 2H, *J* = 8.7 Hz), 6.80 (*pseudo*-d, 2H, *J* = 8.7 Hz), 3.96 (s, 6H), 2.22 (s, 3H). ^{13}C NMR (125 MHz, $CDCl_3$) δ: 149.06, 145.15, 141.66, 137.15, 137.00, 136.51, 136.15, 135.02, 129.70, 128.54, 128.16, 124.92, 124.64, 124.30, 124.14, 124.09, 123.97, 112.74, 111.09, 56.28, 20.55. HR-MS (ESI): calcd for $C_{39}H_{27}NO_2S_6$ $[M+H]^+$, 734.0439; found, 734.0455.

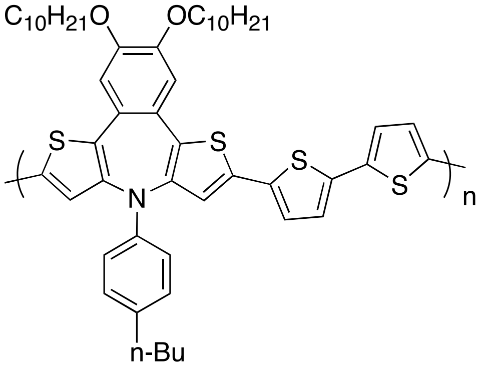

Polymer 10. Compound **6b** (0.077 g, 0.081 mmol), **9** (0.040 g, 0.081 mmol), and $Pd_2(dba)_3$•$CHCl_3$ (4.2 mg, 5 mol %) were dissolved in THF (1 mL). The mixture was degassed by freeze-pump-thaw (3 cycles) and (t-$Bu_3PH)BF_4$ (2.6 mg, 11 mol %) and KF (0.028 g, 0.49 mmol) were added under gentle Ar stream. The mixture was allowed to stir at 60 °C for 24 h, at which time the mixture was cooled to room temperature and methanol was added to precipitate. The filtered solid was re-dissolved in $CHCl_3$ and added to methanol to precipitate again. The product was filtered out and dried under air. Yield: 0.043 g (62%) of dark red solid. GPC (polystyrene standard): M_n = 4980, M_w = 7810, PDI = 1.57. ^1H NMR (300 MHz, $CDCl_3$) δ: 7.20 (aromatic C–H), 7.12 (aromatic C–H), 7.04 (aromatic C–H), 6.96 (aromatic C–H), 6.82 (aromatic C–H), 4.07 (aliphatic C–H), 2.50 (aliphatic C–H), 1.86 (aliphatic C–H), 1.54 (aliphatic C–H), 1.29 (aliphatic C–H), 0.89 (aliphatic C–H).

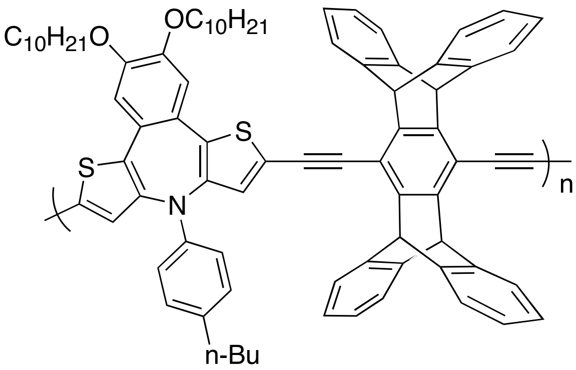

Polymer 12. Compound **6b** (0.077 g, 0.081 mmol) and **11** (0.039 g, 0.081 mmol) were dissolved in degassed diisopropyamine (0.6 mL) and toluene (1.8 mL). Under gentle Ar stream $Pd(PPh_3)_4$ (3.7 mg, 4 mol %) and CuI (1.5 g, 10 mol %) were added. The mixture was allowed to stir at 60 ºC for 24 h, at which time the mixture was cooled to room temperature and methanol was added to precipitate. The filtered solid was re-dissolved in $CHCl_3$ and added to methanol to precipitate again. The product was filtered out and dried under air. Yield: 0.069 g (73%) of yellow solid. GPC (polystyrene standard): M_n = 16900, M_w = 35700, PDI = 2.11. ^{1}H NMR (300 MHz, $CDCl_3$) δ: 7.62 (aromatic C–H), 7.46 (aromatic C–H), 7.23 (aromatic C–H), 7.14 (aromatic C–H), 7.01 (aromatic C–H), 5.89 (aliphatic C–H), 4.19 (aliphatic C–H), 2.58 (aliphatic C–H), 1.94 (aliphatic C–H), 1.58–1.28 (aliphatic C–H), 0.94 (aliphatic C–H), 0.88 (aliphatic C–H).

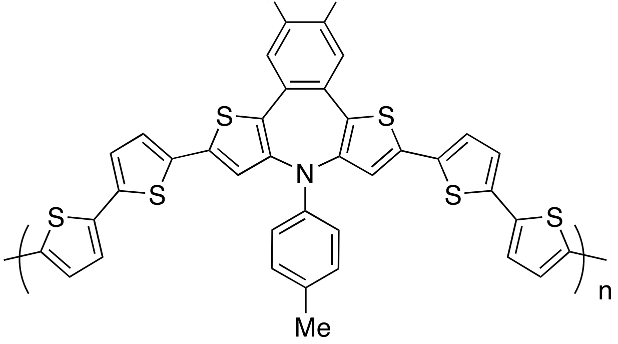

Poly(8). FeCl3 (0.049 g, 0.3 mmol) was added to the $CHCl_3$ (1 mL) solution of compound **8** (0.022 g, 0.03 mmol) and the mixture was allowed to stir at room temperature for 15 h, at which time aqueous NH_4OH was added. The mixture was sonicated for 10 min, and added dropwise to methanol. The precipitates were filtered and suspended in small amount of $CHCl_3$. The mixture was then sonicated again for 10 min, and precipitated out in methanol. The product was filtered and dried under air. Yield: 0.009 g (41%) of dark red solid.

References and Notes

(1) *Metal-Catalyzed Cross-Coupling Reactions,* 2nd ed.; Diederich, F., de Meijer, A., Eds.; Wiley-VCH: Weinheim, 2004.

(2) (a) Guram, A. S.; Rennels, R. A.; Buchwald, S. L. *Angew. Chem. Int. Ed.* **1995,** *34,* 1348–1350. (b) Driver, M. S.; Hartwig, J. F. *Tetrahedron Lett.* **1995,** *36,* 3609–3612.

(3) For the amination of heteroacryl halides: (a) Hooper, M. W.; Utsunomiya, M.; Hartwig, J. F. *J. Org. Chem.* **2003,** *68,* 2861–2873. (b) Hooper, M. W.; Hartwig, J. F. *Organometallics* **2003,** *22,* 3394–3403. (c) Charles, M. D.; Schultz, P.; Buchwald, S. L. *Org. Lett.* **2005,** *7,* 3965–3968.

(4) (a) Nozaki, K.; Takahashi, K.; Nakano, K.; Hiyama, T.; Tang, H. –Z.; Fujiki, M.; Yamaguchi, S.; Tameo, K. *Angew. Chem. Int. Ed.* **2003,** *42,* 2051–2053. (b) Ogawa, K.; Rasmussen, S. C. *J. Org. Chem.* **2003,** *68,* 2921–2928. (c) Koeckelberghs, G.; De Cremer, L.; Vanormelingen, W.; Dehaen, W.; Verbiest, T.; Persoons, A.; Samyn, C. *Tetrahedron* **2005,** *61,* 687–691.

(5) (a) Wolfe, J. P.; Buchwald, S. L. *J. Org. Chem.* **2000,** *65,* 1144–1157. (b) Shekhar, S.; Ryberg, P.; Hartwig, J. F.; Mathew, J. S.; Blackmond, D. G.; Strieter, E. R.; Buchwald, S. L. *J. Am. Chem. Soc.* **2006,** *128,* 3584–3591.

(6) Tova, J. D.; Swager, T. M. *Adv. Mater.* **2001**, *13*, 1775–1780.

(7) Song, C.; Swager, T. M. *Macromolecules*, **2005**, *38*, 4569–4575, and references therein.

(8) Yu, H. -h.; Xu, B.; Swager, T. M. *J. Am. Chem. Soc.* **2003,** *125,* 1142–1143.

(9) Sugiyasu, K.; Song, C.; Swager, T. M. *Macromolecules*, **2006**, *39*, 5598–5600.

(10) Zhu, S. S.; Swager, T. M. *J. Am. Chem. Soc.* **1997,** *119,* 12568–12577.

(11) Kilbinger, A. F. M.; Feast, W. J. *J. Mater. Chem.* **2000,** *10,* 1777–1784.

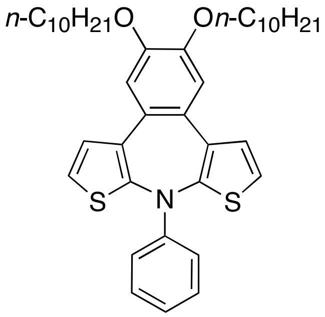
n-C10H21O
On-C10H21
S
N
S

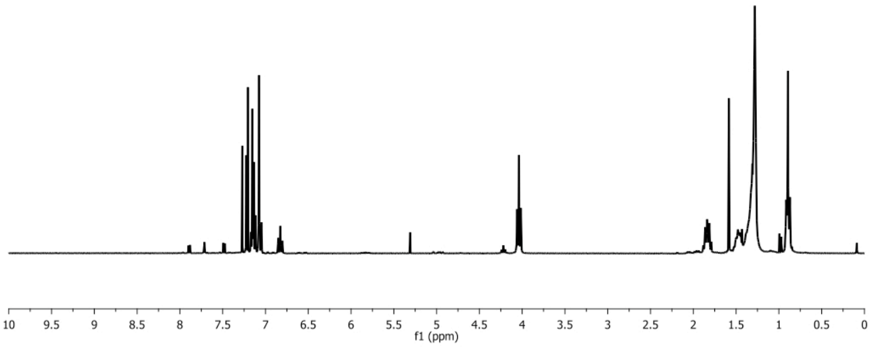

Spectrum 1. ^{1}H-NMR spectrum of **2** (300 MHz, CDCl$_3$).

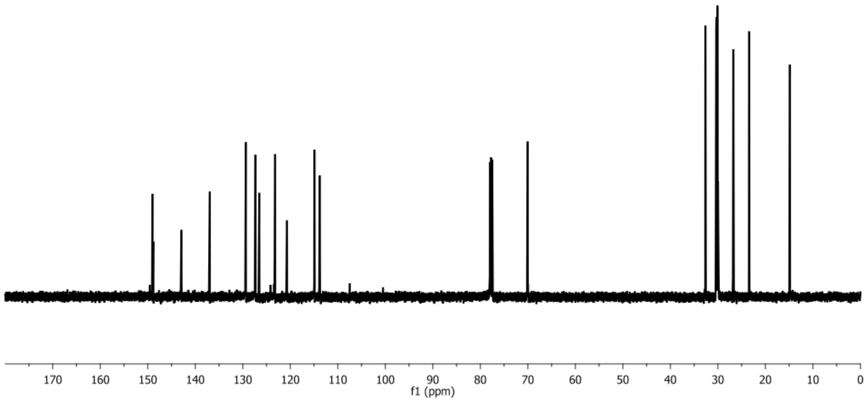

Spectrum 2. ^{13}C-NMR spectrum of **2** (125 MHz, CDCl$_3$).

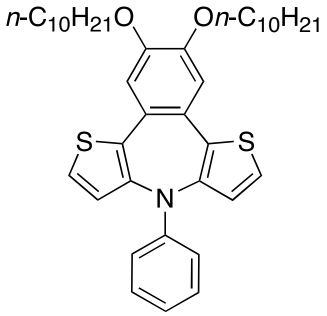
n-C10H21O
On-C10H21
S
S
N

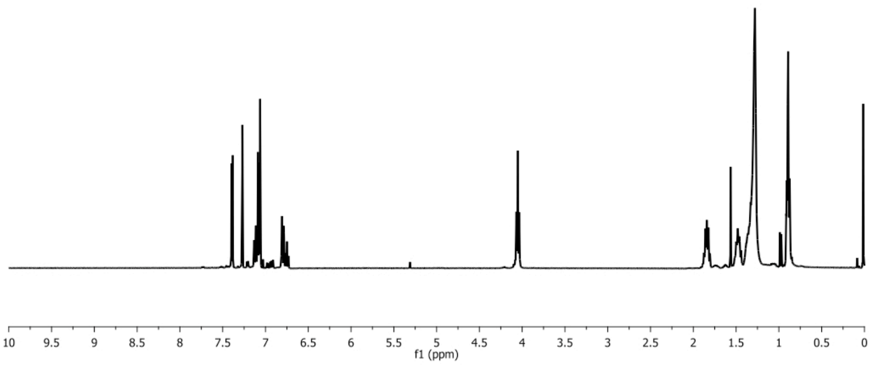

Spectrum 3. ^{1}H-NMR spectrum of **4a** (400 MHz, $CDCl_3$).

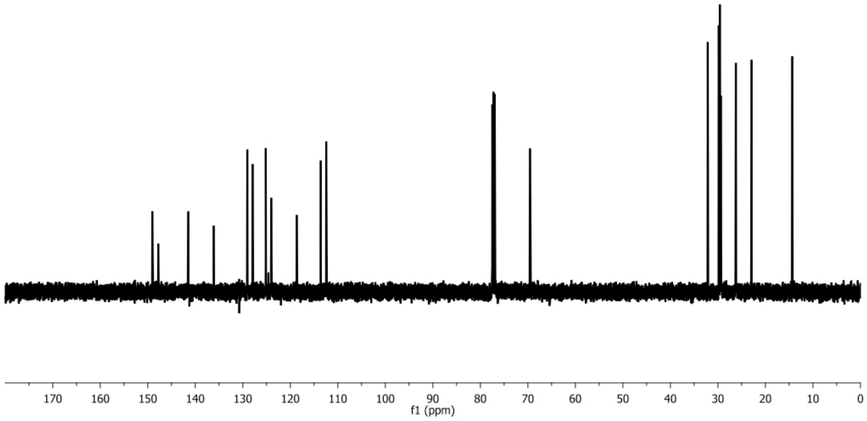

Spectrum 4. ^{13}C-NMR spectrum of **4a** (125 MHz, $CDCl_3$).

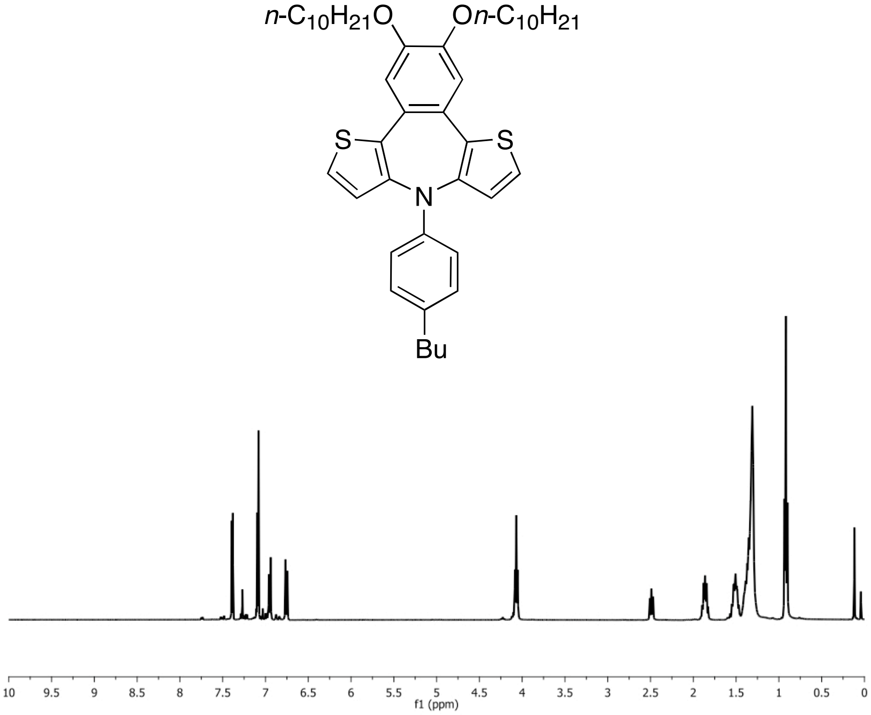

Spectrum 5. ^{1}H-NMR spectrum of **4b** (400 MHz, $CDCl_3$).

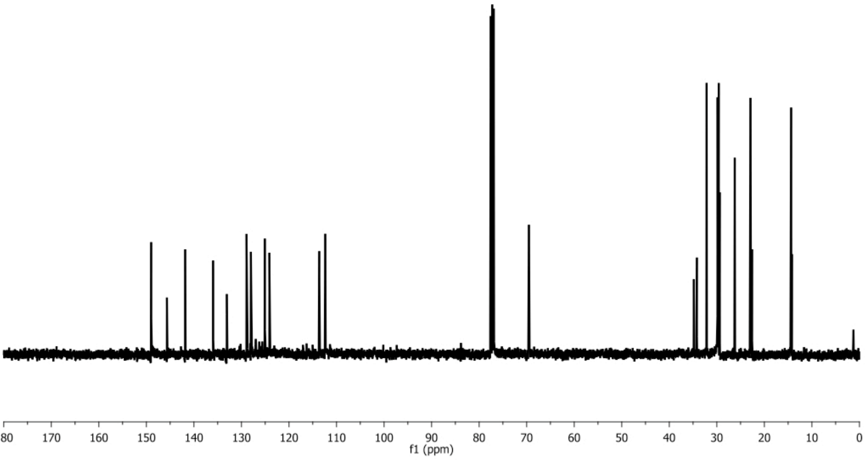

Spectrum 6. ^{13}C-NMR spectrum of **4b** (100 MHz, $CDCl_3$).

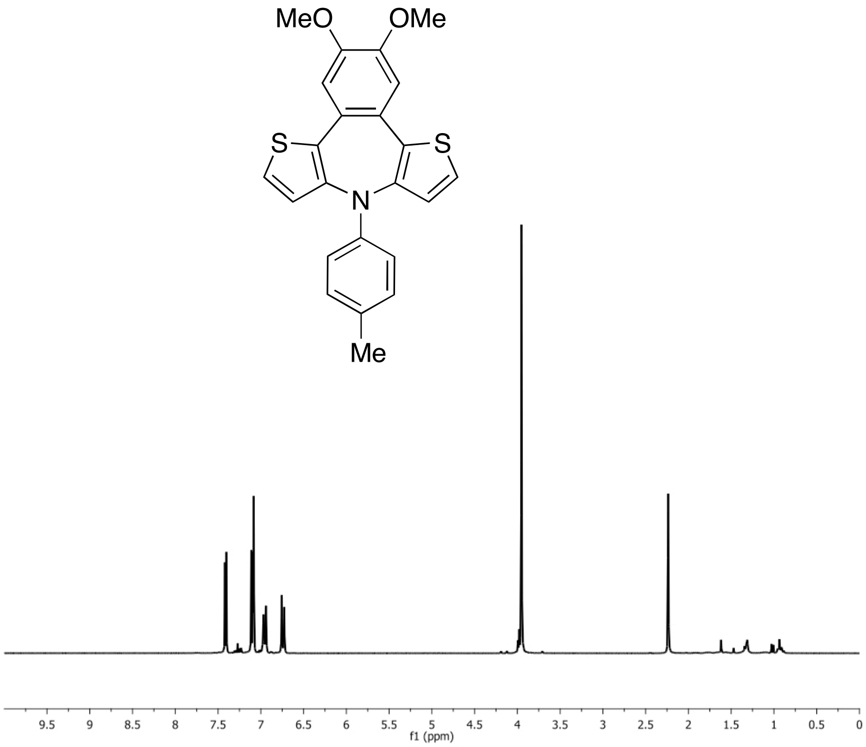

Spectrum 7. ^{1}H-NMR spectrum of **4c** (300 MHz, $CDCl_3$).

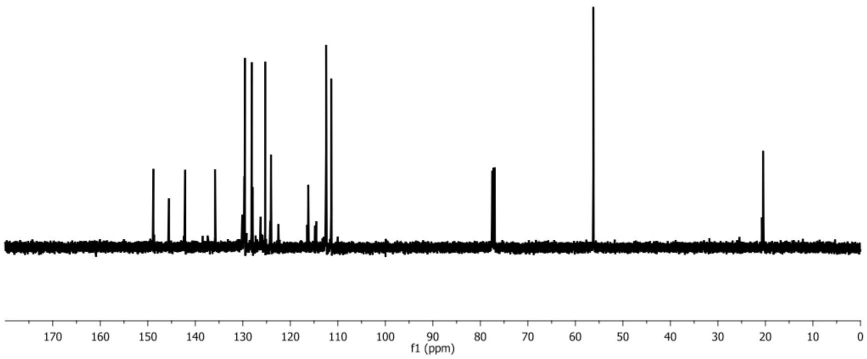

Spectrum 8. ^{13}C-NMR spectrum of **4c** (125 MHz, $CDCl_3$).

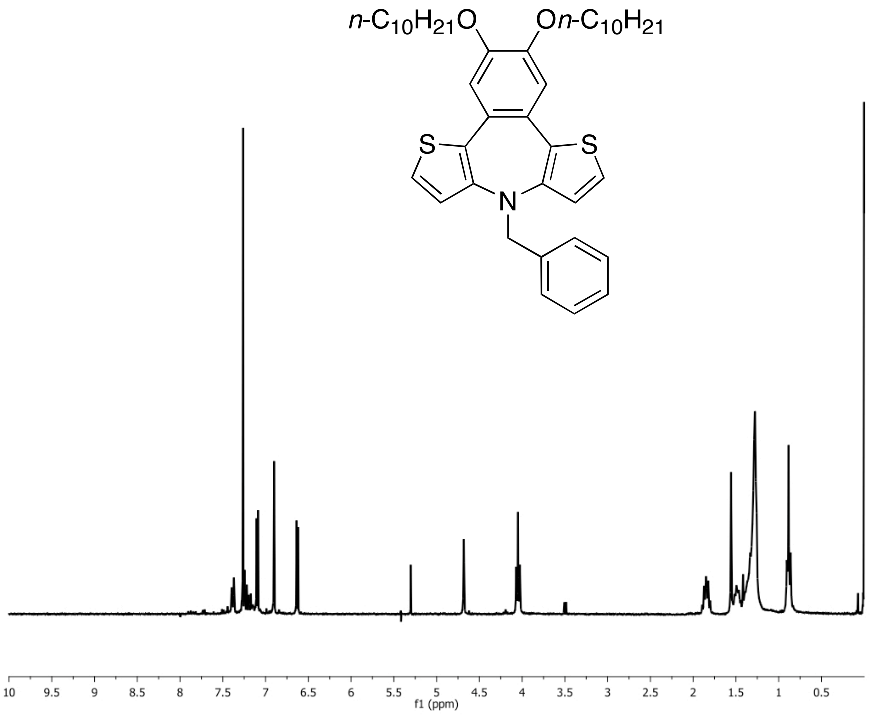

Spectrum 9. ^{1}H-NMR spectrum of **5** (300 MHz, CDCl$_3$).

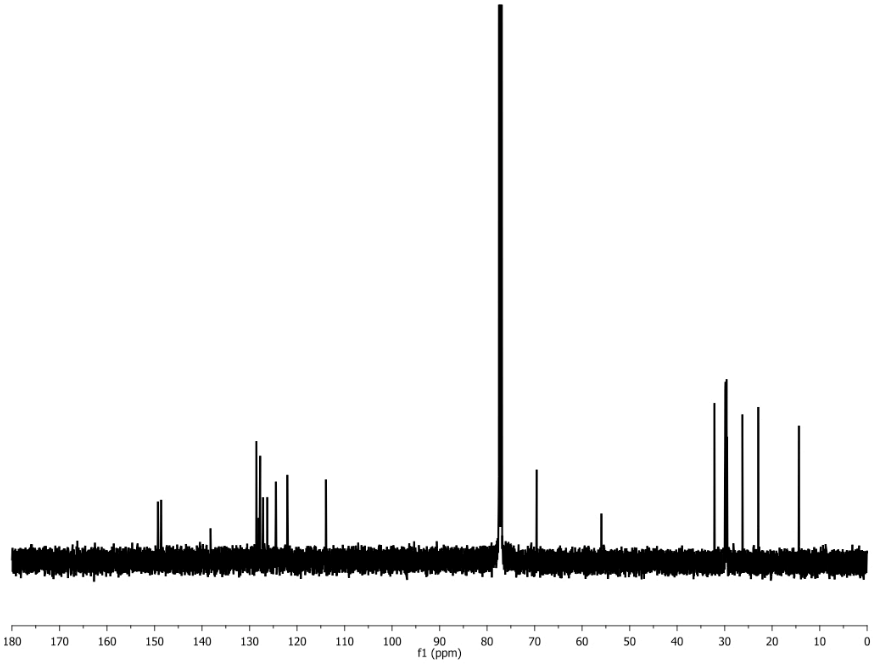

Spectrum 10. ^{13}C-NMR spectrum of **5** (125 MHz, CDCl$_3$).

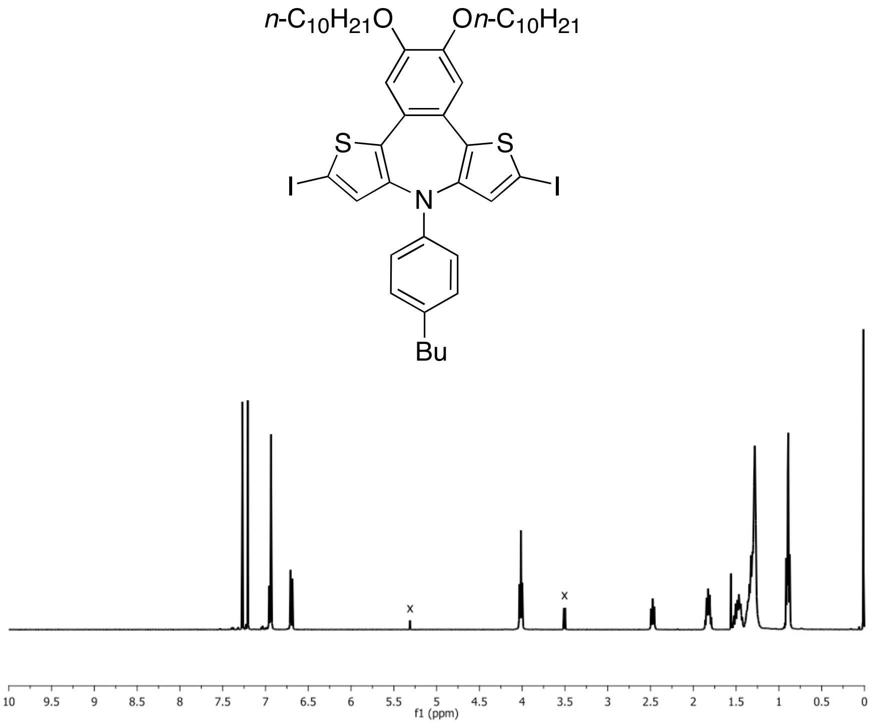

Spectrum 11. ^{1}H-NMR spectrum of **6b** (400 MHz, $CDCl_3$).

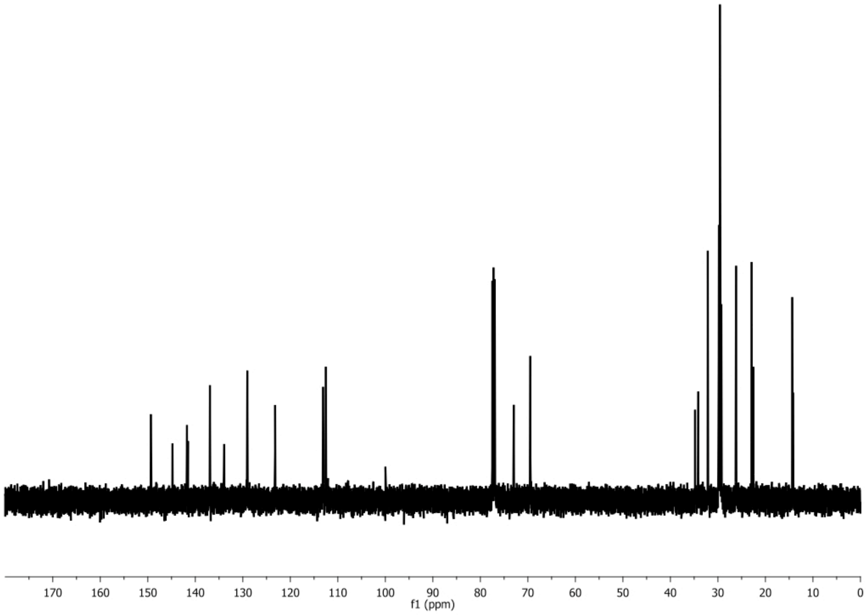

Spectrum 12. ^{13}C-NMR spectrum of **6b** (125 MHz, $CDCl_3$).

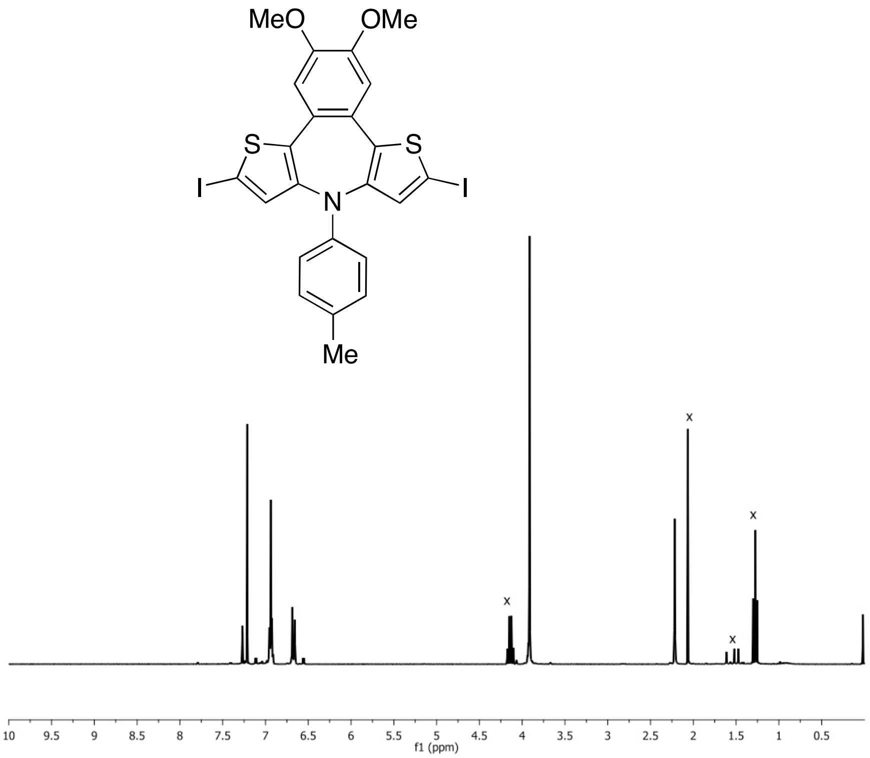

Spectrum 13. ^{1}H-NMR spectrum of **6c** (300 MHz, $CDCl_3$).

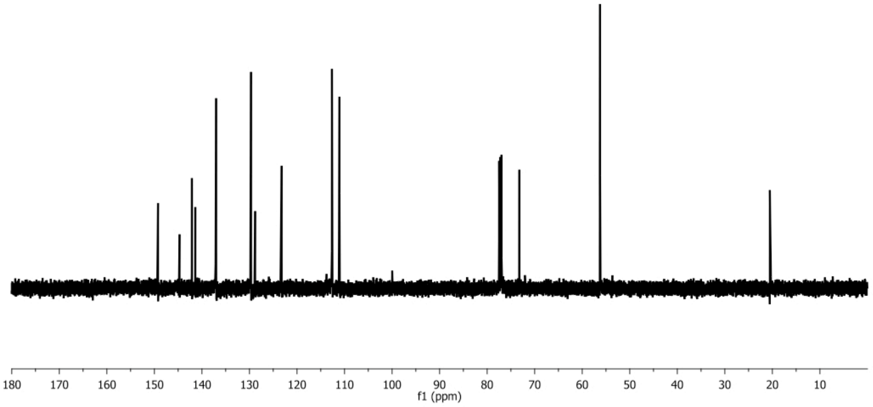

Spectrum 14. ^{13}C-NMR spectrum of **6c** (125 MHz, $CDCl_3$).

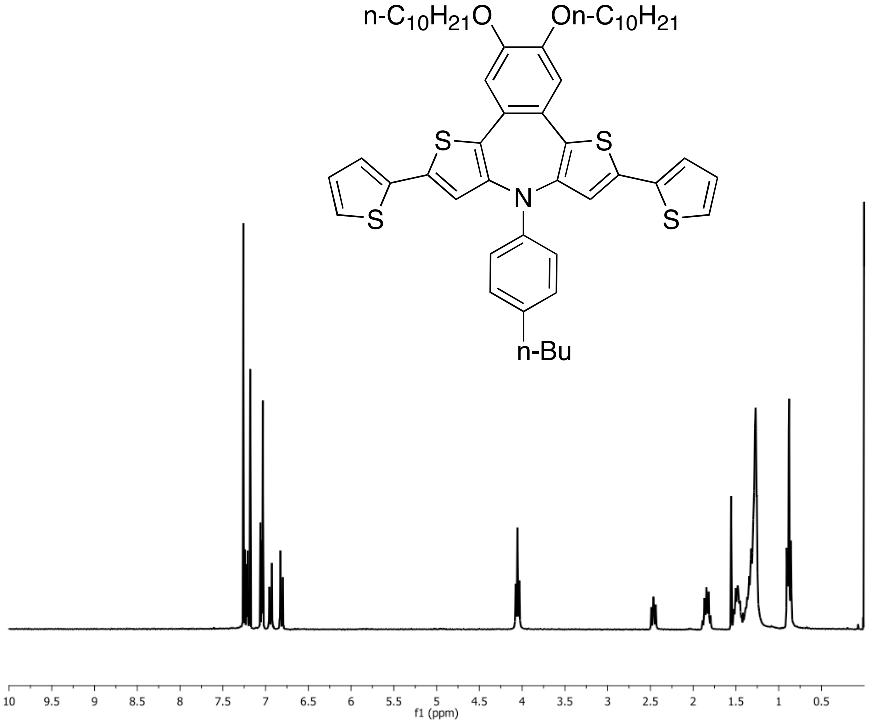

Spectrum 15. ^{1}H-NMR spectrum of **7** (300 MHz, $CDCl_3$).

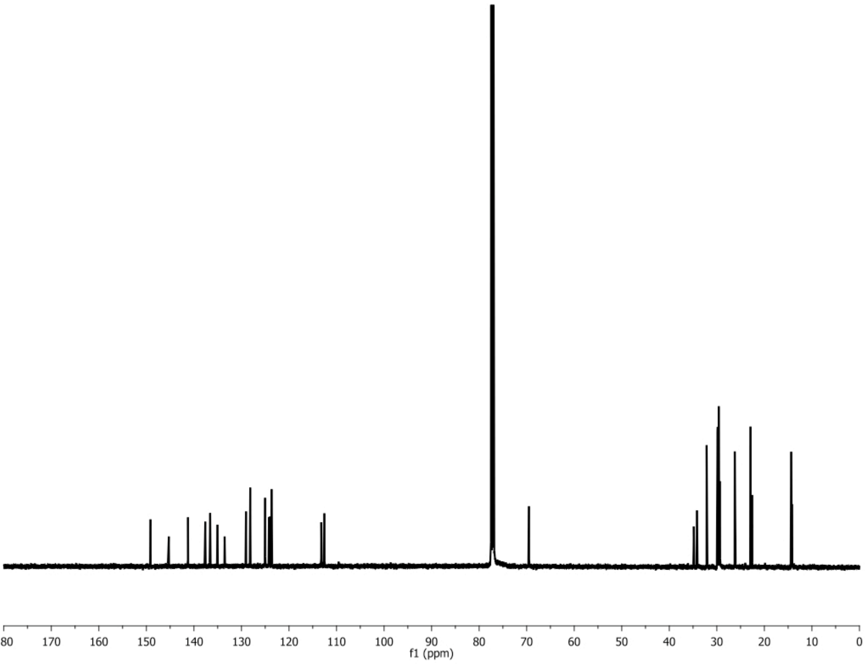

Spectrum 16. ^{13}C-NMR spectrum of **7** (125 MHz, $CDCl_3$).

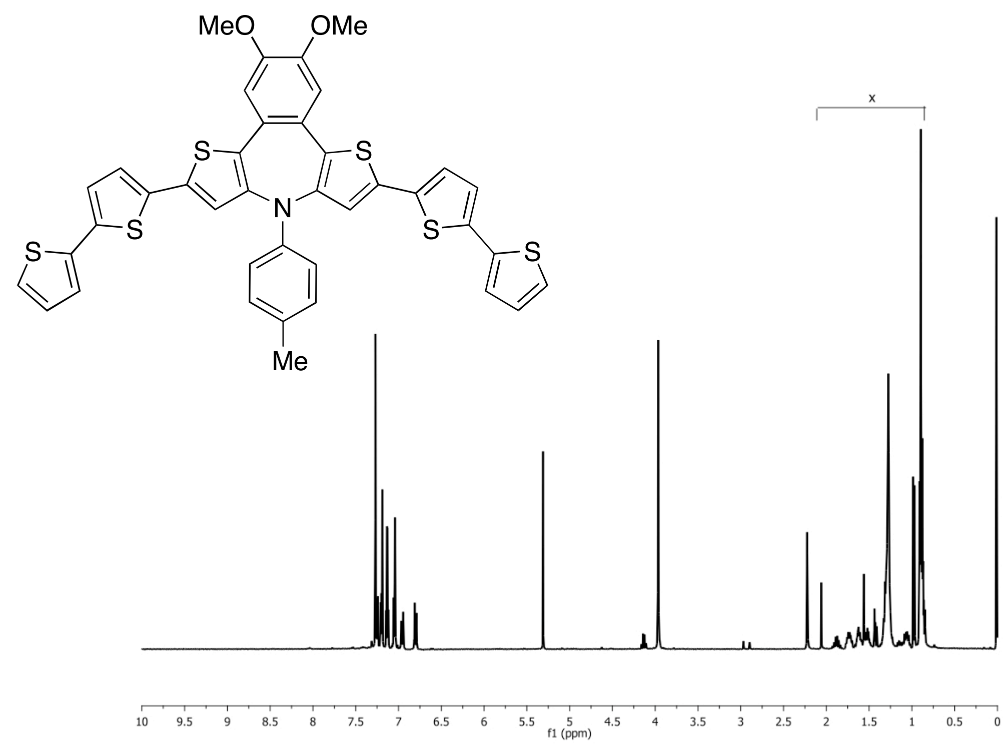

Spectrum 17. ^{1}H-NMR spectrum of **8** (400 MHz, $CDCl_3$).

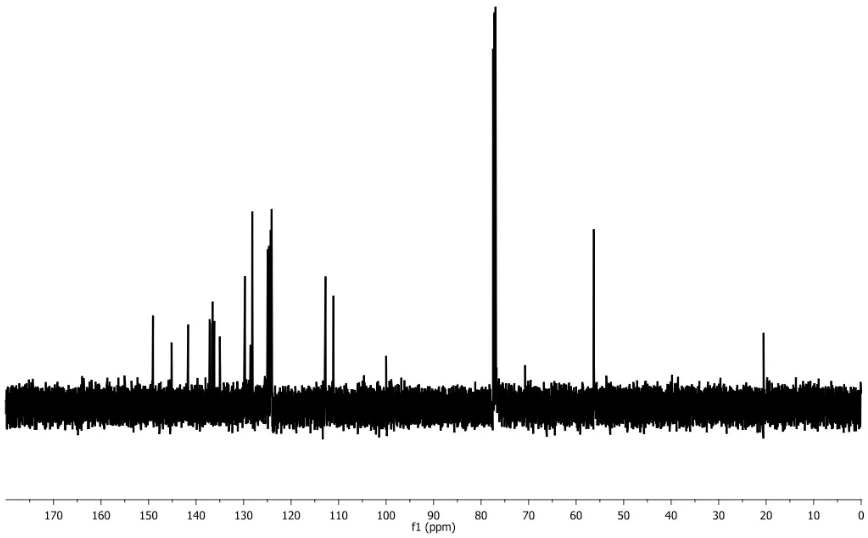

Spectrum 18. ^{13}C-NMR spectrum of **8** (125 MHz, $CDCl_3$).

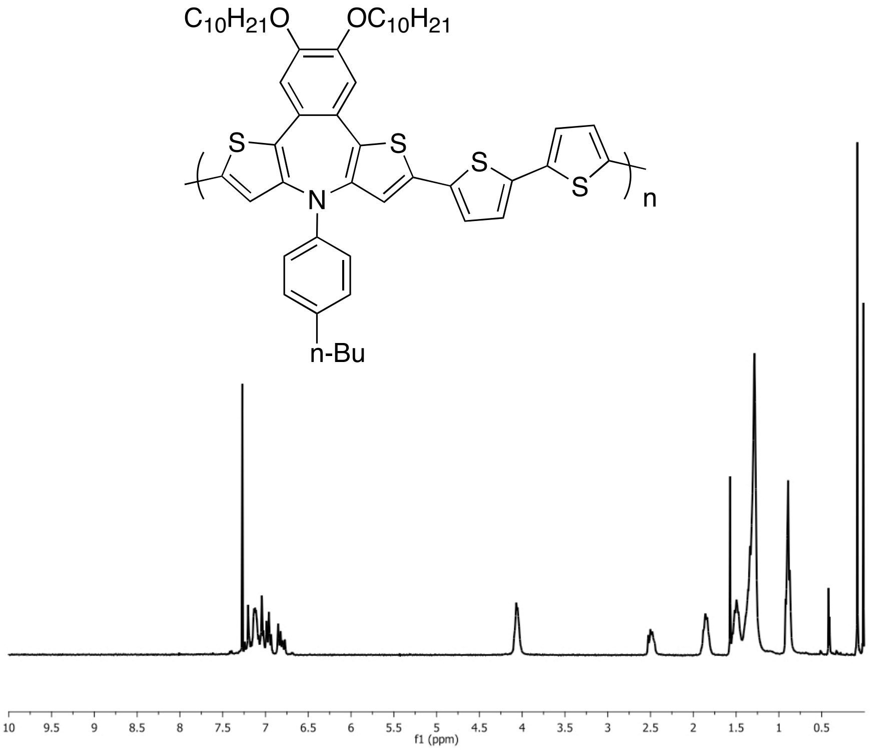

Spectrum 19. ^{1}H-NMR spectrum of **10** (400 MHz, $CDCl_3$).

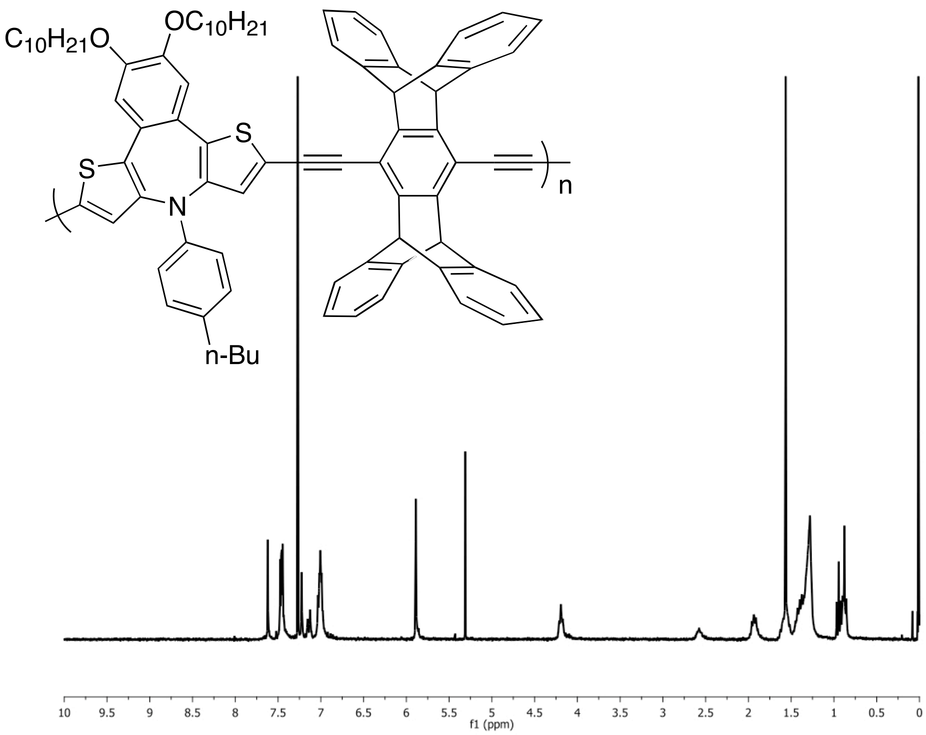

Spectrum 20. ^{1}H-NMR spectrum of **12** (400 MHz, $CDCl_3$).

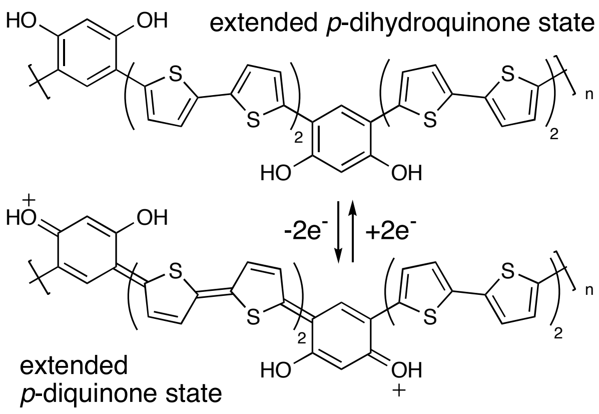
extended *p*-dihydroquinone state
-2e⁻
+2e⁻
extended
p-diquinone state

PMPT-OH

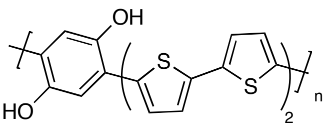

PPPT-OH

Chapter 7

Highly Conductive Poly(phenylene thienylene)s:

m-Phenylene Linkages Are Not Always Bad

Portions of this chapter have been published in

Song, C.; Swager T. M. *Macromolecules* **2005,** *38,* 4569-4576.

Introduction

The demand for highly stable, highly conductive, and easily processable conjugated polymers in organic electronic and optoelectronic applications has led to extensive studies over the past two decades.[1] Major advances have been realized through novel design or synthetic modifications of conjugated polymers. For example, soluble and thus processable polythiophenes have been achieved by incorporating flexible subtsituents such as alkyl chains at 3-position.[2-4] Polythiophenes also have been electronically tuned by aid of electron-donating and/or electron-withdrawing substituents.[4,5] Another approach is to modify the backbones by hybridizing thienylenes with other conjugated molecules, such as various types of phenylenes.[6,7] However, in the design of new highly electron/hole conductive polymers, *meta*-linkages between conducting segments are generally excluded because they interrupt conjugation. In fact, *meta*-linkages have usually been introduced in order to reduce conjugation in a tunable manner, for example, in synthesizing polymers with blue emission.[8] It appears to be widely accepted that *meta*-linkages in polymers are something to be avoided if one wishes to produce systems with high conductivity that is generally associated with delocalized carriers.

Our group recently reported a calix[4]arene-based conducting polymer,[9] which is not fully conjugated but instead contains electroactive segments between insulating bridges. In such a system, phenol groups were found to play a crucial role in the electropolymerization and the conduction pathway. The polymer also demonstrated an intriguing proton-dopable property, in which the segments were proposed to fluctuate between *p*-dihydroquinone-like and *p*-diquinone-like states (similar to what is shown for the materials of interest here in Scheme 1). Considering those features, phenol functionalities could be useful for designing conducting polymer sensors.

Scheme 1.

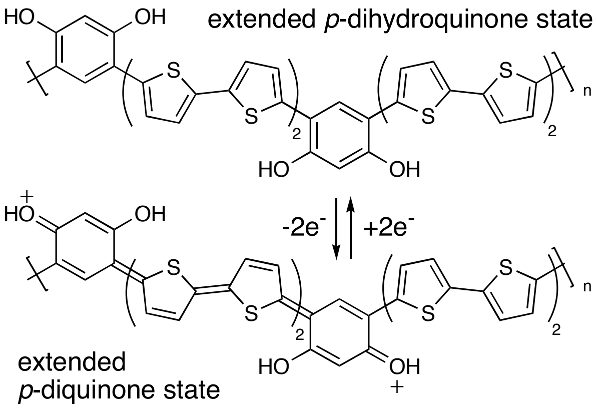

PMPT-OH

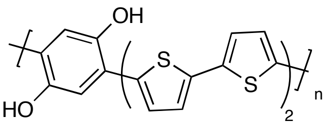

PPPT-OH

Our present study was motivated to investigate the potential of phenols as functional moieties in non-segmented (i.e. those have a continous interconneted π-system) conducting polymers. We proposed that, when strategically located, phenols would endow a non-conjugated *meta*-linked polymer with electroactive and conductive properties that are similar to, or even better than, those of a related *para*-isomer. In this study, two isomeric phenol containing polymers were prepared: poly(*m*-phenylene tetrathienylene)s (**PMPT**s) and poly(*p*-phenylene tetrathienylene)s (**PPPT**s) (Scheme 1). In **PMPT**s, when they are oxidized, it is plausible that the charges are localized on the phenolic oxygens. Upon oxidation, the initially non-conjugated backbone becomes highly delocalized with both aromatic and quinoid structures in the same chain, a scheme that has been utilized in the design of small band-gap polymers.[10] In this work, a series of **PMPT**s and **PPPT**s were synthesized and characterized by several electrochemical methods. The in-situ conductivities of two isomeric polymers were compared by using interdigitated microelectrodes[11] and their electronic transitions were also compared by UV-Vis spectroelecrochemistry.

Monomer Synthesis

The syntheses of the monomers are outlined in Scheme 2. Attempts to synthesize the *meta*-linked monomer **2a** by Stille-coupling between 4,6-diiodoresorcinol and 5-tri-*n*-butylstannyl-2,2'-bithiophene failed. Subsequently, the phenol groups were protected with acetyl or TBDMS groups. Although protected monomers **2b-c** could be obtained by Stille-coupling in good to high yields, deprotection to **2a** was complicated by its instability to air, giving black intractable products. Therefore, removal of the protecting group was carried out in post-polymerization modification. For comparison, an *O*-alkyl version **2d**, a non-substituted version **3**, and *para*-linked isomers **4b-c** were synthesized under similar conditions.

Scheme 2.[a]

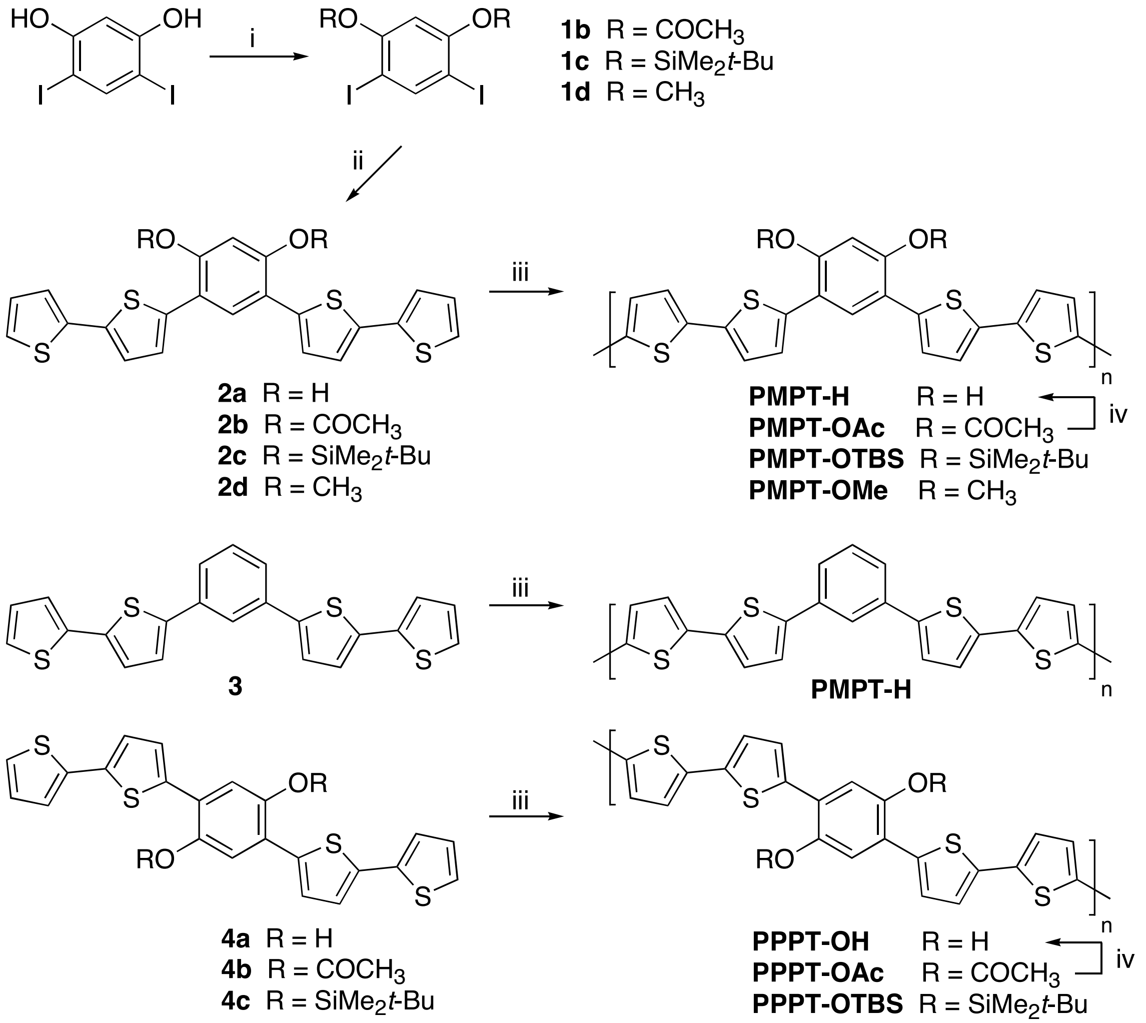
HO
OH
I
I
i
RO
OR
I
I
1b R = $COCH_3$
1c R = $SiMe_2t$-Bu
1d R = CH_3
ii
S
2a R = H
2b R = $COCH_3$
2c R = $SiMe_2t$-Bu
2d R = CH_3
iii
n
PMPT-H R = H
PMPT-OAc R = $COCH_3$
PMPT-OTBS R = $SiMe_2t$-Bu
PMPT-OMe R = CH_3
iv
3
PMPT-H
4a R = H
4b R = $COCH_3$
4c R = $SiMe_2t$-Bu
PPPT-OH R = H
PPPT-OAc R = $COCH_3$
PPPT-OTBS R = $SiMe_2t$-Bu

[a]Reagents: (i) Acetic anhydride, pyridine, RT. (**1b**); TBDMSCl, imidazole, DMF, RT. (**1c**); MeI, K_2CO_3, DMF, RT. (**1d**) (ii) 5-Tri-*n*-butylstannyl-2,2'-bithiophene, Pd cat., toluene or DMF, 80 °C or RT. (iii) Electropolymerization under swept potential conditions in CH_2Cl_2 containing *ca* 2 mM of monomers and 0.1 M $TBAPF_6$ as a supporting electrolyte. (iv) Hydrazine, RT.

Electropolymerization.[15]

All monomers were polymerized via oxidative coupling under swept potential conditions. Electropolymerizations were performed in CH_2Cl_2 solutions containing *ca* 2 mM of monomers and 0.1 M of $TBAPF_6$ as a supporting electrolyte. In most cases, CH_2Cl_2 proved to be a good solvent for electropolymerization. However, when monomers were too soluble in CH_2Cl_2 (**2c** or

4c), or when the working electrode had a large surface area (ITO coated glass electrode or gold coated PETE), a significant amount of the resulting polymer failed to be deposited onto the electrode. This could be attributed to the solubility of initially coupled oligomers. This effect was especially evident when *O*-TBDMS versions (**2c** or **4c**) were polymerized in CH_2Cl_2. It was observed that oxidized oligomers diffused away from the electrode surface. This problem was overcome by adding CH_3CN, a poor solvent. Depending on the solubility of each monomer, a 1:1 to 1:3 mixture of CH_2Cl_2:CH_3CN was used for electropolymerizations.

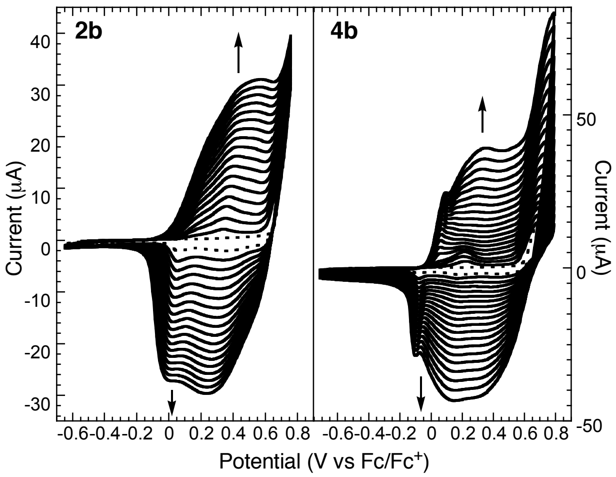

Figure 1. Electropolymerization (100 mV/s) of **2b** (left) and **4b** (right) on Pt button electrodes in CH_2Cl_2 with 0.1 M $TBAPF_6$ as a supporting electrolyte. Dotted lines represent the first scan

Figure 1 shows the cyclic voltammograms (CVs) during the polymerization of **2b** and **4b**. The initial oxidation of monomer **2b** occurred at a potential slightly higher than **4b** reflecting the non-conjugated nature of the *meta*-linkage. For both materials, all subsequent scans displayed much lower potential oxidation onsets, thereby indicating that electroactive polymer had deposited onto the electrode. The oxidation peak potential of poly(**2b**) (**PMPT-OAc**) and poly(**4b**) (**PPPT-OAc**) were minimally different. Table 1 summarizes the electrochemical results for monomers (**2b-d**, **3**, **4b-c**) and their polymers. As expected, the electron-donating effect of methoxy groups results in a lower oxidation potential for monomer **2d**. The *O*-TBDMS versions **2c** and **4c** also oxidized at low potentials for the same reason.

Table 1. Electrochemical Results. Monomer Oxidation Potentials ($E_{a,m}$) and Polymer Oxidation / Reduction Potentials ($E_{a,p}$ / $E_{c,p}$).

monomer	$E_{a,m}$ (V)[a]	$E_{a,p}$ (V)	$E_{c,p}$ (V)
2b[b]	>0.8	0.41, 0.68	0.05, 0.33
2c[c]	0.57	0.12, >1.0	0.14
2d[d]	0.47	0.37, 0.61	0.01, 0.41
3[b]	0.81	>1.0	-0.10
4b[b]	0.69	0.20, 0.36, 0.72	-0.18, 0.18
4c[c]	0.48	0.74	0.41

[a] All Potentials measured vs Fc/Fc$^+$ at scan rate 100 mV/s. [b] Performed in CH_2Cl_2. [c] Performed in a mixed solvent of CH_2Cl_2 and CH_3CN. [d] Performed in CH_3CN.

Deprotection to Give Free –OH Groups

PMPT-OAc and **PPPT-OAc** were chosen to generate free –OH versions, **PMPT-OH** and **PPPT-OH**, respectively, because the acetyl groups can be easily removed by addition of hydrazine. As-grown polymer films on several types of electrodes were exposed to hydrazine vapor, under which the films immediately became crimson in color. After *ca* 15 min, the films were washed with copious amounts of MeOH, then with CH_2Cl_2. Figures 2 and 3 show the FT-IR and UV-Vis spectra, respectively, of films before and after exposure to hydrazine. It is clearly observed that the strong C=O vibration disappeared after exposure to hydrazine. The weaker than expected C-H and O-H stretching vibrations in spectra C and D in Figure 2 are a result of the thin nature of the films grown from **PPPT-OAc** and **PPPT-OH**, which results in broad and weak signals. The hydrazine reaction did not significantly affect the UV-Vis absorption (Figure 3), hence we conclude the acetyl groups were successfully removed to leave free –OH without degradation of the polymer structure.

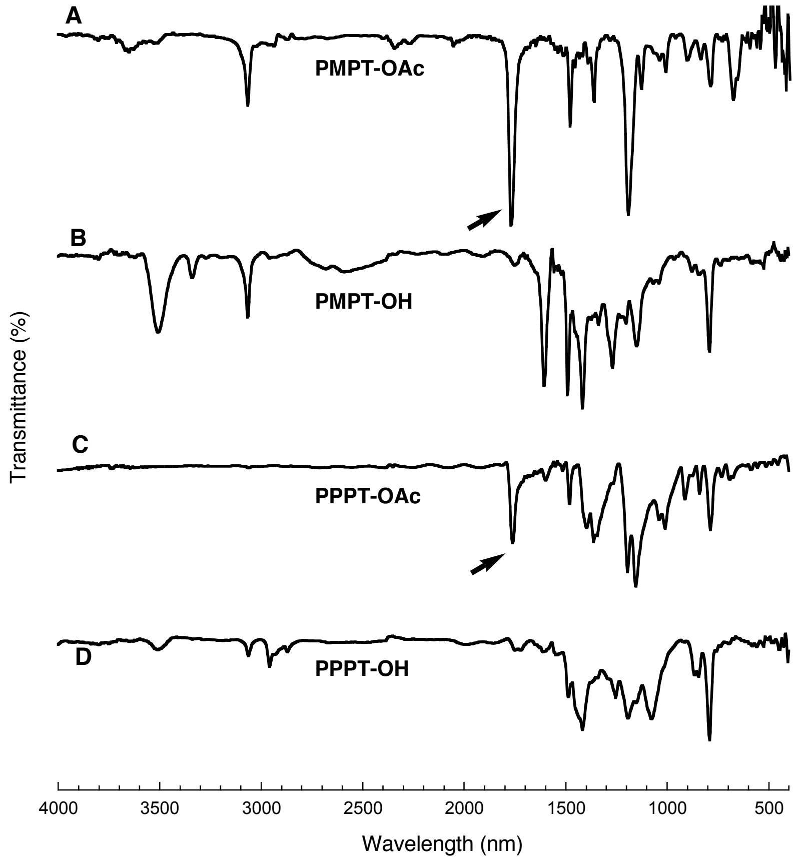

Figure 2. Specular reflectance FT-IR spectra of **PMPT-OH** (B) and **PPPT-OH** (D). The strong C=O stretchings (arrows) of **PMPT-OAc** (A) and **PPPT-OAc** (C) disappeared when exposed to hydrazine. The spectra were measured from films deposited onto gold-coated PETE.

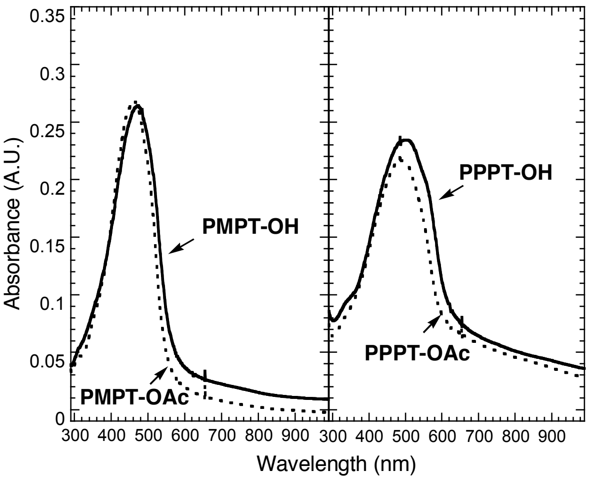

Figure 3. UV-Vis spectra of **PMPT-OH** (left; solid line) and **PPPT-OH** (right; solid line). Dotted lines represent UV-Vis absorption of **PMPT-OAc** (left) and **PPPT-OAc** (right). The spectra were measured from films deposited onto ITO-coated glass.

Polymer Electrochemistry Comparisons of *meta* vesus *para*

Figure 4 compares the CVs of the **PMPT**s and the **PPPT**s. We observed two broad, poorly resolved oxidation and reduction peaks in both **PMPT-OAc** and **PPPT-OAc** and their CVs were quite similar with the exception of the first oxidation peak. Interestingly for **PPPT-OAc**, we observed a well-resolved low-potential redox couple, similar to those reported for polythiophenes with long alkoxy substituents.[5,6] We also observed that this redox couple was more pronounced at low scan rates and thin films. This is most evident for the reduction cycle of **PPPT-OAc**, which suggests that it is more sensitive to ion diffusion or that a structural relaxation has occurred in the oxidized state. However, after the first oxidation, the electrochemistry of both *O*-Ac polymers became similar, which suggests that the lone pairs of the acetoxy groups in **PMPT-OAc** are capable of contributing to the delocalization suggested in Scheme 1.

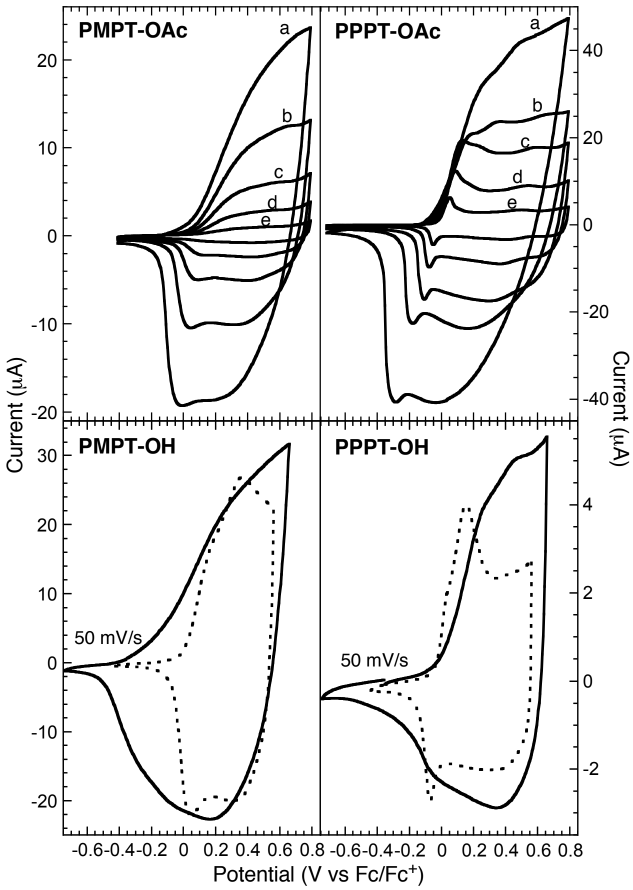

Figure 4. (Top) The CVs of **PMPT-OAc** (left) and **PPPT-OAc** (right) at different scan rates: (a) 200 mV/s, (b) 100 mV/s, (c) 50 mV/s, (d) 25 mV/s, (e) 10 mV/s. (Bottom) The CVs of **PMPT-OH** (left) and **PPPT-OH** (right). Dotted line represents the CV before exposure to hydrazine. All measurements were carried out in CH_2Cl_2 with 0.1 M $TBAPF_6$ onto Pt button electrodes.

Deprotection of the acetyl groups changed the electrochemistry of the polymers dramatically, especially for **PMPT-OAc**. For **PPPT-OH** we observed a broader electroactivity and a loss of the low-potential redox-activity shown for **PPPT-OAc**. The oxidation onset potential of **PPPT-OH** remained approximately the same as that of **PPPT-OAc**. In contrast, the oxidation onset potential of **PMPT-OH** shifted to lower potential and the polymer's CV was much broader than the acetate derivative. This latter feature is attributed to the formation of extended *p*-diquinone states that are more favored in the deprotected form because of the superior ability of the –OH group to stabilize positive charges. Although the free -OH subsituents seemed to improve the polymers' electroactivity, oxidized **PMPT-OH** and **PPPT-OH** were not stable under ambient conditions. All electrochemical measurements of those polymers were performed in a glove box under a nitrogen atmosphere.

Meta vesus *para* In-situ Conductivity Measurement

It is not surprising, considering the similarity of the CVs, that we find the conductivity of the *meta*-linked **PMPT-OAc** is of the same order of magnitude as the *para*-linked **PPPT-OAc** (Figure 5). In the potential-conductivity profile of **PMPT-OAc**, the conductivity increased rapidly from *ca* 0 V and reached a plateau above *ca* 0.3 V (vs Fc/Fc^+). The conductivity profile of **PPPT-OAc** behaved in a similar manner. This conductivity plateau results from the limit of an interchain charge hopping process.[16,17] As in the case of polythiophenes, the interchain charge transport in **PMPT**s and **PPPT**s operates due to the proximity of the polymer backbones, providing multi-channel electronic connectivity. It would appear that the *meta*-linkages do not hamper the conduction pathway in this system.

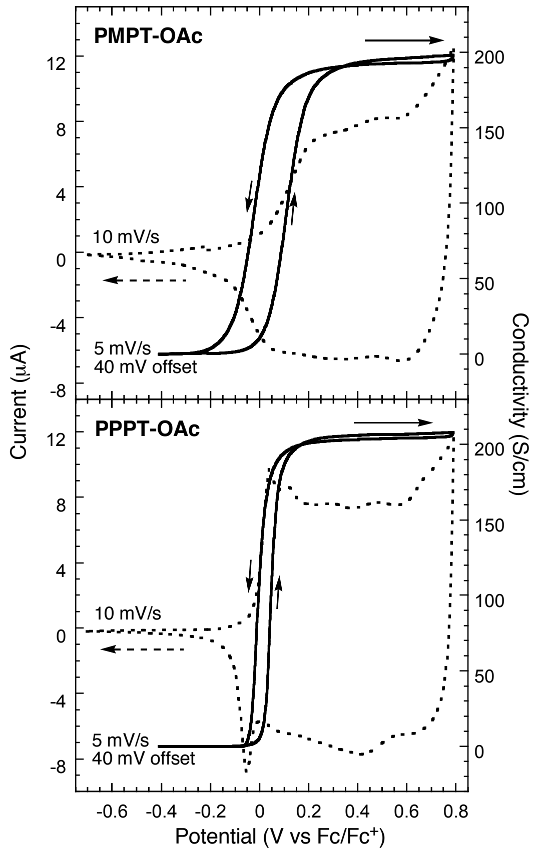

***Figure 5**.* CVs (dotted line) and in-situ conductivity measurements (5 mV/s, offset potential of 40 mV; solid line) of **PMPT-OAc** (top) and **PPPT-OAc** (bottom) on 5 μm interdigitated Pt microelectrodes in CH_2Cl_2 with 0.1 M $TBAPF_6$ as a supporting electrolyte.

The shapes of potential-conductivity profile of the -OH versions, **PMPT-OH** and **PPPT-OH**, resembled their acetate versions (Figure 6). In **PPPT-OH**, the drain current, which is proportional to conductivity, "turns on" at almost the same potential as **PPPT-OAc**. In contrast, the drain current onset is at a much lower potential for **PMPT-OH**. As mentioned above, the free -OH appears to facilitate the formation of extended *p*-diquinone states.

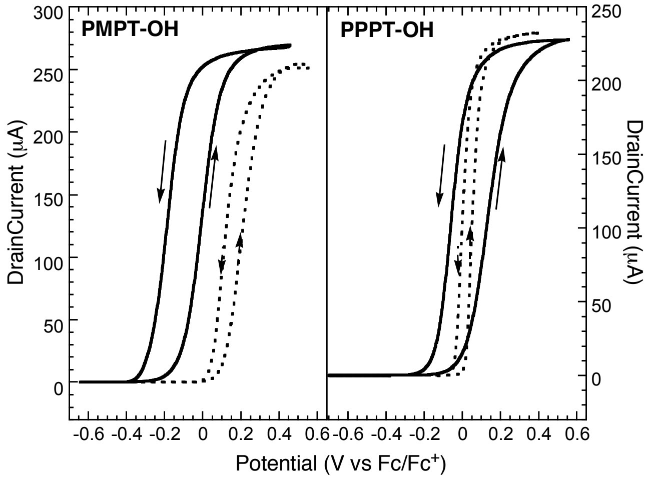

Figure 6. Drain-current profiles (5 mV/s, offset potential of 40 mV; solid line) of **PMPT-OH** and **PPPT-OH** on 5 μm interdigitated Pt microelectrodes in CH_2Cl_2 with 0.1 M $TBAPF_6$ as a supporting electrolyte. The absolute conductivity is proportional to drain current.[11] For comparison, drain-current profiles of **PMPT-OAc** (left, dotted line) and **PPPT-OAc** (right, dotted line) are also plotted.

Meta vesus *Para* Spectroelectrochemistry

UV-Vis spectroelectrochemical studies further reveal that *meta*-linkages produce delocalized electronic structures when the polymers are oxidized. Figure 7 shows in-situ measurements of the UV-Vis absorption of polymers deposited onto ITO-coated glass electrodes. Due to the instability of the oxidized **PMPT-OH** and **PPPT-OH**, only the acetate versions were measured. The UV-Vis spectra of **PPPT-OAc** show a decrease of the original band-gap transition and the buildup of intragap energy states, which appear very similar to those observed for alkoxy substituted poly(phenylene bisthienylene)s.[6] This matches well to polaron-bipolaron model[18] of charge-delocalized π-platforms. It should be noted that even in the non-conjugated **PMPT-OAc**, similar electronic states develop and more delocalized energy states build up at lower applied potentials.

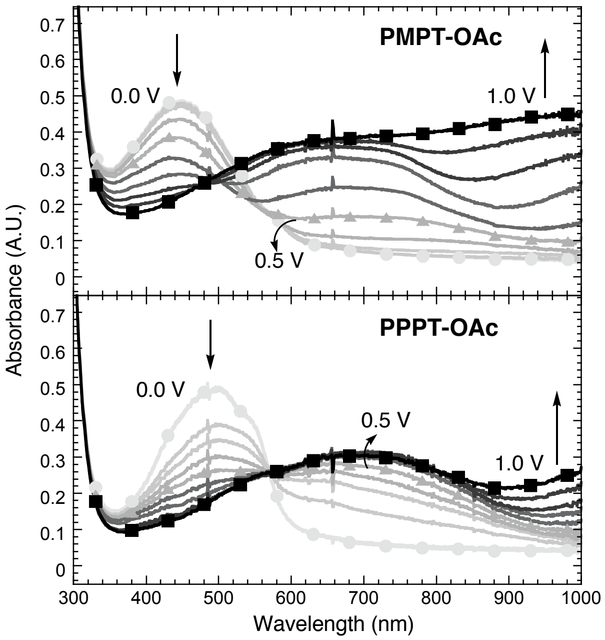

Figure 7. Electronic absorption spectra of **PMPT-OAc** (top) and **PPPT-OAc** (bottom) on ITO-coated glass electrodes in CH_2Cl_2 with 0.1 M $TBAPF_6$ as a supporting electrolyte. The UV-Vis spectra are plotted as a function of oxidation potential from 0.0 V (●) to 1.0 V (■) vs Ag / Ag^+ (0.01 M).

Substituent Effects in PMPTs

To further investigate the electronic properties of these systems, an alkoxy-substituted derivative, **PMPT-OMe**, and a non-substituted derivative, **PMPT-H**, were studied for comparison (Figure 8). As the scan rate increased, the peak potentials of **PMPT-OMe** shifted minimally as shown in Figure 8 (left), while a significant shift of anodic and cathodic peak potentials was observed in **PMPT-H**. We observed two oxidation and reduction peaks in the CV of **PMPT-OMe** similar to that discussed for **PMPT-OAc** (Figure 4). The oxidation in **PMPT-H** occurred at a higher potential than **PMPT-OMe** due to the absence of charge-stabilizing substituents, and peak potentials shifted significantly at fast scan rates. At higher potentials (> 1.0 V vs Fc/Fc^+), **PMPT-H** was unstable and hence we were unable to show a peak in the CV.

When **PMPT-OMe** and **PMPT-H** are compared to **PMPT-OH**, it is apparent that phenol functionalities enhance the electroactivity of the polymer.

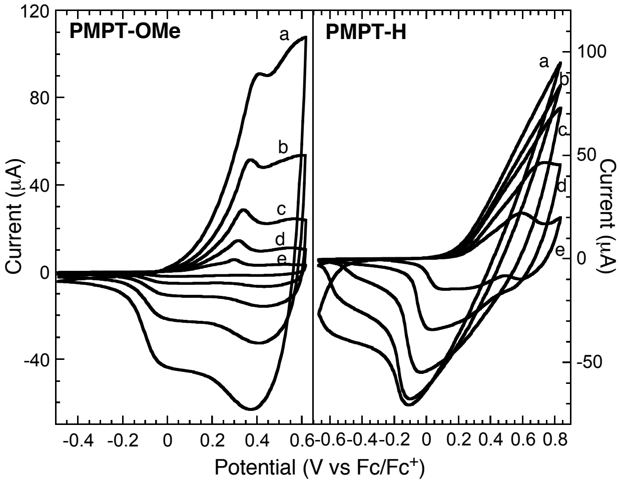

Figure 8. The CVs of **PMPT-OMe** (left) and **PMPT-H** (right) in CH_3CN and CH_2Cl_2, respectively, with 0.1 M $TBAPF_6$ as a supporting electrolyte at different scan rates: (a) 200 mV/s, (b) 100 mV/s, (c) 50 mV/s, (d) 25 mV/s, (e) 10 mV/s.

Figure 9 shows the in-situ conductivity measurements of the **PMPT-OMe** and the **PMPT-H**. The conductivity-potential profile of **PMPT-OMe** resembles that of **PMPT-OAc** and appears to be limited by the interchain charge hopping. However, in **PMPT-H**, the onset is shifted to the significantly higher potential and the conductivity-potential profile passes a peak at *ca* 0.55 V and then increases again, finally reaching a plateau at above 0.8 V (vs Fc/Fc^+). Although there might be a different regime at low potential, or at a low doping level, we suspect that the conductivity of **PMPT-H** is also governed by the interchain charge hopping at a high doping level. The maximum conductivity of **PMPT-OMe** and **PMPT-OAc** were consistently determined to be approximately two-fold greater than that of **PMPT-H**.

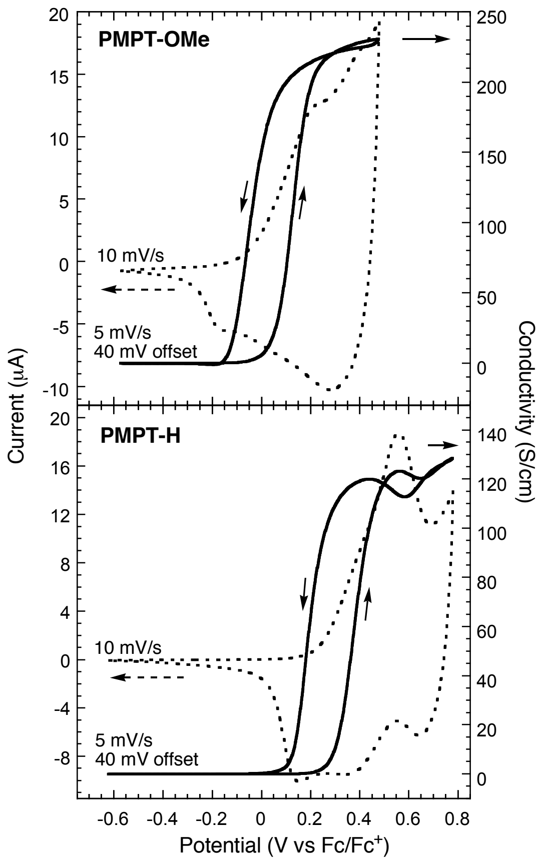

Figure 9. CVs (dotted line) and in-situ conductivity measurements (5 mV/s, offset potential of 40 mV; solid line) of **PMPT-OMe** (top) and **PMPT-H** (bottom) on 5 μm interdigitated Pt microelectrodes in CH_2Cl_2 with 0.1 M $TBAPF_6$ as a supporting electrolyte.

Spectroelectrochemical studies (Figure 10) reveal approximately the same buildup of energy states as the doping level increases. The UV-Vis absorption spectra of **PMPT-OMe** and **PMPT-OAc** are similar at the similar oxidation level. Here again, we observed the stabilizing effect of alkoxy functionalities on positively doped states. In **PMPT-H**, a similar but retarded development of intergap transitions was observed. In addition, the shape of intergap transitions of **PMPT-H** was different from that of **PMPT-OMe** or **PMPT-OAc** (Figure 7, top). We suspect that without the alkoxy or phenolic substituents, delocalized energy states would not be observed in **PMPT**s at a moderate doping level.

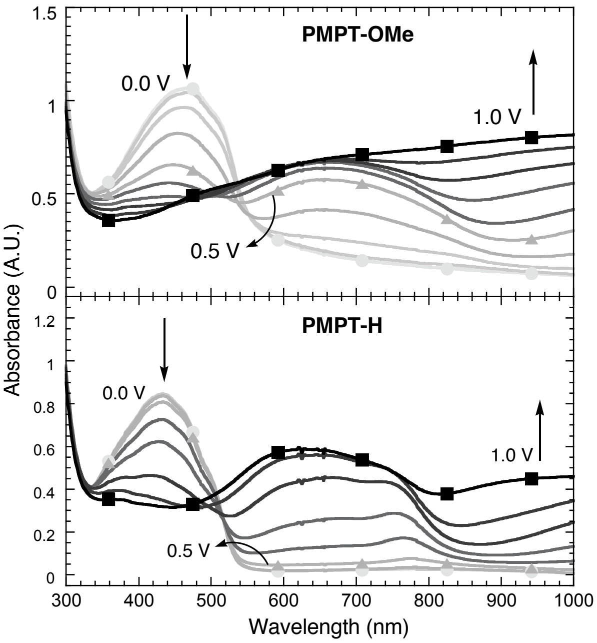

Figure 10. Electronic absorption spectra of **PMPT-OMe** (top) and **PMPT-H** (bottom) on ITO-coated glass electrodes in CH_2Cl_2 with 0.1 M $TBAPF_6$ as a supporting electrolyte, as a function of oxidation potential from 0.0 V (●) to 1.0 V (■) vs Ag / Ag^+ (0.01 M).

Conclusion

We have found that *meta*-linked polymers can be rendered as electroactive as *para*-linked isomers by strategic positioning of phenolic substituents. The maximum conductivities of both *meta*- and *para*-linked polymers in in-situ measurements were similar to each other, but appeared to be limited by an interchain charge transport. Spectroelectrochemical studies demonstrated that there were very delocalized energy states in both systems when they were oxidized. Free -OH substituents showed a marked effect on the *meta*-linked polymer over that of the acetoxy or methoxy substituents, resulting in much lower onset potential in a conductivity-potential profile and broad electroactivity of the polymer.

Experimental Section

Instrumentation. NMR spectra were recorded on a Varian Mercury-300, Bruker Advance-400, or Varian Inova-500 spectrometer. Chemical shifts are referenced to residual solvent peaks. High-resolution mass spectra (HR-MS) were obtained on a Bruker Daltonics APEX II 3 Tesla FT-ICR-MS. Electrochemical studies were carried out using an Autolab PGSTAT 10 or PGSTAT 20 potentiostat (Eco Chemie) in a three-electrode cell configuration consisting of a quasi-internal Ag wire reference electrode (BioAnalytical Systems) submerged in 0.01 $AgNO_3$ / 0.1 M tetrabutylammonium hexafluorophosphate ($TBAPF_6$) in anhydrous CH_3CN, a Pt button (1.6 mm in diameter), 5 μm interdigitated Pt micro, ITO-coated glass (100 Ω sheet resistance), or Au-coated poly(ethylene terephthalate) (PETE) electrode as the working electrode, and a Pt coil or Pt gauze as the counter electrode. The ferrocene/ferrocenium (Fc/Fc^+) redox couple was used as a reference. Half-wave potentials of Fc/Fc^+ were observed between 210-245 mV vs Ag/Ag^+ in CH_2Cl_2 and 80 mV in CH_3CN. For the in-situ conductivity measurements, polymer films were electrochemically deposited on 5 μm interdigitated Pt microelectrodes and placed in a monomer-free solution. Drain current measurements were typically carried out at a 5 mV/s scan rate with a 40 mV offset potential between the two working electrodes. The conductivity was then calculated from the value of the drain current by applying geometrical factors[11] and also corrected with a known material - poly(3-methylthiophene) as 60 S/cm. The polymer film thickness for the conductivity calculation was measured with a surface profilometer (Veeco Dektak 6M Stylus Profiler). The baseline (A) of a bare interdigitated microelectrode was first obtained. Next, the surface profile (B) of a given polymer film on the electrode was measured. Several values of A and B were taken to get averages of each. The thickness was determined by subtracting the averaged value of A from the averaged value of B. Absorption spectra for spectroelectrochemistry were obtained using a HP 8453 diode array spectrometer. FT-IR spectra of polymer films were taken using Nicolet 8700 FT-IR spectrometer with a fixed 30° specular reflectance accessory.

Materials. Spectroscopic grade CH_2Cl_2 and CH_3CN were purchased from Aldrich for electrochemistry. $TBAPF_6$ was recrystallized in ethanol prior to use. 4,6-Diiodobenzene-1,3-diol,[12] 2,5-diiodobenzene-1,4-diol,[13] and 5-tributylstannyl-2,2'-bithiophene[14] were prepared by literature methods. Anhydrous DMF was purchased from Aldrich as Sure-Seal Bottles and used as received. All other chemicals were of reagent grade and used as received.

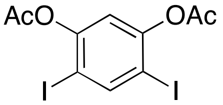

1,5-Diacetoxy-2,4-diiodobenzene (**1b**). In a 100 mL round-bottom flask equipped with a stir bar were combined 4,6-diiodobenzene-1,3-diol (1.08 g, 3 mmol), acetic anhydride (1.42 mL, 15 mmol), and 5 mL of pyridine. After being stirred overnight at room temperature, the mixture was poured into water and extracted with diethyl ether. The organic layer was washed with brine, dried over $MgSO_4$, and evaporated under reduced pressure. The resulting crude product was purified by column chromatography (ethyl acetate:hexane 1:1). Yield: 1.30 g of white solid (97 %). ^{1}H NMR (300 MHz, $CDCl_3$) δ: 8.26 (s, 1H), 6.97 (s, 1H), 2.36 (s, 6H). ^{13}C NMR (100 MHz, $CDCl_3$) δ: 168.1, 152.2, 147.7, 118.1, 88.1, 21.4. HR-MS (ESI): calcd for $C_{10}H_8I_2O_4$ $[M+Na]^+$, 468.8404; found, 468.8383.

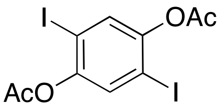

1,4-Diacetoxy-2,5-diiodobenzene. Similar to the synthesis of **1b** except using 2,5-diiodobenzene-1,4-diol. Yield: 1.09 g of white solid (82 %). ^{1}H NMR (400 MHz, $CDCl_3$) δ: 7.53 (s, 2H), 2.36 (s, 6H). ^{13}C NMR (100 MHz, $CDCl_3$) δ: 168.4, 149.6, 132.7, 90.2, 21.3. HR-MS (ESI): calcd for $C_{10}H_8I_2O_4$ [M+Na]$^+$, 468.8404; found, 468.8416.

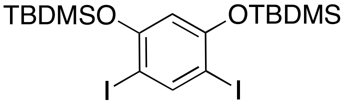

1,5-Bis(*tert*-butyldimethylsilanyloxy)-2,4-diiodobenzene (**1c**). In a 100 mL round-bottom flask equipped with a stir bar were combined 4,6-diiodobenzene-1,3-diol (1.45 g, 4 mmol), TBDMSCl (1.8 g, 12 mmol), and 20 mL of anhydrous DMF under Ar. After being stirred for 10 min, imidazole (1.38 g, 20 mmol) was added to the mixture and it was stirred overnight at room temperature. The mixture was poured into water and extracted with diethyl ether. The organic layer was then washed with brine, dried over $MgSO_4$, and evaporated under reduced pressure. The resulting crude product was purified by column chromatography (dichloromethane:hexane 1:15). Yield: 2.30 g of white solid (97 %). ^{1}H NMR (400 MHz, $CDCl_3$) δ: 8.04 (s, 1H), 6.40 (s, 1H), 1.07 (s, 18H), 0.28 (s, 12H). ^{13}C NMR (100 MHz, $CDCl_3$) δ: 156.4, 147.1, 109.5, 81.3, 26.0, 18.6, -3.8. HR-MS (ESI): calcd for $C_{18}H_{32}I_2O_2Si_2$ [M+Na]$^+$, 612.9922; found, 612.9895.

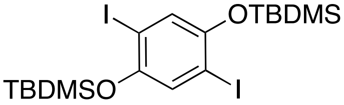

1,4-Bis(*tert*-butyldimethylsilanyloxy)-2,5-diiodobenzene. Similar to the synthesis of **1c** except using 2,5-diiodobenzene-1,4-diol. Yield: 2.34 g of white solid (99 %). ^{1}H NMR (400 MHz, $CDCl_3$) δ: 7.18 (s, 2H), 1.05 (s, 18H), 0.26 (s, 12H). ^{13}C NMR (100 MHz, $CDCl_3$) δ:

150.4, 128.0, 89.7, 26.1, 18.5, -3.9. HR-MS (ESI): calcd for $C_{18}H_{32}I_2O_2Si_2$ $[M+Na]^+$, 612.9922; found, 612.9904.

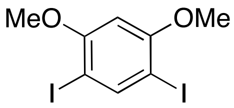

1,5-Dimethoxy-2,4-diiodobenzene (**1d**). In a 100 mL round-bottom flask equipped with a stir bar were combined 4,6-diiodobenzene-1,3-diol (1.09 g, 3 mmol), K_2CO_3 (4.15 g, 30 mmol), and 30 mL of DMF under Ar. Iodomethane (0.936 mL, 15 mmol) was slowly added to the mixture and it was stirred for 6h at room temperature. The mixture was diluted with ethyl acetate and the organic layer was washed with water and brine, dried over $MgSO_4$, and evaporated under reduced pressure. The resulting crude product was filtered through a pad of silica gel, eluding with dichloromethane. The solvent was evaporated under reduced pressure, and the resulting solid was further purified by recrystallization (dichloromethane, hexane). Yield: 1.07 g of white solid (91 %). ^1H NMR (400 MHz, CD_2Cl_2) δ: 8.03 (s, 1H), 6.40 (s, 1H), 3.88 (s, 6H). ^{13}C NMR (100 MHz, CD_2Cl_2) δ: 160.3, 147.3, 96.4, 75.5, 57.0. HR-MS (ESI): calcd for $C_8H_8I_2O_2$ $[M+Na]^+$, 412.8506; found, 412.8522.

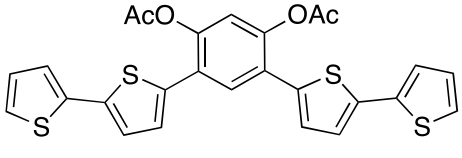

1,5-Diacetoxy-2,4-bis([2,2’]bithiophen-5-yl)benzene (**2b**). In a Schlenk tube equipped with a stir bar were combined **1b** (0.446 g, 1 mmol), $Pd_2(dba)_3$ (31 mg, 3 mol %), $P(t\text{-}Bu_3)$ (24 mg, 6.6 mol %), and 10 mL of toluene under Ar. To the mixture was added 5-tributylstannyl-2,2’-bithiophene (1.37 g, 3 mmol) and stirred for 48 h at 80 °C. The reaction mixture was then cooled to room temperature, diluted with ethyl acetate, and filtered through a pad of silica gel. The silica gel was thoroughly washed with ethyl acetate, and the solvent was evaporated under reduced pressure. The crude solid was washed with diethyl ether, and then further purified by recrystallization (dichloromethane, hexane). Yield: 0.262 g of pale yellow solid (50 %). ^{1}H NMR (300 MHz, CD_2Cl_2) δ: 7.91 (s, 1H), 7.32 (d, 2H, J = 3.8 Hz), 7.29 (dd, 2H, J = 5.3, 1.1 Hz), 7.25 (dd, 2H, J = 3.6, 1.1 Hz), 7.21 (d, 2H, J = 3.8 Hz), 7.07 (s, 1H), 7.06 (dd, 2H, J = 5.3, 3.6 Hz), 2.36 (s, 6H). ^{13}C NMR (100 MHz, CD_2Cl_2) δ: 169.3, 146.6, 139.0, 137.4, 136.4, 129.5, 128.5, 127.7, 126.0, 125.4, 124.55, 124.52, 119.4, 21.8. HR-MS (ESI): calcd for $C_{26}H_{18}O_4S_4$ $[M+Na]^+$, 544.9980; found, 544.9999.

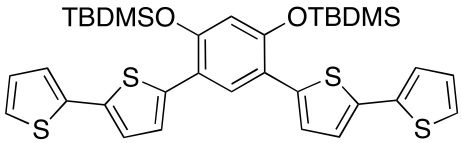

1,5-Bis(*tert*-butyldimethylsilanyloxy)-2,4-bis([2,2']bithiophen-5-yl)benzene (**2c**). In a Schlenk tube equipped with a stir bar were combined **1c** (1.18 g, 2 mmol), $Pd_2(dba)_3$ (104 mg, 5 mol %), P(*t*-Bu_3) (81 mg, 0.4 mmol), and 15 mL of toluene under Ar. To the mixture was added 5-tributylstannyl-2,2'-bithiophene (2.73 g, 6 mmol) and stirred for 48 h at 80 °C. The reaction mixture was then cooled to room temperature, diluted with ethyl acetate, and filtered through a pad of silica gel. The silica gel was thoroughly washed with ethyl acetate, and the solvent was evaporated under reduced pressure. The crude solid was washed with cold hexane, and then further purified by recrystallization (dichloromethane, hexane). Yield: 0.872 g of yellow solid (65 %). ^{1}H NMR (400 MHz, $CDCl_3$) δ: 7.72 (s, 1H), 7.25 (d, 2H, J = 3.6 Hz), 7.21 (dd, 2H, J = 5.2, 1.2 Hz), 7.18 (dd, 2H, J = 3.6, 1.2 Hz), 7.15 (d, 2H, J = 3.6 Hz), 7.04 (dd, 2H, J = 5.2, 3.6 Hz), 6.53 (s, 1H), 1.00 (s, 18H), 0.27 (s, 12H). ^{13}C NMR (100 MHz, $CDCl_3$) δ: 152.4, 138.7, 138.2, 136.4, 129.4, 128.0, 125.8, 124.1, 123.6, 123.2, 119.6, 111.5, 26.2, 18.8, -3.6. HR-MS (ESI): calcd for $C_{34}H_{42}O_2S_4Si_2$ $[M+H]^+$, 667.1679; found, 667.1683.

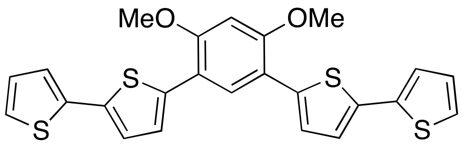

1,5-Dimethoxy-2,4-bis([2,2']bithiophen-5-yl)benzene (**2d**). In a Schlenk tube equipped with a stir bar were combined **1d** (0.390 g, 1 mmol), $Pd_2(dba)_3$ (31 mg, 3 mol %), P(*t*-Bu_3) (13 mg, 6.6 mol %), LiCl (170 mg, 4 mmol), and 10 mL of DMF under Ar. To the mixture was added 5-tributylstannyl-2,2'-bithiophene (1.37 g, 3 mmol) and stirred overnight at room temperature. The reaction mixture was diluted with dichloromethane, and filtered through a pad of silica gel. Most of the solvent was evaporated under reduced pressure. The residue was diluted with ethyl acetate, washed with brine (×2), dried over $MgSO_4$, and evaporated under reduced pressure. The resulting residue was precipitated with hexane, and the crude solid was washed with copious amounts of hexane. The product was further purified by recrystallization (dichloromethane, hexane). Yield: 0.347 g of yellow solid (74 %). ^1H NMR (400 MHz, CD_2Cl_2) δ: 7.89 (s, 1H), 7.38 (d, 2H, *J* = 3.8 Hz), 7.23-7.25 (m, 4H), 7.18 (d, 2H, *J* = 3.8 Hz), 7.05 (dd, 2H, *J* = 5.1, 3.7 Hz), 6.64 (s, 1H), 4.00 (s, 6H). ^{13}C NMR (100 MHz, CD_2Cl_2) δ: 156.7, 138.6, 138.2, 136.7, 128.4, 127.7, 125.6, 124.6, 124.0, 123.7, 116.4, 96.7, 56.4. HR-MS (ESI): calcd for $C_{24}H_{18}O_2S_4$ $[M]^+$, 466.0184; found, 466.0176.

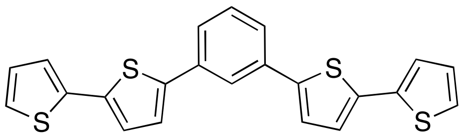

1,3-Bis([2,2’]bithiophen-5-yl)benzene (**3**). In a Schlenk tube equipped with a stir bar were combined 1,3-diiodobenzene (0.337 g, 1 mmol), $PdCl_2(PPh_3)_2$ (37 mg, 5 mol %), and 10 mL of toluene under Ar. To the mixture was added 5-tributylstannyl-2,2’-bithiophene (1.37 g, 3 mmol) and stirred overnight at 80 °C. The reaction mixture was then cooled to room temperature, diluted with dichloromethane, and filtered through a pad of silica gel. The solvent was evaporated under reduced pressure, and the resulting residue was precipitated with hexane. The crude solid was washed with hexane, and further purified by recrystallization (dichloromethane, hexane). Yield: 0.350 g of bright yellow solid (86 %). ^{1}H NMR (400 MHz, CD_2Cl_2) δ: 7.83 (pseudo-t, 1H, J = 1.7 Hz), 7.54 (dd, 2H, J = 7.7, 1.7 Hz), 7.41 (t, 1H, J = 7.7 Hz), 7.33 (d, 2H, J = 3.8 Hz), 7.27 (dd, 2H, J = 5.1, 1.1 Hz), 7.25 (dd, 2H, J = 3.7, 1.1 Hz), 7.20 (d, 2H, J = 3.8 Hz), 7.06 (dd, 2H, J = 5.1, 3.7 Hz). ^{13}C NMR (100 MHz, CD_2Cl_2) δ: 142.9, 137.7, 137.6, 135.2, 130.1, 128.5, 125.2, 125.1, 124.8, 124.3, 123.0. HR-MS (ESI): calcd for $C_{22}H_{14}S_4$ $[M+H]^+$, 407.0051; found, 407.0042.

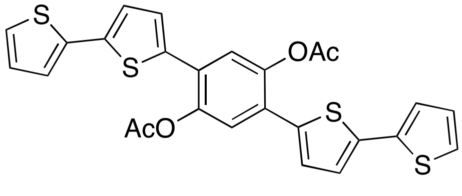

1,4-Diacetoxy-2,5-bis([2,2’]bithiophen-5-yl)benzene (**4b**). In a Schlenk tube equipped with a stir bar were combined 1,4-diacetoxy-2,5-diiodobenzene (0.446 g, 1 mmol), $PdCl_2(PPh_3)_2$ (37 mg, 5 mol %), and 10 mL of toluene under Ar. To the mixture was added 5-tributylstannyl-2,2’-bithiophene (1.37 g, 3 mmol) and stirred overnight at 80 °C. The product precipitated as the reaction progressed. The reaction mixture was then cooled to room temperature. The product was filtered out, and washed thoroughly with diethyl ether. The crude product was then redissolved with dichloromethane, and passed through a pad of silica gel. The silica gel was thoroughly washed with dichloromethane, and the solvent was evaporated under reduced pressure. The resulting solid was then further purified by recrystallization (dichloromethane, hexane). Yield: 0.429 g of pale yellow solid (82 %). ^{1}H NMR (500 MHz, THF-d_8) δ: 7.60 (s, 2H), 7.43 (d, 2H, *J* = 3.8 Hz), 7.37 (m, 2H), 7.29 (m, 2H), 7.23 (d, 2H, *J* = 3.8 Hz), 7.04 (dd, 2H, *J* = 5.0, 3.5 Hz), 2.38 (s, 6H). ^{13}C NMR (125 MHz, THF-d_8) δ: 169.0, 145.5, 139.7, 138.0, 136.9, 128.9, 128.2, 127.6, 126.0, 124.92, 124.86, 124.1, 21.5. HR-MS (ESI): calcd for $C_{26}H_{18}O_4S_4$ [M+Na]$^+$, 544.9980; found, 544.9992.

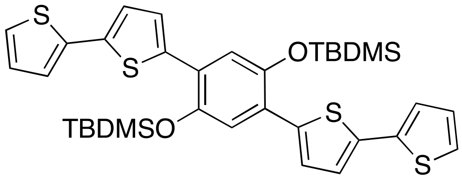

1,4-Bis(*tert*-butyldimethylsilanyloxy)-2,5-bis([2,2']bithiophen-5-yl)benzene (**4c**). In a Schlenk tube equipped with a stir bar were combined 1,4-bis(*tert*-butyldimethylsilanyloxy)-2,5-diiodobenzene (0.177 g, 0.3 mmol), $PdCl_2(PPh_3)_2$ (11 mg, 5 mol %), and 3 mL of toluene under Ar. To the mixture was added 5-tributylstannyl-2,2'-bithiophene (0.341 g, 0.75 mmol) and stirred for 20 h at 80 °C. The product precipitated as the reaction progressed. The reaction mixture was then cooled to room temperature. The product was filtered out, and washed thoroughly with ethyl acetate. The crude product was then redissolved with dichloromethane and passed through a pad of silica gel. The silica gel was thoroughly washed with dichloromethane, and the solvent was evaporated under reduced pressure. The resulting solid was then further purified by recrystallization (dichloromethane, hexane). Yield: 0.194 g of pale yellow solid (97 %). ^{1}H NMR (400 MHz, $CDCl_3$) δ: 7.32 (d, 2H, *J* = 3.8 Hz), 7.23 (dd, 2H, *J* =

5.2, 1.0 Hz), 7.21 (dd, 2H, *J* = 3.6, 1.0 Hz), 7.16 (d, 2H, *J* = 3.8 Hz), 7.15 (s, 2H), 7.05 (dd, 2H, *J* = 5.2, 3.6 Hz), 1.03 (s, 18H), 0.27 (s, 12H). ^{13}C NMR (100 MHz, $CDCl_3$) δ: 146.4, 138.6, 138.0, 137.2. 128.1, 126.4, 124.8, 124.4, 123.8, 123.5, 119.6, 26.3, 18.8, -3.5. HR-MS (ESI): calcd for $C_{34}H_{42}O_2S_4Si_2$ $[M+H]^+$, 667.1679; found, 667.1706.

References and Notes

(1) (a) *Conjugated Polymers*; Bredas, J. L., Silbey, R., Eds.; Kluwer Academic Publishers: Dordrecht, Netherlands, 1991. (b) *Organic Electronic Materials*; Farchioni, R., Grosso, G., Eds.; Springer: New York, 2001.

(2) Sato, M.; Tanaka, S.; Kaeriyama, K. *J. Chem. Soc., Chem. Commun.* **1986**, 873.

(3) Jen, K. Y.; Miller, G. C.; Elsenbaumer, R. L. *J. Chem. Soc., Chem. Commun.* **1986**, 1346.

(4) Roncali, J. *Chem. Rev.* **1992**, *92*, 711.

(5) Zotti, G.; Gallazzi, M. C.; Zerbi, G.; Meille, S. V. *Synth. Met.* **1995**, *73*, 217.

(6) Child, A. D.; Sankaran, B.; Larmat, F.; Reynolds, J. R. *Macromolecules* **1995**, *28*, 6571.

(7) (a) Sarker, H.; Ong, I.; Sarker, S.; Searson, P. C.; Poehler, T. O. *Synth. Met.* **2000**, *108*, 33. (b) Pei, J.; Yu, W. -L.; Ni, J.; Lai, Y. -H.; Huang, W.; Heeger, A. J. *Macromolecules* **2001**, *34*, 7241. (c) Bouachrine, M.; Bouzakraoui, S.; Hamidi, M.; Ayachi, S.; Alimi, K.; Lere-Porte, J. -P.; Moreau, J. *Synth. Met.* **2004**, *145*, 237.

(8) (a) Reddinger, J. L.; Reynolds, J. R. *Macromolecules* **1997**, *30*, 479. (b) Liao, L.; Pang, Y. *Macromolecules* **2001**, *34*, 7300. (c) Hong, S. Y.; Kim, D. Y.; Kim, C. Y.; Hoffmann, R. *Macromolecules* **2001**, *34*, 6474.

(9) Yu, H. -h.; Xu, B.; Swager, T. M. *J. Am. Chem. Soc.* **2003**, *125*, 1142.

(10) (a) Jenekhe, S. A. *Nature* **1986**, *322*, 345. (b) Chen, W. -C.; Liu, C. -L.; Yen, C. -T.; Tsai, F. -C.; Tonzola, C. J.; Olson, N.; Jenekhe, S. A. *Macromolecules* **2004**, *37*, 5959.

(11) (a) Kingsborough, R. P.; Swager, T. M. *Adv. Mater.* **1998**, *10*, 1100. (b) Kingsborough, R. P.; Swager, T. M. *J. Am. Chem. Soc.* **1999**, *121*, 8825.

(12) Nicolet, B. H.; Sampey, J. R. *J. Am. Chem. Soc* **1927**, *49*, 1796.

(13) Zhou, Q.; Swager, T. M. *J. Am. Chem. Soc* **1995**, *117*, 12593.

(14) Zhu, S. S.; Swager, T. M. *J. Am. Chem. Soc* **1997**, *119*, 12568.

(15) Chemical polymerization with $FeCl_3$ was attempted, but produced insoluble materials that could not be characterized.

(16) *Electroactive polymer electrochemistry*; Lyons, M. E. G., Ed.; Plenum: New York, 1994.

(17) (a) Miller, L. L.; Mann, K. R. *Acc. Chem. Res.* **1996**, *29*, 417. (b) Cornil, J.; Beljonne, D.; Calbert, J. -P.; Bredas, J. L. *Adv. Mater.* **2001**, *13*, 1053.

(18) (a) Bredas, J. L.; Street, G. B. *Acc. Chem. Res.* **1985**, *18*, 309. (b) Heeger, A. J.; Kivelson, S.; Schrieffer, J. R.; Su, W. -P. *Rev. Mod. Phys.* **1988**, *60*, 781.

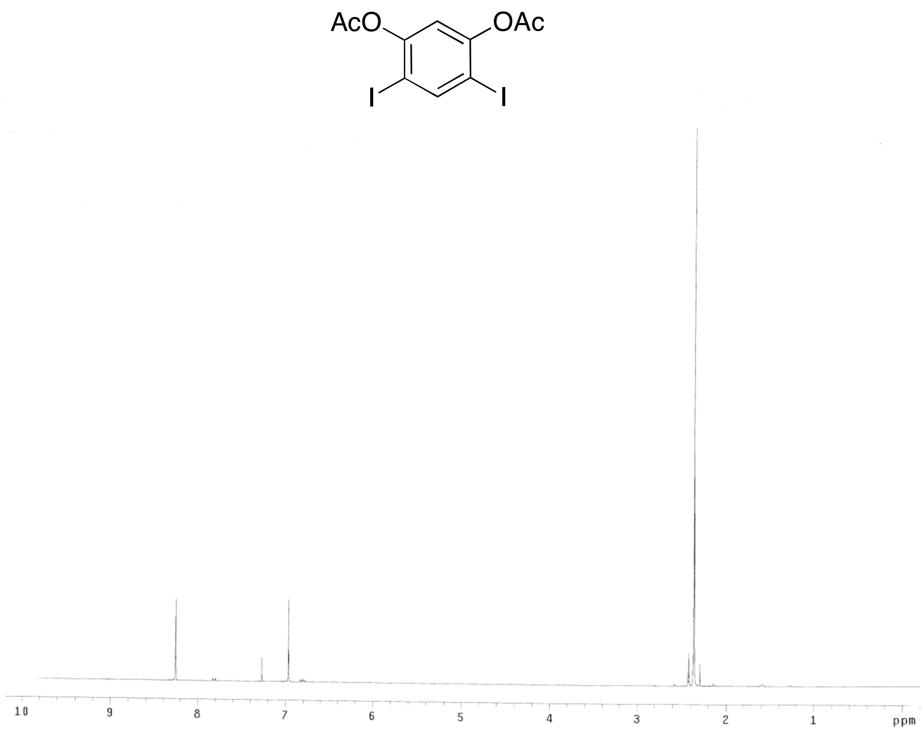

Spectrum 1. ^{1}H-NMR spectrum of **1b** (500 MHz, $CDCl_3$).

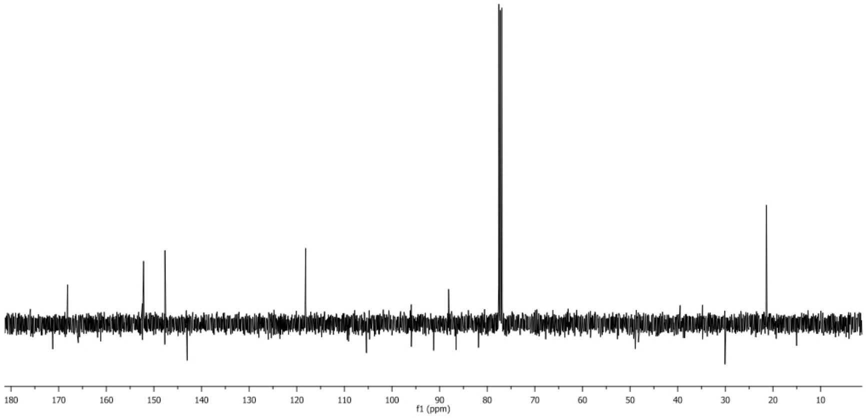

Spectrum 2. ^{13}C-NMR spectrum of **1b** (100 MHz, $CDCl_3$).

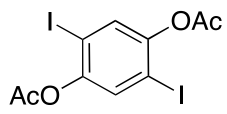

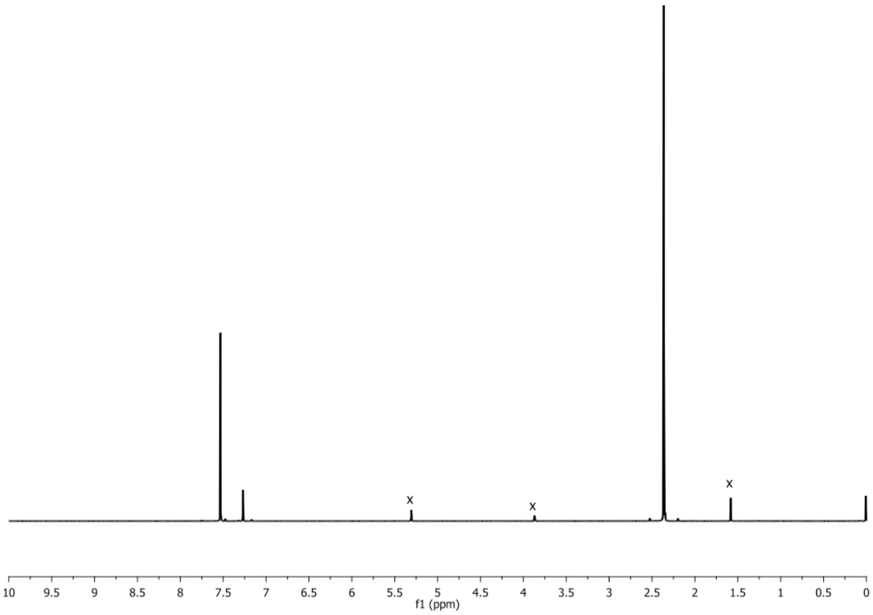

Spectrum 3. ^{1}H-NMR spectrum of **1,4-diacetoxy-2,5-diiodobenzene** (400 MHz, $CDCl_3$).

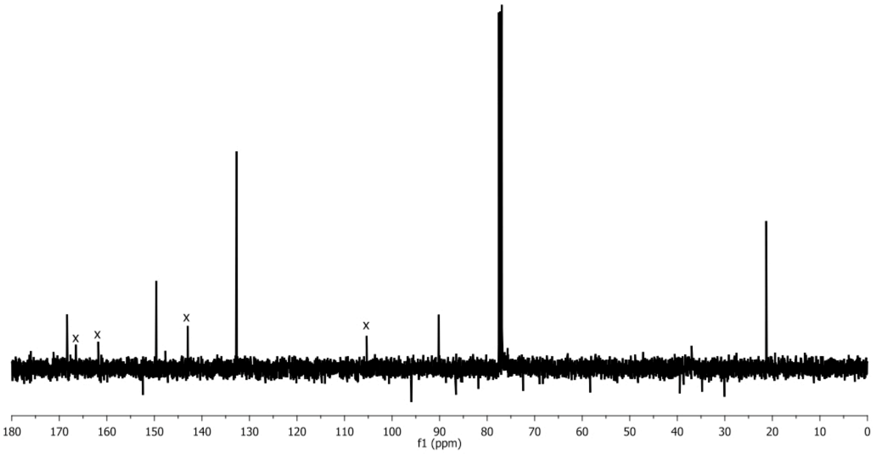

Spectrum 4. ^{13}C-NMR spectrum of **1,4-diacetoxy-2,5-diiodobenzene** (100 MHz, $CDCl_3$).

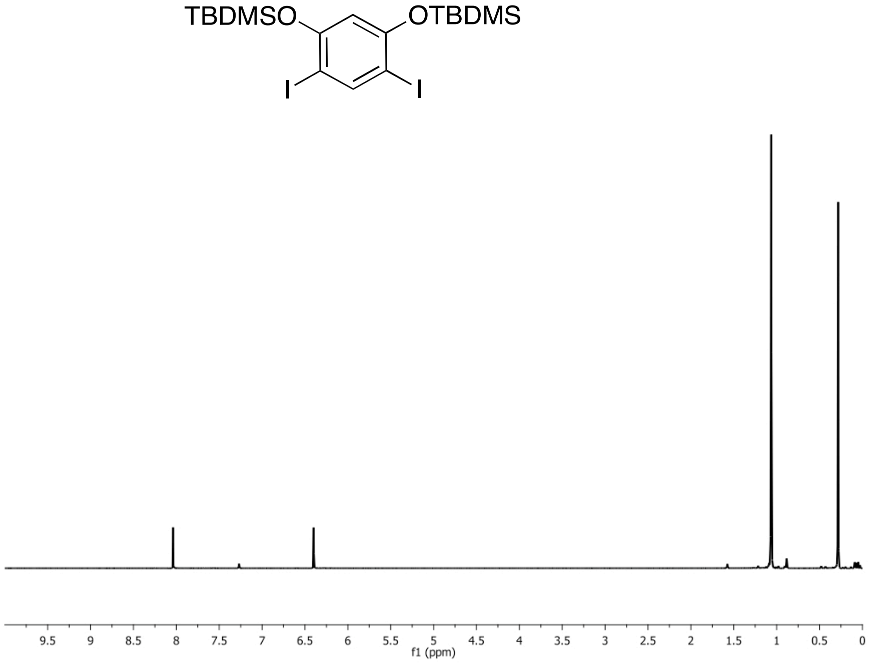

Spectrum 5. ^{1}H-NMR spectrum of **1c** (400 MHz, $CDCl_3$).

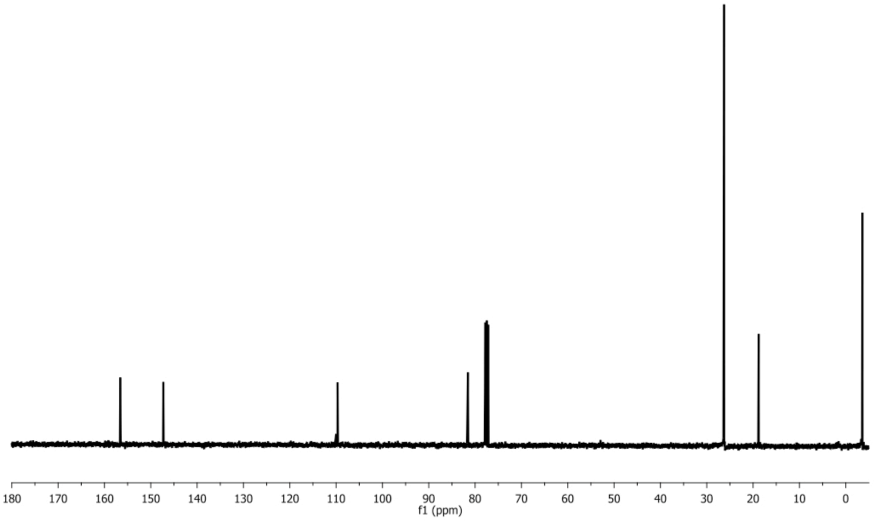

Spectrum 6. ^{13}C-NMR spectrum of **1c** (100 MHz, $CDCl_3$).

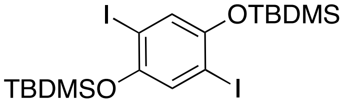

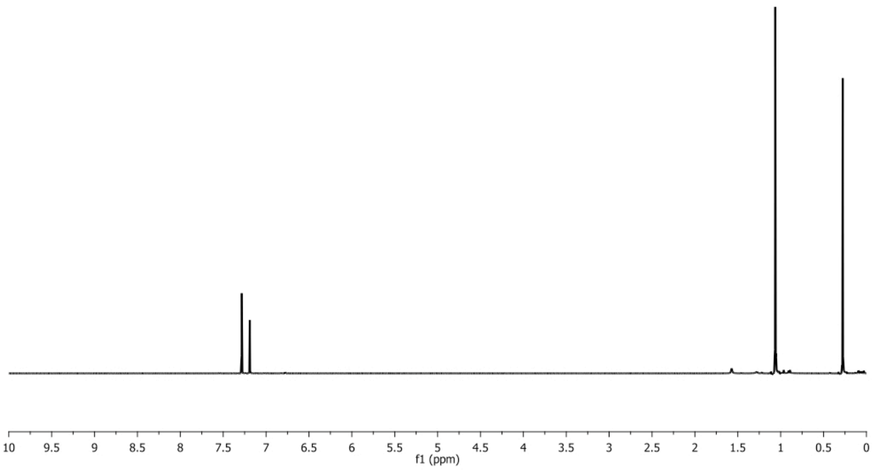

Spectrum 7. ^{1}H-NMR spectrum of **1,4-bis(t-butyldimethylsilanyloxy)-2,5-diiodobenzene** (400 MHz, $CDCl_3$).

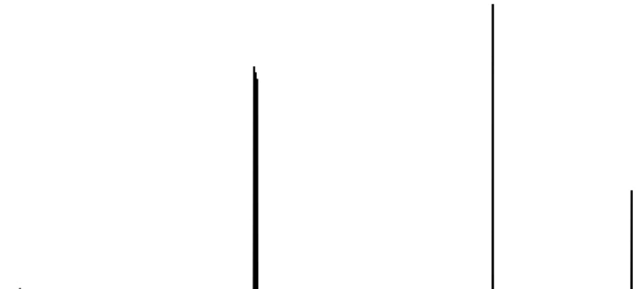

Spectrum 8. ^{13}C-NMR spectrum of **1,4-bis(t-butyldimethylsilanyloxy)-2,5-diiodobenzene** (100 MHz, $CDCl_3$).

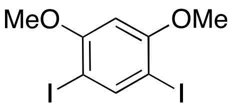

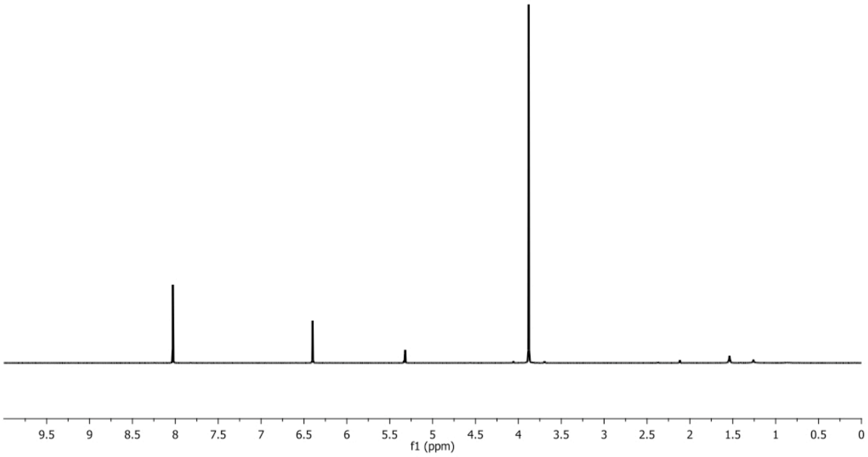

Spectrum 9. ^{1}H-NMR spectrum of **1d** (400 MHz, CD_2Cl_2).

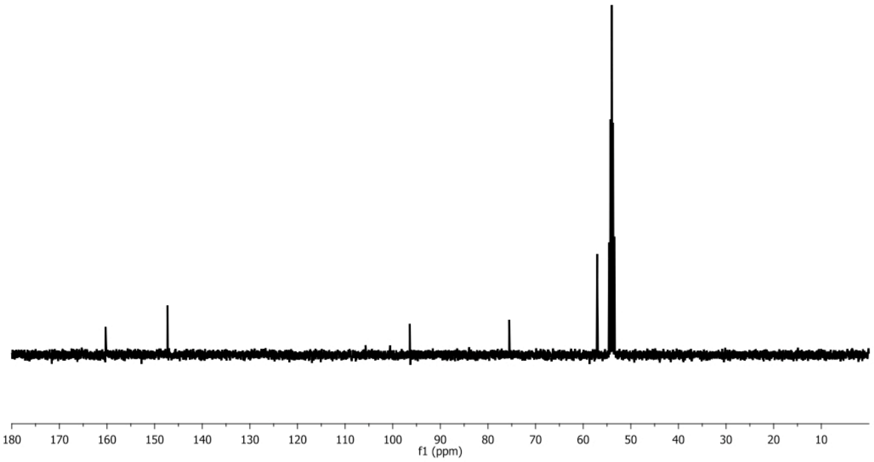

Spectrum 10. ^{13}C-NMR spectrum of **1d** (100 MHz, CD_2Cl_2).

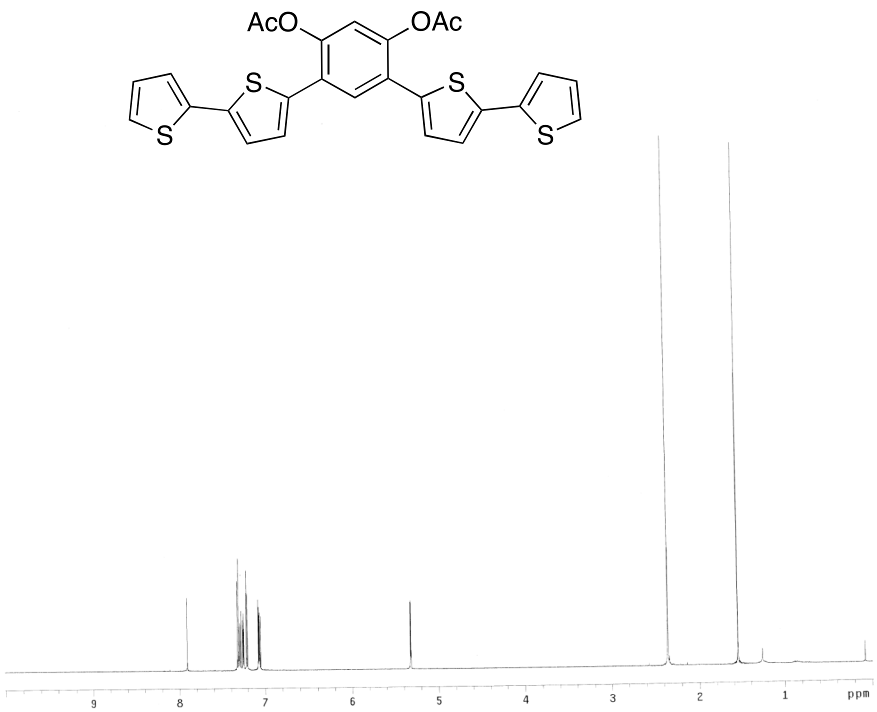

Spectrum 11. ^{1}H-NMR spectrum of **2b** (500 MHz, CD_2Cl_2).

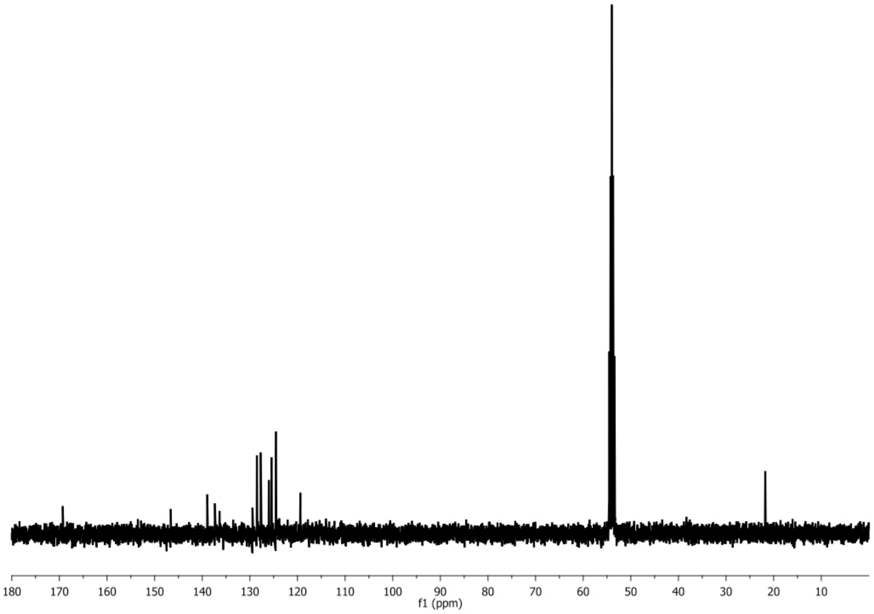

Spectrum 12. ^{13}C-NMR spectrum of **2b** (100 MHz, CD_2Cl_2).

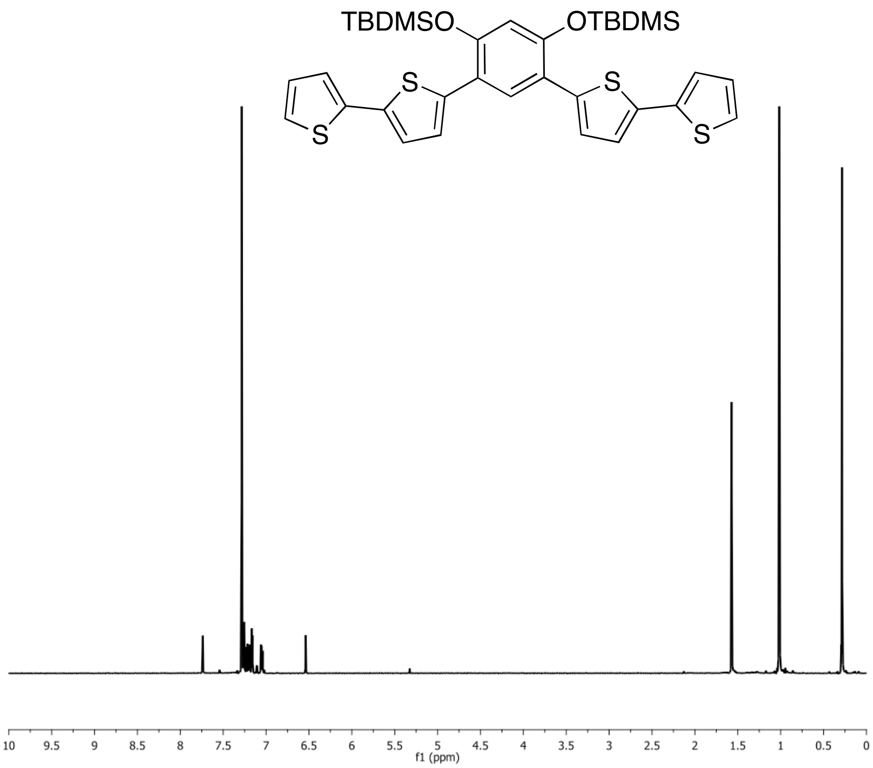

Spectrum 13. ^{1}H-NMR spectrum of **2c** (400 MHz, $CDCl_3$).

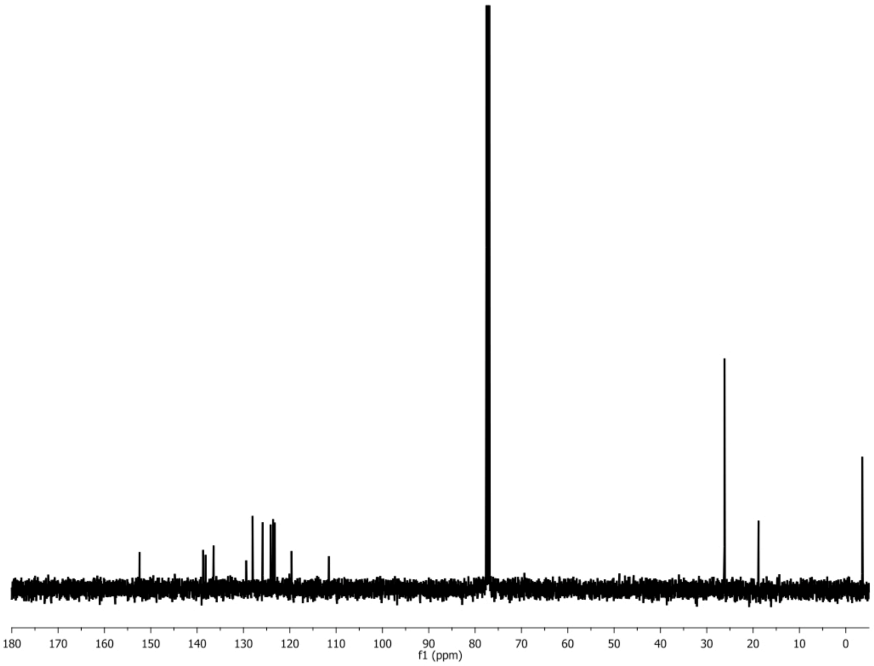

Spectrum 14. ^{13}C-NMR spectrum of **2c** (100 MHz, $CDCl_3$).

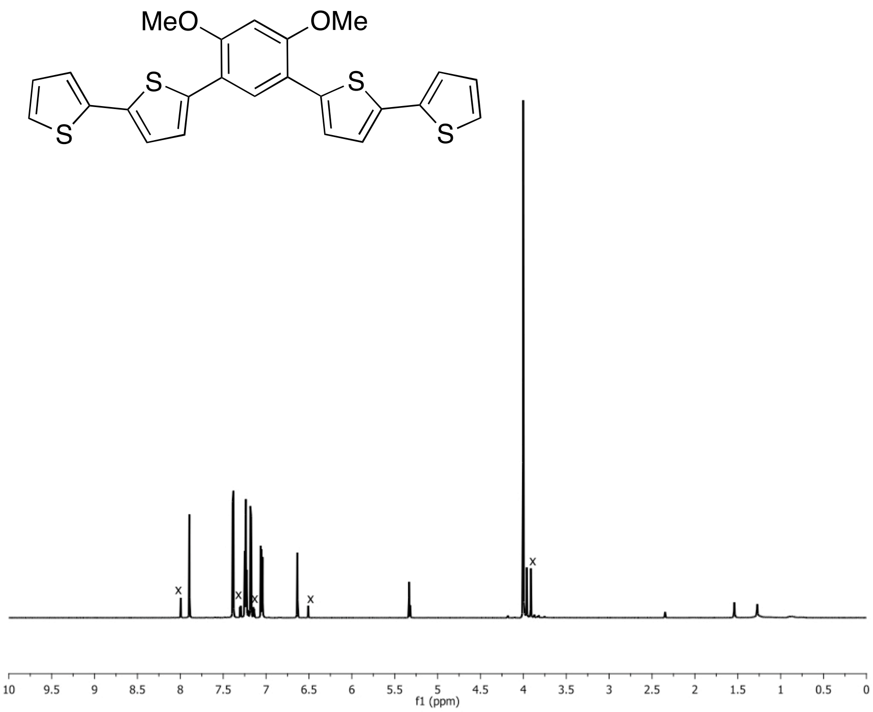

Spectrum 15. ^{1}H-NMR spectrum of **2d** (400 MHz, CD_2Cl_2).

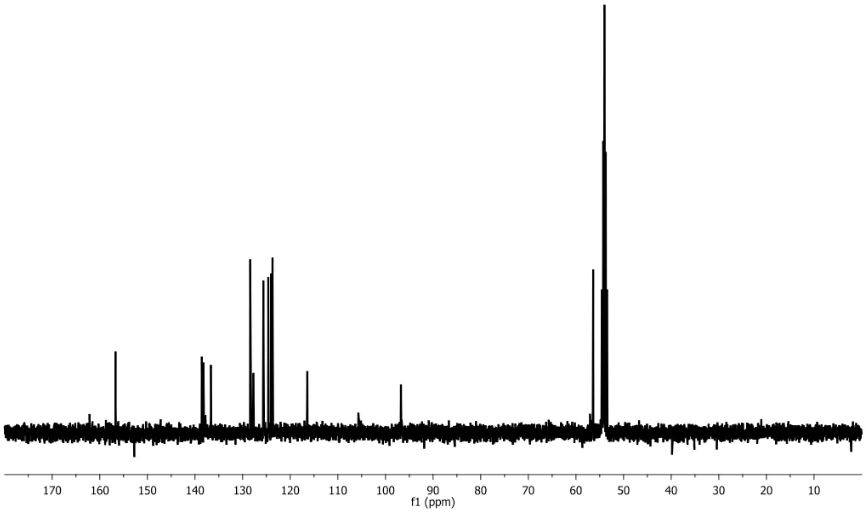

Spectrum 16. ^{13}C-NMR spectrum of **2d** (100 MHz, CD_2Cl_2).

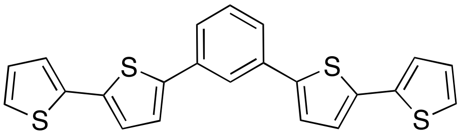

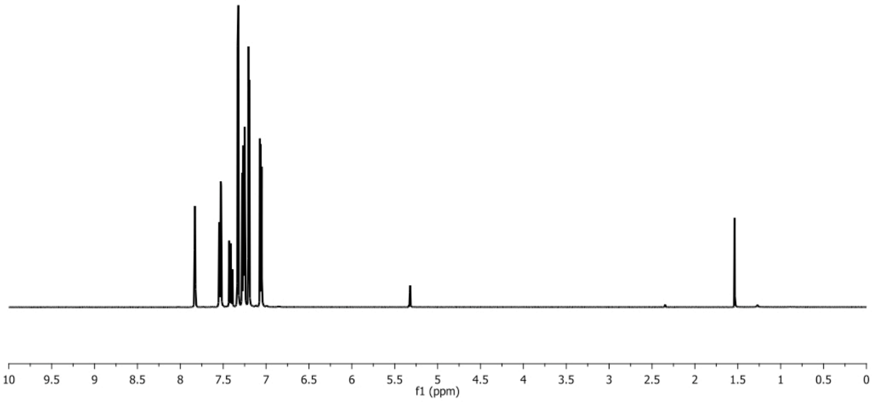

Spectrum 17. ^{1}H-NMR spectrum of **3** (400 MHz, CD_2Cl_2).

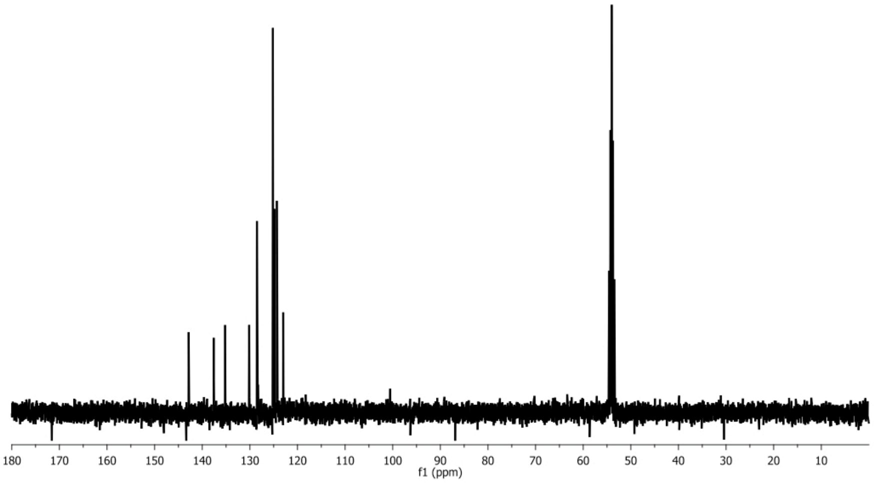

Spectrum 18. ^{13}C-NMR spectrum of **3** (100 MHz, CD_2Cl_2).

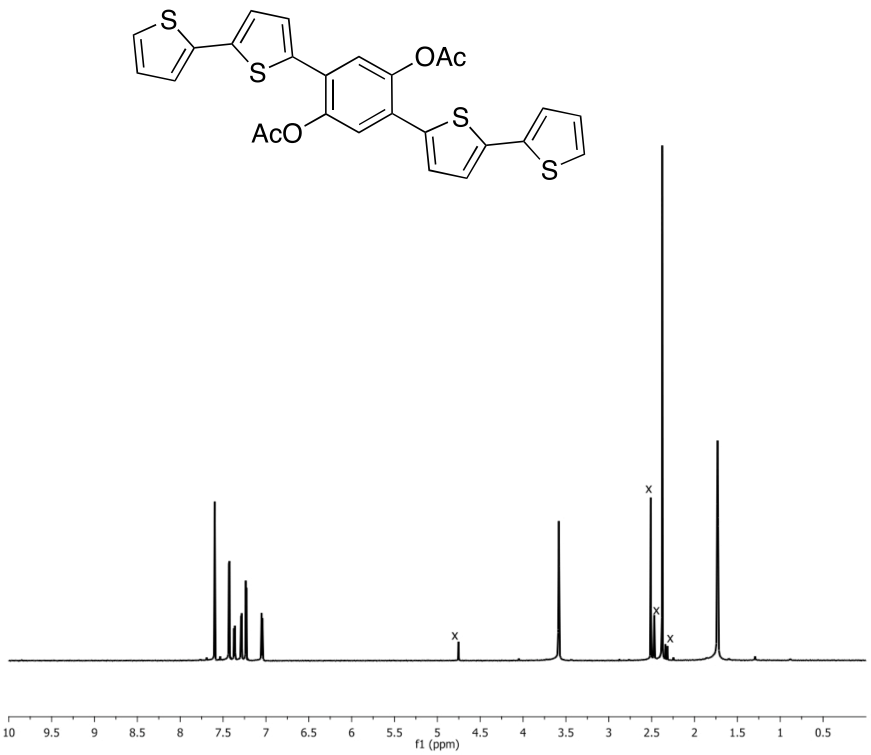

Spectrum 19. ^{1}H-NMR spectrum of **4b** (500 MHz, THF-d_8).

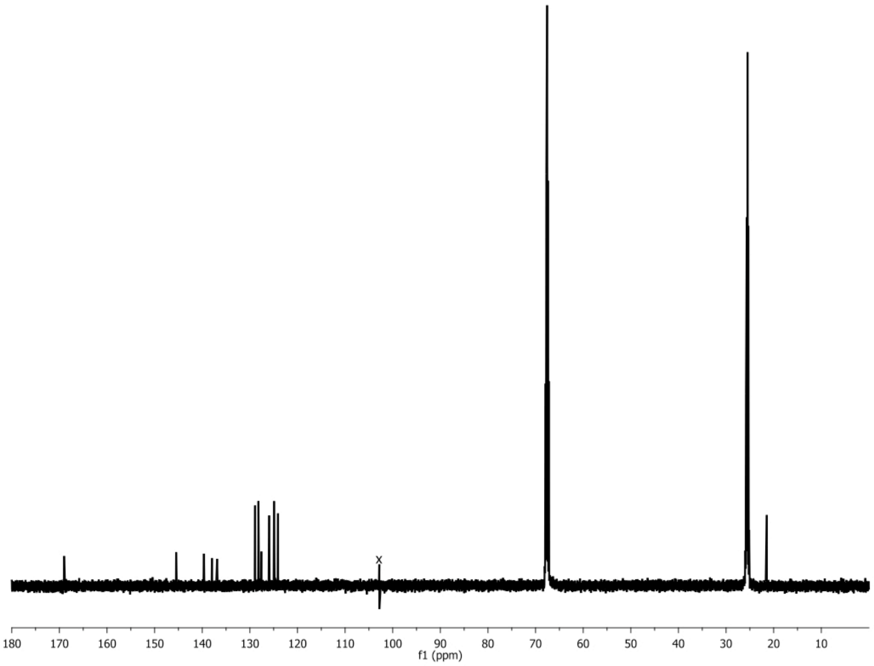

Spectrum 20. ^{13}C-NMR spectrum of **4b** (125 MHz, THF-d_8).

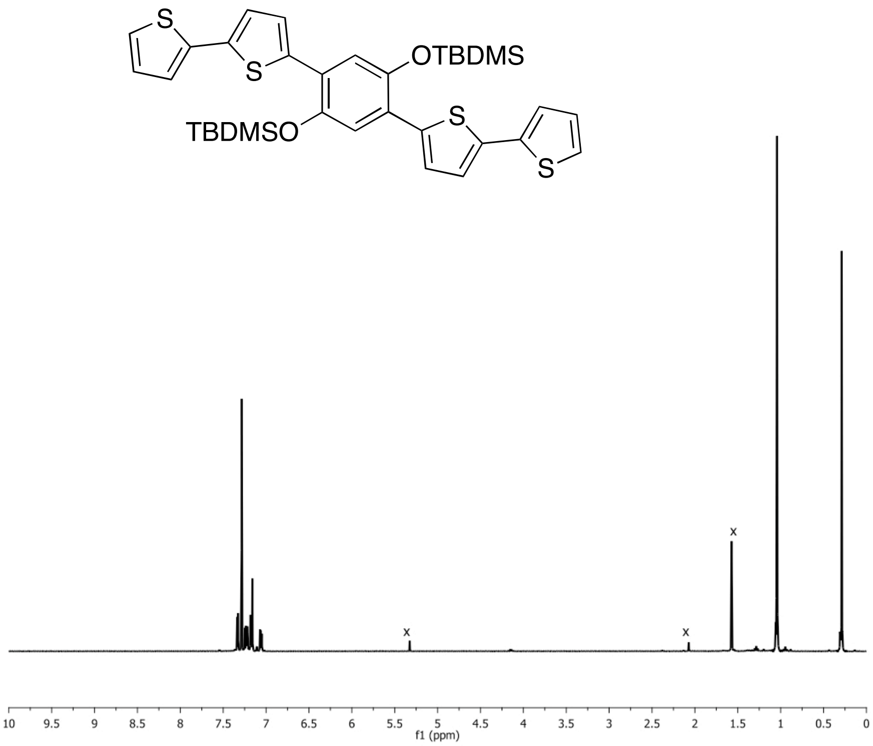

Spectrum 21. ^{1}H-NMR spectrum of **4c** (400 MHz, $CDCl_3$).

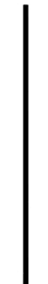

Spectrum 22. ^{13}C-NMR spectrum of **4c** (100 MHz, $CDCl_3$).

Changsik Song

77 Massachusetts Avenue #18-014
Cambridge, MA 02139
617-452-5097 (office) 617-388-9149 (cell)
cssong@mit.edu

EDUCATION

Massachusetts Institute of Technology, Cambridge, MA

***Ph.D.**,* Organic Chemistry (*expected) September 2007*

Thesis Title: Design and Synthesis of Molecular Actuators and Sensors

Korea Advanced Institute of Science and Technology, Daejeon, Korea

B.S., Chemistry, *summa cum laude* *August 2001*

RESEARCH EXPERIENCE

Massachusetts Institute of Technology, Cambridge, MA *1/2003 – present*

Graduate Student with **Prof Timothy M. Swager**. Design and synthesis of electronic functional materials and their application to actuators and sensors. Investigations of unconventional “molecular” actuating mechanism (vs “swelling” mechanism). Syntheses and characterization of various conducting polymers with interesting structures. Development of a new polarizing agent for DNP that works in aqueous media.

Korea Advanced Institute of Science and Technology, Daejeon, Korea *6/2001 – 6/2002*

Research Assistant with **Prof Sunggak Kim**. Development of new radical reactions for alkylation to carboxylic imides.

TEACHING EXPERIENCE

Massachusetts Institute of Technology, Cambridge, MA *Fall 2002/Spring 2003/Spring 2005*

Teaching Assistant in the undergraduate labs: general chemistry and intermediate organic chemistry. Taught experimental skills, graded reports, and had discussions.

PRESENTATIONS

1. **American Chemical Society Spring 2007 National Meeting**, Chicago, Il *3/2007*
   Song, C.; Swager, T. M. “π-Dimer Formation as the Driving Force for Calix[4]arene-based Molecular Acuators”.
2. **Materials Research Society 2005 Fall Meeting**, Boston, MA *11/2005*
   Song, C.; Swager, T. M. “Poly(Thienyl-1,1’-Binaphthol)s: Conducting Polymer Sensor for Amines”.

3. **The Sixth International Symposium on Functional π-Electron Systems**, Ithaca, NY *6/2004*
   Song, C.; Swager, T. M. “Highly Conductive Poly(phenylene thienylene)s: m-Phenylene linkages Are Not Always Bad”.

PUBLICATIONS

1. Song, C.; Hu, K.-N.; Joo, C.-J.; Swager, T. M.; Griffin, R. G. “TOTAPOL: A Biradical Polarizing Agent for Dynamic Nuclear Polarization Experiments in Aqueous Media” *J. Am. Chem. Soc.* **2006**, *128*, 11385-11390.
2. Sugiyasu, K.; Song, C.; Swager, T. M. “Aromaticity in Tropone-Containing Polythiophene” *Macromolecules* **2006**, *39*, 5598-5600.
3. Song, C.; Swager, T. M. “Highly Conductive Poly(phenylene thienylene)s: m-Phenylene linkages Are Not Always Bad” *Macromolecules* **2005**, *38*, 4569-4576.
4. Kim, S.; Lim, C.-J.; Song, C.; Chung, W.-J. “Novel Radical Alkylation of Carboxylic Imides” *J. Am. Chem. Soc.* **2002**, *124*, 14306-14307.

Acknowledgements

He who sacrifices thank offerings honors me… (Psalms 50:23)

I used to think I have had all the blessings because I deserve them. I believe I have the ability to accomplish many difficult things, including this Ph.D. thesis, and it is my efforts that get things done! But now I realize I am nothing and, without any help (from above and around) I would have not finished this 5-year race. Looking back, I have to admit that it was a truly blessed time, regardless of how many ups and downs I've had, and thus I owe many thanks to people around me.

First of all, I am deeply grateful to my advisor, Prof. Tim Swager, for his tremendous supports and encouragements. He is an unusual professor with such a passion of science balancing with taking good care of his group members. His brilliant creativity saved my research several times from standstills or dead ends. I also would like to thank Prof. Greg Fu and Prof. Sarah O'Connor for valuable advices and suggestions, and for always being helpful. It was a great honor to have such professors in the thesis committee. I have never even imagined to have a conversation with world famous professors. I would like to thank Prof Robert Griffin and Dr Kan Hu for allowing me to involve the biradical DNP project. I really enjoyed the collaboration with them.

Swager group is a definitely pleasant place to work. I am indebted to the post-docs and graduate students, who are all outstanding, during my years in the Swager group. I have to thank Dr. Bruce Yu, an actuator guy, for paving the way for my research. I followed him in many aspects. Building 13 crews, Zhihua Chen, Drs. Brad Holliday, Michael Büschel, Jocelyn Nadeau, Sandra Rifai, Craig Breen, and Eléna Ishow, all helped me get through the early days of graduate life. Sandra and Craig invited my wife and me to their wedding and we really enjoyed the "American culture". Their friendship thus far is very much appreciated. Zhihua is really a good friend and a devoted scientist who have also had managed the "satellite" lab, which made me do the research without any insufficiency. Basement boys, Drs. Akihiro Ohira and Koji Arimitsu, and Takeshi Igarashi, shared most of the time and had lots of fun together.

I would like to thank Andrew Satrijo, Jean Bouffard, Vanessa Peréz, and Jessica Liao, some of who already got their Ph.D., with Zhihua for being wonderful same-year friends. Their enthusiasm and friendship inspired me a lot. Others like Drs. Kenichi Kuroda, Jordan Wosnick, Alex Paraskos, Juan Zheng, Phoebe Kwan, Paul Byrne, Karen Villazor, Nate Vandesteeg, Sam Thomas, John Amara, and Gigi Bailey always greeted me with smiles and taught me not only chemistries, but also how to use various instruments that I never expected to handle. I was privileged to work with them and other outstanding students like Scott Meek, Yong Yang, Eric Dane, Julian Chan, Trisha Andrew, Fei Wang, and Brett VanVeller. I wish them a great luck on their research.

Post-docs' expertise was undoubtedly a great help. I would like to express my gratitude to all post-docs, Evgueni Nesterov, Shigeyuki Yagi, Paul Kouwer, Lokman Torun, Guy Joly, Christine Espino, Lars Geiger, Hongwei Gu, Masashi Hasegawa, Ivory Hills, Johan Hoogboom, Katsuhiro Maeda, Anne McNeil, Koji Miki, Ryo Takita, Kazunori Sugiyasu, Mark Taylor, Koushik Venkatesan, Dahui Zhao, and Wei Zhang for their unlimited helps, discussions, proofreadings, and so on. Especially, Ryo, Kazu, and Koushik allowed me to join their literature meeting, in which we shared our own views, broadened horizons of each, and had fun! I will never forget their friendships.

I have to give special thanks to Korean family, Hyuna Kang, Inja Song, Jeewoo Lim, Drs. Dongwhan Lee, Jinho Oh, Taehyun Kim, and Youngmi Kim. On top of their great help on research, they were like a shelter when my emotions went astray. I wish I did not reduce any good reputations of Korean scientists that all others have been building so far. Korean friends outside the group like Namyong Kim, Sungji Kim, Junghyun Choi, Seungjip Choi, Sungho Yoon, Yongwon Jung, Soonsil Hyun, Inhee Jung, Hoesung Jung, Mihee Lim, Kihyun Choi, Jongho Park, Sunghee Son, Yoon-aa Choi, Taeho Shin, Changhoon Lee, Yoonju Song, Heesun Han, Sungyu Han, and Jongnam Park were all kind enough to offer me a cup of coffee when failed reactions depressed me. As same-year students, Mihee, Kihyun, and Jongho shared lots of first-year frustrations with me, and I deeply appreciate their fellowships.

First Korean Church in Cambridge has been an important part of my life since I came to MIT. The non-English speaking, "foreign" student felt much loneliness, homesick, and depression, but the church was where my soul and spirit gained comforts from above. I would like to give my true appreciation to Pastor Taewhan Kim and all brothers and sisters there, especially to 7GY and CJN2. Without their prayers and love through Christ, I would have not even sustained the graduate life.

I am mostly grateful to my parents and my two younger brothers. There is nothing to compare with their unconditional love and support. [절 낳아주시고 길러주시고 늘 기도와 격려를 아끼지 않으시는 부모님께 뭐라고 감사의 말씀을 드려야 할까요. 부모님의 수고와 인내와 헌신과 교육에 대한 열정이 아니었던들, 어떻게 제주도 촌구석에서 이곳 미국까지 올 생각이나 했을까 싶습니다. 지금까지 고생하신 두분에게 이 작은 결실이 위로가 되길 바라고, 위로부터 오는 참 안식과 평화를 얻게 되시길 늘 기도합니다. 늘 기도로 사랑으로 응원해 주시는 장모님께 같은 감사의 말씀을 전합니다. 하시는 사역에 늘 하나님의 도우심이 함께 하시길, 그리고 언젠가 저희가 같이 동역할 수 있게 되길 빕니다.] I have to thank my dear Yunmi, but the words in this world are not enough to express my heart. She is just perfect for me, and I am always sorry not to love her enough that she deserves. May God continually bless on her research and keep her health.

I realized it is God who chose and called me to this place. He first loved me and visited me even though I did not know Him. He is so good and faithful. He made this fruit possible, through the help of every single person around me, and He deserves all the credits. I always pray that my life will be worthy of Him. Glory be to Him, always.

Everything comes from him; Everything happens through him; Everything ends up in him.
(Romans 11:36)